

MODELING & SIMULATION OF GASIFICATION OF INDIAN COAL

A DISSERTATION

*Submitted in partial fulfillment of the
requirements for the award of the degree
of*

INTEGRATED DUAL DEGREE

(Bachelor of Technology & Master of Technology)

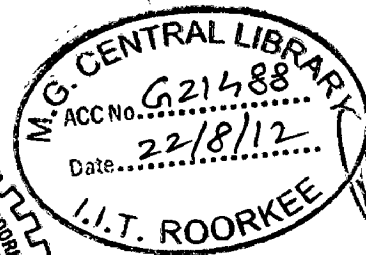
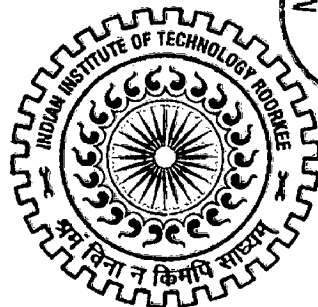
in

CHEMICAL ENGINEERING

(With Specialization in Hydrocarbon Engineering)

By

GOVIND KUMAR SINGH



**DEPARTMENT OF CHEMICAL ENGINEERING
INDIAN INSTITUTE OF TECHNOLOGY ROORKEE
ROORKEE -247 667 (INDIA)
JUNE, 2012**

CANDIDATE'S DECLARATION

I hereby declare that the work, which is being presented in this dissertation, entitled “**MODELING & SIMULATION OF GASIFICATION OF INDIAN COAL**”, submitted in partial fulfillment of the requirements for the award of **Integrated Dual Degree** (Bachelor of Technology and Master of Technology) in **Chemical Engineering** with specialization in **Hydrocarbon Engineering**, is an authentic record of my own work carried out during the period from June 2011 to June 2012, under the supervision of **Dr. Bikash Mohanty**, Professor, Department of Chemical Engineering, Indian Institute of Technology Roorkee.

Date - ~~11~~, June 2012

Place - Roorkee

Govind Kumar Singh
(Govind Kumar Singh)

CERTIFICATE

This is to certify that the above statement made by the candidate is correct to the best of my knowledge.

Bikash Mohanty

Bikash Mohanty

Professor,

Department of Chemical Engineering

Indian Institute of Technology Roorkee

Roorkee, Uttarakhand-247667

ACKNOWLEDGEMENT

A dissertation or any publication can reach to the acme only by the proper guidance, cooperation and kind words of the individuals involved. It is my pleasure to express my gratitude to all of them.

I wish to express my deep sense of gratitude and sincere indebtedness to my supervisor **Dr. Bikash Mohanty**, Professor, Department of Chemical Engineering, Indian Institute of Technology Roorkee for his kind cooperation and encouragement that he provides me to bud new ideas in tackling the various situations while doing the dissertation work. His undying determination to get the best out of his students served as inspiration for completion of this report. Prolonged discussions with him have not only helped me in my dissertation work but also helped me in exploring myself. He has been a constant source of inspiration to me. His unique way of explaining things using examples related to day to day life are truly praiseworthy.

I wish to express my profound gratitude to **Dr. V. K. Agrawal**, Professor, Head cum Chairman, DAC, Chemical Engineering Department, IIT Roorkee for providing all the facilities which have made it possible for me to complete this work. I am also indebted to the faculty members of Chemical Engineering Department especially **Dr. Vimal Kumar Singh**, who have taught me during last five years.

In addition to the Department of Chemical Engineering, IIT Roorkee and administration whose help and resources I have used from time to time, I thank the brains behind the scientific publications, chemical engineering books and research papers whose guidance I have drawn on to complete this work.

I should not forget to express my wholehearted thanks to **Mr. Vijay Singh**, Incharge, Heat Transfer Research Lab and also to **Mr. Amit Rai, Mr. Brajesh Kumar Singh, Mr. Deepak Kumar Dwivedi and Mohd. Shueab** for helping me a lot during my thesis work.

Lastly, I will be always grateful to Him and also my parents whose blessings are always with me.

GOVIND KUMAR SINGH

ABSTRACT

In 21st century, most of the countries including India are facing energy crisis due to accrued energy demand and decline in production of liquid and gaseous fuels. Most of the conventional oil and gas fields have already been exploited and efforts are on now to exploit sources like coal, oil sands, gas hydrates etc. for energy production. India has fourth largest reserves of coal in the world which can be used as a shield against the overwhelming energy crisis. However, most of the coal available in our country is low grade coal, having very high ash content and low sulfur content. In general, they are not amenable to the “standard” gasification process based on commercial entrained flow gasifiers. Instead, they are amenable to less developed fluidized bed gasification technology.

Design, optimization & scale up of fluidized bed coal process have been a challengeable problem due to its complex reaction and transfer mechanism. Therefore, efforts are required to develop the fluidized bed gasification technology through pilot plant studies and numerical modeling. Numerical modeling can be used for tailoring the flow patterns and temperature profiles inside the gasifiers to optimally match the demands made by the kinetics of gasification reactions.

The present work focuses on the modeling and simulation of a pilot scale bubbling fluidized bed gasifier (BFBG) for the gasification of high ash Indian coal. For this purpose, a two dimensional model with quadrilateral cells is developed using FLUENT 12.0 software, taking into account the drying, volatilization, gasification and combustion processes. In the model, the exchange of mass, momentum and energy between solid (secondary phase) and gaseous phase (primary phase) has been described using Eulerian –Eulerian approach. The solid phase is described by kinetic theory of granular flows. The reaction system inside the gasifier involves 4 heterogeneous and 4 homogeneous reactions covering 6 species in gaseous phase (CO, CO₂, H₂, N₂, O₂ and H₂O) and coal in solid phase. The kinetics for the homogeneous reactions is described using eddy dissipation model available in FLUENT while for heterogeneous reactions, a user defined function (UDF) code with Arrhenius kinetics is written in C. The calibration and validation of the model has been done using experimental data generated in a pilot scale BFBG at Central Institute of mining & fuel research (CIMFR), Dhanbad, India. The computed exit gas

composition as well as temperature profile inside the gasifier is in good agreement (error within 10 %) with experimental data.

The flow behaviors, volume fraction and velocity profiles of gas and solid phases in the bed and freeboard zones have been predicted using this model. Also, this model has been used to study the effect of superficial gas velocity, temperature and pressure on the performance of the gasifier. Temperature & CO₂ concentration were found to decrease while CO & H₂ concentration increased along the length of gasifier. The concentration of combustible gases like CO & H₂ increased with temperature while that of H₂O and CO₂ decreased with temperature. The effect of pressure was not very significant and a small decrease in concentration of CO & H₂ and increase in concentration of CO₂ was observed with pressure.

In order to scale up the bubbling fluidized bed gasifier facility at CIMFR, Dhanbad, further case study simulations with various Indian coals having different ash content is required. Also, a disperse particle model (DPM) study of the model is necessary to determine the effect of air distributor holes on the bubble formation and hydrodynamics of the gasifier.

TABLE OF CONTENTS

CANDIDATES' DECLARATION	i
ACKNOWLEDGEMENT	ii
ABSTRACT	iii
CONTENTS	v
LIST OF FIGURES	ix
LIST OF TABLES	xii
NOMENCLATURE	xiv
CHAPTER 1 INTRODUCTION	1- 4
1.1 Motivation and Scope of the Thesis	1
1.2 Objective	4
CHAPTER 2 LITERATURE REVIEW	5- 48
2.1 Gasification Process	5
2.1.1 How it is different from combustion	5
2.1.2 Process description	6
2.1.3 Chemical reactions	7
2.1.4 Parameters affecting syngas compositions	8
2.1.5 Thermodynamic equilibrium	15
2.2 Gasifiers	16
2.2.1 Updraft gasifier	18
2.2.2 Downdraft gasifier	18
2.2.3 Entrained bed gasifier	19
2.2.4 Fluidized bed gasifier	21
2.2.5 HT Winkler Process	23
2.2.6 KBR Transport gasifier	24
2.3 Selection of gasifier for Indian coal	26
2.3.1 Description of Indian coal	26
2.3.2 Selection of gasifier	27
2.4 Modeling approach used for fluidized bed gasifiers	29
2.4.1 One dimensional models	29
2.4.2 Two dimensional models	29
2.4.3 Eulerian granular models	30

	2.4.4	Three dimensional models	30
	2.4.5	Prior Art	31
CHAPTER 3	MULTIPHASE MODEL SELECTION & DEVELOPMENT		49- 65
	3.1	Multiphase modelling approach	49
	3.1.1	Multiphase modeling of Bubbling Fluidized bed gasifier	49
	3.1.2	Eulerian Lagrange Approach	49
	3.1.3	Eulerian- Eulerian Approach	50
	3.1.4	Eulerian Granular Approach	52
	3.1.5	Choosing the correct multiphase model	52
	3.1.6	Turbulence models in FLUENT	53
	3.1.7	Drag models in FLUENT	54
	3.1.8	Interphase heat transfer	56
	3.1.9	Virtual mass effect	56
	3.1.10	Lift force	56
	3.2	Model development	57
	3.2.1	Hydrodynamics	57
	3.2.2	Solid pressure	59
	3.2.3	K- ϵ per phase turbulence model	60
	3.3.4	Granular Eulerian model	61
	3.3.5	Energy conservation	62
	3.3.6	Chemical reactions	63
	3.3.7	Species transport equations	65
CHAPTER 4	PRPBLEM DESCRIPTION & SOLUTION TECHNIQUE		66- 93
	4.1	Geometry	67
	4.1.1	3D geometry in Ansys design modular	67
	4.1.2	2D geometry in Gambit	72
	4.2	Meshing	74
	4.2.1	Edge & face meshing	74
	4.2.2	Boundary conditions	76
	4.2.3	Grid optimization	77
	4.3	FLUENT model setup	79
	4.3.1	Mesh quality	79

4.3.2	Solver preferences	79
4.3.3	Models	80
4.3.4	Materials	81
4.3.5	Phases	82
4.3.6	Phase interaction	84
4.3.7	Operating & boundary conditions	84
4.3.8	Monitors	84
4.3.9	Customization of FLUNT for BFBG problems	85
4.4	Solution Techniques	86
4.4.1	Overview of flow solvers	86
4.4.2	Solution Method in FLUENT for Multiphase Flows	86
4.4.3	Time-Advancement Algorithm	87
4.4.4	Discretization	87
4.4.4.1	Finite Volume Method (FVM)	88
4.4.4.2	Spatial Discretization	88
4.4.4.3	Temporal Discretization	89
4.5	Algorithm used for Present work	91
CHAPTER 5	RESULTS AND DISCUSSION	94- 143
5.1	Basic Gasifier Model	95
5.1.1	Calibration & Validation	95
5.1.2	Temperature contours along height & width of gasifier	95
5.1.3	Velocity contours along the height & width of gasifier	97
5.1.4	Predominant reactions along the height of gasifier	99
5.1.5	Contours of species along height & width of gasifier	100
5.1.6	Bed Fluidization	102
5.2	CIMFR gasifier model	105
5.2.1	Calibration & Validation	105
5.2.2	Temperature Profile	106
5.2.3	Reaction rate profile	110

5.2.4	Contours of species mole fraction	118
5.2.5	Volume fraction profile	126
5.2.6	Velocity profile	127
5.2.7	Tar concentration profile	131
5.2.8	Calculation of calorific value of syngas	131
5.3	Parametric study	134
5.3.1	Fluidization at different air velocity	134
5.3.2	Effect of temperature on syngas performance	140
5.3.3	Effect of pressure on syngas performance	142
5.4	Some insights on design modification of CIMFR BFBG pilot plant	143
CHAPTER 6	CONCLUSIONS AND RECOMMENDATIONS	144- 146
6.1	BASIC Model	144
6.2	CIMFR Model	145
6.3	Recommendations	146
CHAPTER 7	REFERENCES	147- 156
APPENDIX- A	Pilot plant Data	A1- A2
APPENDIX- B	UDF for heterogeneous reactions	B1- B2
APPENDIX- C	Sample data & results	C1- C2

LIST OF FIGURES

Fig. No.	Title	Page No.
1.1	Oil & Gas consumption (1960- 2006)	1
1.2	India's growing coal import	2
2.1	Classification of gasification process based on gasifying medium	9
2.2	Products of gasification reaction as a function of oxygen-to- coal ratio	10
2.3	Relation between CO concentration, carbon conversion, gasification efficiency and gas velocity	11
2.4	Syngas composition Vs. Operating temperature	11
2.5	Syngas composition Vs. Operating pressure	12
2.6	Effect of varying bed compositions on syngas composition	14
2.7	Classification of gasifiers	16
2.8	Updraft gasifier	18
2.9	Downdraft gasifier	19
2.10	Entrained bed gasifier	19
2.11	Circulating fluidized bed gasifier	21
2.12	High temperature Winkler fluidized bed process	23
2.13	KBR transport gasifier	24
2.14	Schematic diagram of fluidized bed gasification model used by Robert et al. 1988	31
2.15	Cundall's representation of normal contact force	32
2.16	Schematic diagram showing two phase theory with concept of net flow	34
2.17	Schematic diagram of cell model applied by Hamel et al. 2001	36
2.18	Schematic view of Gaussian particle size distribution	38

2.19	Phases, fluids and exchanges in Chejne's coal gasification model	38
2.20	Schematic representation of the model developed by Pengmei et al. 2008	43
2.21	Calculation process of the model equations used by Pengmei et al. 2008	44
2.22	Experimental & predicted molar fractions (Cornejo et al. 2011)	47
3.1	Hierarchy of Multiphase Models	53
3.2	Turbulence Models	53
4.1	Flowchart of solution Approach	66
4.2	Sketching panel of Ansys design modular	67
4.3	Closed loop sketch in the ZX plane generated using polyline	68
4.4	Central body of the BFBG geometry obtained after revolve 1 operation	69
4.5	Sketch for coal inlet & syngas outlet	69
4.6	Details of Revolve 8 (Add material operation)	70
4.7	3D geometry of bubbling fluidized bed gasifier	70
4.8	A closer view of coal inlet & syngas outlet section	71
4.9	Gambit user interface used for generating 2D geometry	72
4.10	Generating 2D geometry in Gambit	73
4.11	Geometry of 2D section of bubbling fluidized bed gasifier	74
4.12	Edge meshing in Gambit	75
4.13	Experimental set up and FLUENT gasifier geometry	76
4.14	Boundary condition types assigned in Gambit	77
4.15	Variation of Temperature and CO mole fraction with number of cells (grid optimization)	78
4.16	Patch in FLUENT	85
4.17	Solution Algorithm used by FLUENT	102

5.1	Contour of Temperature profile (Basic Model)	96
5.2	Contour & Vectors of phase 2 velocity profile (Basic Model)	97
5.3	Major reactions taking place along the height of the gasifier (Basic Model)	99
5.4	Contours of mole fraction of syngas components (Basic Model)	100
5.5	Bed fluidization at different air velocity as a function of time (Basic Model)	102
5.6	Comparison of predicted values and experimental results	106
5.7	Contour of temperature distribution inside the gasifier	107
5.8	Reaction pattern along the height of the gasifier	108
5.9	Axial temperature distribution inside the gasifier	109
5.10	Axial profile of heterogeneous and homogeneous gasification reactions rate	111
5.11	Contours of mole fraction of syngas components	118
5.12	Axial profile of mole fraction of syngas components	121
5.13	Contour of volume fraction of phase 2	126
5.14	Contour and vectors of velocity profile of phase 2	127
5.15	Contour of mass fraction of Tar	131
5.16	Calorific value of exit syngas as a function of time & Temperature	133
5.17	Bed fluidization at different air velocity as a function of time	135
5.18	Effect of temperature on mole fraction of syngas components	140
5.19	Effect of pressure on syngas composition	142

LIST OF TABLES

Table No.	Title	Page No.
2.1	Differences between combustion and gasification processes	5
2.2	Effect of coal quality on gasifier performance	13
2.3	Characteristics of different types of gasifiers	17
2.4	Characteristics of important entrained flow processes	20
2.5	Commercial fluidized bed processes	22
2.6	Advantages and disadvantages of moving, fluidized and entrained bed gasifiers	25
2.7	Proximate analysis of various Indian coals	26
2.8	Typical proximate analysis of Indian, Indonesian & South African coal	27
2.9	Quality of Indian coals (1970s- 1990s)	27
2.10	Classification of gasifiers based on suitability for Indian coals	28
2.11	Summary of salient features of discrete element model and two fluid model	34
2.12	Comparison of performance from isothermal and non-isothermal model with experimental data (Ross et al. 2005)	40
2.13	Solver parameters (Cornejo et al. 2011)	46
3.1	Arrhenius parameters of heterogeneous reactions	64
3.2	Kinetics of homogeneous reactions	64
4.1	Mesh size information for 3 cases	75
4.2	Comparative study of case transitions	79
4.3	Results of mesh quality check	79
4.4	Characteristics of solver	80
4.5	Model selection for bubbling fluidized bed gasifier	80

4.6	Properties of coal feedstock	81
4.7	Granular parameters for secondary phase	82
4.8	Material properties used in FLUENT	83
4.9	Operating & boundary conditions for gasifier models	84
5.1	Basic model validation (predicted values vs. literature data)	95
5.2	CIMFR model validation	105
5.3	Average rate of reactions	110
5.4	Desired syngas composition for different end uses	143

4.6	Properties of coal feedstock	81
4.7	Granular parameters for secondary phase	82
4.8	Material properties used in FLUENT	83
4.9	Operating & boundary conditions for gasifier models	84
5.1	Basic model validation (predicted values vs. literature data)	95
5.2	CIMFR model validation	105
5.3	Average rate of reactions	110
5.4	Desired syngas composition for different end uses	143

NOMENCLATURE

A	Constant in Syamlal O'Brien drag model
B	Constant in Syamlal O'Brien drag model
C_D	Drag coefficient, (-)
C_p	Calorific capacity, J/ kg K
d	Coal particle mean diameter, m
e	Coefficient of restitution for particle collision
F	Force, N
g_0	Radial distribution function
g	Gravitational acceleration, m/ s ²
h	Specific enthalpy, j/ kmol kg
k	Thermal conductivity, W/ mK
Nu	Nusselt number
P	Pressure, P
Pr	Prandtl number
q	Heat flux, w/ m ²
Q	Heat transfer intensity between phases, W·m ⁻² ·sr ⁻¹
Re	Reynolds number
S	Source term
t	Time, s
T	Temperature, K
U	Velocity, m/ s
Y	Mass fraction

Greek Symbols

α	Volume fraction
λ	Bulk viscosity, kg/ m- s
ε	Turbulent kinetic energy dissipation rate, m ³ / s ³
κ	Turbulent kinetic energy, m ² / s ²

μ	Molecular viscosity, kg/ m s
τ	Stress tensor, Pa
C_p	Calorific capacity, J/ kg K
ρ	Density, kg/ m ³
Θ	Granular Temperature, m ² / s ²
ϕ	Switch function, Equation

Subscripts

g	Gas phase
s	Solid phase
p, q	Fluid phase

CHAPTER- 1

INTRODUCTION

In 21st century, most of the countries including India are facing energy crisis due to accrued energy demand and decline in production of liquid and gaseous fuels. Most of the conventional oil and gas fields have already been exploited. The worldwide rate of conventional crude oil production peaked at the end of 2004, and has remained between 72 and 74 million barrels per day (mbpd) ever since. However, the demand of energy is continuously increasing especially in the developing countries like India and China as evident from Fig. 1.1. Therefore, efforts are on now to exploit sources like coal, oil sands, gas hydrates etc. for energy production. Unconventional liquids (0.5 Mb/day in 2007 to 2.0 Mb/day in 2009 and estimated to be 5.0 Mb/day in 2030) have been responsible for nearly all of the growth in world “oil” production since 2005. [11]

1.1 MOTIVATION & SCOPE OF THE THESIS

According to United States Energy Information Administration, India has fourth largest reserves of coal (10.2 %) in the world after America (27.1 %), Russia (17.3 %) and China (12.6 %). According to the Ministry of Coal, India is currently the third largest producer of coal in the world, with a production of about 533 million tons (MT) of hard coal and 40 MT of lignite in 2009–10. India has relatively large reserves of coal (285.862 billion tons as on 1st April, 2011[71]) compared to crude oil (728 million tons) and natural gas (686 billion cubic meters). This vast coal reserve can be used as a shield against the overwhelming energy crisis.

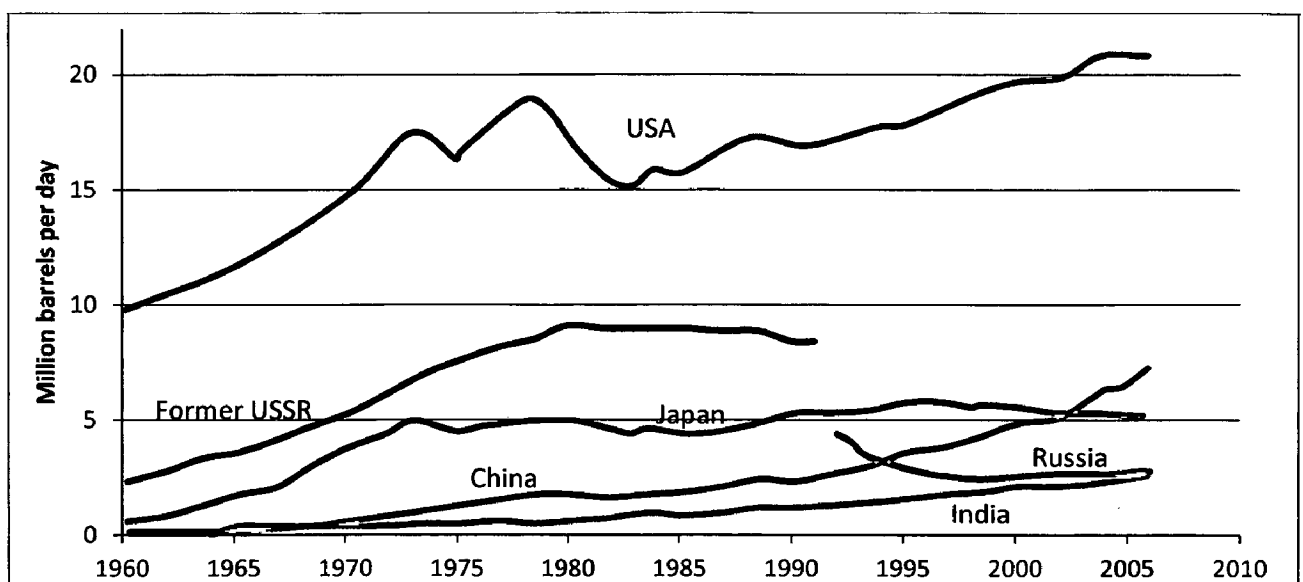


Fig. 1.1: - Oil and gas consumption (1960 – 2006) [2]

Conventionally, in India, coal is utilized mainly for producing electricity in coal fired power plants. In these conventional power plants, coal is combusted in low efficiency combustors where only a third of the energy value of coal is actually converted into electricity [130]. This is because a lot of heat is wasted in power generation cycle due to irreversibility of the process (Second law of thermodynamics). Also, these combustors cause large emission of CO₂, SO₂, and particulate matter and degrade air quality and show inverse impact on human health. Emission of CO₂ from coal combustion has been identified as major fugitive in increasing atmospheric CO₂ concentration strongly affecting the world's climate [5]. Therefore, mitigating climate change will require deep reduction in CO₂ emissions, especially from coal use.

Most of the coal available in our country is low grade coal, having very high ash content and low sulfur content. The ash content of Indian coal is as high as 40 % and average ash content is around 30 %, which is very high. This ash has high silica/ quartz and alumina content, which melt by absorbing heat in the conventional combustors and becomes corrosive to the gasifier material [24]. Also, it is an excess burden on the transportation and beneficiation part. This is one of the reasons of rising coal import in India as shown in Fig. 1.2, even though we have large reserves of coal. [65]. Therefore, the demand of the present time is to develop “Clean coal technologies” to put a curb on the import of non-coking coals and make efficient utilization of this vast resource in an economical and environment friendly manner [66].

All these technologies viz. gasification, underground coal gasification, co-gasification with pet coke, oxyfuel combustion, direct coal liquefaction and carbon capture & storage have gained fabulous momentum in terms of research. However, concerns exist regarding the economic viability of these technologies and the timeframe of delivery, potentially high hidden economic costs in terms of corrosion, social and environmental damage [127], and the costs and viability of disposing of ash and other toxic matter.

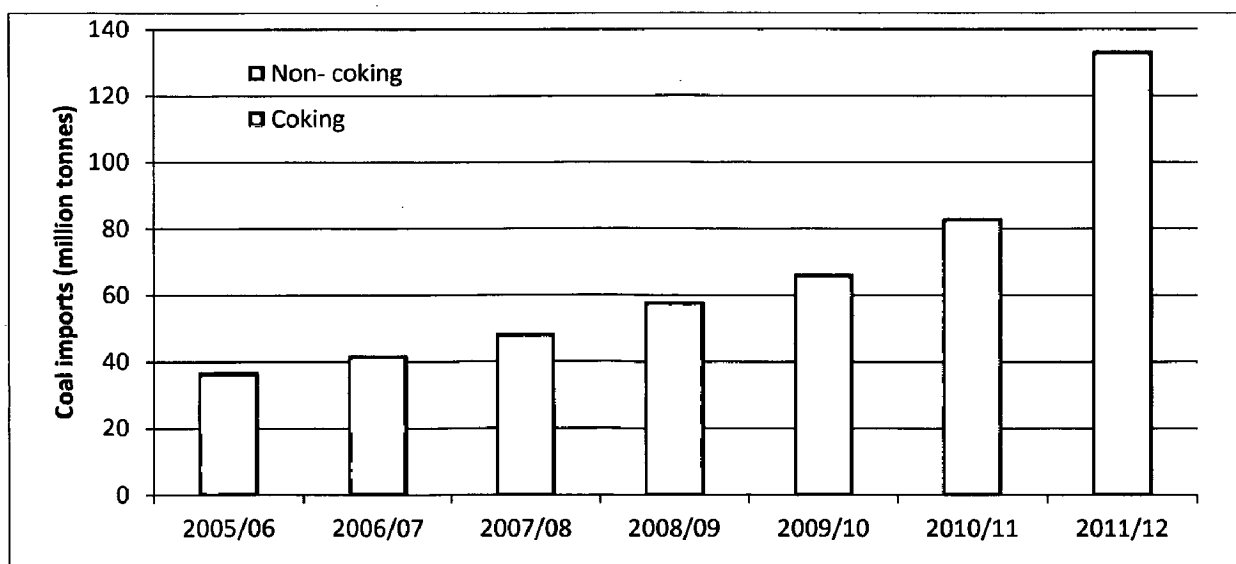


Fig. 1.2 Indian's growing coal import
 Source: Ministry of coal, Karvi stock broking

Gasification is the oldest and commercially most established technique. Coal gasification plants in general have better emissions profiles than conventional power plants and their higher operating efficiencies allow for significant reductions in pollutants. CO₂ emissions for one are reduced roughly by 20 % and can be further reduced to zero by adding carbon capture & sequestration technologies (CCS) [69]. Syngas derived from coal gasification is virtually free from NO_x and emits extremely low SO_x, NO_x and particulate matter on burning or in integrated gasification combined cycle (IGCC). During gasification process, Sulfur in coal gets converted to hydrogen sulfide and can be captured by acid gas removal process.

Efficiency gains are another benefit of coal gasification. Coal gasification based power plant gets dual benefit from the gases it produces. First, the syngas, cleaned of impurities, are fired in a gas turbine to generate electricity. The hot exhaust of the gas turbine, and some of the heat generated in the gasification process, is then used in heat recovery steam generators (HRSG) to generate steam for use in a steam turbine generator. This dual source of electric power, called "IGCC" is much more efficient (fuel efficiency up to 50%) in converting coal's energy into electricity [130].

This capability to produce electricity, hydrogen, and various other chemicals while eliminating nearly all air pollutants and potentially greenhouse gas emissions makes coal gasification one of the most promising technologies for energy plants of the future. Now, plants based on coal gasification are operating commercially in United States (California- 110 MW, Florida- 250 MW) and in other nations [69]. Experts predict that gasification will be at the heart of the future generations of clean coal technology plants and may be the most flexible process for the production of clean burning hydrogen [131]. The last 10-15 years have seen the renaissance of gasification technology as evident from Fig. C.2. [120]

Gasification of coal was considered in India as early as the 1970s, but Indian coals, in general, are not amenable to the "standard" gasification process based on commercial entrained flow gasifiers due to their high ash content and high ash fusion temperature [21]. Standard Indian coals can be gasified using fluidized-bed and moving-bed gasifiers. However, fluidized bed is preferred over moving bed due to its high thermal efficiency and continuous operation.

Although several small-scale demonstration plants were built in Europe and the U.S. based on fluidized bed technology, there is significantly low investment in fluidized bed gasification technology worldwide, as it is not relevant for most coals of Indonesian, American & European origin. However, it is quite amenable for use with Indian coals, and there has been some R&D on developing a fluidized-bed gasification process in India, primarily led by the Council for Scientific and Industrial Research, the Indian Institute of Chemical Technology, and BHEL [5].

In the late 1990s, BHEL developed a pilot IGCC plant using fluidized-bed gasifier and currently, BHEL and NPTC are collaborating on a 100 MW IGCC demonstration plant based on Indian

coals [108]. Central Institute of mining & fuel research (CIMFR), Dhanbad has also setup bubbling fluidized bed gasifier in their Digwadih campus at Dhanbad for pilot scale study.

In addition to government sector, the private players are also displaying interest in gasification process for efficient coal utilization. Naveen Jindal-led Jindal Steel and Power (JSPL) have awarded a technology contract to the US-based KBR Group to construct three transport gasifier with the capacity of 1, 20,000 nm³/hour (a unit for the compressed air/gas requirement) at the coal gasification plant at Angul in Orissa. [78].

Pilot plant initiatives have been taken by both government and private sectors. However, setting up a gasification plant is cost intensive and the similar prediction on the performance of gasifier can be made by using modeling and simulation techniques. Numerical modeling has become an essential and cost effective tool for design, optimization and scaling up gasification processes. This can be used to easily predict flow behaviors and temperature profiles of gas and solid phases in the bed and freeboard zones, which are difficult to be measured by pilot plant experiments.

Several works on modeling & simulation of coal gasification [17, 18, 31, 32, 54, 57, 58, 60, 62, 72, 79, 84, 89, 91, 99, 102, 103, 107, 113, 117, 125, 128, 136, 138, 146 and 147] in fixed, fluidized and entrained bed gasifiers is reported in literatures. However, most of the work is done on low ash coals having ash content between 2- 5 %. There is hardly any report on modeling and simulation of gasification of high ash Indian coal ($\approx 40\%$).

1.2 OBJECTIVE

In view of the above discussion, the present work has been taken up with the following objective: -

- a) To identify a suitable gasifier for the gasification of Indian coal.
- b) To develop a precise numerical model of CIMFR bubbling fluidized bed gasifier pilot plant in FLUENT 12 using Eulerian Granular model with Indian coal as feed material.
- c) To validate the model using experimental results obtained from CIMFR, Dhanbad.
- d) To study the hydrodynamics and fluidization behavior of the bubbling fluidized bed gasifier pilot plant.
- e) To study the temperature distribution and composition of product species along the length of gasifier.
- f) To study the effect of temperature, pressure & superficial velocity on the performance of the gasifier.

CHAPTER- 2

LITERATURE REVIEW

The present study aims at modeling & simulation of gasification of Indian coal. The objectives of the present work are given in Chapter 1. To meet those objectives, a literature review was conducted on the relevant aspects such as chemistry of Indian coal, gasification process and gasifiers, selection of gasifier, hydrodynamics of the bubbling fluidized bed, multiphase, drag and heat transfer models used for simulation of the bubbling fluidized bed gasifier by other investigators in this field.

2.1 GASIFICATION PROCESS

The gasification covers the conversion of any carbonaceous fuel to a gaseous product with a usable heating value. [23] The process starts with drying of the feedstock as soon as they are introduced in the gasifier and heated. The dry feedstock is then pyrolysed (devolatilization) and converted to char with further increases in its temperature. Gasification is a result of chemical reactions between carbon present in the feedstock and steam, CO₂ and hydrogen in the gasifier vessels as well as reaction between the product gases. These reactions are endothermic in nature to a large extent and thus the thermal energy to drive the gasification reactions must be provided by the combustion of the char or dry feedstock in some cases. [76].

2.1.1 How it is different from combustion: Gasification is not a combustion process but rather a conversion process [46]. Here, the fuel is combined with limited steam and oxygen in a heated, pressurized vessel. The atmosphere inside the vessel is starved of oxygen to prevent or limit combustion, and the result is partial oxidation of the fuel to produce a syngas. Table 2.1 shows some key differences between gasification & combustion process [76]: -

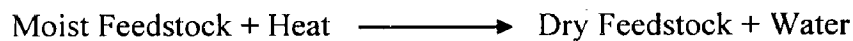
Table 2.1: Difference between Combustion & Gasification

Features	Gasification	Combustion
Purpose	Creation of valuable products from carbonaceous material	Generation of heat, destruction of waste
Process type	Thermal & chemical conversion using no or limited Oxygen,	Complete combustion using excess Oxygen.
Raw Gas composition	H ₂ , CO, H ₂ S, NH ₃ & particulates	CO ₂ , H ₂ O, SO ₂ , NO _x & particulates
Operating pressure	Atmospheric to high	Atmospheric
Operating Temperature	1300 – 2700 ° F	1500- 1800 ° F
Gas clean up	➤ Syngas cleanup at atmospheric	➤ Flue gas cleanup at

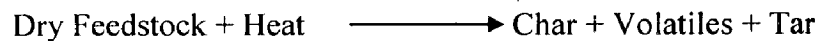
	<p>to high pressures depending on the gasifier design.</p> <ul style="list-style-type: none"> ➤ Treated syngas used for chemical, fuels, or power generation. ➤ Recovers sulfur species in the fuel as sulfur or sulfuric acid. ➤ Clean syngas primarily consists of H₂ and CO. 	<p>atmospheric pressure.</p> <ul style="list-style-type: none"> ➤ Treated flue gas is discharged to atmosphere. ➤ Acid gas removal generates a waste that must be landfilled. ➤ Clean flue gas primarily consists of CO₂ and H₂O
--	---	---

2.1.2 Process Description: - As the feedstock proceeds through the gasifier, the following physical, chemical and thermal processes may occur sequentially or simultaneously depending on the reactor design and the feedstock material.

- 1.) **Drying:** - As the feedstock is heated and its temperature increases, water is the first component to get evolved.

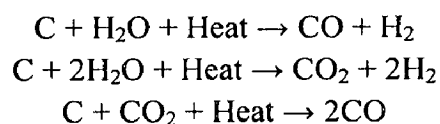


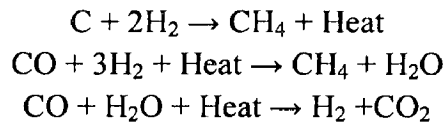
- 2.) **Devolatization:** - As the temperature of the dry feedstock increases, pyrolysis takes place and the feedstock is converted to char.



Depending on the origin of the feedstock, the volatiles may include H₂O, H₂, N₂, O₂, CO₂, CO, CH₄, H₂S, NH₃, C₂H₆, and very low levels of unsaturated hydrocarbons such as acetylenes, olefins, and aromatics. Any compound with molecular weight greater than Benzene is called Tar. Char is the residual solids consisting of organic and inorganic materials. After pyrolysis, the char has a higher concentration of carbon than the dry feedstock.

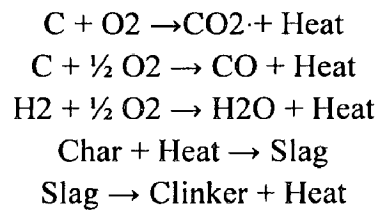
- 3.) **Gasification:** - Gasification is the result of chemical reactions between carbon in the char and steam, carbon dioxide, and hydrogen in the gasifier vessel as well as chemical reactions between the resulting gases. Gasification reactions can be represented by:





Depending on the gasification process conditions, the remaining char may or may not have significant amount of organic content or heating value.

- 4.) **Combustion:** - The thermal energy that drives the gasification reactions must be provided directly by combusting some of the char or dry feedstock or in some cases, the volatiles within the gasifier or indirectly, by combusting some of the feedstock char, or clean syngas separately and transferring the required heat to the gasifier. The following chemical and thermal reactions may take place when char or dry feedstock is burned: -



Combustion of char or feedstock produces ash, unreacted organic material, which can be melted into liquid slag. Slag can be re-solidified to form clinker.

2.1.3 Chemical Reactions: - The principal chemical reactions during the process of coal gasification can be classified as follows:

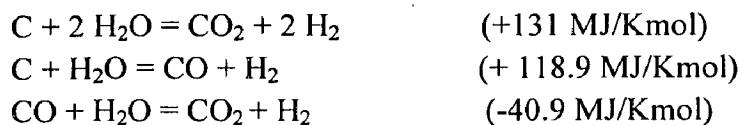
a.) Combustion: -



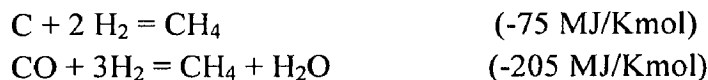
b.) Boudouard: -



c.) Water Gas Reaction: -

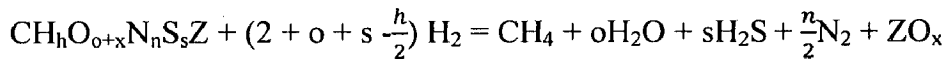
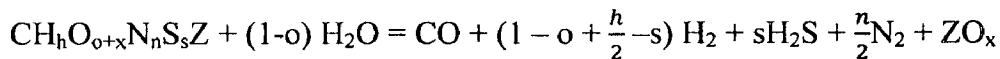
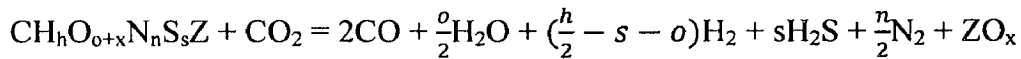
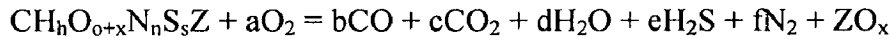


d.) Methanation: -



Most of the oxygen inserted into the gasifier either as pure oxygen or air is consumed in combustion reactions (a) to provide the heat necessary to dry the solid fuel, break up chemical bonds and raise the reactor temperature to drive the gasification reactions (b, c, d).

However, Valero et al., 2006 [3] provides a more detailed description of the gasification reactions. They considered that the formula of the char obtained from devolatilization reaction, containing C, H, N, S, O and mineral matter may be assumed to be $CH_hO_{o+x}N_nS_sZ$. The gasification reactions can then be represented as follows: -



2.1.4 Parameters affecting syngas composition: - The composition of the syngas obtained from the gasifier depends strongly on the following parameters: -

- 1.) Gasifying medium
- 2.) Equivalence Ratio: -
- 3.) Gasifier Operating Temperature
- 4.) Gasifier Operating Pressure
- 5.) Feedstock Composition
- 6.) Bed Material
- 7.) Feedstock preparation and particle size
- 8.) Reactor heating rate
- 9.) Residence time
- 10.) Plant configuration such as : -
 - a) Feed System: -Dry or Slurry
 - b) Feedstock reactant flow Geometry
 - c) Mineral removal system: - Dry ash or slag
 - d) Heat Generation and transfer method-Direct/Indirect
 - e) Syngas cleanup system

Gasifying Medium: - In general, coal gasification can be done using air, oxygen or steam as the gasifying medium. Gasification with air results in syngas with low higher heating value in the range of 3.5 – 10 MJ/ m³ due to inherent dilution with N₂ present in the air [51]. Conversely, gasification with oxygen results in syngas with HHV of 10 – 20 MJ/ m³ and gasification with steam results in even higher heating value in the range of 20-35 MJ/ m³. However, air gasification is more widely used compared to oxygen and steam gasification due to its economical and operational advantages. A schematic representation of different gasification medium and the resulting syngas quality is shown in Fig. 2.1 [76, 33]

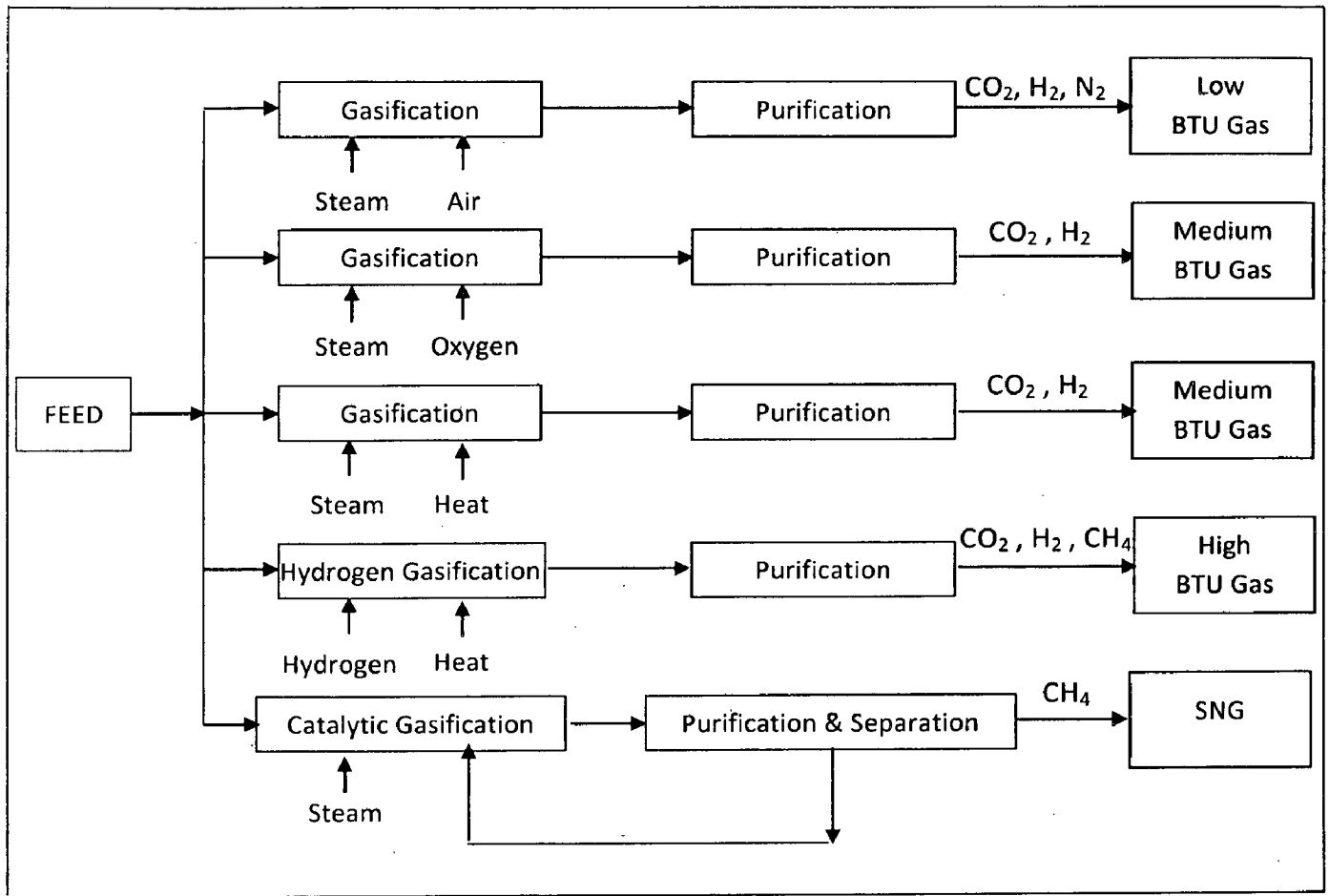


Fig. 2.1 Classification of Gasification process based on gasifying medium

In hydrogen gasification [33], the fuel stock is converted to gaseous fuel in the presence of hydrogen under high pressure. For this process, it is critical to maintain stringent reaction conditions due to highly volatile nature of hydrogen. Weil et al. (1978) [135] used preheated hydrogen mixed with peat at the entrance of fluidized bed gasifier. The reactor was operated as an entrained flow reactor in an isothermal heat-up mode. He observed that increasing the temperature from 426°C to 760°C increased carbon monoxide and hydrocarbon gases from 8% to 18% and 41% to 63%, respectively.

Equivalence Ratio: - Equivalence ratio is the most influential parameter in any gasification process. An increase in equivalence ratio increases the temperature inside the gasifier while ER decrease increases the char formation inside the gasifier. Combustible products decreases with an increase in ER with the formation of higher amount of CO₂ as well as total gas yield [118] greatly diminishing the heating value of the final syngas. At the equivalence ratios of 0.25, 0.20 and 0.17, the higher heating value of the produced gas from biomass air gasification were 6.48, 6.19 and 5.98 MJ/Nm³, respectively [42]. Tar concentration decreases with increase in equivalence ratio. This is mainly due to the following two reasons: -

- Higher temperature as a result of higher ER increases reaction rate of the chemical products.
- Higher ER supplies additional oxygen for the cracking of Tar into lower hydrocarbons.

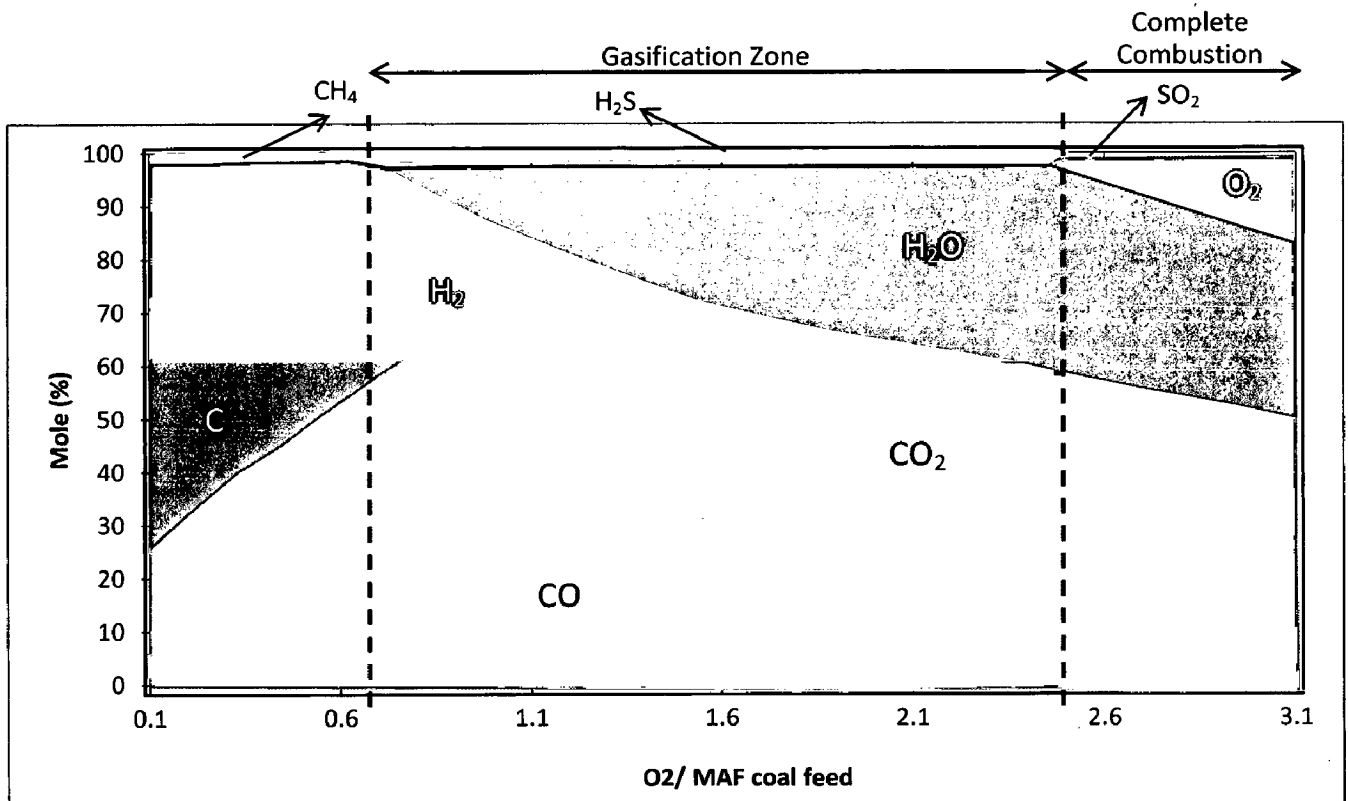


Fig. 2.2 Products of gasification reactions as a function of oxygen-to- coal ratio

Increasing the equivalence ratio also results in lower pressure drops both in the dense bed and the freeboard regions when the gasifier operated at different fluidization velocities and bed heights. Therefore, it is very important to maintain an optimal value of equivalence ration in the gasifier to obtain the desired product composition. The range of oxygen to fuel ratio for the gasification reaction to occur is illustrated in Fig. 2.2 [74, 89]:

Superficial Velocity: - The Superficial Velocity is the ratio of volume flow rate of syngas to the cross-sectional area of the gasifier and can be thought as one independent parameter unconstrained to a particular gasifier size. Higher SV promotes burning as well as reaction rate and decreases the residence time of coal in the system [43] .Higher burning rate increases the temperature of the gasifier. An overall increase in combustibles (except CH₄ which shows no appreciable change) is reported with increase in SV. The tar content initially decrease reaching the minimum level followed by an increase with SV is reported in the literature [124]. Increase in tar content beyond optimum SV is due to the short residence time of the tar vapors inside the gasifier and slowing down cracking.

Fang et al. 2001 studies the effect of superficial velocity on gasification reaction. They observed that the CO concentration, carbon conversion and gasifier efficiency increases when gas velocity decreases under same fuel feed rate as evident from Fig. 2.3 [144].

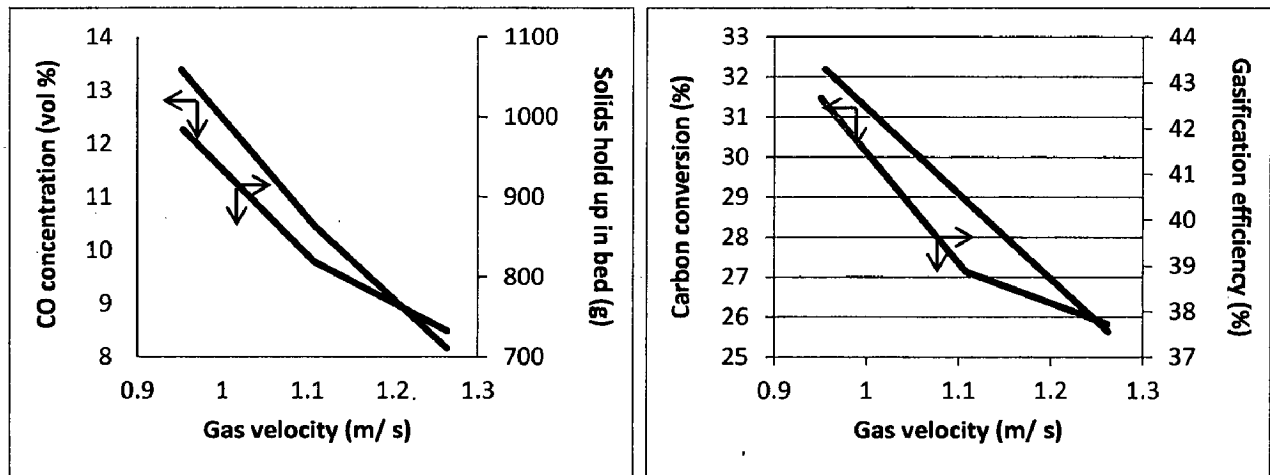
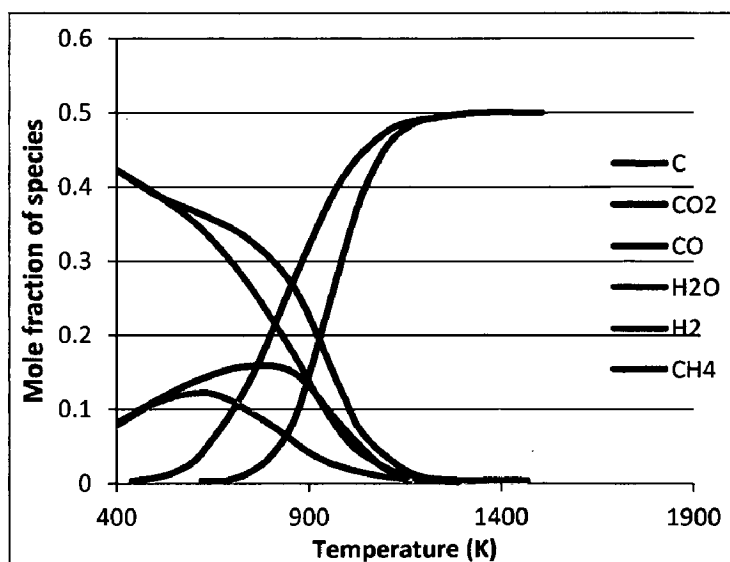


Fig. 2.3 Relationship between CO concentration, carbon conversion, gasification efficiency and gas velocity

Gasifier operating Temperature: - The gasification rate as well as overall performance of the gasifier is temperature dependent. All gasification reactions are normally reversible and equilibrium point of any of these reactions can be shifted by changing the temperature. Harris et al. (2005) [61] presented gasification conversion data for a suite of Australian coals reacting with Oxygen/ Nitrogen mixtures at 2.0 MPa pressure and at temperatures up to 1773 K. An increase in the temperature increases the mass conversion efficiency, reduces the tar content as well as char inside the gasifier.



Combustible gas yield increases due to higher tar cracking resulting in higher syngas yield and heating value. CO content increases with increase in temperature as the endothermic reactions are more favored at higher temperatures. The composition of syngas from gasification of biomass as a function of gasifier operating temperature is shown in Fig. 2.4.

Uniformity of temperature in a radial as well as in axial direction inside the reactor is very important for efficient

Fig. 2.4 syngas composition vs. operating temperature

mixing in a fluidized bed. Generally, less than 100 °C difference in total riser height is acceptable.

Utioh et al. (1989) reported increases in hydrocarbon gases, especially CH₄ and C₂H₄ (ethylene) and decrease in yield of higher hydrocarbons (C₃ – C₈) with increases in temperature above 650 °C indicating the onset of cracking/ reforming reactions [133].

Gasifier Operating Pressure: - High-Pressure gasification reduces the size of the gasifier for the same amount of feedstock and can act to reduce the need for further compression when the gasification products are intended for subsequent use in the Fischer-Tropsch process or other chemical synthesis process which require high pressure.

Increase in pressure in a fluidized bed increases turbulence and thus increase in gas-particle interaction is observed. Increase in pressure also results in bubble instability and bubble splitting in fluidized bed. Wiman and Almstedt [73] have defined a parameter called bed expansion ratio (δ) as follows:

$$\delta = ((H_{fl} - H_{MF}) / H_{fl})$$

Where,

H_{fl} = fluidization height at given condition

H_{mf} = minimum fluidization height

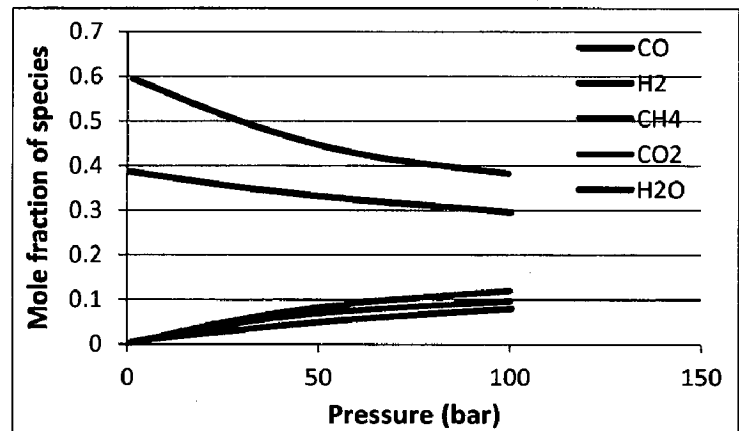


Fig. 2.5 syngas composition vs. operating pressure

Their finding shows a significant increase in δ with increase in pressure. However, the rate of increase drops with increase in pressure and levels off once the pressure reaches around 1 MPa.

Duan et al., 2011 [44] worked on the gasification of bituminous coal to determine the effect of pressure on coal gasification in a turbulent circulating fluidized bed gasifier. They observed that the higher pressure improves the product quality because of better fluidization in the reactor. Coal gasification at higher pressure shows advantages in terms of higher heating value (increased by 16.6% when the pressure is increased from 0.1 to 0.3 MPa.) and coal conversion (increased from 57.52 % to 76.76 %).

The effect of pressure on syngas composition is evident from Fig. 2.5. CO and H₂ yield decreases while CO₂, H₂O and CH₄ yield increases with increase in pressure resulting in higher heat content yield.

Feed stocks Composition: - The reactivity of different coal and char depends on a number of factors: -

- a) The porosity of coal i.e. its inner structure, surface and active sites.
- b) The crystal structure of fixed carbon
- c) The catalytic effect of ash components in the coal

Young (low-rank) coals such as brown coal have a large specific surface and thus a high reactivity. On the other hand, older coals, particularly anthracitic coals, have a poor reactivity. Reactivity is enhanced by alkalis, particularly potassium. Table 2.2 summarizes the effect of coal quality on the gasifiers' performance: -

Table 2.2: Effect of coal quality on gasifier performance

S. No.	Parameter	Importance
1	Moisture	Influences gasifier efficiency and determines whether process will be dry or slurry feed
2	Volatile Matter	Determines the extent and rate of gasification reactions
3	Heating Value	Determines plant dimensions and generation capacity
4	Ash Content	Lowers system efficiency and increases slag production and disposal cost
5	Ash Fusion Temp.	Influences melting ability of the coal ash
6	Slag Viscosity	Influences smooth slag flow between packed bed particles.
7	Char Reactivity	Influences the extent of carbon conversion
8	Sulphur	Causes corrosion in heat exchangers
9	Nitrogen	NOx emissions
10	Chlorine	May produce HCL which can poison gas cleaning system catalyst

Bed Material: - Proper consideration of bed material in a fluidized bed is important for achieving proper homogenization of feed particles and efficient heat transfer so that minimum temperature gradient is realized within the riser. In many cases, bed material can itself act as a catalyst facilitating efficient tar cracking. Presence of Ni in the bed material can promote low temperature gasification of coal preventing ash melting. Catalytic steam gasification can be carried out in the presence of Alkali and Alkaline earth catalysts converting coal directly into H₂/CH₄ rich gases under mild conditions. Armstrong et al. 2011 studied the effect of char- limestone bed material on syngas composition. He considered 3 different cases: -

- a) A bed with a 50- 50 ratio of char and limestone.
- b) Char dominating bed (75 % char- 25 % limestone) and
- c) Limestone dominating bed (25 char- 75% limestone)

From these studies, he stated that the composition of char and limestone can greatly influence the concentration of the gaseous products. He observed that increasing the percentage of char in the bed results in an increase in CO and decrease in CO₂ as evident from Fig. 2.7. This is due to a higher presence of char promoting the combustion reaction leading to more CO₂ being produced. The CO₂ is consumed by the Boudouard reaction to produce more CO [81].

Increasing the amount of char would increase the instances of all heterogeneous reactions taking place, including further up the bed where the steam gasification reaction produces further CO and H₂. This is also observed in Fig. 2.6 where there is an increase in the concentration of H₂ with increasing char content.

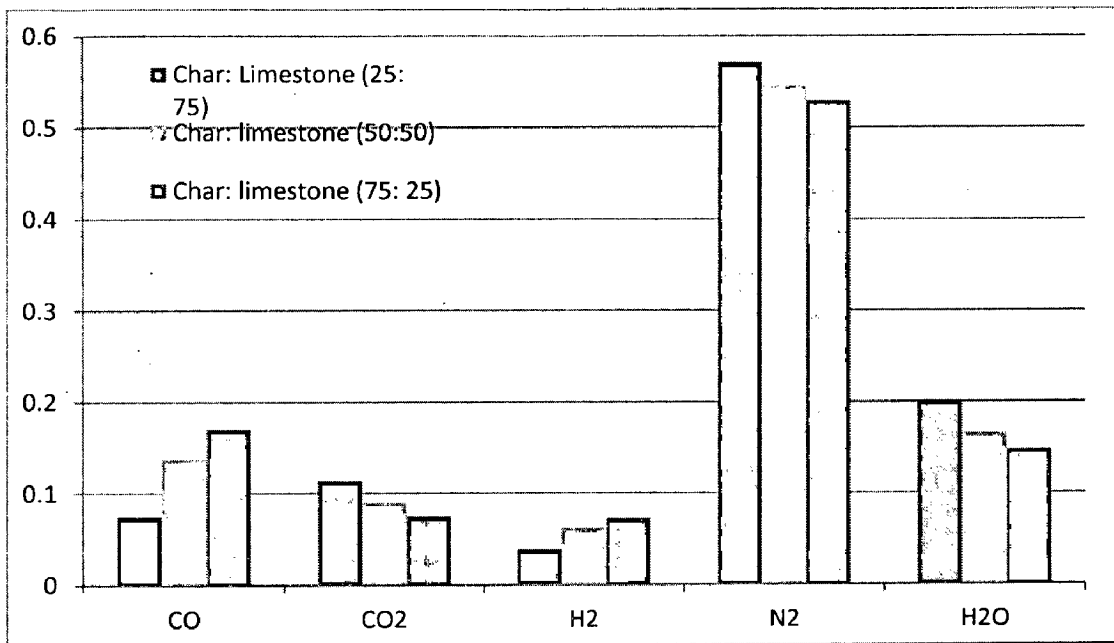


Fig. 2.6 Effect of varying bed compositions on syngas composition

Feedstock Preparation and Particle size: - The particle size of the feedstock depends largely on the feedstock preparation which in turn affects the reactivity of the feedstock for gasification. The reactivity of coal for gasification increases as the particle size decreases at a given temperature [145]. Molina et al. [1] showed the initial gasification rate of char as a function of particle size. From their experiment, they observed that the reaction rate decreases as the particle size increases. Also, the particle size has significant effect on the selection of predictive models. The shrinking core model is found to be better for higher particle sizes whereas the volume reaction model is better for smaller particle sizes.

Fixed bed gasifiers have lower feedstock size restrictions compared to fluidized bed gasifiers. The maximum particle size suggested for a conventional downdraft gasifier with throated design is one-eighth of the reactor throat diameter [51]. Entrained bed gasifiers are most sensitive to the particle size and require pulverized feedstock (90% passing through 200 mesh size) [35, 102].

Size of solid fuel particles has to be less than 1 mm [36]. The larger particles form bridges preventing the efficient flow of feedstock inside the gasifier while the smaller particles interferes with the air/ gasifying agent passage creating high pressure drop and consequently may result in gasifier shut-down. Decrease in particle size reduces the heat loss due to radiation and enhances the thermal conductivity in the oxidation and reduction zones but it also increases the pressure drop inside the gasifier.

2.1.5 Thermodynamic Equilibrium: - The Boudouard, water gas shift and the Methanation reactions are reversible reactions i.e. that they may proceed from both right to left as well as from left to right directions. In general, the forward and backward reactions both take place simultaneously and at different rates.

For any given temperature, the reaction rates are proportional to the quantity of reactants available to drive the reaction in the direction under consideration.

The forward reaction rate r_f for the CO shift reaction can be written as: -

$$r_f = k_f * [CO] * [H_2O]$$

Similarly,

$$r_r = k_r * [CO_2] * [H_2]$$

Therefore, temperature dependent equilibrium constant for the CO shift reaction can be written as: -

$$K_p = k_f / k_r = ([CO_2] * [H_2] / [CO] * [H_2O])$$

Assuming ideal gases, the equilibrium constant can also be written as: -

$$K_p = [P_{CO_2} * P_{H_2}] / [P_{CO} * P_{H_2O}]$$

Similarly, the equilibrium constant for other reactions can be expressed as: -

Boudouard Reaction: -	$K_p = P_{CO}^2 / P_{CO_2}$
Methanation Reaction: -	$K_p = P_{CH_4} / P_{H_2}$

2.2 GASIFIERS

Warnecke [109] classified the gasifier broadly in four categories based on the movement of solids and fluids inside the reactor: -

- a.) Quasi non-moving or self-moving feedstock
- b.) Mechanically moved feedstock
- c.) Fluidically moved feedstock
- d.) Special Reactors

Special reactors include the spouted bed gasifier and the cyclone gasifier. Fig. 2.7 shows a schematic classification of different types of gasifier.

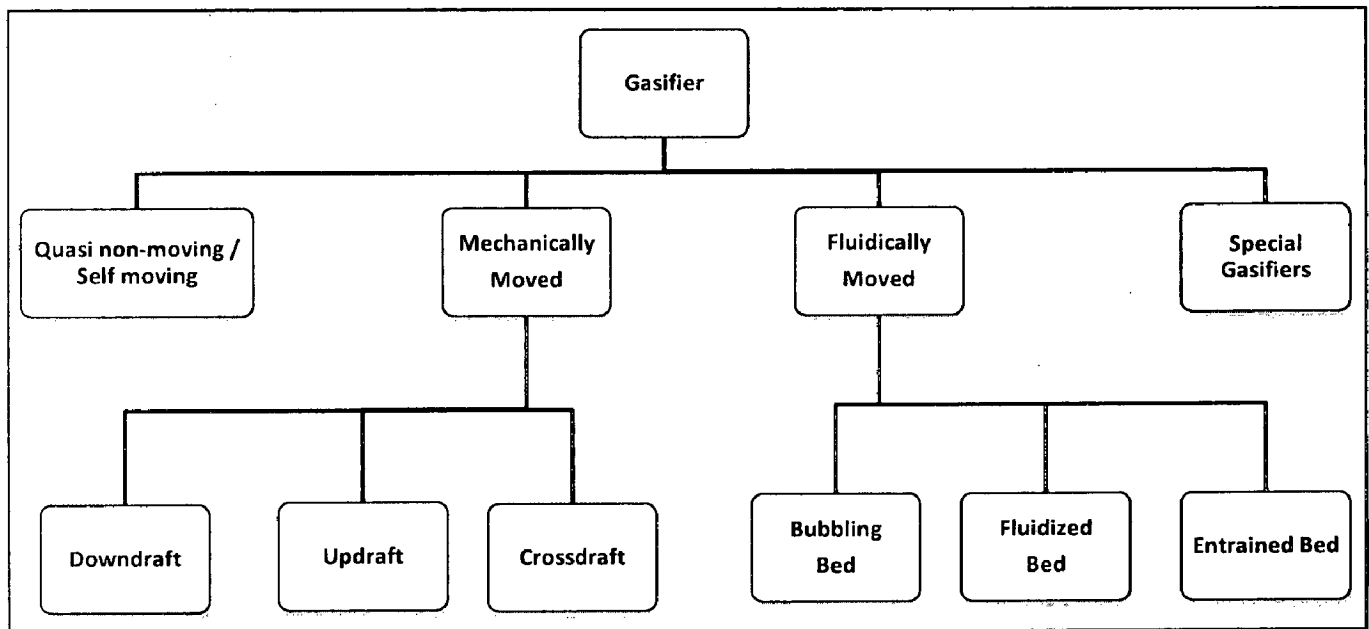


Fig. 2.7: Classification of Gasifiers

According to study done by Knoef, 2000, the following five are the most widely used type of gasifier and hence are of central importance: -

- a) Updraft Gasifier
- b) Downdraft Gasifier
- c) Bubbling fluidized Bed
- d) Circulating Fluidized bed
- e) Entrained Bed

The characteristics of these common types of gasifier and the difference between them are given in the Table 3.1 [46, 101, 119, 51, 68, and 74]: -

Table 2.3 Characteristics of different type of gasifiers

Characteristics	Gasifier Type					
	Moving Bed		Fluidized Bed		Entrained Bed	
	Downdraft	Updraft	Bubbling	Circulating	Dry Fed	Slurry Fed
Residence Time	In range of hours		Lower		Seconds or tens of seconds	
Gasifier Size	High space requirement for higher throughput		Low space requirement Enhanced heat transfer Faster gasification		Demand higher plant size	
Temperature Profiles	Non - uniform temperature distribution radial direction		Uniform temperature distribution inside the gasifier		Uniform Temperature profile	
Permissible particle size	< 50 mm		< 5 mm, more sensitive to particle size		< 100 micro m	
Reaction zone temperature	800 -1100 °C		800 – 1000 °C		1100 – 1500 °C	
Ability to handle fine particle	Limited		Good		Unlimited	
Moisture content	Very flexible		Flexible			
Gas exit temperature	600 -800 °C	250 °C	900 – 1050 °C		1250 -1600 °C	
Tar concentration	very low (0.01-6 g/ Nm ³)	very high (50 g/ Nm ³)	6-12 g/ Nm ³		No tar formation	
Carbon conversion efficiency	Very Good		Fair	Good	High	
Thermal efficiency	Very good	excellent	Good	Very good	Lower (syngas cooling)	
LHV of syngas	Poor	Poor	Poor	Fair		
Cold gas efficiency	≈ 80 %		≈ 90 %		≈ 70 %	
Gas clean up	High cleaning required	Relatively clean gas	Clean up required for dust and tar		Clean up required	
Dust content in syngas	High	Low	Higher dust content	-	-	
Energy requirement for	Low		High	High		

operation						
Investment	Higher investment		Lower investment		-	
Steam demand	High (Dry bottom) Low (Slagging)		Moderate		Low	
Oxidant demand	Low		Moderate		High	
Acceptance of caking coal	Yes		Possibly		Yes	
Typical processes	Refill Energy Inc.	Lurgi	HTW, HRL	KBR	Shell, Prenflo - Dry	GE Energy, E-Gas
Other Characteristics	HC s in gas		Low carbon conversion		High carbon conversion	
Applications	Small to medium scales		Large scales		Large Scales	

Now, let us discuss these gasifier types especially the fluidized bed and entrained bed gasifiers in more detail.

2.2.1 Updraft Gasifier: - In this type of gasifier, the movement of the feedstock and the gasifying agent are in opposite directions and therefore they are also called as counter-current gasifier. Here, the syngas formed is not forced to pass through the hot high temperature combustion zone and hence the **tar content is high in the syngas obtained from this gasifier.**

On the other hand, the temperature of syngas exiting from this gasifier is lower around (200-300°C) and hence the **thermal efficiency of this kind of gasifier is high.** A schematic of this

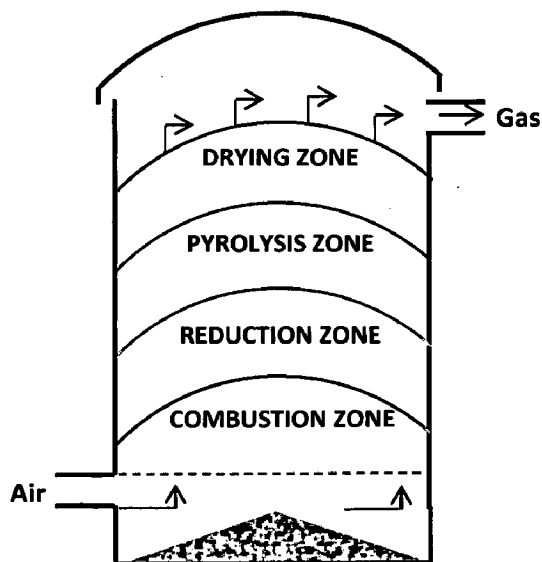


Fig. 2.8 Updraft Gasifier

type of gasifier is shown in figure 2.8. Due to high tar content in the syngas, a subsequent tar cleaning system is needed, which can become a major investment if the end-process requires tar-free syngas.

2.2.2 Downdraft Gasifier: - In a downdraft gasifier, the feedstock and gasifying agent both move in the same direction as shown in Fig. 2.9.

Here, the gases have to pass through the high-temperature combustion zone and therefore the amount of **tar is significantly lower than that in an updraft gasifier.**

The particulate content is however higher for **downdraft gasifier** and also the **thermal efficiency is lower** since syngas draws an appreciable amount of energy while passing through the high-temperature zone inside the gasifier.

Note: - One of the major drawbacks of moving bed gasifiers (updraft & downdraft) is that they have moving parts which are absent in other type of gasifiers. Therefore, they require a relatively high amount of maintenance [132].

2.2.3 Entrained Bed Gasifier: - Entrained bed gasifiers are the most widely used gasifiers with different technologies like BBP, Hitachi, MHI, PRENFLOW, Shell, E gas and Texaco. In this type of gasifiers, coal and other solid particles concurrently reacts with steam and oxygen or air in suspended fluid flow / entrained mode.

Entrained bed gasifiers requires pulverized feed stocks (90 % passing through 200 mesh) which may be injected either in dry or in slurry state. Size of the solid fuel particles has to be less than 1 mm [36]. Semisolid feed stocks such as visbreaking tars as well as asphalt from de-asphalting can be injected in molten phase.

Temperature of gasification may exceed 1500°C and the residence time is of the order of 1 s.

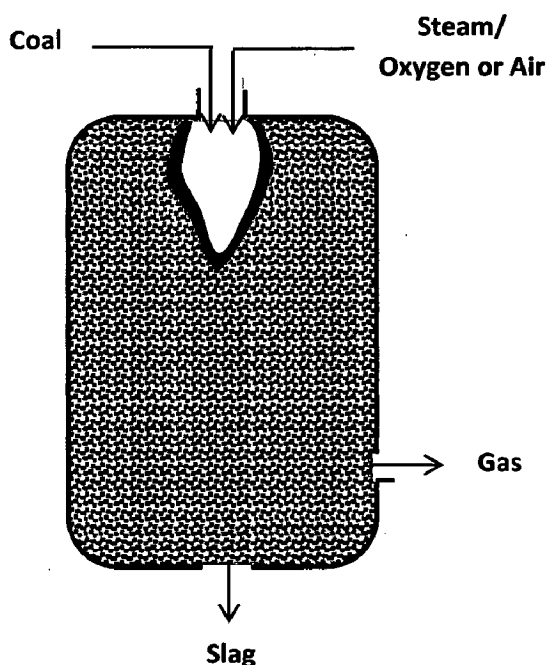


Fig. 2.10 Entrained bed Gasifier

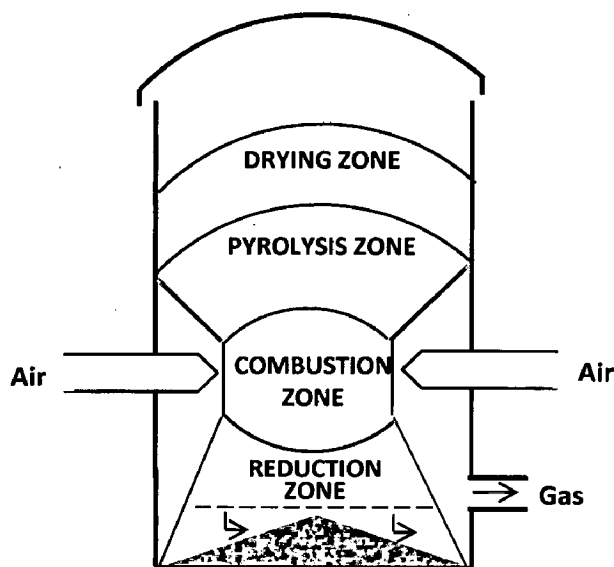


Fig. 2.9 Downdraft Gasifier

High operating temperature effectively destroys all hydrocarbons, tars, oils and phenols which may be formed during the devolatilization process and also removes most of the mineral matter in feed stocks as slag. The units are usually operated at high pressures in the range of 2.94 – 3.43 MPa.

Entrained bed gasifiers are more versatile as they can accept both solid and liquid fuels and can be operated at high temperatures (above ash slagging temperature) to ensure high carbon conversion. However, such high temperature has an adverse impact on the burner and refractory life and thus requires the use of expensive materials for construction as well as

sophisticated high temperature heat exchangers for cooling syngas.

Recent development in entrained bed gasifiers is ConocoPhillips two stage gasification process also known as **E-Gas Technology** [102, 47]. In this gasifier, the slurry feedstock reacts readily with oxygen in the first stage gasifier to form hydrogen, CO, CO₂ and Methane. High temperature in the first stage gasifier ensures complete conversion of all feed stocks materials and also traps organic materials as ash and metal as slag. Hot syngas from the horizontal first stage gasifier enters the vertical second stage gasifier, where additional slurry is added to increase the syngas quantity.

All entrained-flow gasifiers are of the slagging type, which implies that the operating temperature is above the ash melting point. This ensures destruction of tars and oils and, if appropriately designed and operated, a high carbon conversion of over 99% can be achieved, although some coal-water slurry-fed plants do not achieve this in a single pass and must recycle carbon to achieve it. Moreover, entrained-flow gasifiers produce the highest quality synthesis gas because of the low methane content. Entrained-flow gasifiers have relatively high oxygen requirements, and the raw gas has high sensible heat content.

The various designs of entrained-flow gasifiers differ in their feed systems (dry coal fed in a high-density fluidized state or coal-water slurries), vessel containment for the hot conditions (refractory or membrane wall), configurations for introducing the reactants and the ways in which sensible heat is recovered from the raw gas. Table 2.4 [23] provides characteristics of some other important entrained flow processes: -

Table 2.4 Characteristics of important entrained flow processes

Process	Stages	Feed	Flow	Reactor Wall	Syngas Cooling	Oxidant
Koppers- Totzek	1	Dry	Up	Jacket	Syngas Cooler (SC)	Oxygen
Shell SCGP	1	Dry	Up	Membrane	Gas Quench & SC	Oxygen
Prenflo	1	Dry	Up	Membrane	Gas Quench & SC	Oxygen
Siemens	1	Dry	Down	Membrane	Water Quench & SC	Oxygen
GE Energy	1	Slurry	Down	Refractory	Water Quench / SC	Oxygen
E-Gas	2	Slurry	Up	Refractory	2 Stage Gasification	Oxygen
MHI	2	Dry	Up	Membrane	2 Stage Gasification	Air
Eagle	2	Dry	Up	Membrane	2 Stage Gasification	Oxygen

2.2.4 Fluidized bed Gasifier: - In fluidized bed gasifier, feed stocks and air or oxygen is injected from the bottom of the gasifier as shown in Fig. 2.11. High levels of back mixing ensures a uniform temperature distribution inside the gasifier, which is usually operated at a temperature well below the ash fusion temperature (900 – 1050°C) to avoid ash melting thereby avoiding clinker formation and loss of fluidity of the bed

The required average particle size is 8 mm and residence time of the feedstock in the gasifier is typically 10-100 s. The main advantage of this type of gasifier is that it can be operated at various loads which results in high turndown flexibility [102].

The main disadvantages of the fluidized bed gasifiers are the extent of carbon conversion and the carryover of the particles having high carbon content. Therefore, to achieve high carbon conversion, the carried over fines are collected and recycled back in the gasifier with fresh feed stocks. The system of choice for fluidized bed gasification of coal includes: -

- a) Bubbling fluidized bed process (BFB)
- b) Circulating fluidized bed process. (CFB)
- c) Agglomerating fluidized bed process. (AFB)

Bubbling and Circulating Fluidized Bed process: These two processes differ with respect to the fluidizing velocity and the gas path. Bubbling beds have relatively low gas velocities. Therefore, very little solids are transported out of the bubbling bed. However, in circulating fluidized bed, velocity is close to pneumatic flow. Therefore, small particles are converted in one pass or are entrained with the gas. These entrained solids are recycled after passing through a cyclone.

The high slip velocities in circulating fluidized bed gasifiers ensure good mixing of gas and solid and thus promote excellent heat and mass transfer. Another advantage of CFB process is that the shape and size of the particle is less important. Hence, this type of gasifier is most suitable for gasification of biomass and wastes and presently there is rapid shift in the fluidized bed design from bubbling to circulating fluidized bed.

Agglomerating fluid-bed process: - The idea behind agglomerating fluid-bed processes is to have a localized area of higher temperature where the ash reaches its softening point and begin to fuse. The purpose of this concept is to allow a

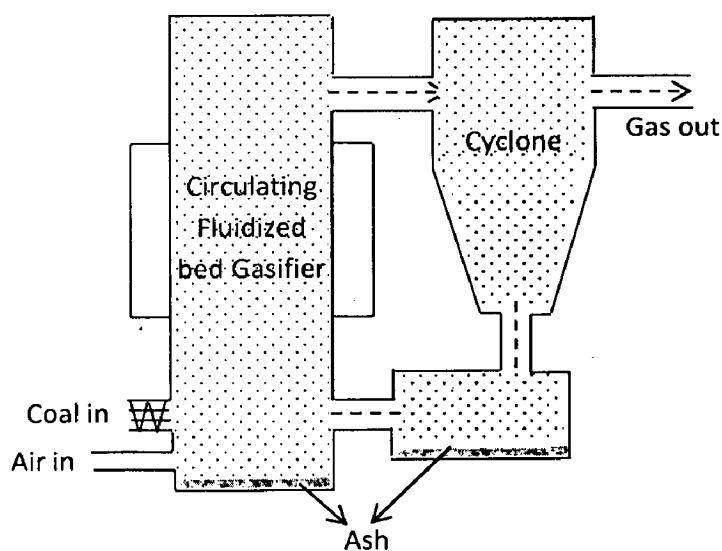


Fig. 2.11 Circulating fluidized bed

limited agglomeration of ash particles that, as they grow and become too heavy to remain in the bed, fall out at the bottom. This preferential separation of low-carbon ash particles is designed to permit a higher carbon conversion than conventional fluid-bed processes [14]. A potential advantage for such processes over conventional fluid beds is that the problem of a leachable ash is less serious because of the ash agglomeration step incorporated near the burner(s) in the bottom of the reactor. The burner(s) in these gasifiers have two functions:

- a) Introducing the fluidizing gas,
- b) Creating a hot region where ash agglomeration occurs.

This two-in-one feature is definitely nice, but always put restrictions on the operation when trying to operate in the “no-go” temperature range between the ash softening point and the ash melting point. Some commercial fluidized bed processes are given in Table 2.5

Table 2.5 Commercial Fluidized bed Processes [23, 36]

Technology Supplier	Country	Coal feed type	Oxidant	Fluidized bed type	P (psi)	T (°C)
KRW	U.S	Dry	Air	Agglomerating	290	900
Envirotherm	Germany	Dry	Air	Circulating	-	-
IGT U. Gas	U.S, Finland, India	Dry	Air	Agglomerating	-	-
Rheinbraun HTW	Germany	Dry	Air	Circulating	145-435	800
Foster Wheeler	Sweden	Dry	Air	Circulating	-	905
BHEL	India	Dry	Air/ Steam mixture	-	188	1000
KBR Transport Gasifier	-	Dry	Air	Circulating	-	870-1000

From India perspective, we will discuss the following 4 fluidized bed gasification processes in detail: -

- a) BHEL fluidized bed gasification process
- b) HT Winkler fluidized bed gasification process
- c) Transport Gasifier (KBR).

BHEL Gasifier: The BHEL pressurized fluid bed gasifier is developed especially for local coals and conditions. India’s most coal reserves have very high ash content and so there is significant saving in Oxygen by choosing a non- slagging system [23].

In this type of gasifier, a mixture of steam and air is fed through a grate which also serves the purpose of ash removal. A gas cooler is used to recover a part of the sensible heat and superheat

steam for the gasifier. Gas cooling and tar condensation are done by water quenching. In the late 1990s, BHEL developed a pilot IGCC plant using fluidized-bed gasifier and Currently, BHEL and NPTC are collaborating on a 100 MW IGCC demonstration plant based on Indian coals. [108]

2.2.5 HT Winkler Process: The high temperature wrinkler process was developed by Rheinbraun especially for lignite coals. Since, India has reserves of lignite in the south, so this technology is useful from Indian perspective. This process is basically a development of the original atmospheric fluid bed gasification process and is shown in Fig. 2.12.

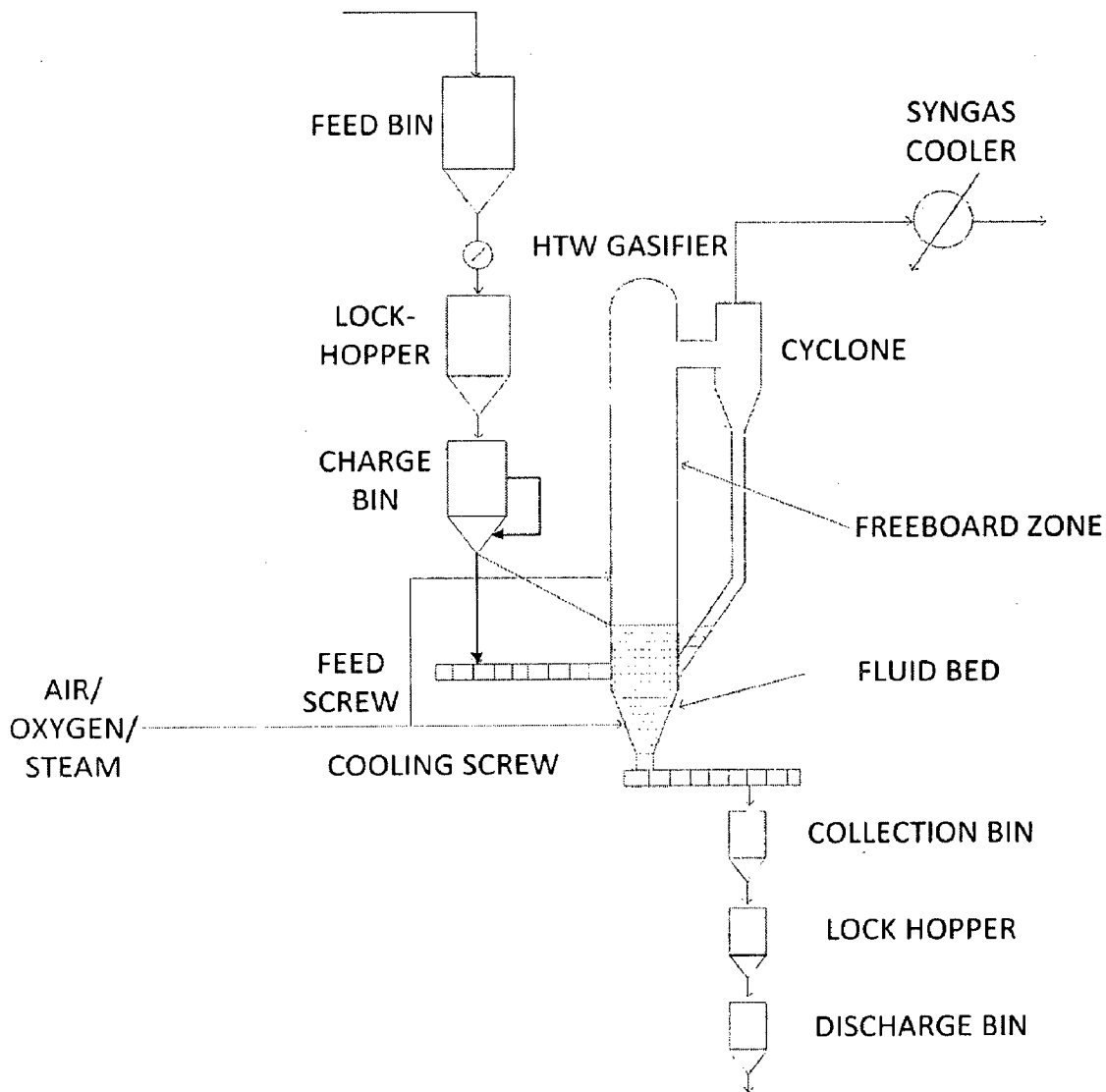


Fig. 2.12 High Temperature Winkler fluidized bed process

In the original wrinkler process, fluid bed is maintained by a blast which enters the reactor via a conical grate area at the base. An additional amount of blast is fed in above the bed to assist

gasification of small, entrained coal particles. This also raises the temperature above that of the bed itself, thus reducing the tar content of the syngas. Development in high temperature wrinkler process included raising the pressure so as to increase output and reduce compression energy; raising operating temperatures so as to improve gas quality and carbon conversion, and include solids recycle from the cyclone to the fluid-bed as a further measure to increase carbon conversion [112].

2.2.6 KBR Transport gasifier: - This gasifier comprises features of both fluidized bed and entrained bed gasifier and is an example of high velocity regime fluid bed gasifier having a velocity of 11-18 m/s in the riser [121]. The objective of this development was to demonstrate higher circulation rates, velocities and riser densities than in conventional circulating beds, resulting in higher throughput and better mixing and heat transfer rates.

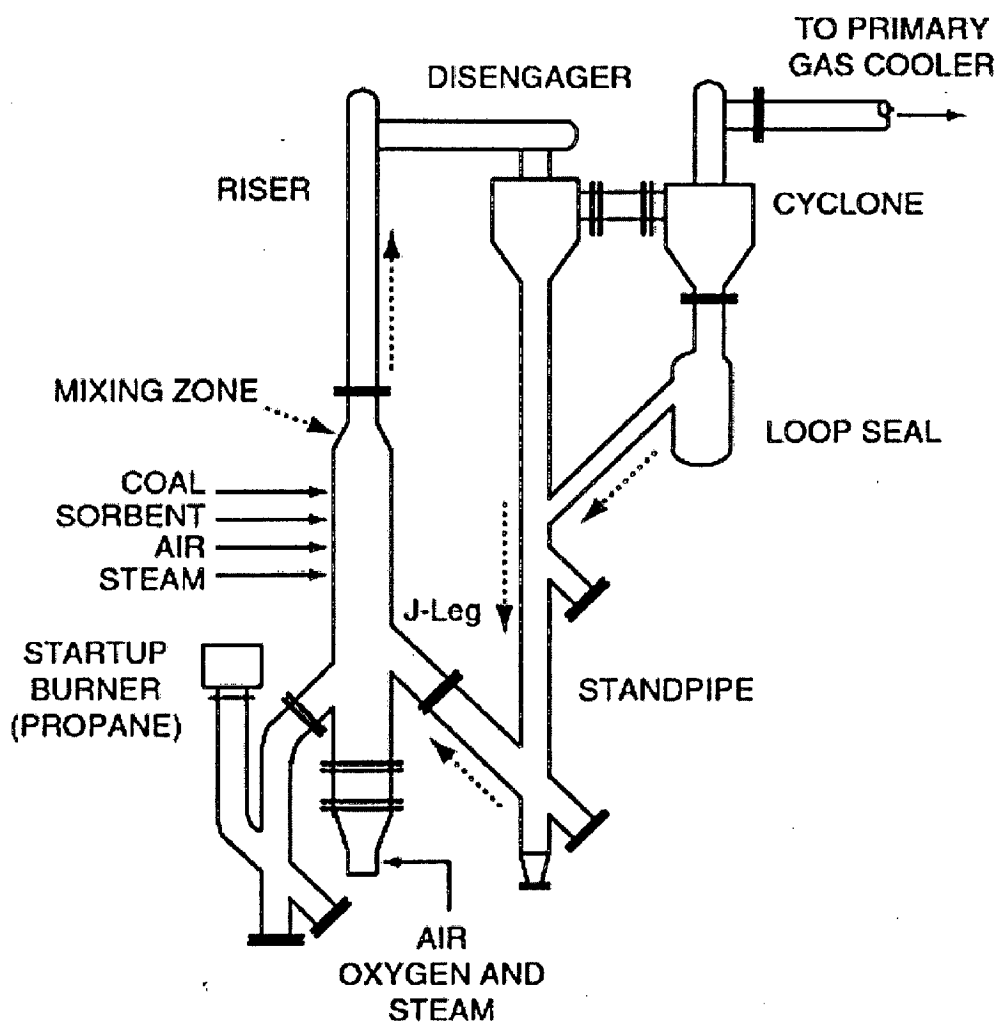


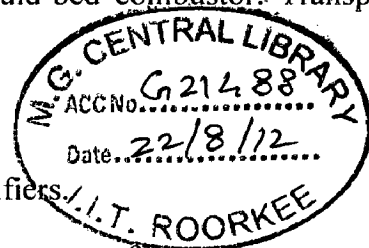
Fig. 2.13 KBR Transport gasifier
Source: Smith et al., 2002

The fuel and sorbent (limestone for sulfur removal) are fed to the reactor through separate lock-hoppers. They are mixed in the mixing zone with oxidant and steam, and with recirculated solids from the standpipe. The gas with entrained solids moves up from the mixing zone into the riser. The riser outlet makes two turns before entering the disengager, where larger particles are removed by gravity separation. Smaller particles are largely removed from the gas in the cyclone. The solids collected by the disengager and cyclone are recycled to the mixing zone via the standpipe and J-leg (Fig. 2.13).

Gas exiting the cyclone passes through the hot gas cleanup loop and proceeds to the gas quench train. Solids removed from the cyclone are reintroduced into the riser. A solid stream is withdrawn from the standpipe via a cooling auger system to provide a means of removing the accumulated ash and spent sorbents.

The sorbent added to the fuel reacts with the sulfur present to form CaS. Together with a char-ash mixture, this leaves the reactor from the standpipe via a screw cooler. These solids and the fines from the candle filter are combusted in an atmospheric fluid-bed combustor. Transport gasifiers have following advantages over conventional gasifiers: -

- a.) High Throughput and medium cold gas efficiency
- b.) Simultaneous removal of Sulfur
- c.) Comprises features of both entrained and fluidized bed gasifiers



Finally, to conclude a summary of the advantages and disadvantages of the three types of gasifiers viz. moving bed, entrained bed and fluidized bed gasifiers is given in Table 2.6: -

Table 2.6 Advantages & Disadvantages of Moving, Entrained and Fluidized bed gasifiers

ENTRAINED BED GASIFIERS	
Advantages	Disadvantages
More versatile	Requires pulverized feed stocks (90 % passing through 200 mesh)
Can operate with both liquid and solid feed	Operating Temperature above ash fusion temperature
High operating temperature effectively destroys all hydrocarbons, tars, oils and phenols	High temperature has an adverse impact on the burner and refractory life.
Higher carbon conversion due to high operating temperature.	Requires the use of expensive materials for construction
Most widely used type of gasifiers	Requires sophisticated high temperature heat exchangers for cooling syngas.

	Not suitable for high ash content feed stocks
FLUIDIZED BED GASIFIERS	
Advantages	Disadvantages
High level of back mixing, uniform temperature throughout gasifier	Low extent of carbon conversion.
Operate well below ash fusion temperature	Carryover of particles having high carbon content.
Avoid ash melting, clinker formation	Carried over fines needs to be recycled with fresh feeds.
Prevents loss of fluidity of the bed	Velocity close to pneumatic flow is required
Suitable for high ash coals	
Moving Bed Gasifier [77]	
Advantages	Disadvantages
High moisture tolerance	Moving parts, high maintenance costs.
Simple operation	Low throughput per unit reactor volume
Minimum fuel preparation	High tar content in gas
High efficiency	Channeling
Low solids carryover	

2.3 SELECTION OF GASIFIER FOR INDIAN COAL

2.3.1 Description of Indian coal

Table 2.7 gives the proximate analysis & ultimate analysis of various Indian coal samples.

Table 2.7 Proximate analysis of various Indian coals

Proximate Analysis	Singareni	Kushmanda	Singrauli	Jharia	Neyveli
Moisture	9.6	10	12	13	42.52
Volatile Matter	23.3	23	20.1	17.51	24.5
Fixed Carbon	32.9	25	27.9	28.22	19.5
Ash	34	40.5	40.0	36.08	7.5
Sulfur	0.363	0.28	0.31	0.41	0.63
HHV	4133.3	5590	3641.6	3300	2850

Also, for comparison purpose, the proximate analysis of Indian, Indonesian and South African coals is given in Table 2.8. From Table 2.7 & 2.8, it is evident that most of the coal available in our country is low grade coal, having very high ash content and low sulfur content [12].

Fig. 2.8: Typical proximate analysis of Indian, Indonesian and S. African coal

TYPICAL PROXIMATE ANALYSIS OF VARIOUS COALS			
Parameter	Indian Coal	Indonesian Coal	South African Coal
Moisture	5.98	9.43	8.5
Ash	38.63	13.99	17
Volatile Matter	20.70	29.79	23.28
Fixed Carbon	34.69	46.79	51.22

The ash content of Indian coal is as high as 40 % and average ash content is around 30 %, which is very high. Also, we have observed in the past few decades that the quality of Indian coal is deteriorating i.e. with time we are getting Indian coal with higher ash content as evident from Table 2.9.

Deteriorating Quality of Indian Coal			
	1970s	1980s	1990s
Fixed Carbon	36.5 %	32.4 %	25 %
Volatile Matter	25.5 %	21.6 %	18 %
Moisture	10 %	16 %	12 %
Ash	28 %	30 %	45 %
HHV (Kcal/Kg)	4750	4050	3000

This ash melts by absorbing heat in the conventional combustors and also its chemistry is such that it is very in silica and alumina and is corrosive due to high quartz content [24]. Amount of ash in the coal also affects the syngas composition, cleaning cost and cold gas efficiency. Therefore, selection of gasifier for the gasification of Indian coals requires special consideration.

Table 2.9: Quality of India coal (1970s – 1990s)

2.3.2 Selection of Gasifier: The slagging, entrained-flow gasifier is the well-developed gasifier for power generation today. However, it operates at very high temperature above the ash fusion temperature of the bed and requires a finely powdered feedstock with low ash content that can be injected into the gasifier at high pressures, so that the coal can be gasified quickly in the one-pass-through system. Ash is removed as a molten slag, which requires the feedstock coal to have low ash-fusion temperatures. Therefore, this type of gasifier generally is not compatible with most Indian coals, which have both high ash content and high ash-fusion temperature such as 1400 °C [116, 2]. High ash content in the feed decreases the efficiency and also increases the slug production and causes disposal problems.

However, according to BHEL, the problem is not serious in case of fluidized bed gasifiers as they operate much below the ash fusion temperature. In fact, fluidized bed gasifiers operate better with coals having high ash content as the ash released from the coal lowers the temperature of the bed and increases the efficiency of the process. Also, there is significant savings in oxygen by using a non-slugging system [23].

Therefore, **fluidized bed gasifiers are preferred over entrained bed gasifiers for Indian coals** due to the following reasons: -

- a.) Indian coal has high ash content and since entrained bed gasifier operates above ash fusion temperature, the slug production and disposal problem is high.
- b.) Indian coals have very high ash fusion temperature of the order of 1500 C, making it difficult to use entrained bed gasifiers.
- c.) The ash present in Indian coal contains abrasive quartz which may erode the syngas cooling system if gets fused as in case of entrained bed gasifiers.
- d.) Fluidized bed gasifiers operate at temperature below ash fusion temperature and therefore it is free from the above problems. In addition ash released from the coal lowers the temperature of the bed and increases the efficiency of the fluidized bed process.

Moving bed process has also been found acceptable in view of availability of indigenous capability [25]. However, its application is limited due to lower throughput per unit reactor volume, high maintenance costs, tar content in syngas and channeling. On the basis of above discussion, Table 2.10 provides a list of gasifiers which are suitable and not suitable for gasification of Indian coal [116]

Table 2.10: Classification of gasifiers based on suitability for Indian coal

Gasifiers Not suitable for Indian coal			
Slurry Feed			Dry Feed
GE Gasifier (WHB)	GE Gasifier (quench)	E-Gas Gasifier	Shell/ Prenflow Gasifier
Gasifiers suitable for Indian coal			
Fluidized bed	Transport		Moving Bed
U-Gas, HTW No Slagging Medium Oxidant Use Medium Cold Gas Eff.	U-Gas, HTW No Slagging Medium Oxidant Use Medium Cold Gas Eff. High Throughput		Lurgi Gasifier No Slagging Low Oxidant Use High cold gas Eff. Require lump coal

Note: - The entrained-flow gasifier can, however, be used with tertiary Indian coals tertiary coals are located in Assam and other northeastern states, as well as Jammu and Kashmir, which have lower ash content and lower ash-fusion temperature, although they suffer from high sulfur content. [5]

2.4 MODELING APPROACH USED FOR FLUIDIZED BED GASIFIERS

From the above discussion, it is inferred that the gasification of Indian coal can be carried out in bubbling fluidized bed gasifier. However, it has been a challengeable problem to scale up fluidized bed coal process due to its complex reaction and transfer mechanism [141].

Therefore, numerical modeling has become an essential and cost effective tool for design, optimization and scaling up the combustion [45, 94, 141, 143] and gasification [17, 18, 31, 32, 54, 57, 58, 60, 62, 72, 79, 84, 89, 91, 99, 102, 103, 107, 113, 117, 125, 128, 136, 138, 146 and 147] processes in fixed, fluidized and entrained bed gasifiers as reported in literatures. Most of the initial models were one- dimensional in nature [60]. These were based on two phase concept: bubble phase and emulsion phase.

2.4.1 One Dimensional Model: - The first two phase model was proposed by Toomey and Johnstone [128]. Many improvements were made to the original two phase model to simulate coal gasification process of bubbling fluidized bed gasifiers [17, 60, 113 and 140]. However, the inherently existed drawbacks are impossible to be solved due to its empirical nature in the description of gas and particles in motion and interactions without solving the momentum balance equations [145].

2.4.2 Two Dimensional Model: - In recent years, two dimensional models based on mass conservation and momentum balance equations for gas and solid have been applied to simulate the hydrodynamics of bubbling fluidized bed. Two approaches have been proposed: -

- a) Discrete Element Method (DEM) - Based on molecular dynamics. Also known as Eulerian- Lagrangian approach.
- b) Two Fluid Model (TFM) - Based on assumption that gas and solid phase form two interpenetrating continua. Also, known as Eulerian- Eulerian Approach [48].

A characteristic feature of the bubbling fluidized bed is the chaos motion of large number of particles in the bed. Therefore, the fundamental procedure is to simulate complex particles stresses resulting from multi body collisions. In DEM, researchers have applied: -

- a) Soft sphere simulation: - In this approach, researchers have applied empirical equation of restitution & friction to describe particle collisions and to predict frequency of pressure fluctuations, bubble formation and particle segregation.

- b) **Hard sphere simulation:** - In this approach, empirical spring stiffness and friction coefficient were performed to describe particle collisions and to predict frequency of pressure fluctuations, bubble formation and particle segregation [63, 64, 112 and 129].

However, if we need to model complex industrial problems like the bubbling fluidized bed gasifiers, the huge computational time put DEM at disadvantage [20, 48]. On the other hand, TFM saves computational time and provides mean particulate flow fields which are convenient to analyze for making decisions in engineering design. TFM can also be used to compute observed bubbles and clusters and also flow regime [49].

2.4.3 Eulerian Granular Model: - In [10, 13, 16, 50], kinetic theory of granular flow was introduced into Eulerian- Eulerian model (TFM) in analogy with kinetic theory of gas molecules to improve the description of particle collision. Enwald and Almstedt, 1999 applied kinetic theory of granular flow (KTGF) in bubbling fluidized bed model and compared numerical simulation with experimental results. From his comparison, he found the statistical consistency in the prediction of bubble frequency, mean pierced bubble length, mean bubble rise velocity and mean bubble volume fraction.

Using his work as reference, Yang et al. 2005 successfully used TFM for studying the fluid dynamics of gas- solid bubbling fluidized bed. Patil et al. [102, 103] performed a critical comparison of hydrodynamics model for jet bubbling fluidized bed and freely bubbling fluidized beds and concluded that kinetic theory of granular flows was in good agreement with the experimental data.

KTGF based on Eulerian- Eulerian two phase model (TFM) gives reasonable flow description of dense gas solid flows. However, it is difficult to introduce complicated chemical reaction in this model due to complex mechanism of heat transfer and reactions to be modeled. But, scale up and optimal design of industrial reactor cannot be carried out without considering chemical reactions. Therefore, several researchers have worked to incorporate chemical reactions in TFM with reasonable accuracy [145, 26].

2.4.4 Three Dimensional Model: - Wang et al., 2009 [139] developed a three dimensional model of fluidized bed coal gasification. This was followed by Cornejo et al. [26] who developed the first three dimensional model of bubbling fluidized bed gasifier in 2011 using Eulerian-granular approach. The purpose of his work was to develop a modeling methodology within the framework of commercial CFD code FLUENT to describe the coal gasification process in bubbling fluidized bed gasifier. Following this work, Knutson [80] developed a 3D model of advanced Lewis ultra-superheated steam bubbling bed coal gasification in ANSYS 12.1.4 to determine the syngas composition for various ranks of coal based on operational conditions.

2.4.5 Prior Art: - These different approaches for modeling the gasification processes in bubbling fluidized bed gasifiers are discussed in detail in their chronological order:

- 1.) **Robert et al. 1988:** - Robert et al. 1988 developed a steady state model to simulate the North Carolina state university pilot scale fluidized bed coal gasification reactor. They considered an instantaneous devolatilization of coal at the top of the gasifier i.e. in the freeboard zone. The char combustion and gasification reactions were assumed to occur in the fluidized bed as shown in Fig. 2.14.

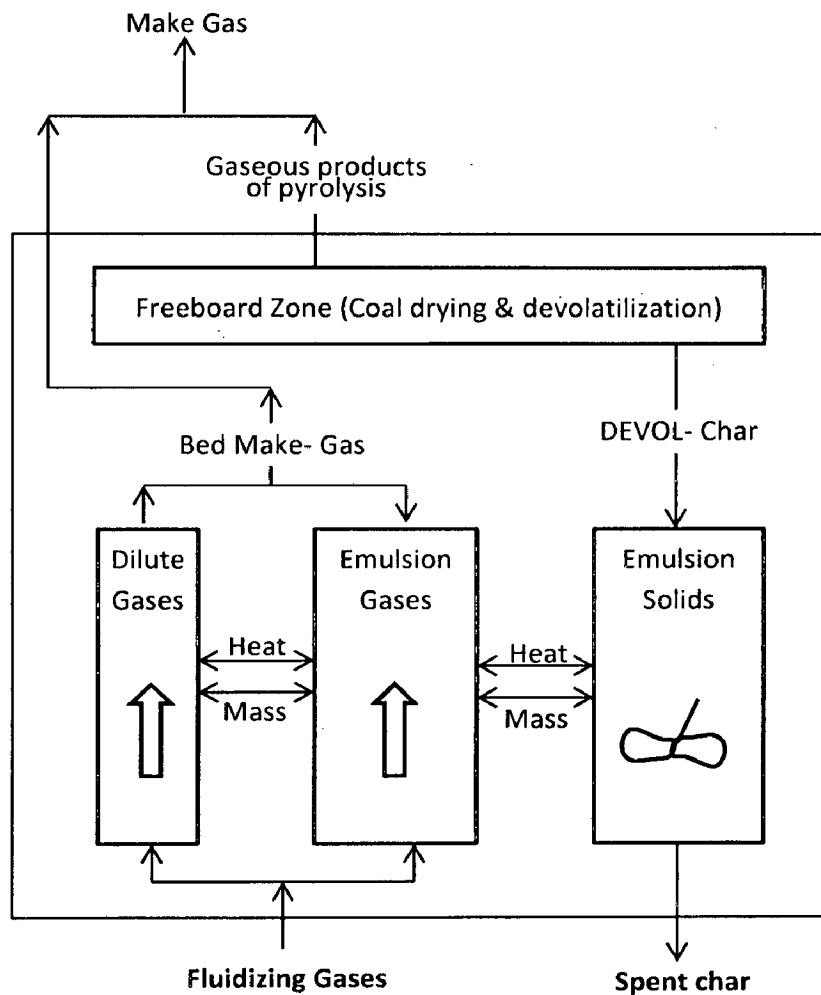


Fig. 2.14: Schematic diagram of the fluidized bed gasification model used by Robert et al. 1988

They developed a two phase (emulsion- gas phase) representation of the fluidized bed incorporating the phenomenon of jetting, bubbling, slugging and mass and heat transfer between phases. Their model enabled them to predict the individual species flow rates and

temperature profiles within the bed provides good correlations with operating parameters of overall carbon conversion, total synthesis gas production, rates of formation of individual species, and average bed temperature.

- 2.) **Saffer et al. 1988:** - Their work deals with the study of Spanish anthracite by mixtures of air and water vapor in a small fluidized bed reactor with a capacity of the order of 20kg/ hr. of coal. They studied the effect of several parameters on the performance of the gasifier and observed that most of these effects can be explained from physic- chemical and kinetic considerations, together with the hydrodynamic behavior of the bed. Also, they made the first attempt to model their gasifier based on the classical description of the behavior of the gas given by J. F. Davidson and D. Harrison.
- 3.) **Desouza-Santos, 1989** developed a comprehensive one dimensional model of a fluidized bed gasifiers taking into account 24 chemical reactions and the devolatilization reactions. They used a model consisting of mass and energy balance equations for individual phases to predict the gasifier performance. The predictions compared favorably with the experimental results.
- 4.) **Tsuji et al. 1993:** Tsuji et al. 1993 performed a numerical simulation of two dimensional gas fluidized bed using discrete particle model. In this model, the motion of individual particles was calculated and the contact force between particles was modeled by Cundall's distinct element method. In this method, the force was expressed with the use of a spring, dash-pot and friction slider as shown in Fig. 2.15.

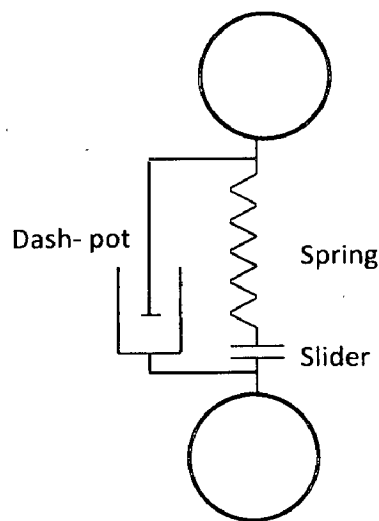


Fig. 2.15: Cundall's representation of normal contact force

The gas was assumed to be inviscid and its flow was solved simultaneously with the motion of the particles taking into account the interaction between particles and gas. Their

simulation gave realistic pictures of particle motion. Formation of bubbles and slugs and the process of particle mixing and pressure fluctuations were observed to occur in the same way as in experiments.

- 5.) **Hoomans et al. 1996:** - Hoomans et al. carried out a discrete particle simulation of bubble and slug formation in a two dimensional gas- fluidized bed using hard sphere approach. In this model, the two dimensional model of the individual spherical particles was directly calculated from the forces acting on them, accounting for the interaction between the particles and the interstitial gas phase.

In their work, they used a collision model based on conservation laws of linear and angular momentum. This model required two important empirical parameters- a restitution coefficient and friction coefficient apart from geometrical factors. The hydrodynamic model of the gas phase was based on the volume averaged Navier-Stokes equation for gas solid two phase flow.

Their simulations of bubble and slug formation in a small two dimensional bed (height 0.50 m, width 0.15 m) with 2400 particles ($d_p = 4$ mm, material: aluminum, $\rho = 2700$ kg m⁻³) showed a strong dependency of the flow behavior with respect to the restitution and friction coefficient. When ideal particles ($e = 1$, $\mu = 0$) were modeled the flow behavior was found to be unrealistic which leads to the conclusion that it is of utmost importance that, in a model that requires a restitution and/or a friction coefficient, these parameters are given realistic values.

Simulations with realistic values for e and μ showed highly realistic flow behavior for D-powder material. Explosive bubble growth followed by a transition to slug flow, which is rather typical for D-powder fluidization, was predicted by the model when bubble formation at a single orifice was simulated. Their model was capable of predicting the formation of slugs when homogenous inflow conditions above minimum fluidization conditions were specified.

- 6.) **Gera et al. 1998:** - Gera et al. compared the discrete particle model and two phase model for the characteristics of bubble formation, motion and eruption at the bed surface. From their work, they inferred that the inter particle friction incorporated into two phase model through the use of solid pressure and viscosity are very sensitive parameters and need to be tuned in for each case running with different set of physical properties. Therefore inaccurate determination of the empirical correlations for solid pressure either through the experiments or through the kinetic theory of granular media will hinder the true bubbling characteristics of fluidized bed in two phase model.

However, DEM does not require any empirical input of solid's rheology which makes it more appropriate for some modeling situations. For the simulations of small beds, the computational time required by TFM and DEM are comparable, but if one requires modeling a system with the millions of particles then TFM would take very small time as compared to the DEM. They presented a summary of the salient features of discrete element model and two fluid models, given in Table 2.11

Table 2.11: Summary of salient features of discrete element method and two fluid models

S No.	Distinct element method	Two fluid model
1	It is possible to account for the individual particles' shape, size, and density. For example, a particle shape approximated by an 'n-sided' polygon can be incorporated in this model.	Particles are characterized by their mean size and density. Different sizes and densities of the particles are treated as the separate phases which would increase the number of conservation equations to solve.
2	Individual particle motion can be traced.	Only averaged particulate motion in a grid cell can be computed.
3	Particle interactions are calculated from coefficient of restitution (e) and friction (μ) between the particles. Different values of (e) can be given for particle-particle collisions and particle-wall collisions.	Particle interaction is normally expressed as a function of porosity and is calculated empirically. Using kinetic theory of granular media, it may also be calculated by the empirical input of coefficients of restitution (e) and friction (μ).
4	Computational time depends on the calculation of particle motion explicitly, and three (1 continuity and 2 momentum equations for a 2-D case) sets of equations for fluid motion iteratively.	Computational time depends on the iterative solutions of six sets of simultaneous differential equations.
5	Considers multiple collisions of particles, based on the soft sphere approach of the molecular dynamics. Hard sphere approach, based on binary instantaneous collisions is also used in the literature.	No such considerations
6	Visualization of the individual particle mixing is possible.	Mixing characterized by integrating the averaged particulate phase velocity to obtain the estimated position of the particles is possible. Particulate mixing is driven by the convection and diffusion processes

7.) **Yan et al. 1998:** - Yan et al. develop an isothermal model incorporating the two phase theory to evaluate the performance of a bubbling fluidized bed coal gasifier. A distinctive feature of their model was the consideration of net flow term from the emulsion to the bubble phase in the conservation equations as shown in Fig. 2.16

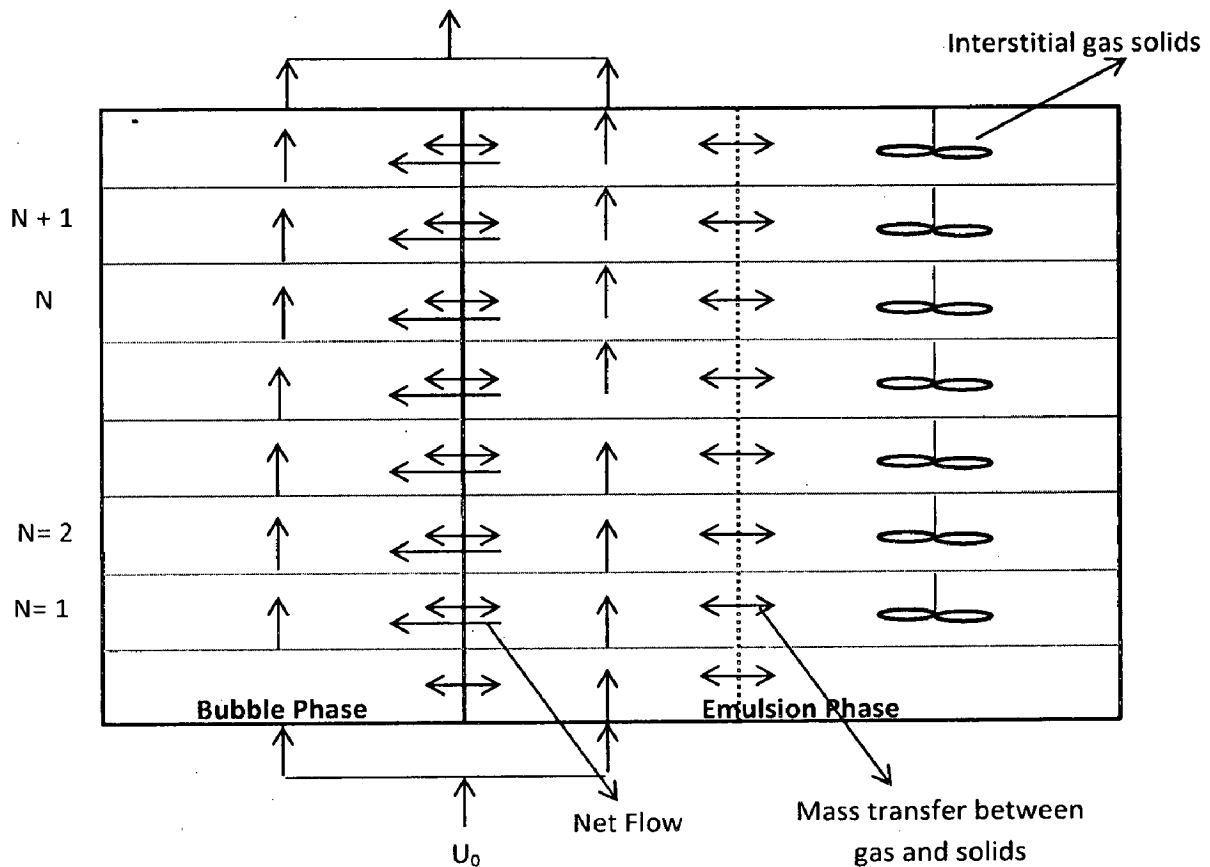


Fig. 2.16: Schematic diagram showing two phase theory with concept of net flow

Their simulations with consideration of the “net flow” term indicate that the overall results compare favorably with available experimental data from an industrial fluidized-bed gasifier reported in the literature while simulations without the net flow were observed to deviate significantly from the experimental results.

The “net flow” was significant, in the range 71–87% relative to the feed gas rate, strongly depending on the coal rank, heterogeneous reaction rates and volatile matter released in the bed. The higher the coal rank, the lower was the net flow and total excess gas flow. They observed that large volume of net flow generated can significantly change the fluidization conditions in the bed and thus alter the reaction rates and mass transfer properties.

8.) **Hamel et al. 2001:** - Hamel et al. developed a mathematical model based on cell model to simulate the gasification process of solids in atmospheric or pressurized bubbling fluidized bed gasifiers. According to cell theory, the gasifier and other required components like cyclone and connection pipes were divided into a number of in series arranged discrete balance segments- so called cells. Each cell was then subdivided (Fig. 2.17) into a solid free bubble phase and an emulsion phase according to two phase theory.

Their model incorporated bed and freeboard hydrodynamics, fuel drying and devolatilization and chemical reaction kinetics and was used to simulate four bubbling fluidized bed gasifiers, from atmospheric laboratory scale up to pressurized commercial scale, processing brown coal, peat and sawdust. The simulation results for overall carbon conversion, temperature and concentrations of gaseous species agreed sufficiently well with published experimental data.

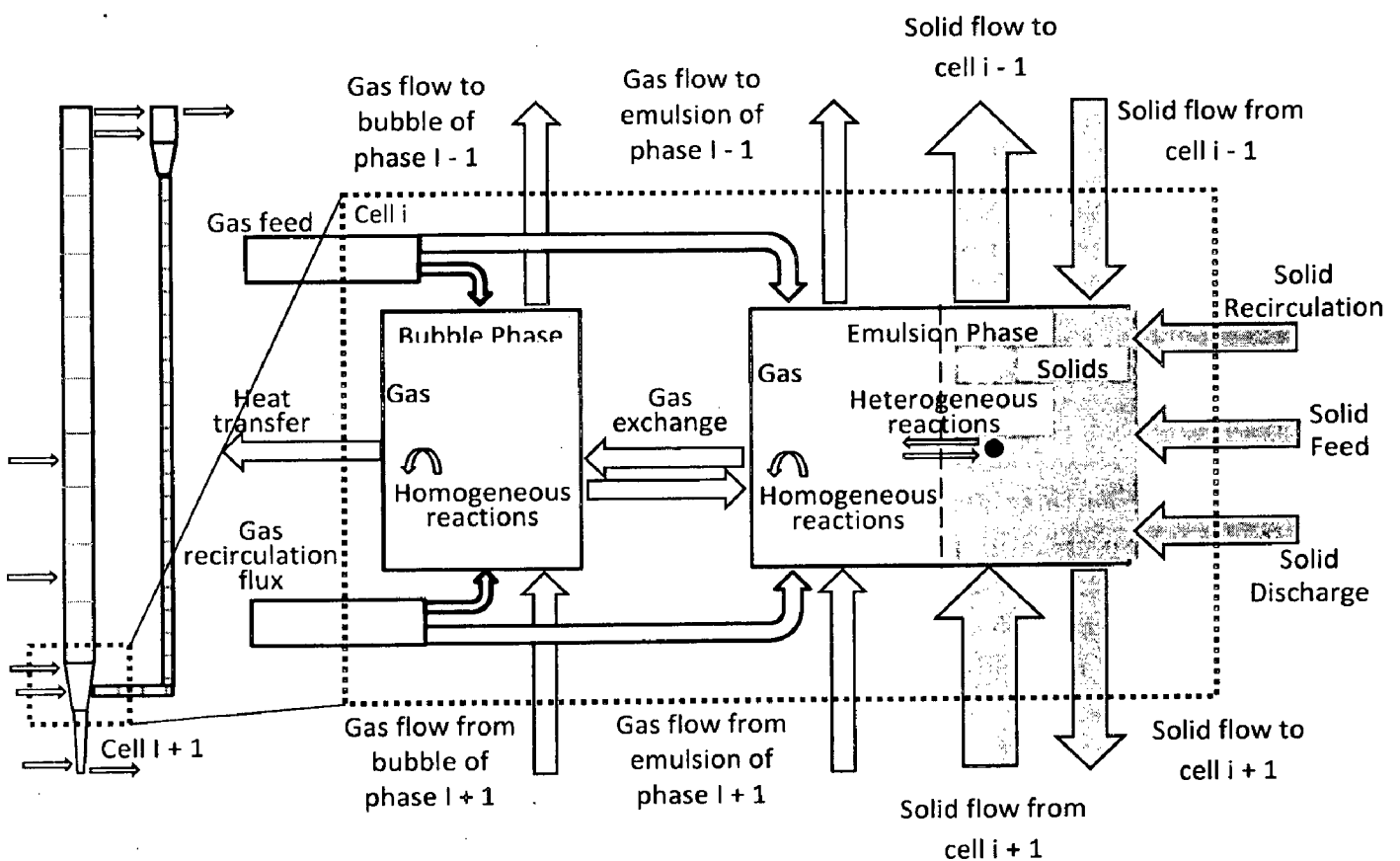


Fig. 2.17: Schematic diagram of cell model applied by Hamel et al. 2001

9.) **Gidaspow et al. 2002:** - Gidaspow et al. presented a critical review on hydrodynamics of fluidization using kinetic theory of granular flow. They experimentally verified an equation of state relating the solid pressure to the granular temperature and the solids volume fraction,

having structure similar to Van der Waals equation for gases. From their experiments, they concluded that the particle viscosity expression obtained from kinetic theory gives the same value as that obtained by classical methods.

They also used particle image velocity meter based on kinetic theory to demonstrate two kinds of turbulence in fluidization: -

- a) Random oscillations of individual particles, measured by the classical granular temperature and
- b) Turbulence caused by the motion of clusters of particles, measured by the average particle normal Reynolds stress.

These two types of turbulence give rise to two kinds of mixing, mixing on the level of a particle and mixing on the level of cluster or bubble. They also programmed a CFD code to compute the granular temperature. For the determination of diffusivity, they expressed particle diffusivity using the concepts of kinetic theory, in agreement with the random walk theory of Ruckenstein [53, 54] as follows: -

$$\text{Diffusivity (D)} = \text{mean free path} * \text{Oscillating velocity}$$

Here, the oscillating velocity is the square root of the granular temperature. This gives diffusivity (D) as: -

$$D = (\text{particle diameter} / \text{solid volume fraction}) * \text{square root of granular temperature}$$

This particle diffusivity is analogous to the molecular diffusivity. The dispersion coefficient D was found to depend on the hydrodynamics of the system. For a bubbling fluidized bed, they expressed it as: -

$$E = \text{bubble diameter} * \text{bubble velocity}$$

Finally, they found that CFD simulations of multiphase flow models by several groups throughout the world correctly predict transient and time averaged behavior of fluidized beds: bubbles, clusters and flow regimes.

- 10.) **Chejne et al. 2002:** - Chejne et al. developed a one dimensional steady state mathematical model and a numerical algorithm to simulate the coal gasification process in fluidized bed. Their model incorporates two phases: - a solid phase and a gaseous phase. The gaseous phase participates in the emulsion with the solid phase and forms the bubble. The solid phase was considered to be composed of carbonaceous material, limestone and/ or inert bed material.

At the feed zone, a Gaussian distribution for the solid particle size is considered in which an average diameter is calculated for each element. Inside the reactor, the shape of the distribution is conserved but the average diameter changes due to attrition, elutriation, consumption, and drag. Attrition only affects the size of the particles. On the other hand, elutriation, consumption and drag also affect the total mass of the element (Fig. 2.18)

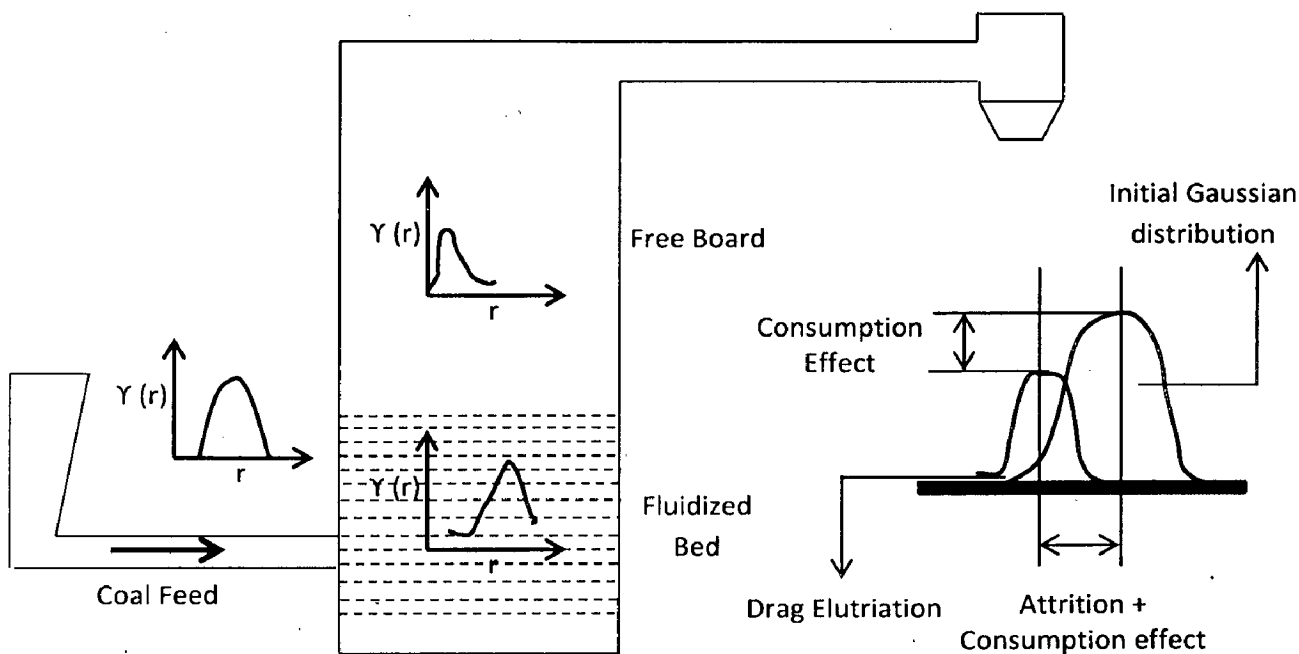


Fig. 2.18 Schematic view of Gaussian particle size distribution

The bubble was considered as a fluid which increases the energy and mass transfer inside the reactor. The bubble helps the solids homogenization and its presence increases the process efficiency and performance. The bridge between the solid and bubble is the gas in the emulsion, because it exchanges mass and energy with both solids and bubble; while these only exchange mass and energy with the gas in the emulsion as shown in Fig. 2.19

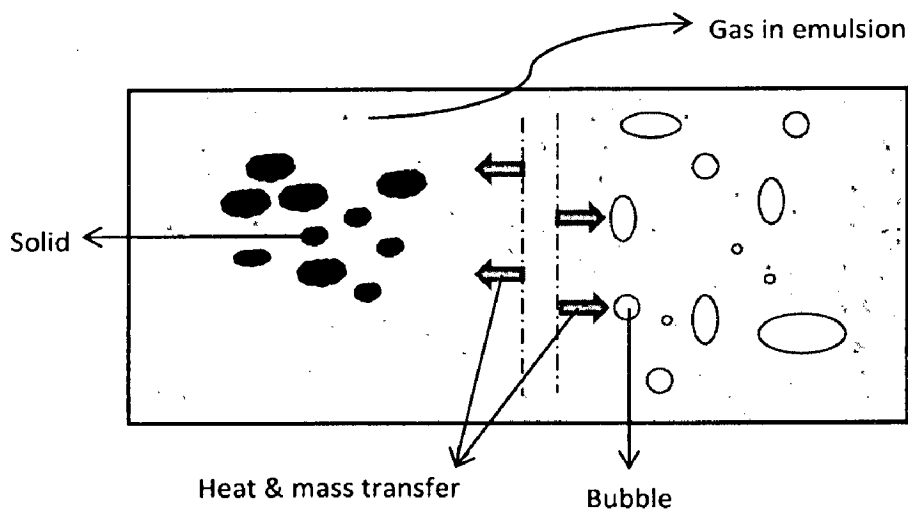


Fig. 2.19 Phases, fluids and exchanges in the Chejne's coal gasification model

They formulated a system of 29 differential and 10 non-linear equations derived from mass, energy and momentum balances for each phase at any point along the bed height and solved it using Gear & Adams method. The model was validated using experimental data from the Universidad de Antioquia and Universidad Nacional-Medellin. After validation, the model was used to optimize the gasification process by varying several parameters, such as excess of air, particle size distribution, coal type, and geometry of the reactor.

- 11.) **Hullin et al. 2005:** - Hullin et al. investigated the solid motion in a gas solid bubbling fluidized bed using hard-sphere model. For this purpose, a discrete particle model of a gas-solids bubbling fluidized bed was developed and the 2D motion of the spherical particles was individually calculated. The turbulent viscosity of the gas phase was predicted by sub grid scale (SGS) model. The interaction between gas and particles phases was governed by Newton's third law.

The radial distribution function was calculated from the simulated spatio-temporal particle distribution. The normal and shear stresses of particles were predicted from the simulated instantaneous particle velocity. The searching list approach of fluid volume-particle volume was developed for the processes of one collision at a time. The pressure and viscosity of particles are obtained from both the kinetic theory of granular flow and the calculated stresses of particles.

From their model, they observed that the results obtained for elastic particles showed an excellent agreement with the kinetic theory of granular flow. The distributions of individual particle velocity are found to be closed to Gaussian distributions. However, for inelastic particles, anisotropy of the particle velocity distribution was observed. The vertical standard deviation of particle velocity was much larger than the lateral standard deviation. The formation of bubbles seemed to disturb spatial homogeneity and resulted in collisional anisotropy. The observed anisotropy becomes more pronounced with increasing degree of inelasticity of the particles.

Results show that the particle pressure calculated from the normal stresses is the same magnitude as the values calculated from the kinetic theory of granular flow. However, a different trend is observed due to the anisotropy flow of particles. The laminar-type shear viscosity of particles calculated from shear stress is smaller than that calculated from the kinetic theory of granular flow.

From their observation, they concluded that the hard-sphere discrete particle model can give detailed information of particle phase since it computes the motion of every individual particle, taking collisions, and external forces acting on the particles directly into account.

Therefore, the discrete particle model can be applied as a valuable research tool to verify and develop closure laws for the continuum models.

However, a limitation for the future applicability of hard-sphere models seems to arise from the significant increase in computation times, since accurate detection of the collision point requires much more computational effort.

- 12.) **Ross et al. 2005:** - Ross et al. developed a one dimensional non- isothermal model of a HT Winkler fluidized bed coal gasifier for using Chinese bituminous coal as feed material. This model was basically an improvement of the isothermal model developed by Yan et al. 1998 [1] to study the non- isothermal behavior of gases and heat transfer mechanism inside fluidized bed gasifier. This was done by incorporating the energy conservation equation for bubble and emulsion phase in the isothermal model. The simulation runs were performed in both the cases –isothermal and non- isothermal. The results of both the simulations is given in Table 2.12

Table 2.12 Comparison of predictions from Isothermal & Non Isothermal model with experimental data

Parameter	Units	Pilot Plant	Isothermal Model	Non- Isothermal Model
Solid temperature (T_s)	K	1223	1223	1238
Bubble phase temperature (T_B)	K		1223	600- 1254- 1210
Emulsion phase temperature (T_E)	K		1223	600- 1238
Total carbon conversion	wt. %	70.1	68.3	71.0
Gas composition (dry)	V %			
CO		10.9	10.7	11.0
H ₂		14.6	16.3	16.3
CO ₂		12.9	12.6	12.5
CH ₄		2.6	2.9	2.8
Total product gas rate	mol/ s		9.45	9.53

From Table 2.13, it is evident that comparisons of overall carbon conversions, operating bed temperatures and individual gas species predicted from both the non-isothermal and isothermal models with experimental data are favorable. The temperature profile of the gas phase predicted from the non-isothermal model follows the trend of the bubble temperature due to a large majority of the product gas flowing through the bed as bubbles.

The temperature of cold feed gas is predicted to experience a heating up period at the lower part of the bed and homogeneous combustion in the gas phase results in a peak temperature in the gas phase. As a consequence of the higher solid temperature predicted from the non-

isothermal model than from the isothermal model, the final product gas molar flow rate and fractional carbon conversion due to gasification predicted from the non-isothermal model are all higher giving better agreeing results compared with experimental data than those predicted from the isothermal model.

- 13.) **Zhou et al. 2006:** - Zou at al. developed a non- premixed combustion model for biomass air steam gasification in a bubbling fluidized bed gasifier using FLUENT 6.0 software. In their model, they used K-ε model for turbulence specification and P-1 radiation model to determine the heat source produced by radiation, to be used in enthalpy balance equation.

For chemical reactions, the have considered a non- premixed modeling approach available in FLUENT. It involves the solution of transport equations for a conserved scalar quantity known as mixture fractions, which is determined as follows: -

$$\text{Mixture fraction} = \frac{Z_i - Z_{i,ox}}{Z_{i,fuel} - Z_{i,ox}}$$

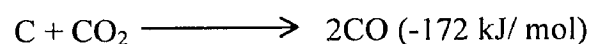
Where,

Z_i = mass fraction for element i

Subscript ox = Oxidizer stream inlet

Subscript fuel = Fuel stream inlet

In this model, the following chemical reactions listed in FLUENT package were used: -



To spread the spread of particle sizes in the biomass, they have adopted a rosin- rammler distribution given by: -

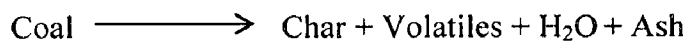
$$\text{Probability} = 1 - \exp\left[-\left(\frac{d}{d_{mean}}\right)^n\right]$$

Here, n is always 2 and d_{mean} is altered to represent different biomass particle sizes.

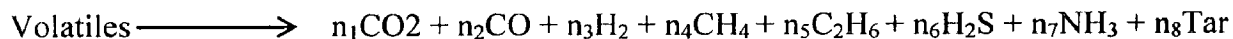
The differential equations were solved using FLUENT by means of finite volume method based on a body fitted grid. The simulation results were compared with the experimental data and the effect of steam to biomass ratio, equivalence ratio and size of biomass particles on the hydrogen yield was studied. From their simulation, they concluded that: -

- a) Hydrogen yield has a nearly exponential relationship with steam to biomass ratio when the ratio is less than 1.35.
- b) Hydrogen yield decreases with equivalence ratio as the oxygen in air reacts with H₂, thereby decreasing its concentration.
- c) The amount of hydrogen produced is higher for smaller particles for a given S/ B and equivalence ratio. The reason may be that the smaller particles can combust or pyrolyze more easily and quickly than large ones.

14.) **Yu et al. 2007:** - Yu et al. developed a new two dimensional numerical model based on Eulerian- Eulerian approach (two phase model) to simulate coal gasification process in a bubbling fluidized bed gasifier. The collision between particles was described using kinetic theory of granular flows. The homogenous reaction rate was obtained from competition between turbulent mixing rate and chemical kinetic rates. For this, they assumed that the gas phase is in turbulent flow and solid phase is in laminar flow. The product of coal pyrolysis was obtained from the proximate analysis of coal sample.



The volatile matter was assumed to be composed of following species and its molecular formula (C_{24.2}H_{46.2}O_{8.5}N_{1.1}S) was determined by combining the elemental analysis of coal with the final pyrolysates: -



The pyrolysis of coal and volatile was considered as an instantaneous phenomenon and their kinetic coefficient was calculated from the mass balance principle. They assumed char particle as spherical particle surrounded by a stagnant boundary layer through which the gas species must diffuse before they react with the coal. The overall char reaction rate was assumed to be controlled by the smaller of the kinetic rates and diffusion rate. The effect of limestone on the heterogeneous reaction rates was neglected.

The air and steam were considered to flow into the bottom of the gasifier at uniform velocity in view of the presence of an air distributor. The outlet pressure was fixed to atmosphere. Initially, they filled the bed with particles up to a height of 1.0 m and the total volume fraction of solids in the bed region was taken as 0.48. To prevent the spacing between particles from decreasing to zero, the maximum particle packing is $r_{s, \text{max}} = 0.64$. At the walls, a zero gradient condition is used for the turbulent kinetic energy and no-slip wall condition for the gas phase and solid phase was used.

The model was validated using experimental data from a pilot plant bubbling fluidized bed gasifier. The prediction results were found to be in agreement with the experimental data. They observed that the calculation errors of CO_2 and N_2 molar fraction were less than 5% and most of other results were within the 20% range.

One or two calculation errors of CH_4 molar fraction were more than 10% and they have explained it by saying that in their work, CH_4 only comes from devolatilization as the reaction of char and H_2 to form CH_4 was neglected in their numerical model. The error in mole fractions of H_2 and CO was higher than CH_4 , CO_2 and N_2 because the effect of limestone on chemical reactions was not considered in their model.

- 15.) **Grabner et al., 2007** presented a numerical simulation of coal gasification at circulating fluidized bed conditions. For this purpose, he considered the pressurized fluidized bed gasifier called the Power High Temperature Winkler gasifier. From the simulation, he observed a core-annular-flow regime which develops up to at least half of the reactor's height. The flow pattern was characterized by a fast, upward, and dilute core flow and by a slow, downward, and concentrated annular flow. Kidney-shaped circulation cells appeared. Increasing reactor diameter resulted in an upward expansion of the circulation cells. Decreasing reactor diameter caused contraction of the circulation cells. The highest turbulence kinetic energy appeared in the transitional region between core and annular flow. The highest rate of dissipation was observed close to the tuyères nozzles.
- 16.) **Pengmei et al. 2008:** - Pengmei et al. developed a steady state, isothermal, one dimensional and two phase mathematical model of biomass gasification kinetics in a bubbling fluidized bed gasifier by considering the features of fluidized bed reactors and kinetic mechanism of biomass gasification. The model assumes the presence of two phases- a bubble and an emulsion phase, with chemical reaction occurring in both the phases as shown

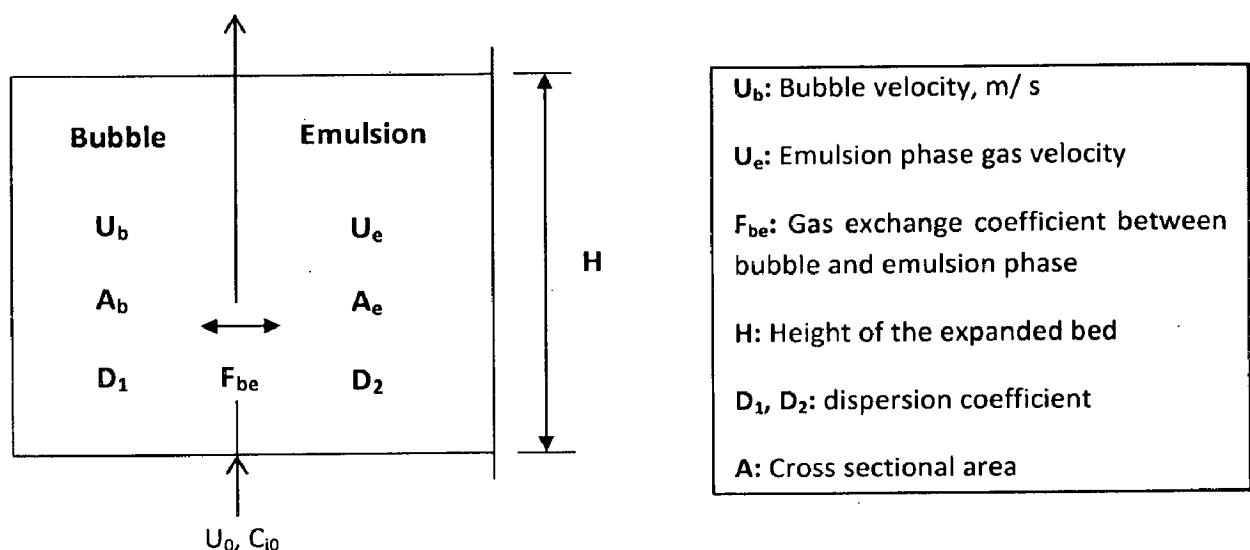


Fig. 2.20 Schematic representation of the model developed by Pengmei et al. 2008) 43

in Fig. 2.20. The gaseous flow in bubble and emulsion phase was considered to be plug-flow i.e. the condition over the fluidized bed cross-section was considered to be uniform and axial diffusion was considered. The reaction system involved char, 5 gas species (CO, CO₂, H₂, H₂O and CH₄) and 8 chemical reactions. The pyrolysis of biomass was assumed to be instantaneous.

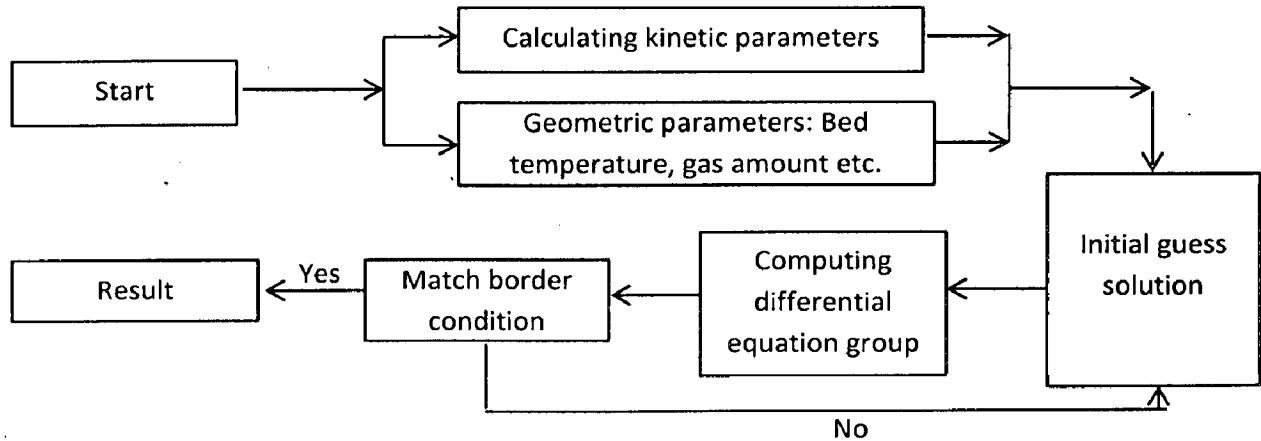
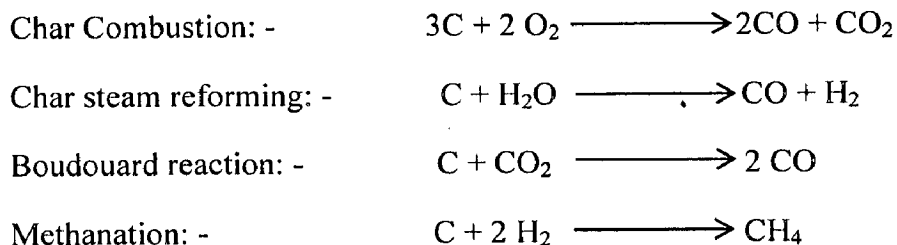


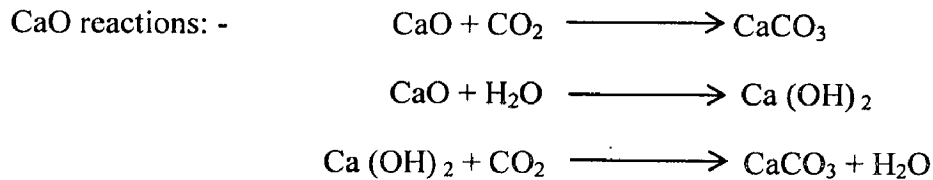
Fig. 2.21 Calculation procedure for the model equations used by Pengmei et al. 2008

17.) **Lu et al. 2008:** - In order to attempt to eliminate the global warming effects, they developed a comprehensive two dimensional model of a high pressure fluidized bed coal gasifier for hydrogen production with in situ fixation of CO₂.

Their model was based on Eulerian Lagrangian approach (DPM) with gas phase treated as a continuum and solid phase is tracked by Lagrangian procedure. Besides, conservation equation for mass, momentum and energy, their comprehensive model also included a particle stochastic tracking model accounting for the particle turbulent dispersion model, a standard K-ε model for gas turbulence, an EDC (Eddy-Dissipation-Concept) model adopted to describe the turbulence-chemistry interaction and a P-1 model used as a radiation model.

This was the first attempt to use Eddy dissipation concept model to simultaneously describe the turbulent mixing and detailed chemical kinetics in pulverized coal gasification. Heterogeneous reactions occurring in their gasifier included coal devolatilization, char reactions and CaO reactions as presented below: -





The developed model was verified with experimental results and was found to be in good agreement with the experimental results in terms of product concentrations and temperature distributions. The relative errors of the main product gas concentrations (H₂ and CH₄) were less than 8%, and the absolute errors of the CO and CO₂ concentration were less than 2%.

- 18.) **Wang et al. 2009:** - Wang et al. developed a comprehensive three dimensional mathematical model to simulate the coal gasification process in fluidized bed coal by considering both gas solid flow and chemical reactions. The primary aim of their work was to develop a promising way to simulate the coal gasification process in fluidized beds.

They modeled the gas phase by K- ε turbulent model while the solid phase was modeled by kinetic theory of granular flow. Coal pyrolysis, homogeneous reactions and heterogeneous reactions were considered in the model. The reaction rate of the homogeneous and heterogeneous reactions was determined by the Arrhenius- Eddy dissipation reaction rate and Arrhenius- diffusion reaction rate.

The simulations were carried out in a coal gasifier of 2 m height and 22 cm diameter. The predicted exit gas composition was in good agreement with the experimental results and therefore, their model was used for studying the flow pattern, gas and particle velocities inside the reactor.

- 19.) **H Lee, S Choi and M Paek, 2010:** - They presented a numerical model for dry feeding entrained bed coal gasifier by simultaneously solving the rate equations for chemical reactions between solid and gas phases. The model described simplified chemical and physical processes inside the gasifier. Chemical reaction processes for coal gasification and combustion were considered along with the simplified gas flow passage in the reactor, so that progress of reactions at the designated spatial location was represented.

They separated the Gasification phenomena of coal particles into devolatilization, gas-phase, and solid-phase reactions. Coal gasifier geometry was simplified to a pseudo-two-dimensional (pseudo-2D) reactor model based on the 1D plug flow concept. The dimension in the pseudo- 2D model was conceptually divided by considering the recirculation effect.

From the model, they observed that as the concentration of oxygen increases, enough carbon conversion was obtained and reactor length shorter than 6m was sufficient to get maximum efficiency at given oxygen to coal ratio. Also, as the oxygen to coal ratio increases, combustion of fuel gases lasted by oxidation reaction of excess oxygen. Therefore, peak temperature was higher as oxygen to coal ratio increases.

The rate of increase of temperature was higher at higher pressure during the early stages of reaction but the peak temperature was lower. This is because high pressure results in high reactivity of endothermic gasification reactions. As pressure increases, the partial pressure of the gasifying agents, CO₂ and H₂O increases. As a result, carbon conversion and cold gas efficiency also increase.

20.) **Cornejo et al. 2011:** - Cornejo et al. developed a three dimensional model to describe the coal gasification process inside bubbling fluidized bed reactors using commercial multi-purpose CFD code FLUENT 6.3. The model was developed taking into account drying, volatilization, combustion and gasification processes. Both gas phase and solid phase were described using Eulerian approach to model the exchanges of mass, energy and momentum between phases. The disperse phase was described using the kinetic theory of granular flows. The chemical model involved five heterogeneous and five homogeneous chemical reactions, tracking seven species in the gas phase (CO₂, CO, H₂O, CH₄, H₂, O₂ and N₂) and one specie in the solid phase (C(s)).

Drying and volatilization rates were estimated by mass conservation. Heterogeneous reaction-rates were determined by combining an Arrhenius kinetic-rate and a diffusion rate using the kinetics/diffusion Surface Reaction Model; the model was implemented within FLUENT through UDFs (User Defined Functions). Homogeneous reaction-rates were described by a turbulent mixing rate using the Eddy Dissipation Model available in FLUENT.

For the discretization of conservation equations, a first order upwind scheme was used in which the quantities at the cell faces are determined by assuming that the cell center values represent an average value and hold throughout the entire cell. The other solver parameters used in their simulation are given in Table 2.13

Table 2.13 Solver Parameters (Cornejo et al. 2011)

Characteristic	Value
Pressure Based	Enable
Formulation	Implicit
Space	3D
Velocity Formulation	Absolute

Gradient Option	Green Gauss Cell based
Porous formulation	Superficial velocity
Pressure Velocity coupling	Phase coupled Simple
Under Relaxation factor	0.1 for all variables

Calculation time was approximately two days in a 3.2 GHz, 8 GB RAM desktop computer. They calibrated and validated the model using existing experimental data from a benchmark coal-gasification case available in the literature. The results obtained from their simulation were in good agreement with experimental data, capturing known phenomena like fluidization-bed height, temperature distribution and species concentrations. Some of their results like syngas composition are shown in Fig. 2.22.

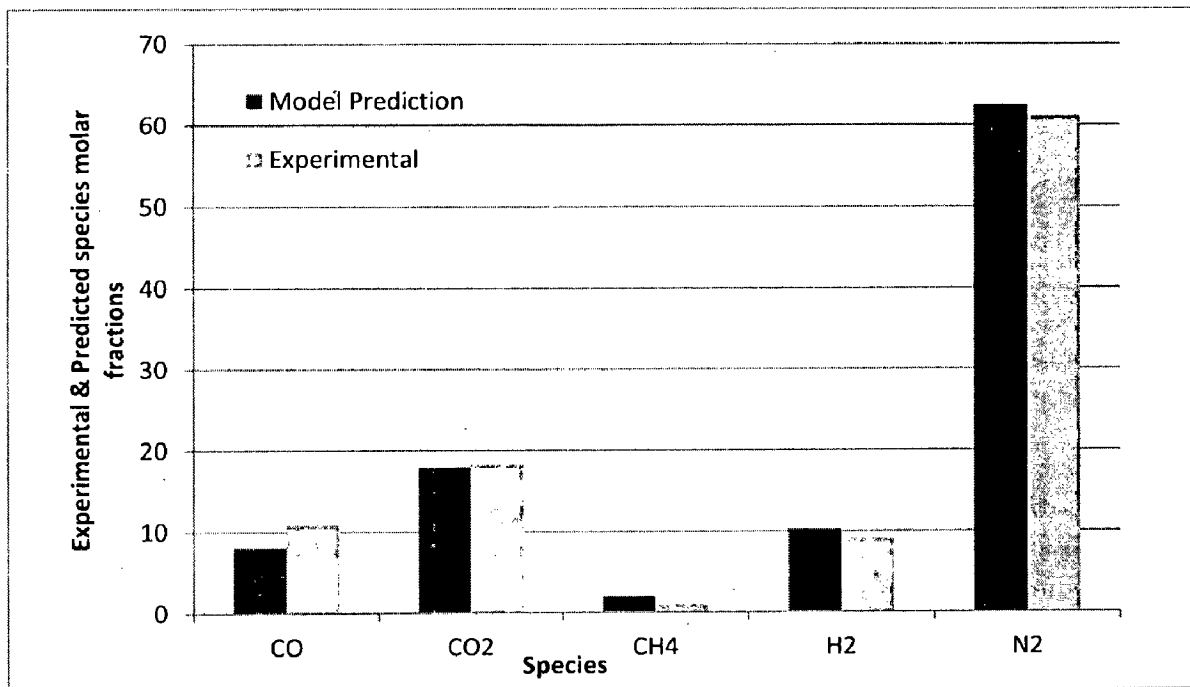


Fig. 2.22 Experimental & Predicted species molar fractions (Cornejo et al. 2011)

21.) **Knudson et al. 2012:** - Ultra superheated steam gasification is used to convert coal to hydrogen. The process known as Lewis USS reforming creates an extremely hot steam flame, which is formed at the tip of the tuyères as the gases enter a fluidized bed containing coal. A major process advantage of steam only gasification is the absence of oxidation of the feedstock material. The main objective of their work was to develop a CFD model of an advanced Lewis USS coal gasifier to :

- a. Determine the syngas composition for various ranks of coal based on operational conditions.

- b. To interpret the transport/ diffusion limitations to describe the mechanism for the water gas shift reaction and determine the reactor configuration that will allow it to reach equilibrium.

For this purpose, they developed a 3D CFD model of Lewis USS bubbling fluidized bed gasifier in ANSYS 12.1.4 commercial software using Eulerian granular model. Using this model, they also studied the hydrodynamic behavior of Geldart B particle size bubbling bed. From their model, they concluded that:

- a) CFD modeling based on first principles for mass/ heat transfer and hydrodynamic behavior in bubbling bed can model the Lewis USS gasifier syngas composition.
- b) Hydrodynamic and transport limitations within the bubbling bed and freeboard dominate over the reaction kinetics, preventing the produced syngas to be at equilibrium within the entire freeboard.
- c) Bubbling bed acts as a flame arrester between the temperatures of 750°C and 900°C.

CHAPTER- 3

MULTIPHASE MODEL SELECTION & DEVELOPMENT

3.1 MULTIPHASE MODELING APPROACH

In multiphase problems, a phase can be defined as an identifiable class of material that has a particular inertial response to and interaction with the flow and the potential field in which it is immersed. For example, different sized solid particles of the same material can be treated as different phases because each collection of particles with the same size will have a similar dynamical response to the flow field. Therefore, Multiphase flow [7- 8] is defined as the simultaneous flow of: -

- a) Matters with different phases (i.e. gas, liquid and solid)
- b) Matters with different chemical substances but with the same phase like (i.e. like oil – water)

In multiphase flows, one phase is considered as a continuous phase (or primary phase) and the others are considered to be dispersed within the continuous phase. Multiphase flow regimes can be grouped into four categories as shown below: -

- a) Gas – Liquid or Liquid-Liquid flows: - Bubbly, droplet, slug and stratified flow
- b) Gas –Solid flows: - Particle laden flows, pneumatic transport and fluidized bed
- c) Liquid – Solid flows: - Slurry flow, hydro transport and sedimentation
- d) Three phase flows

3.1.1 Multiphase Modeling of bubbling fluidized bed gasifier: - The first step in solving any multiphase problem is to determine the appropriate model which can describe a particular flow regime. There are presently two approaches for the multiphase modeling of fluidized bed gasifiers: -

- a) Eulerian Lagrange Approach
- b) Eulerian Eulerian Approach

3.1.2 Eulerian Lagrange Approach : - The Eulerian lagrangian approach is followed by the lagrangian discrete phase model which is based on the following two phases: -

- a) Fluid Phase: -This phase is treated as the continuum by solving the time averaged Navier stokes equation.

- b) **Dispersed phase:** - This phase is assumed to be dispersed in the continuous phase. This phase is solved by tracking a large number of particles, bubbles or droplets through the calculated flow field. This phase can exchange mass, momentum and energy with the continuous phase.

In this model, we compute the trajectories of the particles in the continuous phase under steady as well as unsteady state. Mass, momentum and heat transfer between dispersed and continuous phase is considered but particle – particle interaction is neglected. Therefore, this model is appropriate for modeling particles, droplets or bubbles dispersed at low volumn fraction (less than 10 %) in continuous fluid phase though the particle loading can be as high as fluid loading. For example, this model can be used for

- a) Spray dryers
- b) Coal and liquid fuel combustion
- c) Some partice laden flows

3.1.3 Eulerian - Eulerian Approach: - In this approach, the different phases are treated as interpenetrating continua. The concept of volume fraction is assumed as the volume of a phase cannot be occupied by others. These volume fractions are assumed to be continuous function of space and time and their sum is equal to one. Conservation equations, having similar structure for all phases are derived for each phase. These equations are closed by providing constitutive relation obtained from empirical information or by kinetic theory of gases in case of granular flow. The Eulerian – Eulerian model [7- 8] can be further classified into: -

- a) **Volume of fluid (VOF) model:** - The VOF model is a surface tracking technique applied to fixed Eulerian mesh. It is designed for two or more immiscible fluids where the position of interface between the fluids is of interest. In this case, a single set of momentum equation is shared by the fluids and the volume fraction of each of the fluids in each computational cell is tracked throughout the domain.

$$\frac{\partial(\rho u_j)}{\partial t} + \frac{\partial(\rho u_i u_j)}{\partial x_i} = \frac{\partial P}{\partial x_j} + \rho g_i + F_j + \frac{\partial}{\partial x_j} \mu \left(\frac{\partial y_i}{\partial x_j} + \frac{\partial y_j}{\partial x_i} \right)$$

This model assumes that only one phase is present in each control volume. Therefore, if for a kth fluid, the volume fraction ϵ_k comes out to be: -

- a) $\epsilon_k = 0$, it means the cell is empty of the Kth fluid
- b) $\epsilon_k = 1$, it means the fluid is full of the kth fluid
- c) $0 < \epsilon_k < 1$, it means the cell contains an interface between the phases.

In this model, surface tension and wall adhesion are modeled by an additional source term in the momentum equation. For turbulent flow, single set of turbulent transport equations are solved and also species conservation equations are solved for primary

phases. This model is appropriate for modeling of jet breakup and motion of liquid after a dam break but is inappropriate for flows involving small bubbles like in bubble column.

b) Mixture model: - The mixture model is designed for two or more phases (fluid or particulate). As in the Eulerian model, the phases are treated as interpenetrating continua. The mixture model solves for the mixture momentum equation and prescribes relative velocities to describe the dispersed phases. Applications of the mixture model include particle-laden flows with low loading, bubbly flows, sedimentation, and cyclone separators. The mixture model can also be used without relative velocities for the dispersed phases to model homogeneous multiphase flow.

This model can substitute for Eulerian – Eulerian, Eulerian – Granular and dispersed phase model for to phase problems like: -

- a) Fluid / fluid separation or mixing
- b) Sedimentation of uniform sized particles in liquid
- c) Flow of single sized particles in a cyclone

This model is applicable to relatively small particles (< 50 microns) and low volume fractions (< 10 %) when the primary phase density is much smaller than the secondary phase. Since, in bubbling fluidized bed gasifier, the volume fraction of the dispersed phase is much higher than 10 % (around 30 – 40 %), thus, this model is not suitable for our case.

c) Eulerian model: - The Eulerian model is the most complex of the multiphase models. It solves a set of n momentum and continuity equations for each phase. Coupling is achieved through the pressure and interphase exchange coefficients. This model is appropriate for modeling gas-liquid or liquid-liquid flows (not appropriate for stratified or free surface flows)) where: -

- a) Phases mix or separate
- b) Bubble / droplet volume fraction varies from 0 to 100 % like in case of : -
 - i. Evaporators
 - ii. Boiling
 - iii. Aeration &
 - iv. Separators

In this model, we solve for momentum, enthalpy, continuity and species equation for each phase and track volume fractions. A single pressure field is used for all the phases. Interaction between mean field flows of phases is expressed in terms of drag, virtual and lifts forces.

This model can solve for multiple species and homogeneous reactions for each phases while heterogeneous reactions can be done using UDF. This model allows for heat and mass transfer between phases and includes turbulent models for dilute and dense phase regimes.

The manner in which coupling is handled between different phases depends upon the type of phases involved; granular (fluid-solid) flows are handled differently than non-granular (fluid-fluid) flows. For granular flows, an extension of the Eulerian – Eulerian model is used, known as Eulerian granular Model.

3.1.4 Eulerian Granular Approach: - This model is an extension of Eulerian model for the flow of granular particles (secondary) in a fluid phase (primary). In this model, the granular volume fraction can vary from 0% to the packing limit and the properties of the granular phase are obtained from application of kinetic theory.

In this model, the fluid phase must be assigned as primary phase and multiple solid phases are used to represent the size distribution. Granular temperature and solid pressure field is calculated for each phase.

- Fluid pressure field is shared by all the phases and
- Solid pressure controls the packing limit.

Solid pressure, granular temperature, conductivity, shears and bulk viscosity can be derived based on any of the following three formulations: -

- a) Gidaspow: - Dense fluidized bed applications
- b) Syamlal: - Wide application range
- c) Sinclair: - dilute and dense pneumatic transport lines and risers

3.1.5 Choosing the correct multiphase model: - In general, once you have determined the flow regime that best represents your multiphase system, you can select the appropriate model based on the following guidelines [7- 8]: -

- a) For bubbly, droplet, and particle-laden flows in which the phases mix and/or dispersed-phase volume fractions exceed 10%, use either the mixture model or the Eulerian model.
- b) For slug flows, use the VOF model
- c) For stratified/free-surface flows, use the VOF model
- d) For pneumatic transport, use the mixture model for homogeneous flow or the Eulerian model for granular flow
- e) For fluidized beds, use the Eulerian model for granular flow
- f) For slurry flows and hydro transport, use the mixture or Eulerian model respectively
- g) For sedimentation, use the Eulerian model.

These models are already described in the previous pages. Thus, for the simulation of the bubbling fluidized bed gasifier, Eulerian Granular model has been selected.

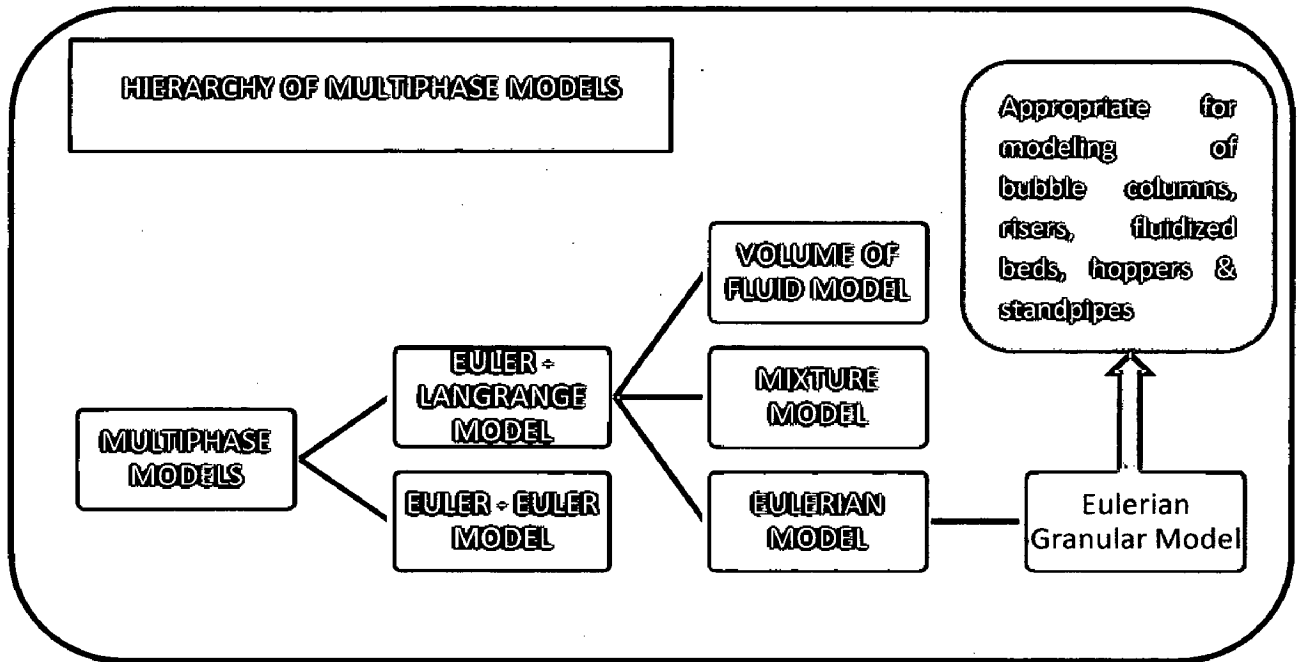


Fig. 3.1 Hierarchy of Multiphase Models

3.1.6 Turbulence Models in FLUENT: - Turbulence models [9, 27, 94, 137] are broadly classified into First order models & second order models, which are further classified into zero equation, one equation two equations models etc. as shown in Fig. 3.2: -

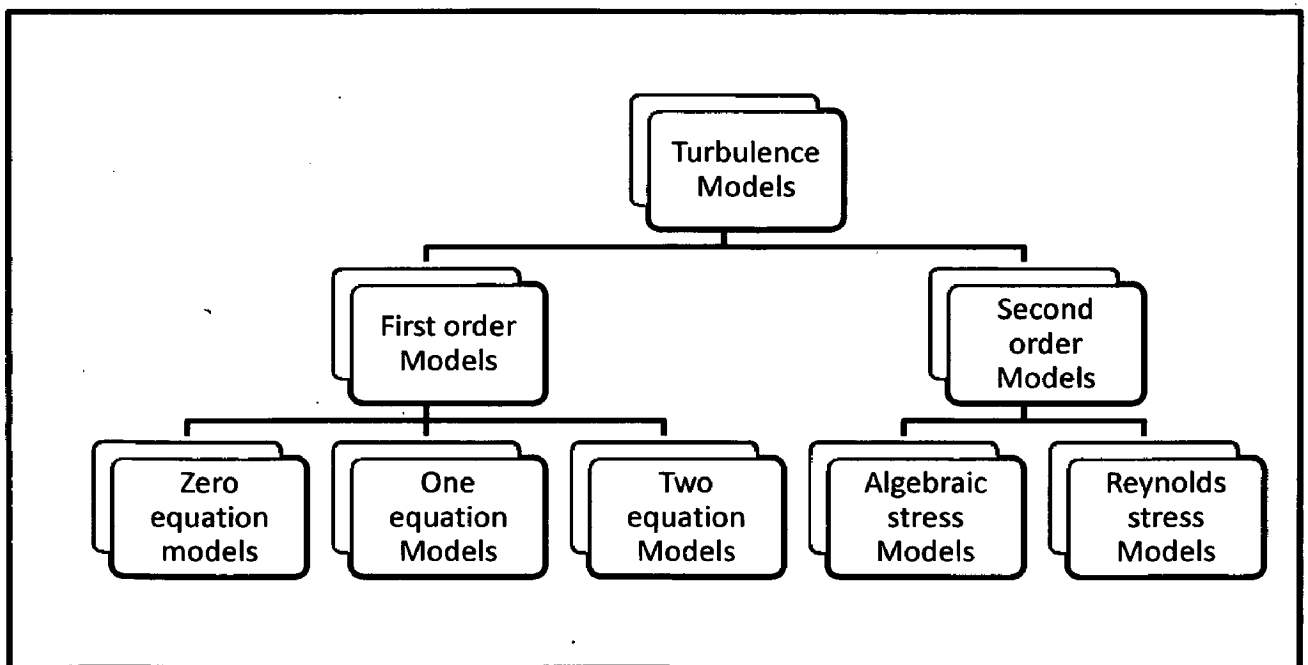


Fig. 3.2 Turbulence Models

Two equation models: - In the two equation models, two PDEs are developed: one for the turbulent kinetic energy (K) and one for the turbulent dissipation rate (ϵ). Ansys fluent includes three methods for modeling turbulence in multiphase flows within the context of the k- ϵ models. The k- ϵ turbulence model options are: -

- **Mixture turbulence model (the default):** - The mixture turbulence model is the default multiphase turbulence model. It represents the first extension of the single-phase k- ϵ model, and it is applicable when phases separate, for stratified (or nearly stratified) multiphase flows, and when the density ratio between phases is close to 1. In these cases, using mixture properties and mixture velocities is sufficient to capture important features of the turbulent flow.

- **Dispersed turbulence model:** - The dispersed turbulence model is the appropriate model when the concentrations of the secondary phases are dilute. In this case, inter-particle collisions are negligible and the dominant process in the random motion of the secondary phases is the influence of the primary-phase turbulence.

Fluctuating quantities of the secondary phases can therefore be given in terms of the mean characteristics of the primary phase and the ratio of the particle relaxation time and eddy-particle interaction time. The model is applicable when there is clearly one primary continuous phase and the rest are dispersed dilute secondary phases.

- **Turbulence model for each phase:** - The most general multiphase turbulence model solves a set of k and ϵ transport equations for each phase. This turbulence model is the appropriate choice when the turbulence transfer among the phases plays a dominant role.

In bubbling fluidized bed gasifier, the turbulence between the phases plays a dominant role. Hence, turbulence model for each phase [26] has been used in BFBG model though it is more calculation intensive as it solve for additional equations for secondary phase.

3.1.7 Drag Models in FLUENT: - The momentum exchange coefficient between gas and solid phase can be given by any of the following drag models: -

- a) **Syamlal – O’ Brien Drag Model [122]:** - Based on measurement of terminal velocity of particles in fluidized / settling beds. According to this model, fluid-solid momentum exchange is given by: -

$$K_{fs} = \left(\frac{3}{4}\right) [(\alpha_s \alpha_g \rho_g) / (V_{r,s}^2 d_s)] C_D (Re_s / V_{r,s}) |V_s - V_g|$$

Where,

$$C_D = [0.63 + 4.8 / (Re_s / V_{r,s})]$$

$V_{r,s}$, the ratio of terminal velocity of multiple and single particle is obtained from the velocity - voidage correlation proposed by Garside and Al – Dibouni (1977): -

$$V_{r,s} = 0.5 [A - 0.06 Re_s + (0.06 Re_s)^2 + 0.12 Re_s (2B - A) + A^2]$$

$$A = \alpha_g^{4.14}, B = 0.8 \alpha_g^{2.65} \quad \text{for } \alpha_g \geq 0.85$$

$$A = \alpha_g^{4.14}, B = 0.8 \alpha_g^{1.28} \quad \text{for } \alpha_g < 0.85$$

Where,

A_s, α_g : - Solid and gas phase volume fraction respectively

V_s, V_g : - Solid and gas phase velocity

b) **Wen – Yu Model** [15]: - Extension of Richardson and Zaki model adapted for high void fraction. The momentum exchange coefficient according to this model is given by:-

$$K_{gs}^{\text{Wen-Yu}} = \frac{3}{4} C_D (\alpha_s \alpha_g \rho_g / d_s) |V_s - V_g| \alpha_g^{-2.65} \quad (\alpha_g \geq 0.8)$$

Where,

$$C_D = [(24/(\alpha_g Re_s)) \{1 + 0.15 (\alpha_g Re_s)^{0.687}\}] \quad Re \leq 1000$$

$$= 0.44$$

$$Re \geq 1000$$

$$Re_s = \{(\rho_g d_s / \mu_g) |V_s - V_g|\}$$

c) **Gidaspow Drag Model** [50]: - Based on Ergun equation in combination with Wen – Yu model. Covers the whole range of void fractions. The momentum exchange coefficient according to this model is equal to the average of Ergun and Wen Yu model:-

$$K_{gs}^{\text{Ergun}} = [\{150(\alpha_s^2 \mu_g / \alpha_g d_s^2)\} + \{1.75(\alpha_s \rho_g / d_s) |V_s - V_g|\}] \quad (\alpha_g \leq 0.8)$$

$$K_{gs}^{\text{Wen-Yu}} = \frac{3}{4} C_D (\alpha_s \alpha_g \rho_g / d_s) |V_s - V_g| \quad (\alpha_g \geq 0.8)$$

And,

$$K_{gs} = (1 - \phi_{gs}) K_{gs}^{\text{Ergun}} + \phi_{gs} K_{gs}^{\text{Wen-Yu}}$$

Where,

$$C_D = [(24/(\alpha_g Re_s)) \{1 + 0.15 (\alpha_g Re_s)^{0.687}\}] \quad Re \leq 1000$$

$$= 0.44$$

$$Re \geq 1000$$

$$Re_s = \{(\rho_g d_s / \mu_g) |V_s - V_g|\}$$

3.1.8 Interphase heat transfer: - For Interphase heat transfer, I have used Gunn, 1978 model which is given by the following equations: -

➤ The interphase heat transfer coefficient is given by:

$$\gamma_{ik} = \frac{6\kappa_k \alpha_i Nu_i}{d_i^2}$$

➤ **Granular Model (Gunn, 1978) :**

$$Nu_s = (7 - 10\alpha_f + 5\alpha_f^2)(1 + 0.7 Re^{0.2} Pr^{1/3}) + (1.33 - 2.4\alpha_f + 1.2\alpha_f^2) Re^{0.7} Pr^{1/3}$$

➤ **Fluid-fluid model :**

$$Nu_i = 2 + 0.6 Re^{0.5} Pr^{0.3}$$

$$Re = \frac{\alpha_k \rho_k |u_i - u_k| d_i}{\mu_k}$$

$$Pr = \frac{C_{p,k} \mu_k}{\kappa_k}$$

3.1.9 Virtual mass effect [34]: - This effect is caused by relative acceleration between phases and is significant when the second phase density is much smaller than the primary phase density as in case of bubble columns.

$$K_{vmfs} = C_{vm} \alpha_s \rho_f \left[\left(\frac{\partial \vec{u}_f}{\partial t} + \vec{u}_f \cdot \nabla \vec{u}_f \right) - \left(\frac{\partial \vec{u}_s}{\partial t} + \vec{u}_s \cdot \nabla \vec{u}_s \right) \right]$$

3.1.10 Lift force [34]: - This force is caused by the shearing effect of the fluid onto the particle and is usually insignificant compared to drag force except when the phases separate quickly and near boundaries.

$$K_{k,fs} = C_L \alpha_s \rho_f (\vec{u}_f - \vec{u}_s) \times (\nabla \times \vec{u}_f)$$

3.2 MODEL DEVELOPEMNT

For the purpose of studying the performance of the CIFR gasification facility, a 2D computational fluid dynamics model has been developed in commercial, multi-purpose CFD software, FLUENT 12.0. Eulerian- Eulerian model was used to describe both the solid and gaseous phases. The turbulence inside the gasifier was modeled using K-ε model with standard wall functions. The operating and boundary conditions were obtained from the experimental setup in CIFR, Dhanbad. The gas solid hydrodynamics, turbulence, energy and gasification models are simplified using the following assumptions in order to decrease the computation time and increase the convergence:

- a) Coal particles are modeled as mono-dispersed, smooth, inelastic and isothermal (internal thermal resistance negligible) spheres [Yu et al. (2007)].
- b) Drying and volatilization are assumed occurring instantaneously in the feed region of the gasifier [O'Brien et al. (2003); Yu et al. (2007); Weimer and Clough (1981)].
- c) The intensity of particles collision does not vary with temperature, i.e., exothermic or endothermic reactions has no impact on the fluctuation of solid phase velocity and hence the temperature variations of the solid phase will not alter the granular temperature [Yu et al. (2007)].
- d) The gas is assumed to be transparent, i.e. the radiative energy is neither absorbed nor emitted [145]. This assumption can be made as the solid phase is dense and continuous in the bed. It is in contact with the walls and the mean free path of radiation is much smaller than the dimension of the solid particle. Also, the bed temperature will rapidly become uniform due to strong agitation of particles. This will limit the contribution of the radiative heat transfer which can be assumed negligible.

3.2.1 Hydrodynamics: - In the fluidized bed gasifier, the volume fraction of the solid phase is greater than 11 %. Therefore, Eulerian granular approach is used to describe the multiphase flow, where both the solid and fluid phase interpenetrates each other exchanging mass, momentum and energy. For this purpose, the concept of phase volume fraction α_q , defined as the volume occupied by each phase, has been used. The volume of phase q, V_q , is given by Cornejo, 2011:

$$V_q = \int_V (\alpha_q) dV \quad \dots (1)$$

Here,

$$\sum_{q=1}^n \alpha_q = 1 \quad \dots (2)$$

The continuity equation for the gas and solid phases are given in terms of these volume fractions as follows [109]: -

$$\frac{\partial}{\partial t} (\alpha_g \rho_g) + \nabla \cdot (\alpha_g \rho_g U_g) = S_{gs} \quad \dots (3)$$

$$\frac{\partial}{\partial t} (\alpha_s \rho_s) + \nabla \cdot (\alpha_s \rho_s U_s) = S_{sg} \quad \dots (4)$$

Here,

α, ρ, U ----- represents volume fraction, density and instantaneous velocity respectively

S_{gs}, S_{sg} ----- represents mass transfer from the gas to solid phase and solid to gas phase respectively

When the continuity equation is used in heterogeneous reactions, there is a mass, momentum and heat exchange between the solid and the gas phases. In the present case, coal reacts with oxygen, steam and CO₂ to change solid phase into gas phase. So, the mass transfer for the phases in equation (3) and (4) can be given by:

$$S_{sg} = wC \sum Y_C R_C = - S_{gs} \quad \dots (5)$$

For the gas phase density in equation (3) & (4), a mixture of ideal gas is assumed.

$$\rho_g = \frac{p}{RT \sum_{i=1}^n \frac{Y_i}{w_i}} \quad \dots (6)$$

Where,

p = Gas pressure, T = Gas mixture mean temperature,

Y_i, w_i = mass fraction and molecular weight of every species.

The momentum equation for the q_{th} phase, in terms of volume fraction, is given by: -

$$\begin{aligned} \frac{\partial}{\partial t} (\alpha_g \rho_g U_g) + \nabla \cdot (\alpha_g \rho_g U_g U_g) \\ = -\alpha_g \nabla p - \phi_{gs} (U_g - u_s) + \nabla \cdot \alpha_g \tau_g + \alpha_g \rho_g g + S_{gs} u_s \quad \dots (7) \end{aligned}$$

Where,

ϕ_{gs} : - Momentum exchange coefficient between solid phase and the gas phase.

G: - Acceleration due to gravity

$S_{gs}u_s$: - Momentum transfer of the coal.

The stress tensor τ_g in equation (7) is obtained from the following relationship:

$$\tau_g = \mu_{1,g} (\nabla U_g + \nabla U_g^T) - 2/3 \mu_{1,g} U_g \quad \dots (8)$$

Similarly, the momentum equation for the solid phase can be expressed as:

$$\begin{aligned} \frac{\partial}{\partial t} (\alpha_g \rho_g U_g) + \nabla \cdot (\alpha_g \rho_g U_g U_g) \\ = -\alpha_s \nabla p - p_s - \phi_{gs}(u_s - U_g) + \nabla \cdot \alpha_g \tau_g + \alpha_g \rho_g g + S_{gs}u_s \end{aligned} \quad \dots (9)$$

Where,

$$\text{Solid stress tensor, } \tau_s = (\lambda_s - 2/3 \mu_s) \nabla u_s + \mu_s (\nabla u_s + \nabla u_s^T) \quad \dots (10)$$

The bulk viscosity, λ_s and solid shear viscosity, μ_s used in equation (10), are calculated using the following expressions given by Gidaspow (1994)

$$\lambda_s = 4/3 \alpha_s \rho_s d_s g_0 (1-\epsilon) (\theta_s / \pi)^{0.5} \quad \dots (11)$$

$$\mu_s = 4/5 \alpha_s^2 \rho_s d_s g_0 (1+e) \sqrt{\frac{\theta_s}{\pi}} \frac{10 \rho_s d_s \sqrt{\pi \theta_s}}{96 (1+e) \epsilon_s g_s} \left[1 + \frac{4}{5 g_0 \alpha_s (1+e)} \right]^2 \quad \dots (12)$$

From the momentum equations (7) and (9), it is evident that drag between the solid phase and the gas phase play a very important role in the momentum exchange. The momentum exchange coefficient is therefore calculated using the drag model of Wen & Yu (1966)

$$\phi_{gs} = \frac{3}{4} C_d \frac{(u_g - u_s)}{d_s} \alpha_g^{-2.65} \quad \dots (13)$$

The drag coefficient C_d is given by: -

$$C_d = 24 / \text{Re} (1 + 0.15 \text{Re}^{0.687}) \quad \text{for } \text{Re} \leq 1000 \quad \dots (14)$$

$$= 0.44 \quad \text{for } \text{Re} > 1000 \quad \dots (15)$$

Where, reynolds number Re is calculated using the expression

$$\text{Re} = \frac{(u_g - u_s) \alpha_g \rho_g d_s}{\mu_g} \quad \dots (16)$$

3.2.2 Solid Pressure: For incompressible granular flows, i.e., when volume fractions are lower than the maximum allowable value, a solid pressure for the granular solid phase (p_s) is estimated in an independent way and used in the momentum equation (9) for solid phase. This granular

pressure will be composed by one kinetic term and a second term due to particle collisions as shown below:

$$p_s = \alpha_s \rho_s \Theta_s + 2 (1+e) \alpha_s^2 g_0 \rho_s \Theta_s \quad \dots (17)$$

Where,

Θ_s – Granular Temperature

e – Coefficient of restitution for particle collision (0.8 – 1, 0.9 for 0.62 mm dia.) [41, 103]

g_0 – Radial distribution function

The radial distribution function g_0 drives the transition from the compressibility condition $r < r_{s, \max}$, where the spacing between solid particles can continuously decrease, to the incompressibility condition $r = r_{s, \max}$, where no additional decrease can take place.

In practice, the radial distribution function is a correction factor that modifies the probability of particle collisions when the granular phase becomes denser. Fluent [96] proposes the following relationship for the same:

$$g_0 = [1 - (\alpha_s / \alpha_{s, \max})^{0.33}]^{-1} \quad \dots (18)$$

3.2.3 K - ϵ per phase Turbulence Model: - In case of bubbling fluidized bed gasifier, the turbulent transfer between the solid and gas phases play a pre-dominant role. Therefore, we have selected K - ϵ per phase model which solves for a set of turbulent kinetic energy and turbulent kinetic energy dissipation equations for each phase though it is more calculation intensive as it solve for additional equations for secondary phase. The K - ϵ conservation equation for per phase turbulence model is given by: -

$$\begin{aligned} & \frac{\partial(\alpha_k \rho_q \bar{U}_q k_q)}{\partial t} \\ & = \nabla \cdot (\alpha_q \frac{\mu_{t,q}}{\sigma_k} \nabla k_q) + (\alpha_q G_{k,q} - \alpha_q \rho_q \epsilon_q) + \sum_{i=1}^n K_{iq} (C_{iq} k_i - C_{qi} k_q) \\ & - \sum_{i=1}^n K_{iq} (\bar{U}_i - \bar{U}_q) \frac{\mu_{t,i}}{\alpha_i \sigma_i} \nabla r_i + \sum_{i=1}^n K_{iq} (\bar{U}_i - \bar{U}_q) \frac{\mu_{t,q}}{\alpha_q \sigma_q} \nabla \alpha_q \end{aligned} \quad \dots (19)$$

The terms C_{iq} and C_{qi} used in the equation (19) can be approximated as: -

$$C_{iq} = 2 \quad \dots (20)$$

$$C_{qi} = 2 \left(\frac{n_{iq}}{1+n_{iq}} \right) \quad \dots (21)$$

The term $\tau_{i,q}$ used in equation (21) is the characteristic time ratio related with the particle dispersion. Finally, turbulent viscosity μ_t can then be calculated using the following equation

$$\mu_t = 0.09 * \rho * \frac{K^2}{\epsilon} \quad \dots (22)$$

3.2.4 Granular Eulerian Model: - The solids stress acting on particles in a dense flow situation is modeled via an additional acceleration in the particle force balance Equation. [103]

$$\frac{du_p}{dt} = F_D(u - u_p) + \frac{g_x(\rho_p - \rho)}{\rho_p} + F_x + F_{interaction} \quad \dots (23)$$

The term $F_{interaction}$ in equation (23) models the additional acceleration acting on a particle, resulting from inter-particle interaction. It is computed from the stress tensor given by the Kinetic Theory of Granular Flows as:

$$F_{interaction} = -\frac{1}{\rho_p} \nabla \cdot \bar{\tau}_s \quad \dots (24)$$

As in a gas, the intensity of velocity fluctuations determines the stresses, viscosity and pressure of the granular phase. The kinetic energy associated with velocity fluctuations is described by a pseudo thermal temperature, known as granular temperature, which is proportional to the norm of particle velocity fluctuations.

The granular temperature of the S_{th} solid phase is proportional to the kinetic energy of the random motion of the particles. The transport equation derived from kinetic theory takes the following form:

$$\frac{3}{2} \frac{\partial(\rho_s \alpha_s \Theta_s)}{\partial(t)} + \nabla \cdot (\rho_s \alpha_s \bar{v}_s \Theta_s) = (P_s \bar{I} + \bar{\tau}_s) : \nabla(\bar{v}_s) + \nabla \cdot (k_{\Theta_s} \nabla(\Theta_s)) - \gamma \Theta_s + \Phi_{ls} \quad \dots (25)$$

Where,

$(P_s \bar{I} + \bar{\tau}_s) : \nabla(\bar{v}_s)$: Generation of energy by the solid stress tensor

$k_{\Theta_s} \nabla(\Theta_s)$: - The diffusion of energy (k_{Θ_s} is the diffusion coefficient)

$\gamma \Theta_s$: - The collisional dissipation of energy

Φ_{ls} : - The energy exchange between the l^{th} fluid phase and s^{th} solid phase.

The diffusional coefficient k_{Θ_s} is given by the equation (26): -

$$k_{\Theta_s} = \frac{15 d_s \rho_s \alpha_s \sqrt{\Theta_s} \pi}{4(41 - 33\eta)} \left[1 + \frac{12}{5} \eta^2 (4n - 3) \alpha_s g_{0,ss} + \frac{16}{15\pi} (41 - 33\eta) \eta \alpha_s g_{0,ss} \right] \quad \dots (26)$$

Where,

$$\eta = \frac{1}{2}(1 + e_{ss}) \quad \dots (27)$$

3.2.5 Energy Conservation: - For energy conservation, the following energy conservation equation is solved for each phase:

$$\begin{aligned} \frac{\partial(\alpha_g \rho_g h_g)}{\partial t} + \nabla \cdot (\alpha_g \rho_g u_g h_g) \\ = -\alpha_g \frac{\partial(P_g)}{\partial t} + \bar{\tau}_g : \nabla(u_g) - \nabla \cdot q_g + S_g + Q_{sg} + S_{sg} h_{sg} + S_{gs} h_{gs} \end{aligned} \quad \dots (28)$$

Here,

- h_g - Specific enthalpy of the gaseous phase.
- q_g : - Heat flux
- S_g : - Source term due to chemical reactions
- Q_{pq} : - Heat transfer intensity between phases p^{th} and q^{th}
- h_{sg} : - Enthalpy at the interface

The rate of heat transfer between phase p and q is assumed to be a function of temperature difference between the two phases: -

$$Q_{pq} = h_{pq} (T_p - T_q) \quad \dots (29)$$

Where,

$$h_{pq} = \frac{6k_p \alpha_q \alpha_p Nu_q}{d_p^2} \quad (\text{assuming convection as main mode of energy transfer}) \quad \dots (30)$$

For the calculation of Nusselt number in case of fluidized bed, Gunn (1978) equation is used which is valid for porosity between (0.35 - 1) and Reynolds number up to 10^5

$$Nu_q (7 - 10\alpha_p + 5\alpha_p^2) \left(1 + 0.7 Re_q^{0.2} Pr^{\frac{1}{3}}\right) + (1.33 - 2.4\alpha_p + 1.2\alpha_p^2) Re_q^{0.7} Pr^{\frac{1}{3}} \quad \dots (31)$$

In the above equation, the phase q^{th} Prandtl number Pr and the Reynolds number Re_q defined by the following equations: -

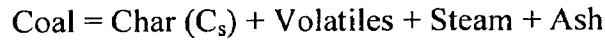
$$Pr = \frac{(C_p)_p \mu_p}{k_p} \quad \dots (32)$$

$$Re = \frac{\rho_l d_p (\bar{v}_q - \bar{v}_l)}{\mu_l} \quad \dots (33)$$

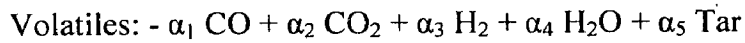
Where,

$(C_p)_p$ is the heat capacity of phase q_{th} at constant pressure.

3.2.6 Chemical Reactions: - In this work, coal drying and volatilization reactions are assumed to occur instantly once the fuel enters the feed zone [17, 145]. Therefore, char, volatiles, ash and steam are formed according to the following equation:



For coal volatilization, the chemical reaction proposed in the ANSYS Euler granular tutorial was used:



These coefficients α_i will be calculated using correlation of Weimer and Clough [135] for the chemical species distribution of the volatile matter. This correlation is shown below: -

$$\text{H}_2 = 0.157 - 0.868 X + 1.338 X^2$$

$$\text{CO}_2 = 0.135 - 0.9 X + 0.196 X^2$$

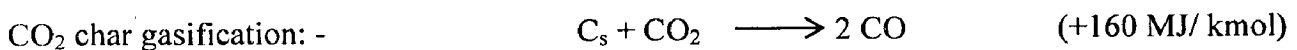
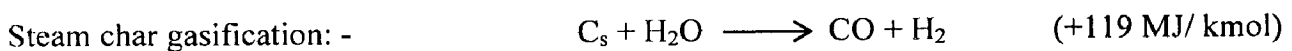
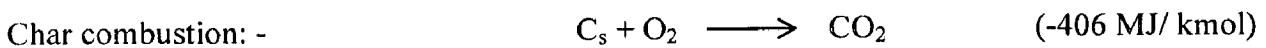
$$\text{CO} = 0.425 - 2.653 X + 1.906 X^2$$

$$\text{H}_2\text{O} = 0.409 - 2.389 X + 4.554 X^2$$

$$\text{Tar} = 0.325 - 7.279 X + 880 X^2 - 12$$

Where, X is the mass fraction of the coal volatile matter in dry / ash free basis.

Char Combustion & Gasification: - For the char (C_s) combustion & Gasification, the chemical model of Weimer & Clough (1981) involving the following heterogeneous chemical reactions is used: -



These heterogeneous reactions between char and gases (O_2 , H_2O , and CO_2) can be described by different reaction mechanisms which take account for possible diffusion effect or further

simplified by kinetic model. Souza-Santos [30] and Chejne and Hernandez [17] used the unreacted core model to combine reaction with diffusion resistance. In Eaton and Smoot's review [39], they presented char oxidation model based on measured intrinsic char kinetic rates and a pore diffusion model.

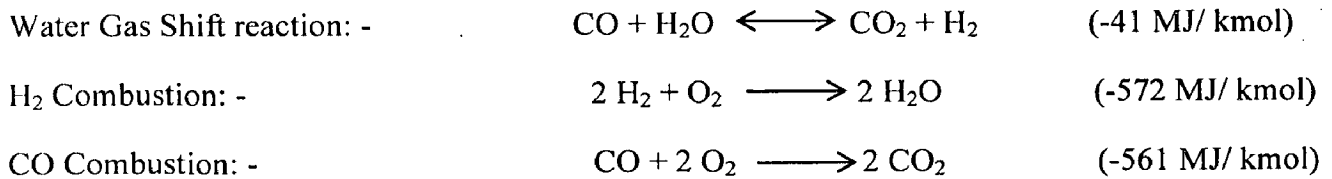
Chen et al. (2000) assumed that the oxygen, carbon dioxide and steam react with char on the char particle surface and the value for reaction order was 0.5. In this study, it is assumed that the char particle is a spherical particle surrounded by a stagnant boundary layer through which gas species must diffuse before they react with the char.

In fluid flows controlled by turbulent fluctuations, chemical kinetics does not play an explicit role in the calculation of homogeneous reaction-rates and these are assumed to be controlled by the turbulent mixing rate Yu et al. (2007). Based on the work of Magnussen and Hjertager (1976), the Eddy Dissipation Model (EDM) was used. In this model, the overall char reaction rate of a particle is controlled by the smaller value of the two rates i.e. diffusion rate and kinetic rate. The kinetic equations of the homogeneous reactions with their Arrhenius parameters are given in Table 3.1.

Table 3.1: - Arrhenius parameters of heterogeneous reactions

Arrhenius kinetics for heterogeneous reactions		
Reactions	Equations	Units
$C_s + O_2 \longrightarrow CO_2$	$K = 17.9 \exp[-13750/T_s]$	$Pa^{-1}s^{-1}$
$C_s + H_2O \longrightarrow CO + H_2$	$K = 0.0000595 \exp[-13650/T_s]$	$Pa^{-1}s^{-1}$
$C_s + CO_2 \longrightarrow 2 CO$	$K = 3.92 \exp[-26927/T_s]$	$Pa^{-1}s^{-1}$

Homogeneous Reactions: - The following homogeneous reactions proposed by Weimer and Clough (1981) [2] is used for modeling the gasifier: -



For homogeneous reactions, it is convenient to use the work of Souza- Santos [30] and Chejne's [17], summarized in Table 3.2.

Table 3.2: - Kinetics of homogeneous reactions

Arrhenius Kinetics of the homogeneous reactions		
Chemical Reactions	Equations (Kg m ⁻³ s ⁻¹)	Arrhenius Equation
CO + H ₂ O → CO ₂ + H ₂	R = K [Y _{CO} Y _{H₂O}]	K = 2780 exp [-1510/ T _g]
CO ₂ + H ₂ → CO + H ₂ O	R = K [Y _{CO₂} Y _{H₂}]	K = 0.0265 exp [3968/ T _g]
2 H ₂ + O ₂ → 2 H ₂ O	R = K/ T _g ^{1.5} [Y _{H₂} ^{1.5} Y _{O₂} ρ _g ^{2.5}]	K = 5.159 * 10 ¹⁵ exp [-3430/ T _g]
CO + 2 O ₂ → 2 CO ₂	R = K [Y _{CO} Y _{O₂} ^{0.5} ρ _g ^{1.5}]	K = 1* 10 ¹⁵ exp [-16000/ T _g]

3.2.7 Species transport equations: -

In the gasifier model, the gas phase is assumed as a mixture of 6 species (CO, CO₂, H₂, N₂, O₂ and H₂O). The conservation equation for these species except N₂ is assumed of the following form: -

$$\frac{\partial (r_g \rho_g Y_{g,i})}{\partial t} + \nabla (r_g \rho_g u_g Y_{g,i}) = -\nabla \cdot r_g J_{g,i} + r_g R_{g,i} + R_{s,i} \quad \dots (34)$$

Here,

$J_{g,i}$ – Diffusion flux of species i in gas phase

$R_{g,i}$ – Net rate of production of homogeneous species i

$R_{s,i}$ – Heterogeneous reaction rate

The diffusion flux of chemical species in gas phase is calculated using Fick's law: -

$$J_{g,i} = -\left(\rho_g D_{m,i} + \frac{\mu_t}{\sigma_Y}\right) \nabla \cdot Y_{g,i} \quad (\sigma_Y - Schmidt No. = 0.7) [145] \quad \dots (35)$$

The diffusion coefficient of the mixture $D_{m,i}$ is calculated using binary mass diffusion coefficient, $D_{m,i}$ as follows: -

$$D_{m,i} = \frac{1 - X_i}{\sum_{j \neq i} \frac{X_j}{D_{i,j}}} \quad \dots (36)$$

CHAPTER- 4

PROBLEM DESCRIPTION & SOLUTION TECHNIQUES

In this work, a CFD model of the bubbling fluidized bed gasifier pilot plant facility has been developed using ANSYS 12. A sequence of various steps employed in modeling and simulation of bubbling fluidized bed pilot plant gasifier is shown in Fig. 4.1. Gasifier selection has been discussed in Chapter 2. The selection of multiphase models is discussed in Chapter 3. In this chapter, we will discuss the gasifier geometry, meshing, fluent set up and solution technique used for the simulations.

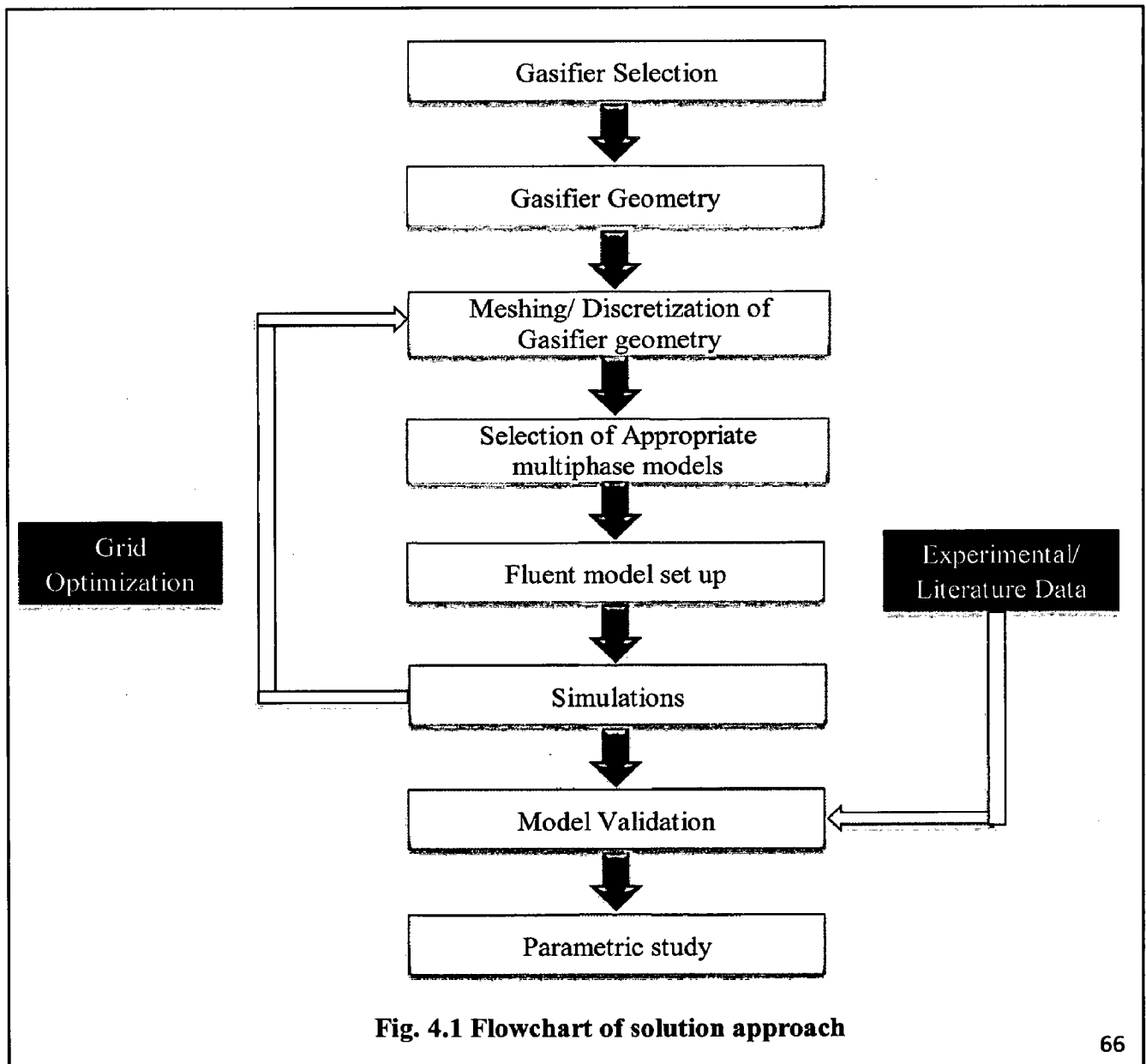


Fig. 4.1 Flowchart of solution approach

4.1 GEOMETRY

The bubbling fluidized bed pilot plant gasifier is 4 m height and has a diameter of 100 mm in the bed zone and 150 mm in the freeboard zone. The diameter of the coal inlet section is equal to 40 mm while that of pressure outlet is equal to 50 mm.

4.1.1 3D Geometry in Ansys design modular: - For the CFD modeling of the bubbling fluidized bed gasifier, a 3D geometry of the gasifier was first generated in Ansys 12 workbench which has integrated design modular for making the geometry as well as meshing the same.

The steps involved in generating the 3D geometry is as follows: -

- a) First, I selected ZX plane and created a new sketch in that plane. Then, I went to the sketching tab and selected the settings tab where I enabled the show grid option and snap option as shown in Fig. 4.2 to take care of the correct dimensions.

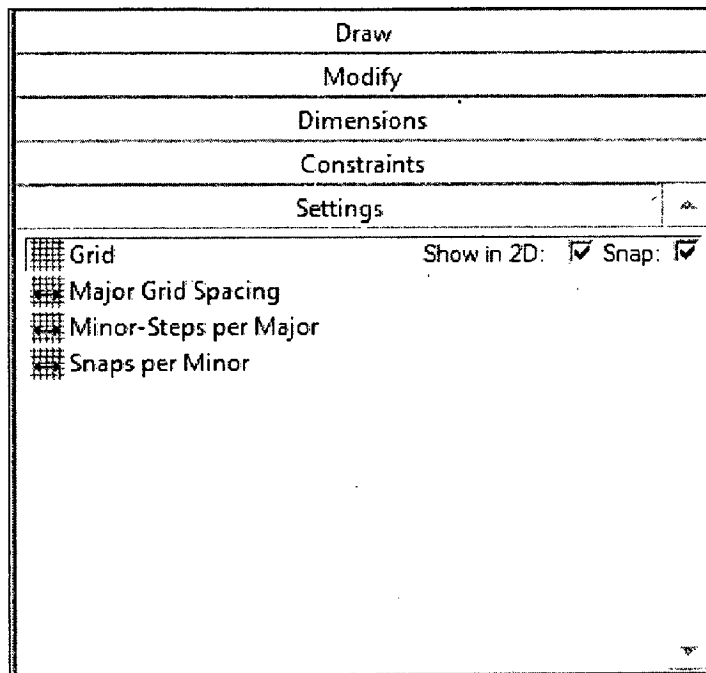


Fig. 4.2 Sketching panel of Ansys design modular

- b) Then, I selected the draw tab of the sketching panel shown in Fig. 4.2 and selected polyline to generate a closed loop sketch on ZX plane as shown in Fig. 4.3.
- c) This closed loop sketch was then revolved around z axis to generate the central geometry of the bubbling fluidized bed pilot plant shown in Fig. 4.4

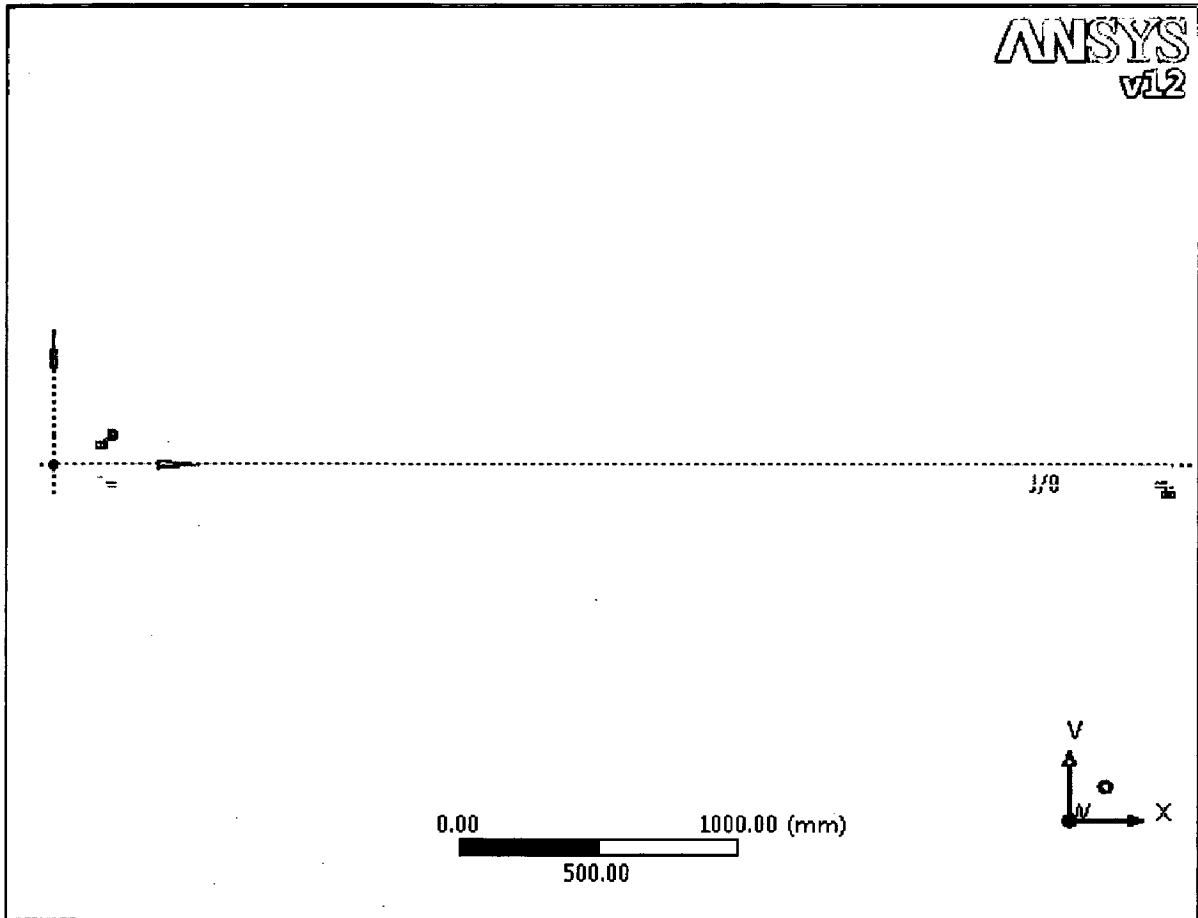


Fig. 4.3: Closed loop sketch in the ZX plane generated using polyline

- d) The next step was to add coal inlet and syngas outlet. For this purpose, two new rectangular sketches were drawn in ZX plane as shown in Fig. 4.5 (a) & 4.5 (b). For coal inlet, a tilted rectangle with an inclination of 45° was drawn while for pressure outlet, a straight rectangle was drawn.
- e) These two rectangles were revolved around their inner edges using command Revolve3 and Revolve7.
- f) In the revolve details, tab shown in Fig. 4.6 “Add material” operation was selected to join these inlets with the central body and form a continuous geometry.

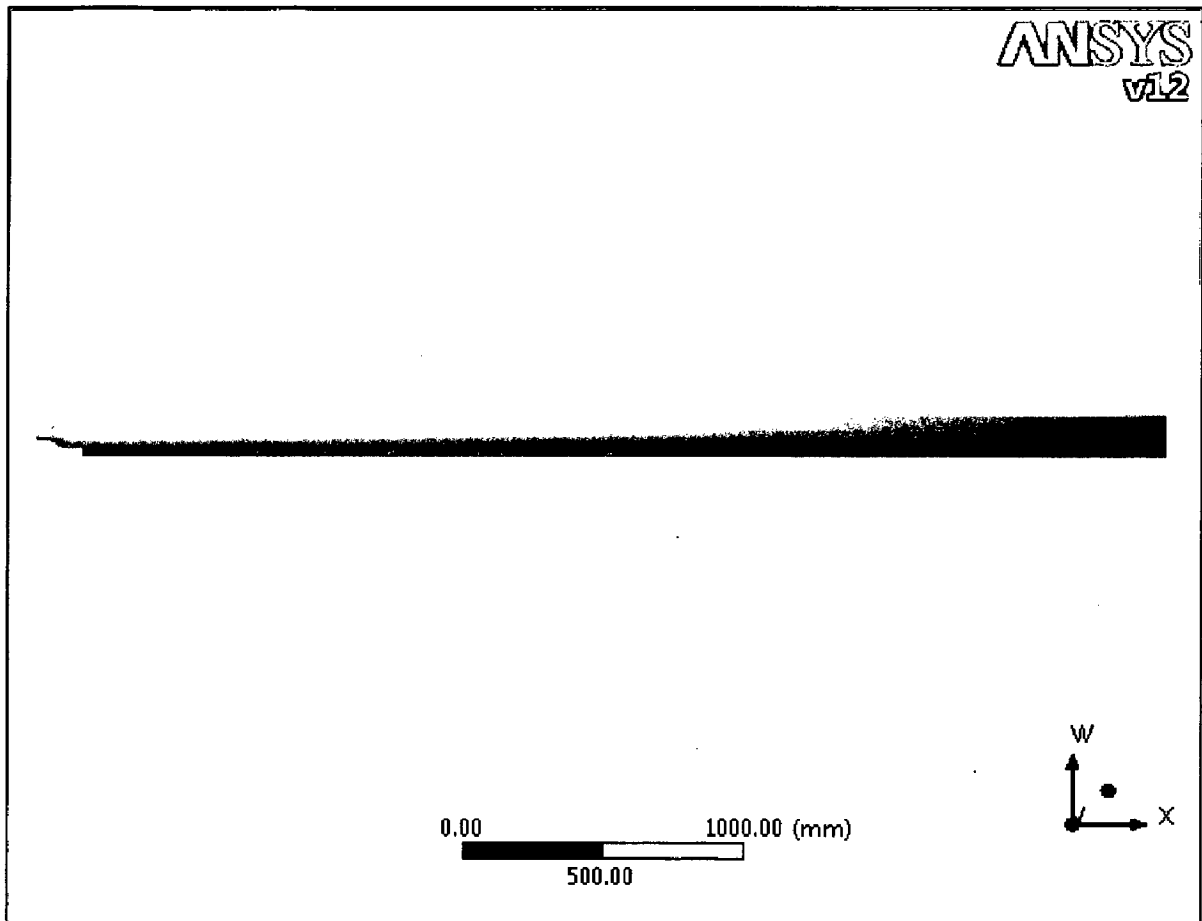


Fig. 4.4: Central body of the BFBG geometry obtained after Revolve1 operation

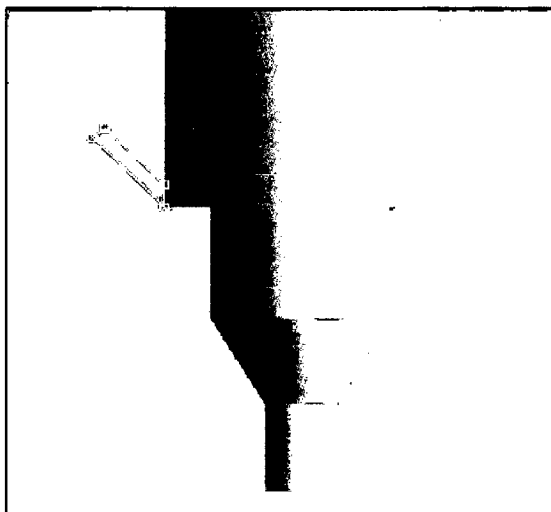


Fig. 4.5 (a): Sketch for coal inlet-

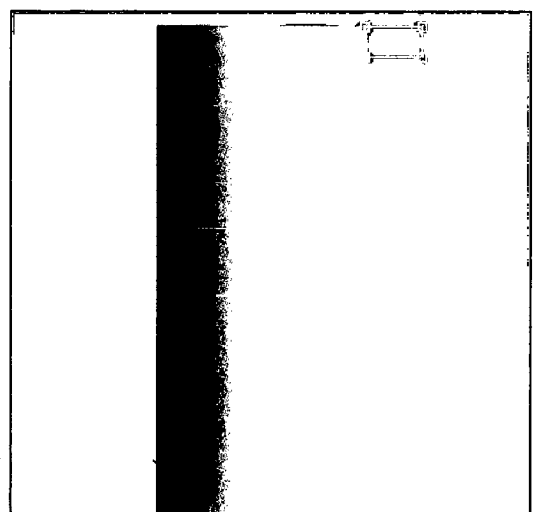


Fig. 4.5 (b): Sketch for syngas

Fig. 4.5 Rectangular sketches for coal inlet and syngas outlet

g) The complete geometry of bubbling fluidized bed gasifier pilot plant obtained after performing the above operations is shown in Fig. 4.7.

Details of Revolve8	
Revolve	Revolve8
Base Object	Sketch5
APC	Apply Cancel
Operation	Add Material
Direction	Normal
<input type="checkbox"/> FD1, Angle (>0)	360 °
As Thin/Surface?	No
Merge Topology?	Yes

Fig. 4.6: Details of Revolve8 (Add material operation)

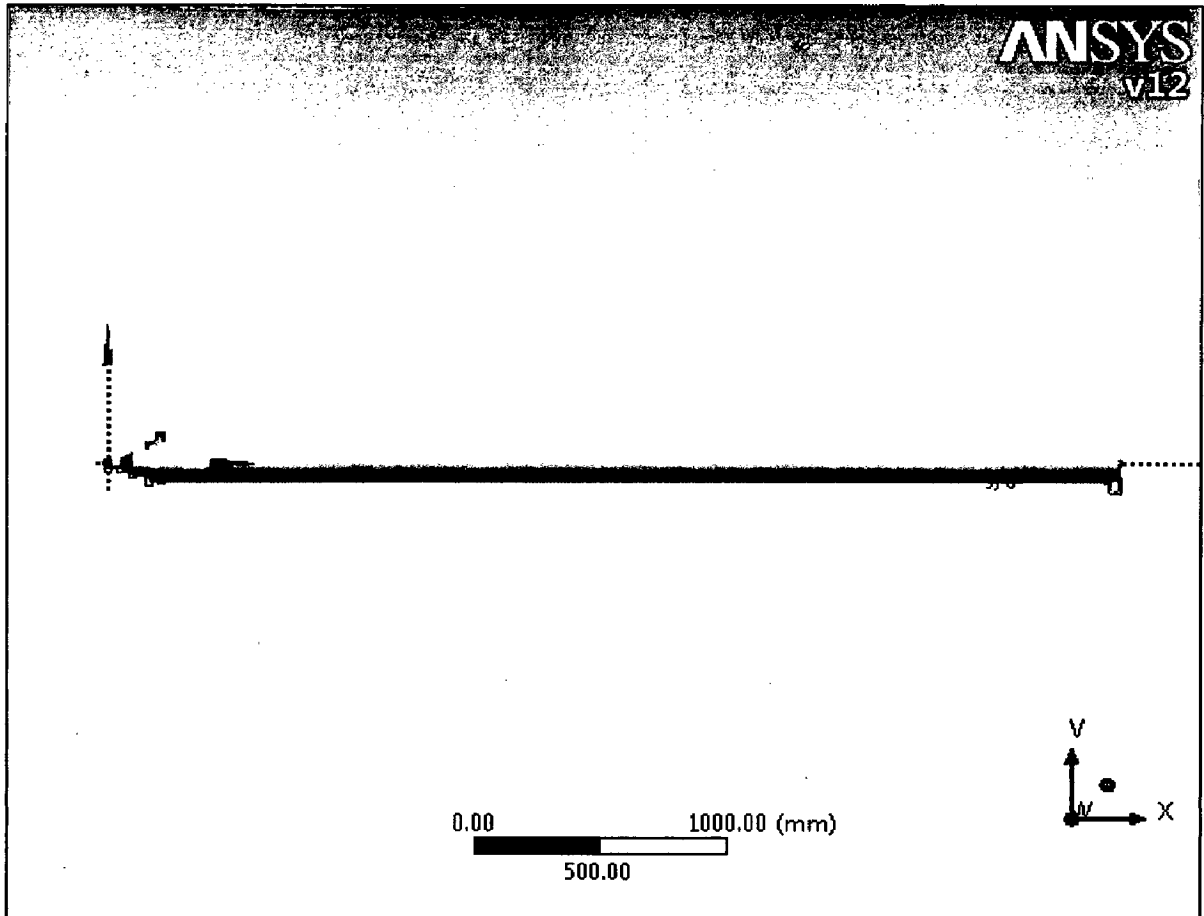


Fig. 4.7: 3D geometry of bubbling fluidized bed gasifier

A closer view of the coal inlet section and syngas outlet section is shown in Fig. 4.8 (a) and 4.8 (b).

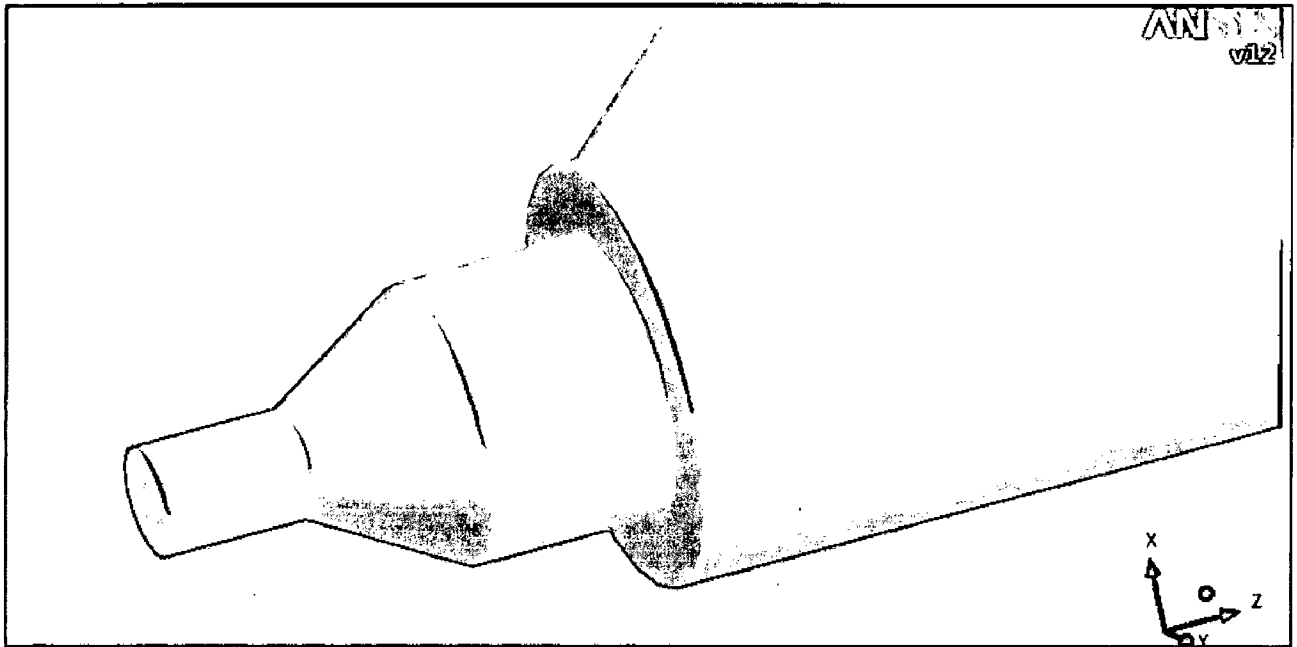


Fig. 4.8 (a): A closer view of coal inlet section

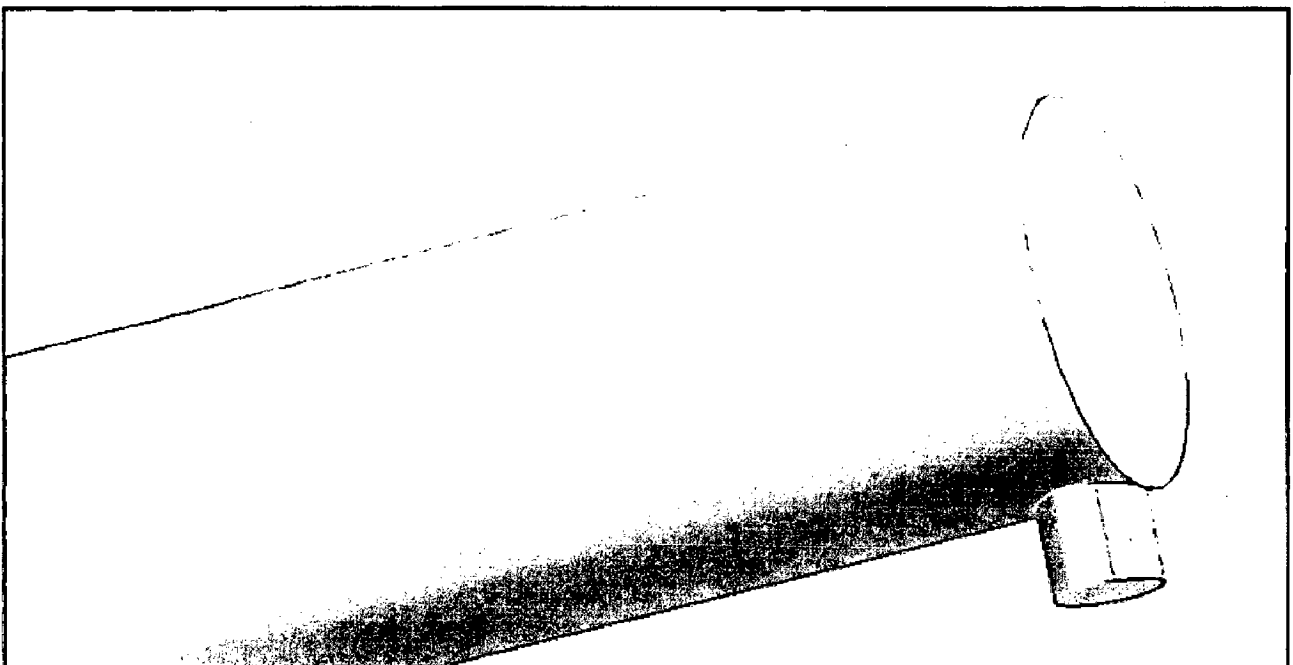


Fig. 4.8 (b): A closer view of syngas outlet section

4.1.2 2D geometry in Gambit: - From the 3D geometry, we can see that the bubbling fluidized bed gasifier has symmetry across the z- x plane. Also, from preliminary study with 3D geometry, we observed that 3D simulation is very time intensive. Therefore, to save the computational time, we decided to take a 2D section of the gasifier along the z- x plane for simulation purpose.

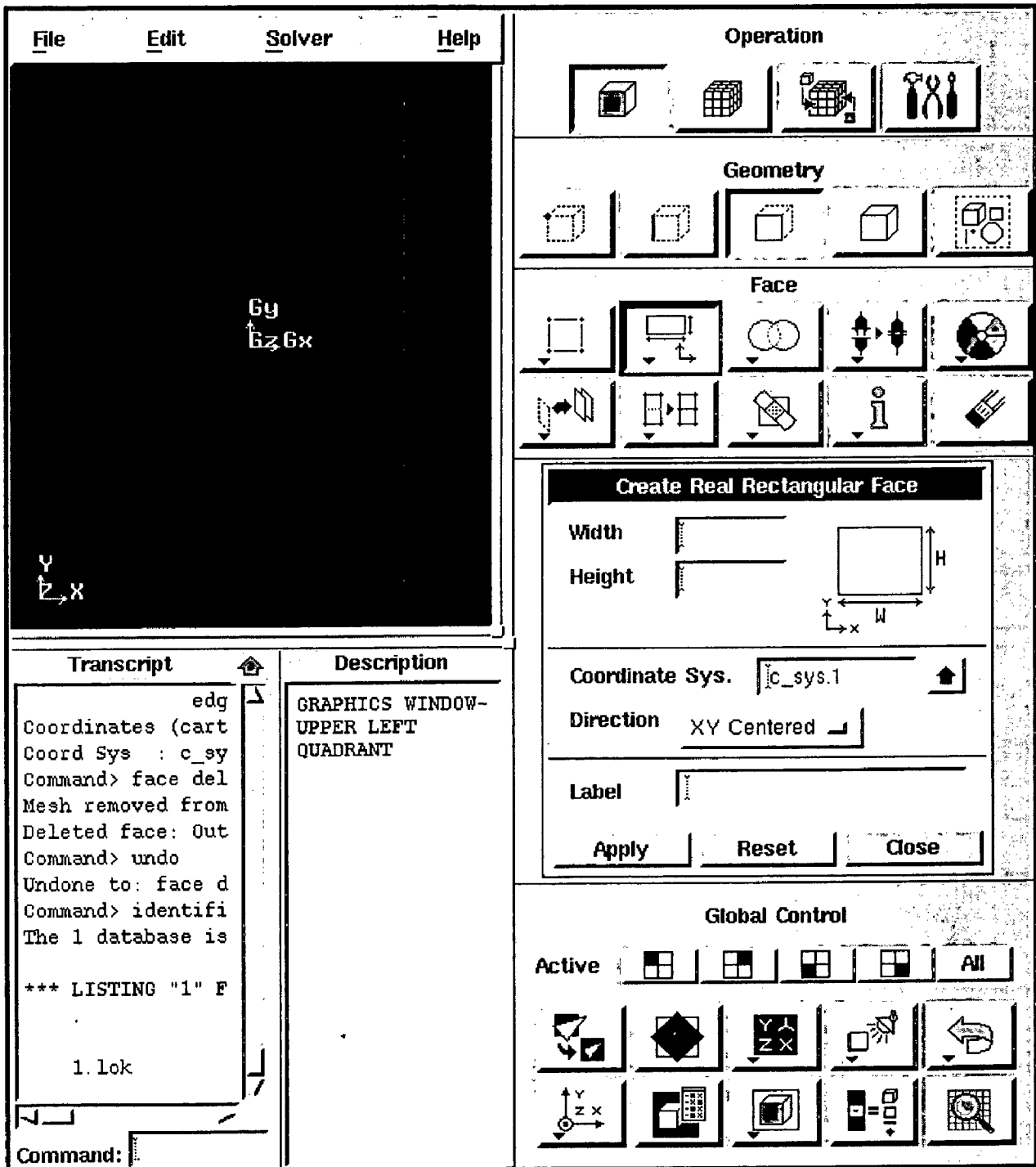


Fig. 4.9: Gambit user interface used for generating 2D

The geometry for the 2D section was generated in Gambit. The Gambit user interface is shown in Fig. 4.9. The steps used for generating the geometry are as follows: -

- a) The first step to create 2 D geometry was to use “create real rectangular faces” option inside face tab to create 4 different rectangular faces shown in Fig. 4.10. These faces include: -
 - a. Freeboard zone
 - b. Bed zone
 - c. Ash outlet Zone
 - d. Pressure outlet zone

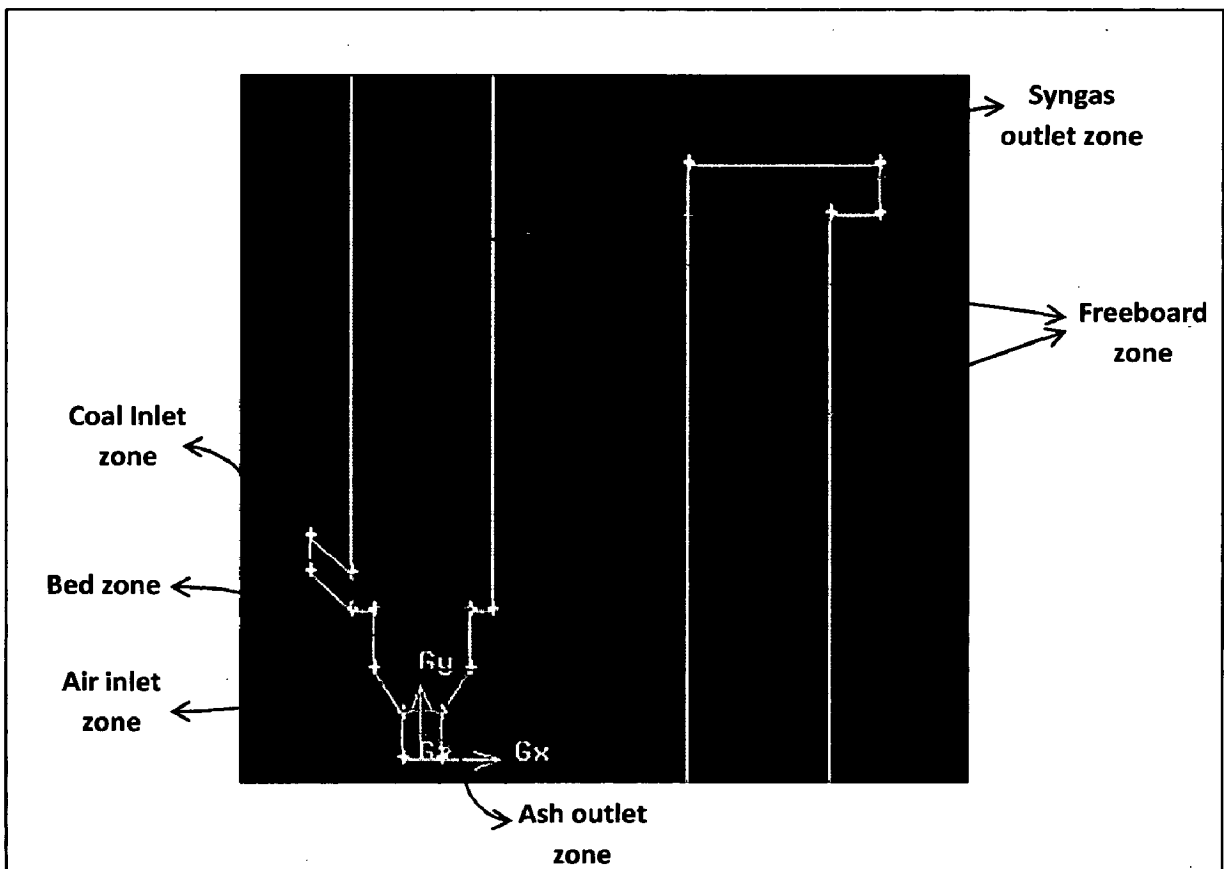


Fig. 4.10: Generating 2D geometry in Gambit

- b) The remaining two zones namely coal inlet and air inlet are not rectangular in shape. Therefore, for generating these zones, we first marked the points. The points were joined to form edges which in turn were joined to form their respective zones.
- c) The different zones forms were then merged using “merge faces” option available under face tab to obtain the final geometry as shown in Fig. 4.11.

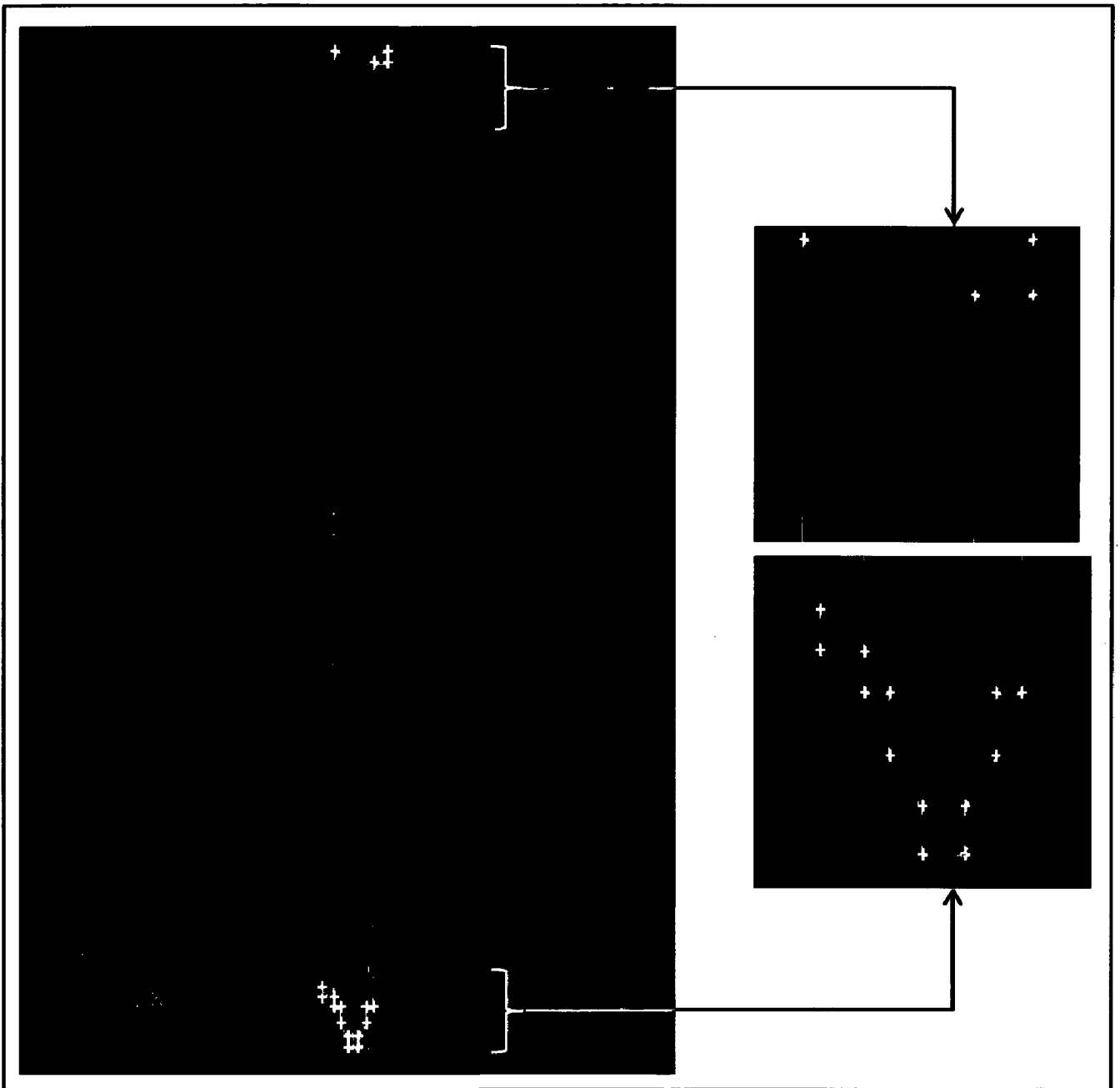


Fig. 4.11: Geometry of 2D section of bubbling fluidized bed gasifier

4.2 Meshing

4.2.1 Edge & Face meshing: - Once the geometry was created, the next step was to go for discretization (meshing). For this purpose, first we selected the edge meshing option from the mesh tab shown in Fig. 4.12. The edge meshing was done with three interval size: -

- a) Case 1: - 2 cm interval size
- b) Case 2: - 1.5 cm interval size

- c) Case 3: - 1 cm interval size
- d) Case 4: - 0.5 cm interval size

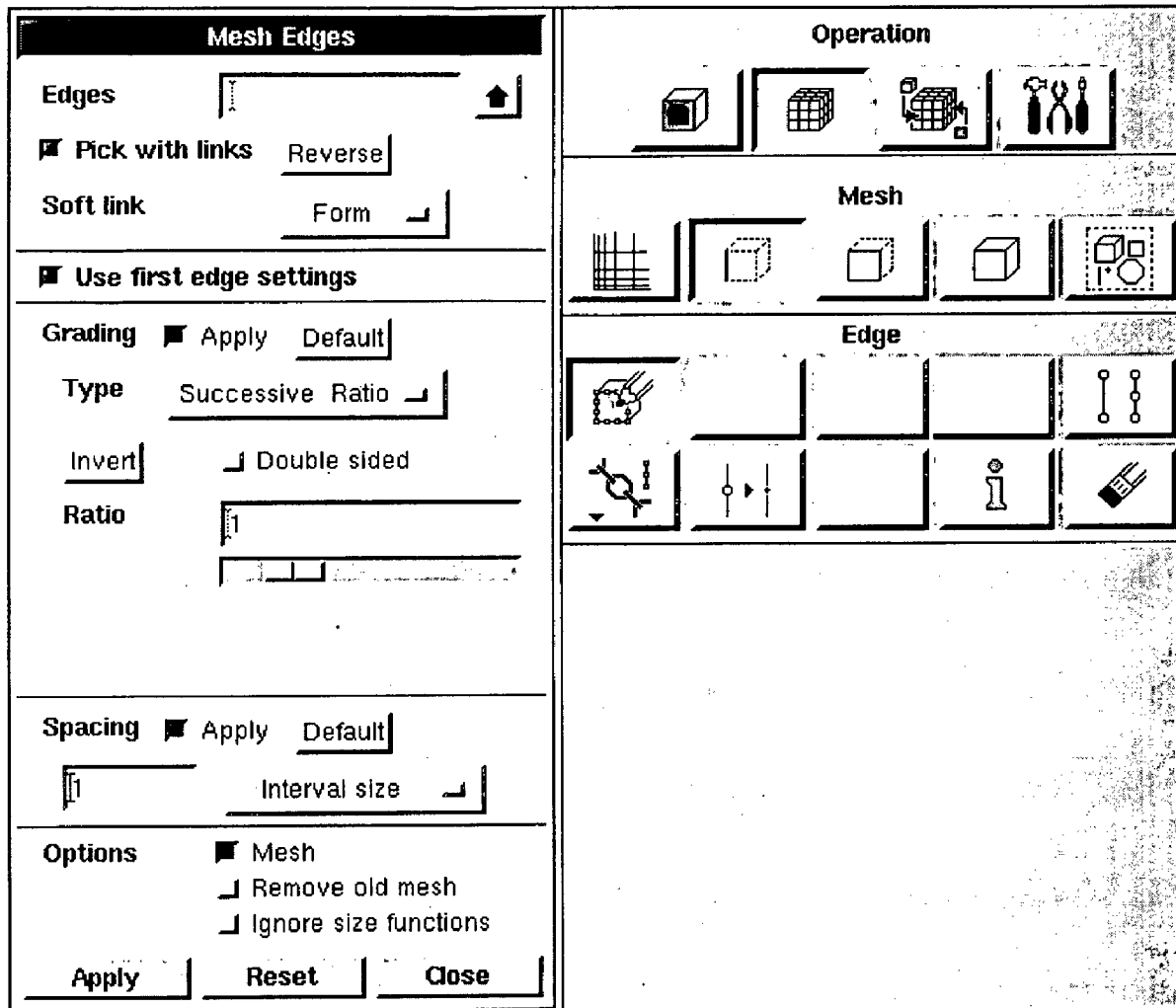


Fig. 4.12 Edge meshing in Gambit

After edge meshing, the face meshing tab was selected and face meshing was done using quad elements with type "pave". The final meshed geometry is shown in Fig. 4.13 along with original bubbling fluidized bed gasifier pilot plant. Four different meshes were obtained in four cases with details given in Table 4.1

Table 4.1 Mesh size info for three cases

Case	Grid Size	Cells	Faces
1	0.5 cm	23685	48218
2	1 cm	6713	13903
3	1.5 cm	2633	5548
4	2 cm	1512	3237

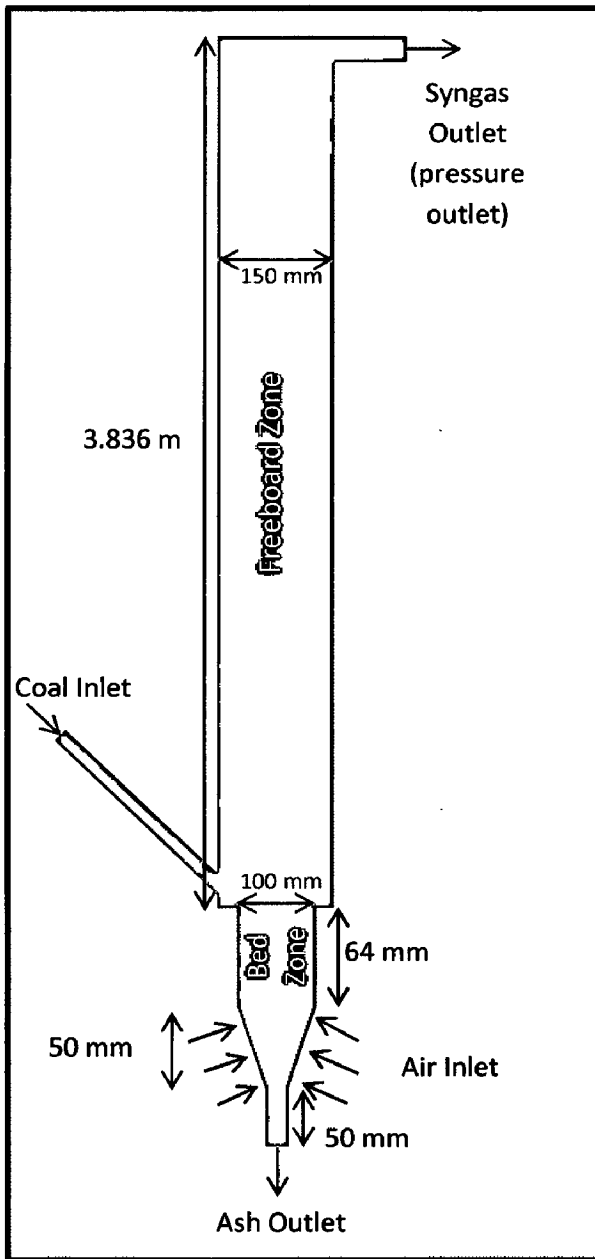


Fig. 4.13 (a)



Fig. 4.13 (b)

Fig. 4.13: Experimental setup and FLUENT Gasifier geometry (a) Flow sheet of the pilot scale BFBG set up at CIFR Dhanbad, (b) Model geometry generated in Gambit.

4.2.2 Boundary conditions: - Mesh generation was followed by assigning boundary condition types to the inlet and outlet boundaries. The coal and air inlet were defined as mass flow inlet while syngas and ash outlet were defined as pressure outlet. The rest of the edges were defined as wall and the interior continuum was defined as fluid. Fig. 4.14 gives a snapshot of boundary type assigned in Gambit.

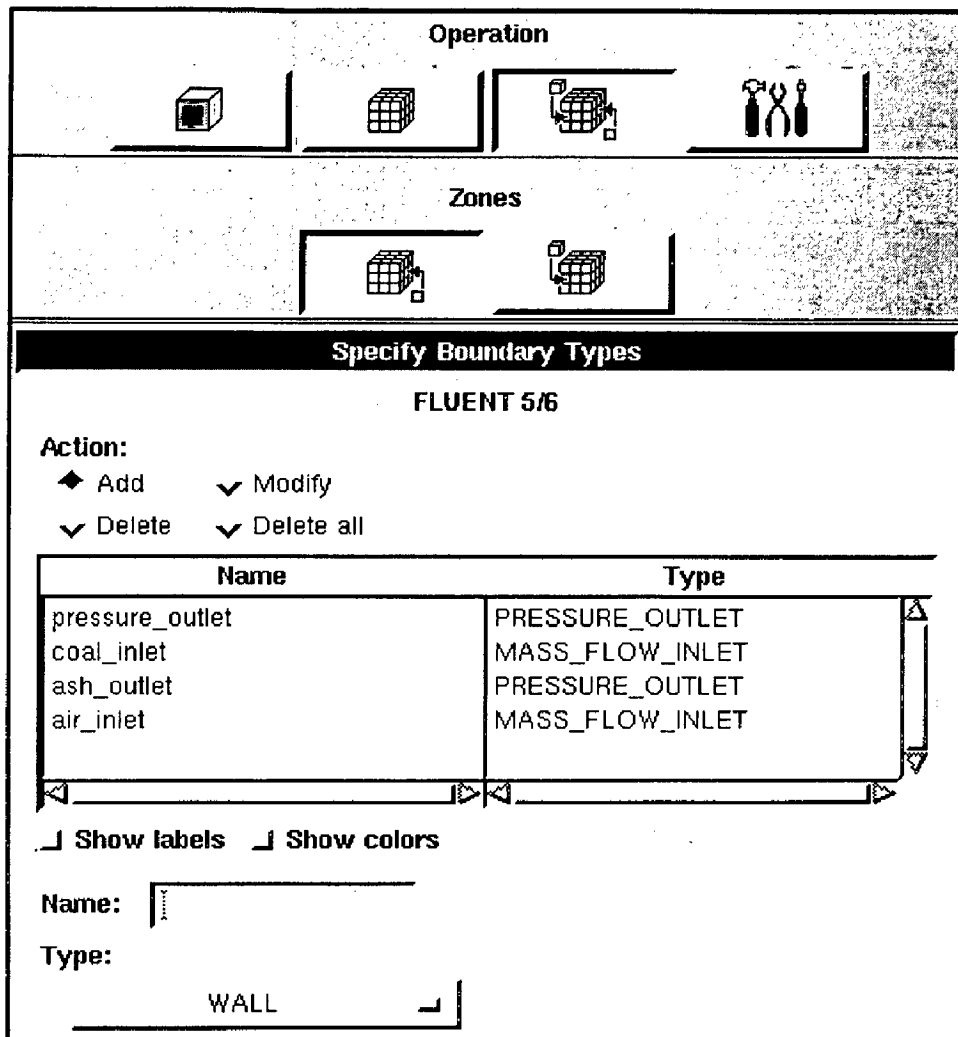


Fig. 4.14: Boundary condition types assigned in Gambit

4.2.3 Grid Optimization: - Grid optimization/ grid independency test is the most significant step in CFD modeling. The results obtained from the model should be independent of the grid size. For this purpose, we generate grids with different mesh sizes and perform simulations with them using same operating and boundary conditions in FLUENT. The simulation results are then compared for some key parameters like temperature or pressure drop to see their variation with grid size.

Initially, the results improve significantly with grid size at the cost of computational time. However, the variation slowly diminishes and after a particular step size, the variation on further refinement becomes so less that investing further computational time appears irrational. At that step size, the grid is said to be optimized and the same grid is used for further simulations, validations and parametric studies.

In my case, I generated four different face meshes from the four cases with grid details given in Table 4.1. These meshes were used for the grid optimization study by performing the simulations for each case. For this purpose, I used temperature & CO prediction as the deciding parameter as most of the gasification reactions are reversible in nature and their extent will depend primarily on operating temperature of the gasifier. Also, CO is the most important components of syngas. Therefore, I have considered their mole fraction as well for the grid optimization purpose. Fig. 4.15 gives the variation of temperature, CO & H₂ mole fraction with grid size.

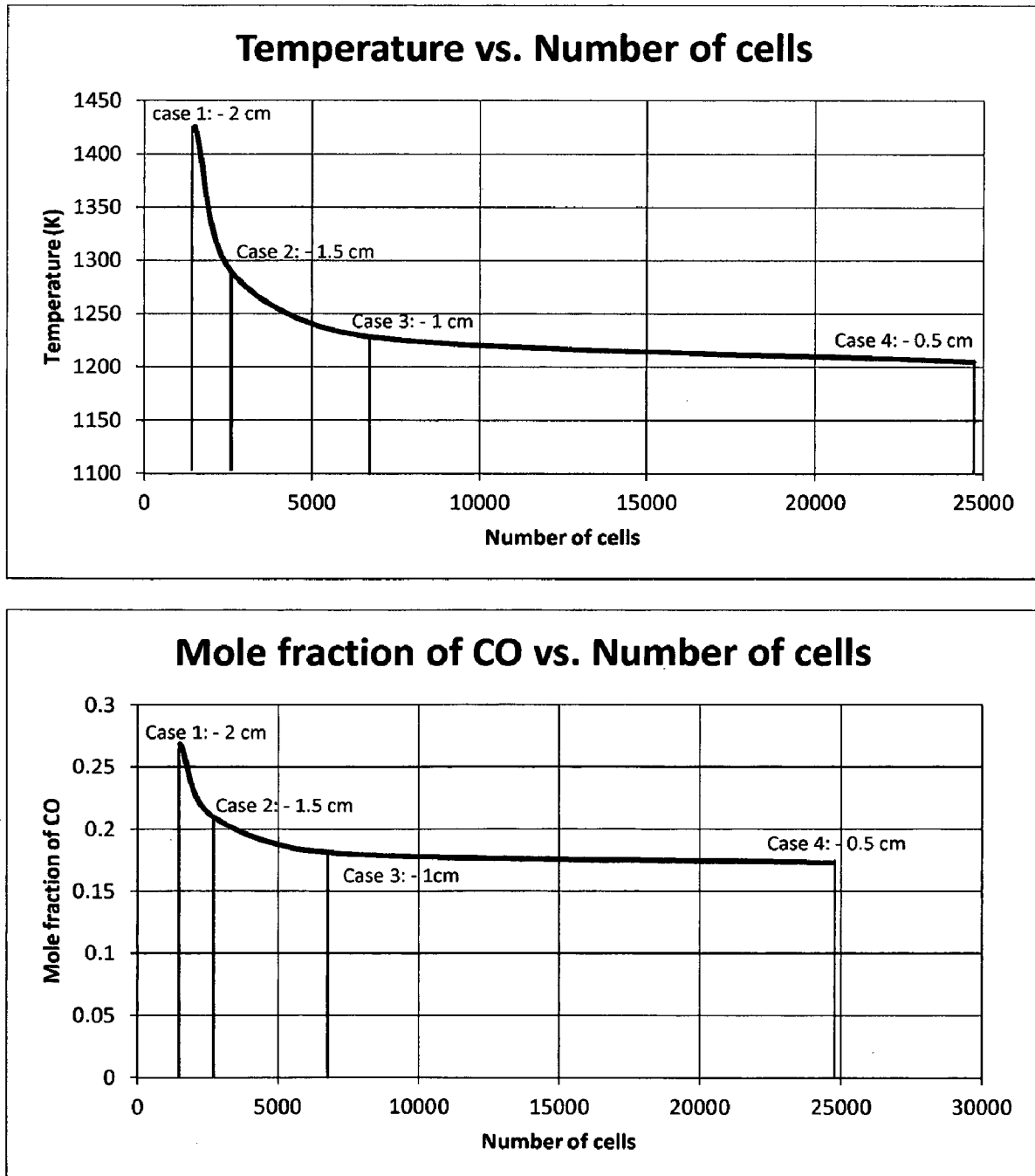


Fig. 4.15: Variation of Temperature & CO mole fraction with Number of cells (Grid optimization)

From Fig. 4.15, it is evident that there is sharp change in temperature prediction as well as CO mole fraction prediction on moving from Case 1 to Case 2, and from Case 2 to Case 3. However, when we change the mesh size from Case 3 to Case 4, the change in Temperature prediction and CO mole fraction prediction is comparatively very low but the numbers of cells and hence the computational time increases significantly. Table 4.2 gives a comparative study of the three transitions.

Table 4.2: Comparative study of case transitions

	$\Delta T_{\text{prediction}}$	$\Delta M_{\text{CO, prediction}}$	ΔN_{cells}
Case 1 to Case 2	138.0056	0.0579	1121
Case 2 to Case 3	59.51995	0.0294	4080
Case 3 to Case 4	23.45274	0.0083	16972

From Table 4.2, it is clear that transition from phase Case 1 to Case 2 is feasible and so is from Case 2 to Case 3. However, the transition from Case 3 to Case 4 is not economical on economics of time. Therefore, Case 3 represents the optimum grid and therefore has been used for all the further studies of bubbling fluidized bed gasifier pilot plant.

4.3 Fluent Model Set up

The model geometry for the CIMFR bubbling fluidized bed gasifier pilot plant was created in Gambit and discretized with 6713 quadrilateral cells. The mesh file was then imported in FLUENT for model set up.

4.3.1 Mesh Quality: - The first step was to check the quality of the mesh for cell squish and aspect ratio. Table 9.1 gives the output of the mesh check along with its quality. The orthogonal quality varies between 0 and 1 where, '0' corresponds to low quality.

Table 4.3 Results of mesh quality check

Mesh Quality		
	Basic Model	CIMFR Model
Maximum Cell Squish	0.375	0.363
Minimum orthogonal quality	0.625	0.637
Maximum aspect ratio	4.8	2.6

4.3.2 Solver Preferences: - From Table 4.3, it is evident that generated mesh is of good quality. The next step involves selecting the appropriate solver preferences. Table 4.4 shows the characteristics of solver used in this simulation.

Table 4.4 Characteristics of solver

Characteristics	Value	
Solver		
Pressure Based	Enable	
Formulation	Implicit	
Space	2 D	
Velocity Formulation	Absolute	
Porous Formulation	Superficial Velocity	
Time	Transient	
Solution Controls		
Transient Formulation	First order Upwind	
Gradient Option	Green Gauss Cell Based	
Pressure- Velocity Coupling	Phase Coupled Simple	
Discretization (for all conservation equations)	First Order Upwind	
Under- Relaxation Factors	Pressure	0.25
	Density	0.8
	Body Forces	0.8
	Momentum	0.6
	Volume Fraction	0.4
	Turbulent Kinetic Energy/ Dissipation rate	0.6
	Turbulent Viscosity	0.8
	Energy	0.9

4.3.3 Models: - In this section appropriate model for hydrodynamics, turbulence and species transport was selected to introduce the physics of bubbling fluidized bed gasifier in our geometry. Table 4.5 provides a summary of different models used in our simulation [15, 97, 135, and 145]: -

Table 4.5 Model selection for bubbling fluidized bed gasifier

Models		
Multiphase	Model	Eulerian
	No. of Phases	2
	Scheme	Implicit
Energy Equation	Enabled	
Viscous	Model	Standard K - ϵ
	Near wall treatment	Std. wall function

	Turbulence multiphase	Per phase Model
Viscous Model constants	cmu	0.09
	C1 Epsilon	1.44
	C2 Epsilon	1.92
	C3 Epsilon	1.3
	TKE prandtl no.	1
	TDR prandtl no.	1.3
	Dispersion prandtl no.	0.75
	Energy prandtl no.	0.85
	Wall prandtl no.	0.85
	Turbulent Schmidt number	0.7
Species	Model	Species Transport
	Reactions	Volumetric
	Turbulence-Chemistry Interaction	Finite rate / Eddy Dissipation

4.3.4 Materials: - The materials solid carbon, hydrogen, nitrogen, carbon monoxide, carbon dioxide, oxygen, air, water (liquid) and water vapor are taken from the fluent database while ash, tar and volatiles have been introduced into the model by properties input. The properties of these materials are given in Table 4.8 for reference [97]. Two mixture templates were created namely:

- a) Mixture gas: - All the gaseous materials like hydrogen, nitrogen, carbon monoxide, carbon dioxide, oxygen, air, water vapor are taken in mixture template -1
- b) Mixture coal: - It comprises of carbon solid, water (liquid), volatiles and ash. The composition of this template was defined according to the proximate analysis of coal samples as given in Table 4.6

Table 4.6 Properties of coal feedstock

	Eastern Coal Field (RajMahal area)	Literature
	(Obtained from CIMFR, Dhanbad)	Liang et al. 2006
Proximate Analysis		
Mineral Matter	48.9 %	1.5 %
Moisture	7.1 %	2.6 %
Volatile Matter	20.4 %	41.8 %
Fixed Carbon	23.6 %	54.1 %

Ultimate Analysis		
Carbon	30.82 %	75.3 %
Hydrogen	1.9 %	5.4 %
Nitrogen	0.6 %	1.8 %
Oxygen	5.55 %	15.6 %
Sulfur	0.24 %	0.4 %
Other Properties		
Mean particle diameter	0.62 mm	0.62 mm
Density	1250 Kg/ m ³	1250 Kg/ m ³
High heating value	2670 Kcal/ kg	7070 Kcal/ Kg

All the homogeneous reactions were considered to occur in mixture gas while the heterogeneous reactions were considered to occur between mixture coal and mixture gas.

4.3.5 Phases: - All the species were defined in the fluid state. There are two phases in this model. The first phase or primary phase is the gas phase consisting of all the gaseous species introduced through mixture template -1. All the homogeneous reactions take place in the primary phase and their kinetics is governed by eddy dissipation model/ Arrhenius kinetics [Table 4.7].

The second or secondary phase consists of four solid species namely solid carbon, volatiles, ash and water (liquid). These are modeled using kinetic theory of granular flows. The maximum particle packing for phase 2 was taken as $r_{s, \max} = 0.64$ to prevent the spacing between particles from decreasing to zero [40]. This was done maintain the fluidization of the bed. The following table gives the various sub-models selected for the same: -

Table 4.7 Granular parameters for secondary phase

Granular Phase Parameters	
Granular	Enabled
Granular temperature model	Phase property
Diameter	2 mm
Granular viscosity	Syamlal - Obrien
Granular bulk viscosity	Lun-et-al.
Frictional viscosity	Schaffer
Solid Pressure	Syamlal - Obrien
Radial Distribution	Syamlal - Obrien

Table 4.8 Material properties used in FLUENT

Properties Species	Density (kg/m ³)	Specific heat Cp (J/kg-k)	Thermal Conductivity k (w/m-k)	Viscosity (kg/m-s)	Molecular Weight (kg/kgmol)	Standard State Enthalpy (j/kgmol)	Standard State Entropy (j/kg mol-k)	Reference Temperature (K)
Combustible Particle	Different for Different samples	2092	0.0454	1.72 e-05	12.0111	0	5731.7471	298
Volatile	1000	2092	0.0454	1.72 e-05	56.168	-18859000	0	298
Ash coal	1500	2092	0.0454	1.72 e-05	120	0	210058.3	298
Tar	1000	1200	0.1	0.001	144	331176	0	298
Carbon monoxide(CO)	1.123	1043	0.025	1.75 e-05	28.010	-1.105 e+08	197531.64	298
Carbon dioxide(CO ₂)	1.788	840.37	0.0145	1.37 e-05	44.010	-3.93 e+08	213720.2	298
Hydrogen (H ₂)	0.08189	14283	0.1672	8.41 e-06	2.016	0	130579.06	298
Water (h ₂ O)	998.2	4182	0.6	0.0010	18.0152	-2.85 e+08	69902.211	298
Water vapor	0.5542	2014	0.0261	1.34 e-05	18.0152	-2.42 e+08	188696.4	298

4.3.6 Phase interaction: - Phase interaction between the two phases was modeled using drag, interphase heat transfer, mass transfer and heterogeneous chemical reaction. The following models were used for this purpose: -

- a) Drag: - Syamlal – O'Brien
- b) Heat: - Gunn
- c) Mass: - Cavitation (check)
- d) Heterogeneous reaction: - Arrhenius kinetics (UDF)/ Diffusion kinetics

The Arrhenius parameters for heterogeneous reactions is given in Table 7.1

4.3.7 Operating & boundary condition: - The operating & boundary conditions for the basic & CIMFR gasifier models, presented in Table 4.9 were obtained from literature & CIMFR, Dhanbad respectively. For CIMFR gasifier model, the bed was initially assumed filled with fuel particles up to a height of 64 mm as per the pilot scale gasifier at CIFR, with a solid-phase volume-fraction of 0.48. However, for basic gasifier model, it was assumed filled to a height of 300 mm. This was done by patching the volume fraction of phase 2 in the solution initialization tab.

The mass flow inlet and pressure outlet boundary conditions has been used for coal, air inlets & syngas outlet respectively. At the walls, no-slip wall condition and zero heat flux (adiabatic wall) was used for the gas phase and solid phase [32]

Table 4.9 Operating & boundary conditions for gasifier models

Operating & boundary conditions		
Parameter	BASIC	CIMFR
Coal Feed	8 Kg/ hr.	12 Kg/ hr.
Air Supply	19.4 Kg/ hr.	320 LPM
Steam Supply	4.6 Kg/ hr.	2.7 Kg/ hr
Air & Steam Temp. at Entrance	420 °C	400 °C
Temperature of reactor	1128 K	1153 K

4.3.8 Monitors: - In monitors, the convergence criteria for all the residuals like that for continuity equation, phase velocity equations, phase k equations and phase epsilon equations were set to absolute value of 0.000001.

4.3.9 Customization of FLUENT for fluidization problems: - For the study of fluidized bed problems in FLUENT, following

- a) **Multiphase Model:** - The volume fraction of secondary phase is very high in case of fluidized bed. Therefore, Eulerian- Eulerian multiphase model should be used instead of Dispersed Phase Model (DPM). DPM tracks individual particles and hence requires high computational time. Also, particle-particle interaction is neglected in DPM and therefore it is not suitable for modeling of reactive fluidized beds like bubbling fluidized bed gasifiers.
- b) **Turbulence Model:** - The turbulence transfer between the phases plays a dominant role in case of bubbling fluidized beds. Therefore, a more intensive turbulent model-K- ϵ per phase model should be used.
- c) **Patch:** - In a bubbling fluidized bed gasifier, we need to form a bed before starting the flow. To define bed region in FLUENT, we need to mark and adapt that portion of the gasifier geometry where bed is present. The marked portion is then patched after initialization with phase 2 volume fraction of 0.48 from the solution initialization tab. For example: - in Fig. 4.16, the red portion represents the patched bed portion.
- d) **Packing Limit:** - In order to maintain a fluidized bed, the particles must not come too close to each other. Therefore, to prevent the spacing between the particles from reducing to zero, a maximum packing limit of 0.64 is used for the granular secondary phase.
- e) **Heterogeneous reaction:** - For reactive fluidized beds, a user defined function must be inserted into FLUENT to incorporate the effect of heterogeneous reaction kinetics. However, for homogeneous reaction, the kinetic parameters can be provided inside the reaction tab of that phase.
- f) **Drag and Lift force:** - In fluidized beds, the drag force plays an important role in the interphase momentum transfer. Therefore, appropriate drag model like Syamlal- O'Brien model should be used.

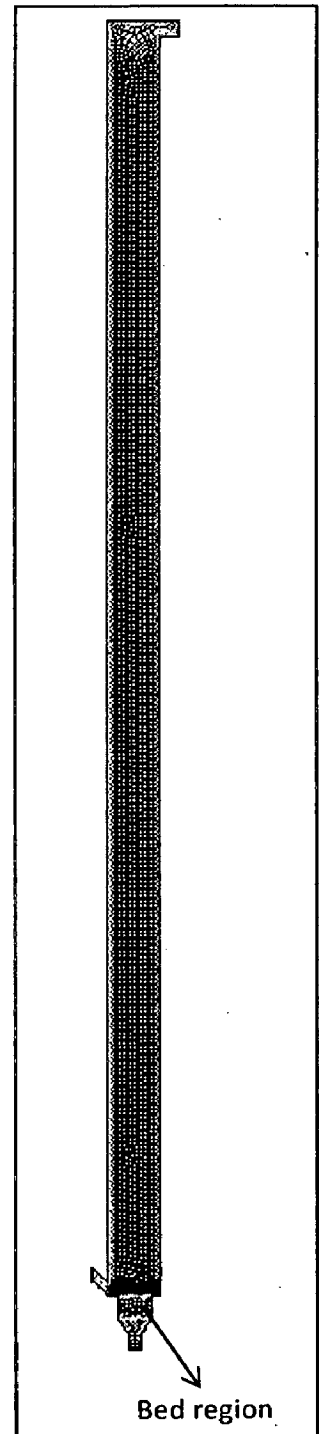


Fig. 4.16 Patch in FLUENT

4.4 SOLUTION TECHNIQUE

This section describes the FLUENT solver methodologies. Details about the solver algorithms used by FLUENT are provided after a brief overview of flow solvers for the solution of the general scalar transport equation. Afterwards, pressure-velocity coupling and time-advancement algorithm are presented for the numerical solution of the general scalar transport equation. Finally, discretization schemes for spatial and temporal derivatives are described along the evaluation methods of gradients and derivatives.

4.4.1 Overview of Flow Solvers

FLUENT allows one of the two numerical methods: pressure- and density-based solver. Whereas the pressure-based approach was developed for low-speed incompressible flows, the density-based approach was mainly used for high-speed compressible flows. However, recently both methods have been extended and reformulated to solve and operate for a wide range of flow conditions beyond their traditional or original intent.

For both methods the velocity field is obtained from the momentum equations. In the density-based approach, the continuity equation is used to obtain the density field while the pressure field is determined from the equation of state. On the other hand, in the pressure-based approach, the pressure field is extracted by solving a pressure or pressure correction equation which is obtained by manipulating continuity and momentum equations. Using either method, FLUENT solves the governing integral equations for the conservation of mass and momentum, and (when appropriate) for energy and other scalars such as turbulence and chemical species. In both cases a control-volume-based technique is used that consists of:

- Division of the domain into discrete control volumes using a computational grid.
- Integration of the governing equations on the individual control volumes to construct algebraic equations for the discrete dependent variables such as velocities, pressure, temperature, and conserved scalars.
- Linearization of the discretized equations and solution of the resultant linear equation system to yield updated values of the dependent variables.

4.4.2 Solution Method in FLUENT for Multiphase Flows

For Eulerian multiphase calculations, FLUENT uses the phase coupled SIMPLE (PC-SIMPLE) algorithm for the pressure-velocity coupling. PC-SIMPLE is an extension of the SIMPLE algorithm to multiphase flows. The velocities are solved coupled by phases, but in a segregated fashion. The block algebraic multigrid scheme is used to solve a vector equation formed by the velocity components of all phases simultaneously. Pressure and velocities are then corrected so as to satisfy the continuity constraint.

The Pressure-Correction Equation

For incompressible multiphase flow, the pressure-correction equation takes the form:

$$\sum_{q=1}^n \frac{1}{\rho_{rq}} \left\{ \frac{\partial}{\partial t} \alpha_q \rho_q + \nabla \cdot \alpha_q \rho_q \vec{u}_q + \nabla \cdot \alpha_q \rho_q \vec{u}_q^* - \left(\sum_{i=1}^m \dot{m}_{iq} - \dot{m}_{qi} \right) \right\} = 0$$

Where ρ_{rq} is the phase reference density for the q^{th} phase (defined as the total volume average density of phase q), u_q' is the velocity correction for the q^{th} phase, and u_q^* is the value of u_q at the current iteration. The velocity corrections are themselves expressed as functions of the pressure corrections.

Volume Fractions

The volume fractions are obtained from the phase continuity equations. In discretized form, the q^{th} volume fraction is given by Equation (38).

$$\alpha_{p,q} \alpha_q = \sum (\alpha_{nb,q} \alpha_{nb,q}) + b_q = R_q$$

These equations satisfy the condition that all volume fractions sum to one as expressed in Chapter-3.

4.4.3 Time-Advancement Algorithm

In the pressure-based solver, the overall time-discretization error is determined by both the choice of temporal discretization (e.g., first-order, second-order) and the manner in which the solutions are advanced to the next time step (time-advancement scheme). Temporal discretization introduces the corresponding truncation error; $O(\Delta t)$, $O[(\Delta t)^2]$, for first-order and second-order, respectively. The approach used here is Iterative time advancement scheme.

Iterative Time-Advancement Scheme

In the iterative scheme, all the equations are solved iteratively, for a given time-step, until the convergence criteria are met. Thus, advancing the solutions by one time-step normally requires a number of outer iterations. With this iterative scheme, non-linearity of the individual equations and inter-equation couplings are fully accounted for, eliminating the splitting error. The iterative scheme is the default in FLUENT.

4.4.4 Discretization

In mathematics, discretization means the process of transferring continuous models and equations into discrete counterparts. This process is usually carried out as a first step toward making them suitable for numerical evaluation and implementation on digital computers. The

stability of the chosen discretization is generally established numerically rather than analytically as with simple linear problems. Special care must also be taken to ensure that the discretization handles discontinuous solutions gracefully. Some of the discretization methods being used are:

4.4.4.1 Finite Volume Method (FVM)

This is the "classical" or standard approach used most often in commercial software and research codes. The governing equations are solved on discrete control volumes. FVM recasts the PDE's (Partial Differential Equations) of the Navier-Stokes equation in the conservative form and then discretize this equation. "Finite volume" refers to the small volume surrounding each node point on a mesh.

In the finite volume method, volume integrals in a partial differential equation that contain a divergence term are converted to surface integrals, using the divergence theorem. These terms are then evaluated as fluxes at the surfaces of each finite volume. Because the flux entering a given volume is identical to that leaving the adjacent volume, these methods are conservative.

Another advantage of the finite volume method is that it is easily formulated to allow for unstructured meshes. This guarantees the conservation of fluxes through a particular control volume. Though the overall solution will be conservative in nature there is no guarantee that it is the actual solution. Moreover this method is sensitive to distorted elements which can prevent convergence if such elements are in critical flow regions. This integration approach yields a method that is inherently conservative (i.e. quantities such as density remain physically meaningful).

$$\frac{\partial}{\partial t} \iiint Q dV + \iint F dA = 0$$

Where Q is the vector of conserved variables, F is the vector of fluxes, V is the cell volume, and A is the cell surface area.

4.4.4.2 Spatial Discretization

By default, FLUENT stores discrete values of the scalar ϕ at the cell centers. However, face values ϕ_f is required for the convection terms and must be interpolated from the cell center values. This is accomplished using an upwind scheme.

'Upwinding' means that the face value ϕ_f is derived from quantities in the cell upstream, or "upwind," relative to the direction of the normal velocity u_n . FLUENT has several upwind schemes: first-order upwind, second-order upwind, power law, and QUICK. I have used the First order upwind scheme.

First-Order Upwind Scheme

When first-order accuracy is desired, quantities at cell faces are determined by assuming that the cell-center values of any field variable represent a cell-average value and hold throughout the entire cell; the face quantities are identical to the cell quantities. Thus when first-order upwind is selected, therefore, in first order scheme, the current face value is taken equal to the cell center value of the upstream cell in the N-1 iteration.

The gradients and the derivatives are evaluated by Green Gauss cell based gradient evaluation method. The discrete form of this method, when used for calculating a scalar ϕ at the cell center c_0 is given by [26]:

$$(\nabla\phi)_{c_0} = \frac{1}{\vartheta} \sum_f \bar{\phi}_f \vec{A}_f \quad \dots (37)$$

In equation (37), ϕ_f is the value of ϕ at the cell face centroid computed with the following equation: -

$$\phi_f = \frac{(\phi)_{c_0} + (\phi)_{c_1}}{2} \quad \dots (38)$$

4.4.4.3 Temporal Discretization

For transient simulations, the governing equations must be discretized in both space and time. The spatial discretization for the time-dependent equations is identical to the steady-state case. Temporal discretization involves the integration of every term in the differential equations over a time step Δt .

A generic expression for the time evolution of a variable ϕ is given by:

$$\frac{\partial\phi}{\partial t} = F(\phi)$$

Where, the function 'F' incorporates any spatial discretization.

Once the time derivative has been discretized, a choice remains for evaluating $F(\phi)$, in particular, which time level values of ϕ should be used in evaluating F : the implicit or explicit time integration method.

Explicit Vs Implicit Method

When a direct computation of the dependent variables can be made in terms of known quantities, the computation is said to be explicit. When the dependent variables are defined by coupled sets

of equations, and either a matrix or iterative technique is needed to obtain the solution, the numerical method is said to be implicit.

In computational fluid dynamics, the governing equations are nonlinear, and the numbers of unknown variables are typically very large. Under these conditions implicitly formulated equations are almost always solved using iterative techniques.

Iterations are used to advance a solution through a sequence of steps from a starting state to a final, converged state. This is true whether the solution required is either one step in a transient problem or a final steady-state result. In either case, the iteration steps resemble a time-like process. The iteration steps usually do not correspond to a realistic time-dependent behavior. In fact, it is this aspect of an implicit method that makes it attractive for steady-state computations, because the number of iterations required for a solution is often much smaller than the number of time steps needed for an accurate transient that asymptotically approaches steady conditions.

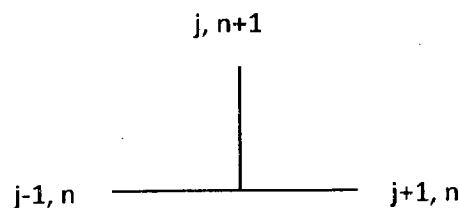
Explicit Method

Using a forward difference at time t_n and a second-order central difference for the space derivative at position x_j , we get the recurrence equation:

$$\frac{u_j^{n+1} - u_j^n}{k} = \frac{u_{j+1}^n - 2u_j^n + u_{j-1}^n}{h^2}$$

This is an explicit method for solving the one-dimensional heat equation

$$\frac{\partial u}{\partial t} = K \frac{\partial^2 u}{\partial x^2}$$



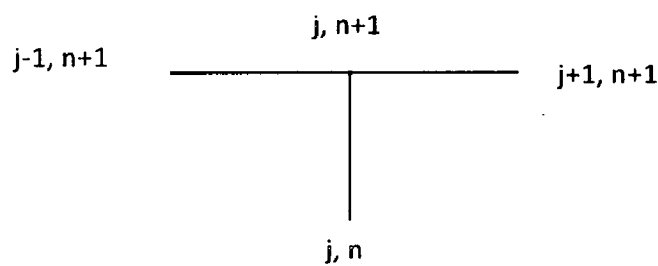
We can obtain u_j^{n+1} from the other values th j, n

$$u_j^{n+1} = ru_{j+1}^n + (1 - 2r)u_j^n + ru_{j-1}^n$$

Where $r = k / h^2$. So, knowing the values at time n you can obtain the corresponding ones at time $n+1$ using this recurrence relation.

Implicit method

If we use the backward difference at time $tn + 1$ and a second-order central difference for the space derivative at position xj we get the recurrence equation:

$$\frac{u_j^{n+1} - u_j^n}{k} = \frac{u_{j+1}^{n+1} - 2u_j^{n+1} + u_{j-1}^{n+1}}{h^2}$$


This is an implicit method for solving the one-dimensional heat equation. We can obtain u_j^n from solving a system of linear equations:

$$u_j^n = (1 + 2r)u_j^{n+1} - ru_{j-1}^{n+1} - u_{j+1}^{n+1}$$

The scheme is always numerically stable and convergent but usually more numerically intensive than the explicit method as it requires solving a system of numerical equations on each time step. The errors are linear over the time step and quadratic over the space step.

4.5. ALGORITHM USED FOR PRESENT WORK

The aim of the present work is to study the performance of the bubbling fluidized bed gasifier. To achieve this, law of conservation of mass, momentum and energy equation are solved by solver FLUENT with associated drag, turbulence, species transport and other constitutive equations. Usually, FLUENT follows the following algorithm to study such a system.

In the present study, I have used pressure based solver to study the hydrodynamics and reaction kinetics inside the bubbling fluidized bed gasifier. The pressure based solver employs an algorithm which belongs to a general class of methods called the projection method, wherein the constraint of mass conservation (continuity) of the velocity field is achieved by solving a pressure correction equation. This pressure equation is derived from the continuity and momentum equations in such a way that the velocity field, corrected by the pressure satisfies the continuity. Since the governing equations are nonlinear and coupled to one another, the solution

process involves iterations, wherein the entire set of governing equations is solved repeatedly until the solution converges.

Two pressure-based solver algorithms are available in FLUENT: a segregated algorithm, and a coupled algorithm. Since, I have used the coupled approach, I have discussed coupled algorithm in the following paragraph.

The Pressure-Based Coupled Algorithm

The pressure-based coupled algorithm solves a coupled system of equations comprising the momentum equations and the pressure-based continuity equation. The remaining equations are solved in a decoupled fashion as in the segregated algorithm.

Since the momentum and continuity equations are solved in a closely coupled manner, the rate of solution convergence significantly improves when compared to the segregated algorithm. However, the memory requirement increases by 1.5 - 2 times that of the segregated algorithm since the discrete system of all momentum and pressure-based continuity equations need to be stored in the memory when solving for the velocity and pressure fields (rather than just a single equation, as is the case with the segregated algorithm).

In the present study, User Defined Functions have been used to specify the drag models and heterogeneous reaction rates. In this case, the solution process for the pressure-based coupled solver (Figure 5.1) begins with an initialization sequence that is executed outside the solution iteration loop. This sequence begins by initializing equations to user-entered (or default) values taken from the FLUENT user interface. The solution iteration loop begins with the execution of ADJUST UDFs. Next, FLUENT solves the governing equations of continuity and momentum in a coupled fashion as shown in Fig. 4.17 and described as follows: -

After initialization, loop begins with user defined adjust, followed by calculation of kinetic parameters and bed properties. This is tailed by momentum conservation & pressure correction equations, turbulent kinetic energy & dissipation rate equations; species transport equation, energy equation and volume fraction equations. After solving the above equations, the properties are updated and checked for convergence and the loop continues until a converged state is reached.

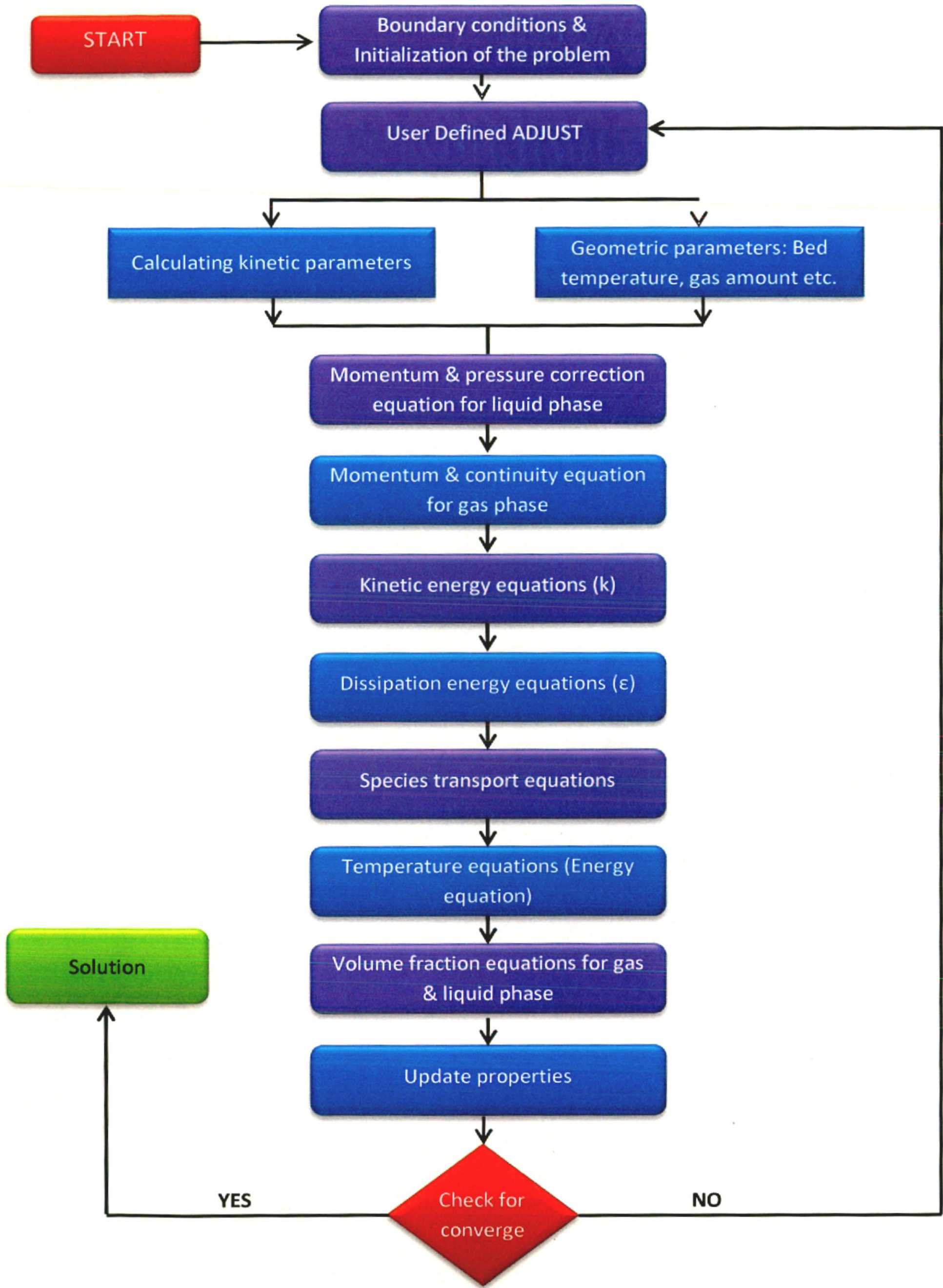


Fig. 4.17: Solution Algorithm used by FLUENT

The objectives of the present dissertation are outlined in Chapter- 1 and literature review is presented in Chapter 2. The basic conservation equations for mass, momentum and energy, various drag & turbulent models and associated constitutive equations used in the present study are given in Chapter 3- Multiphase model selection and development. The problem description and solution technique adopted for the simulation is presented in Chapter- 4.

In the present work, simulation of bubbling fluidized bed gasifier is carried out using CFD code FLUENT 12. First, a basic model was developed using geometry and operating conditions from literature [82]. This model was validated using reported data (Liang et al. 2006). After validation, this model was used as the reference model for developing the CIMFR bubbling fluidized bed gasifier model. The computation time for CIMFR BFBG model on a 3.1 GHz 4GB Ram 32- bit Intel CPU (i3) was around 4 days.

The salient results of the CFD simulations are discussed in this chapter. After solving the model equations using FLUENT CFD code, the results were validated with experimental data obtained from BFBG pilot plant at CIMFR, Dhanbad. Once, the model was validated against literature data and experimental results, it is then used for parametric study to predict the effect of parameters like temperature, pressure and superficial gas velocity on the gasifier performance.

In the first section of this chapter, results of the basic model used as reference model for CIMFR model development and its validation using literature data have been discussed. Also, the effect of superficial air velocity on the fluidized bed height is presented.

In the second section, the results obtained from CIMFR model (developed using Geometry, operating and boundary conditions from CIMFR bubbling fluidized bed gasifier pilot plant) and its validation with experimental data is discussed. The effect of temperature, pressure and superficial gas velocity on the performance of the CIMFR gasifier is also presented thereafter.

Some of the parameters like temperature profile, mole fraction profiles, velocity profile etc. will be discussed in both sections (Base Model & CIMFR Model). An impression of repetition may arise which is not true because these parameters depend on the specific geometry of the gasifier and therefore requires separate discussion for each geometry under consideration.

5.1 Basic Gasifier Model

5.1.1 Calibration & Validation

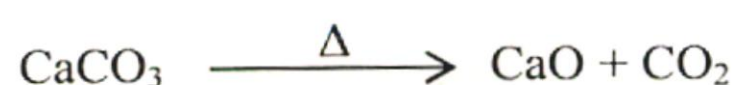
The basic gasifier model was first developed using literature [82] geometry, operating & boundary conditions as given in Chapter-4. The mole fraction of species and temperature predicted by the model is given in Table 5.1 along with results obtained from literature [Liang et al. 2006].

Table 5.1 Basic model validation (Predicted values vs. Literature Data)

Parameters	Predicted Results (Mole Fraction, %)	Results from Literature (Mole Fraction, %)	Error (%)
Syngas Composition			
CO	9.6333	10.5	- 8.254
CO ₂	15.353	14	+ 8.81
H ₂	8.6833	9	-3.51
N ₂	51.34	55	-6.654
Temperature (K)			
	1194	1126	+ 7.383

From Table 5.1, it is evident that the temperature and mole fraction results obtained from the model are in good agreement (error < ± 9 %) with the literature data. The maximum error is 8.81 % in case of mole fraction of CO₂ while the error in mole fraction of H₂ is less than 5 %. The predicted temperature is about +7.4% higher than the temperature reported by Liang et al. 2006. Therefore, this model can be used to study the temperature profiles and mole fraction profiles of different species along the height of gasifier.

The predicted mole fractions of most species (CO, N₂, and H₂) are lower than the literature data while for CO₂, it is higher. The higher value for CO₂ may be due to the presence of limestone with coal (Liang et al. has not considered the presence of lime stone with coal) in the present work, which may decompose at higher temperature to evolve CO₂ by the following reaction: -



5.1.2 Temperature contours along the width and height of gasifier: - The temperature, velocity and presence of reactant control the type of reaction which will take place in a particular zone of the gasifier. Hence these are discussed before the discussion of the product of gasification i.e. CO, CO₂, H₂ etc. are considered.

The contours for the temperature profile inside the gasifier are shown in Fig. 5.1. From the temperature contours, it is evident that temperature rises sharply above the bed region and coal inlet region. After that it almost remains constant in the freeboard zone except in the top right

corner where it decreases gradually. The sharp increase of temperature at the coal entrance and in the bed region is due to dominant exothermic combustion and water gas shift reaction. However, the gradual decrease in temperature at the top right corner is due to endothermic reverse water gas shift reaction (due to reverse flow as can be observed from Fig.5.2(b)) which dominates over exothermic forward water gas shift reaction.

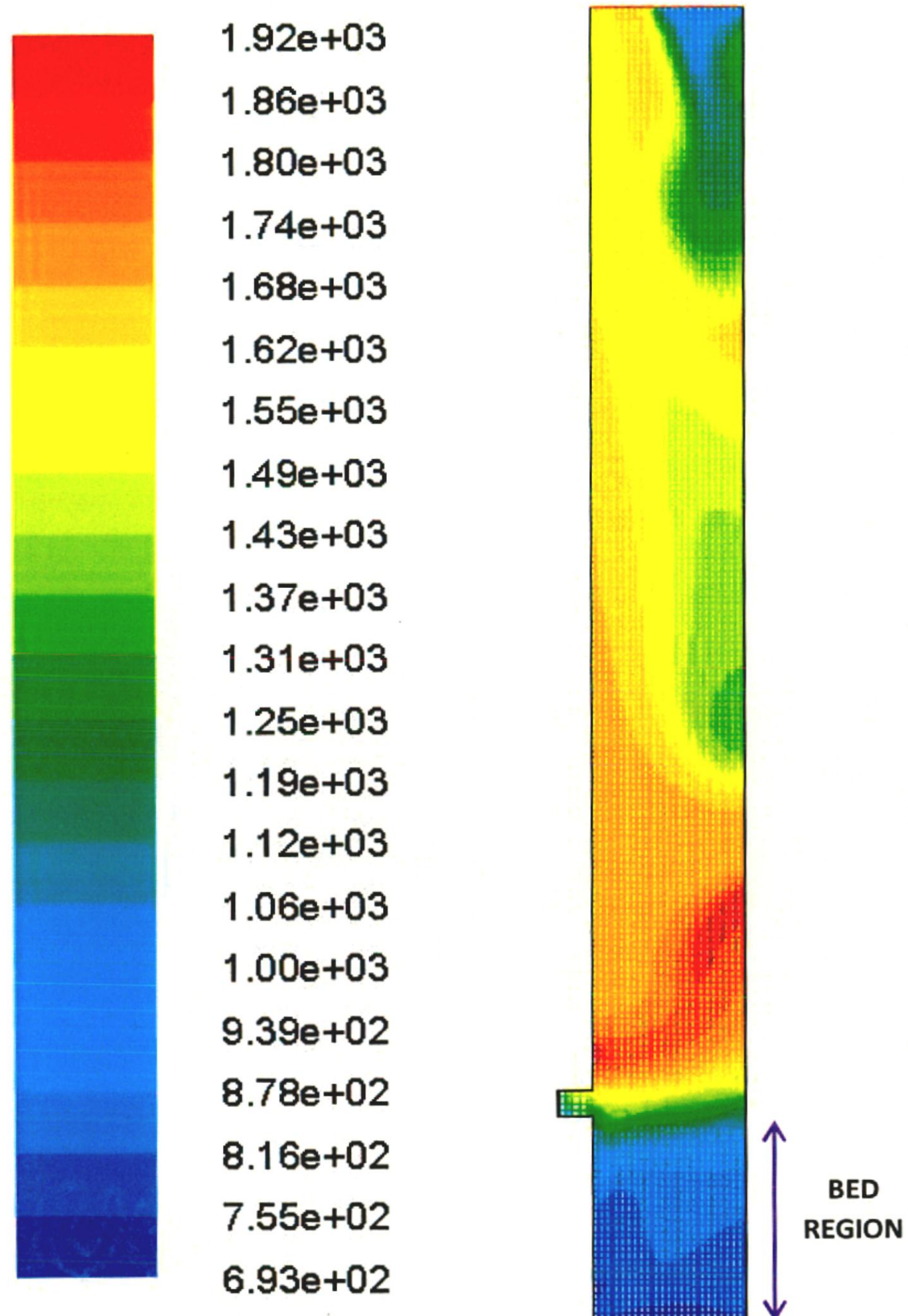


**Fig. 5.1 Contour of temperature profile
BASIC MODEL**

5.1.3 Velocity contours along the height and width of gasifier: -

The contour of phase 2 (coal particles) velocity profile is shown in Fig. 5.2 (a). A vector representation of the same over a selected portion of the gasifier is shown in Fig. 5.2 (b).

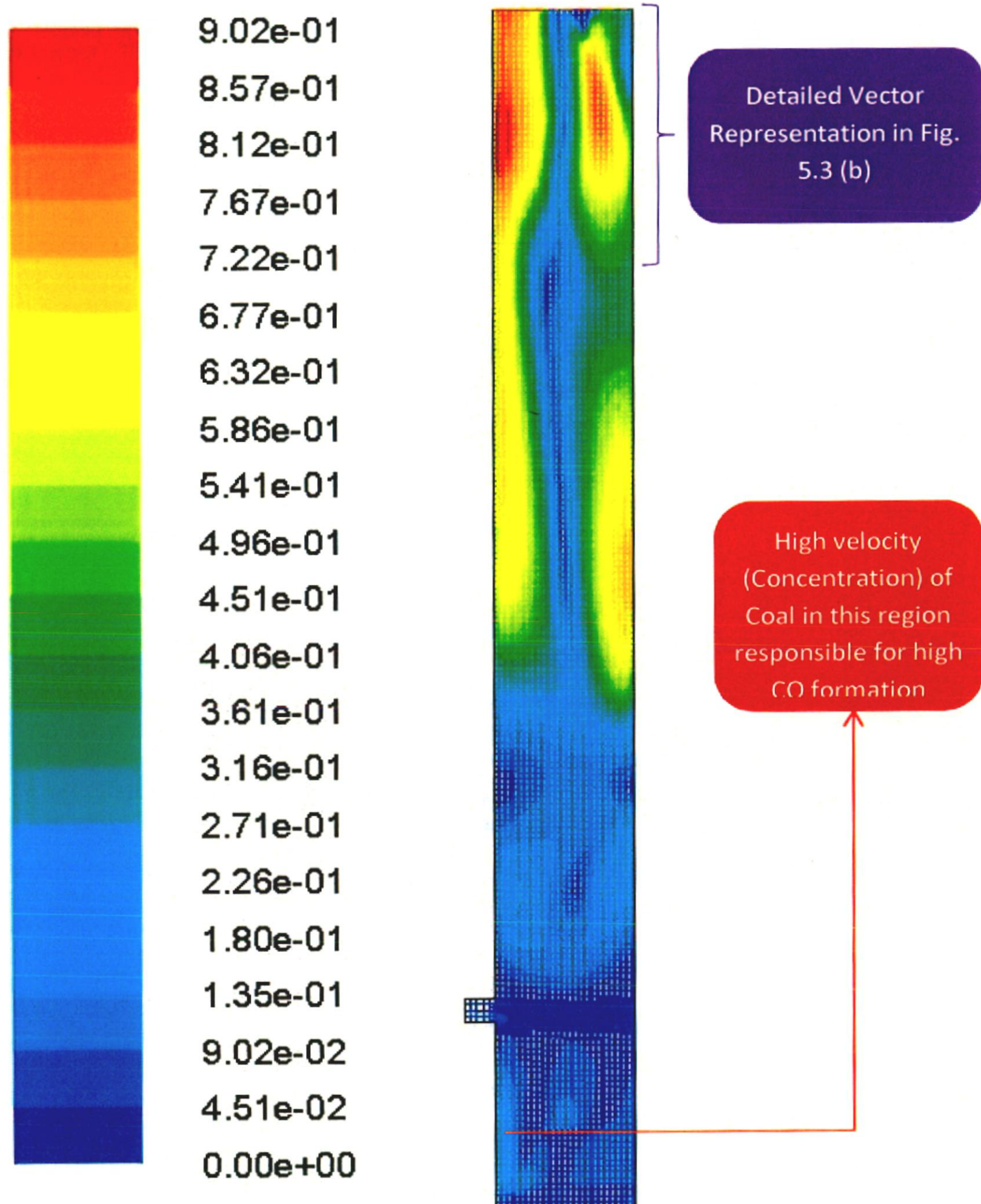
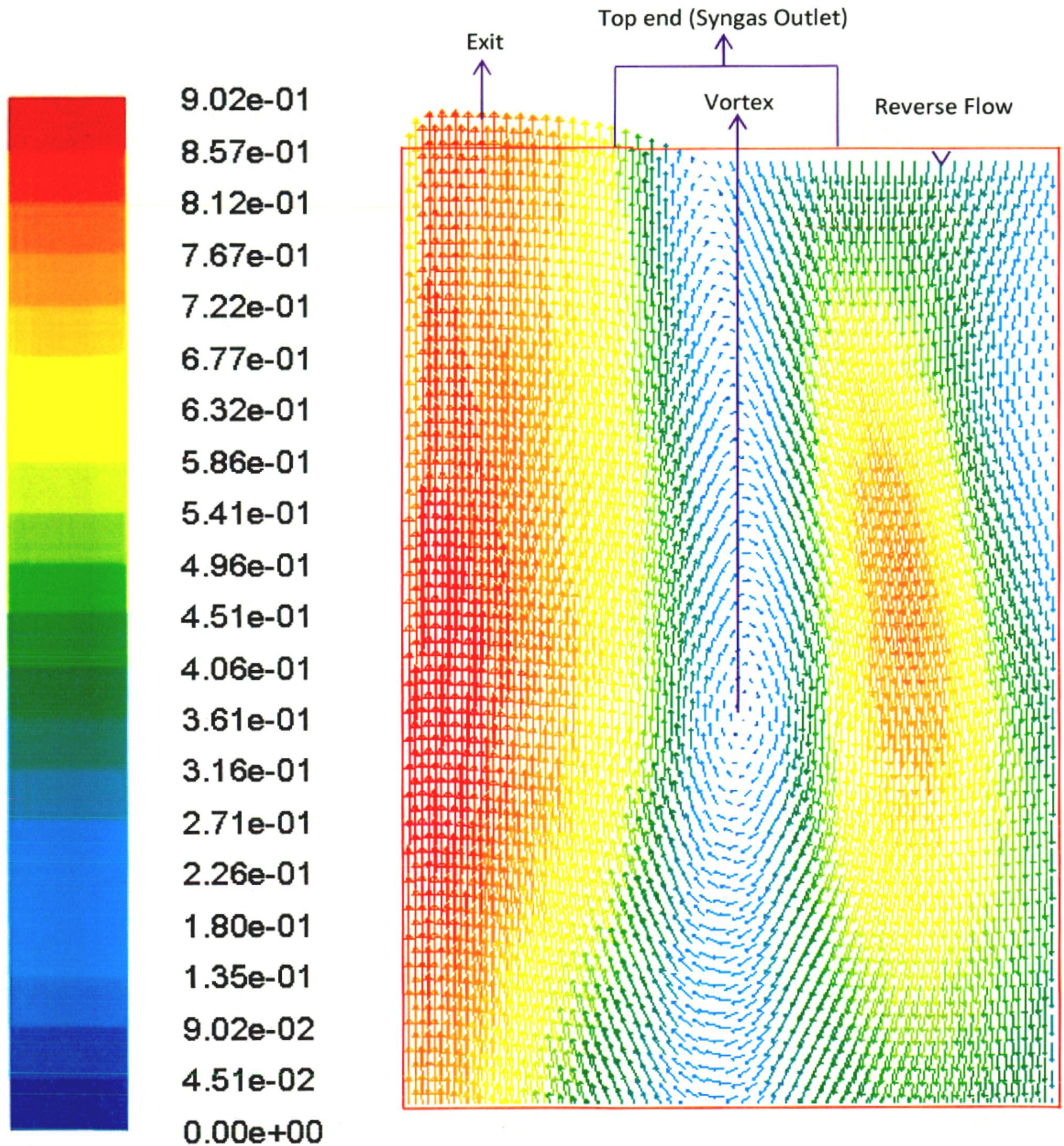


Fig. 5.2 (a) Contour of phase 2 velocity profile
BASIC MODEL



**Fig. 5.2 (b) Vectors of phase 2 velocity
BASIC MODEL**

From the contours of phase 2 velocity profile shown in Fig. 5.2 (a) & 5.2 (b), we can infer that there is high back mixing inside the gasifier due to reverse flow and vortex formation. This is an important characteristic of bubbling fluidized bed gasifier and is responsible for high heat and mass transfer inside the gasifier. Due to this reverse flow, near the exit of the reactor as shown in Fig.1, the reverse water gas shift reaction is taking place.

A vector representation of the velocity profile in the upper portion of freeboard zone near the syngas outlet is given in Fig. 5.2 (b). From this figure, it is apparent that there is a vortex formed in the center region of the gasifier. On the left hand side, syngas is leaving the gasifier while at the right hand side reverse flow is present which retards the flow of syngas from this side. This increases the residence time of syngas in this portion of the fluidized bed and gives rise to the forward and reverse water gas shift reaction. However, the magnitude of velocity on the left hand side is much higher than that on right hand side and therefore, there is net flow of syngas from the gasifier at the syngas outlet.

From Fig. 5.2 (a), it is also evident that the velocity of coal is higher in the left side of the bed zone. Higher velocity in turn means higher amount of coal per unit time (or higher flux of coal particles). This higher flux of coal in this left side region of the bed zone is responsible for higher amount of CO formation in this region.

5.1.4 Predominant reactions along the height of gasifier

In Fig 5.3, the gasifier is shown in horizontal position and shows the predominant reactions occurring in different zones of the gasifier along its height. At the coal entrance and in the bed region, coal is virgin and plenty of oxygen is available. Therefore, combustion reactions like coal & CO combustion plays a dominant role in this region resulting in the formation of CO & CO₂ as evident from Fig. 5.4 (a) & Fig. 5.4 (b).

The formation of CO is highest the lower left corner of the bed region as evident from Fig. 5.4 (a). This is because in this region, the concentration of coal is high and therefore incomplete combustion results in formation of high amount of CO but it gradually gets converted to CO₂ by CO combustion and H₂ by water gas shift reaction as it moves along the height and width of the gasifier.

At the top right portion of the gasifier, forward water gas shift reaction occurs over a larger volume resulting in formation of H₂. However, with increase in concentration of CO₂ reverse water gas shift reaction also begins and becomes dominant in the topmost left portion of the gasifier resulting in formation of CO. Now, reverse water gas shift reaction is endothermic in nature. Therefore, temperature declines gradually in this region of the gasifier as evident from Fig. 5.1.

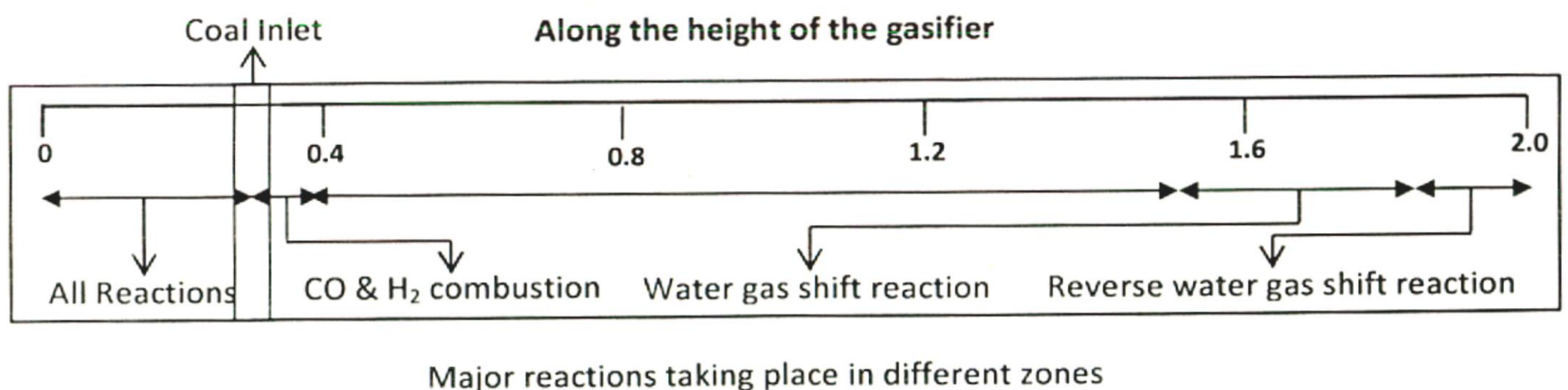


Fig. 5.3 Major reactions taking place along the height of the gasifier

5.1.5 Contours of species along the height and width of Gasifier

Fluent allows plotting contour lines or profiles superimposed on the physical domain. Contour lines are lines of constant magnitude for a selected variable (isotherms, isobars, etc.). A profile plot draws these contours projected off the surface along a reference vector by an amount proportional to the value of the plotted variable at each point on the surface. Contour profile tells us inside distribution of variables like molar concentration of various species, temperature, Pressure, volume fraction, phase velocities etc.

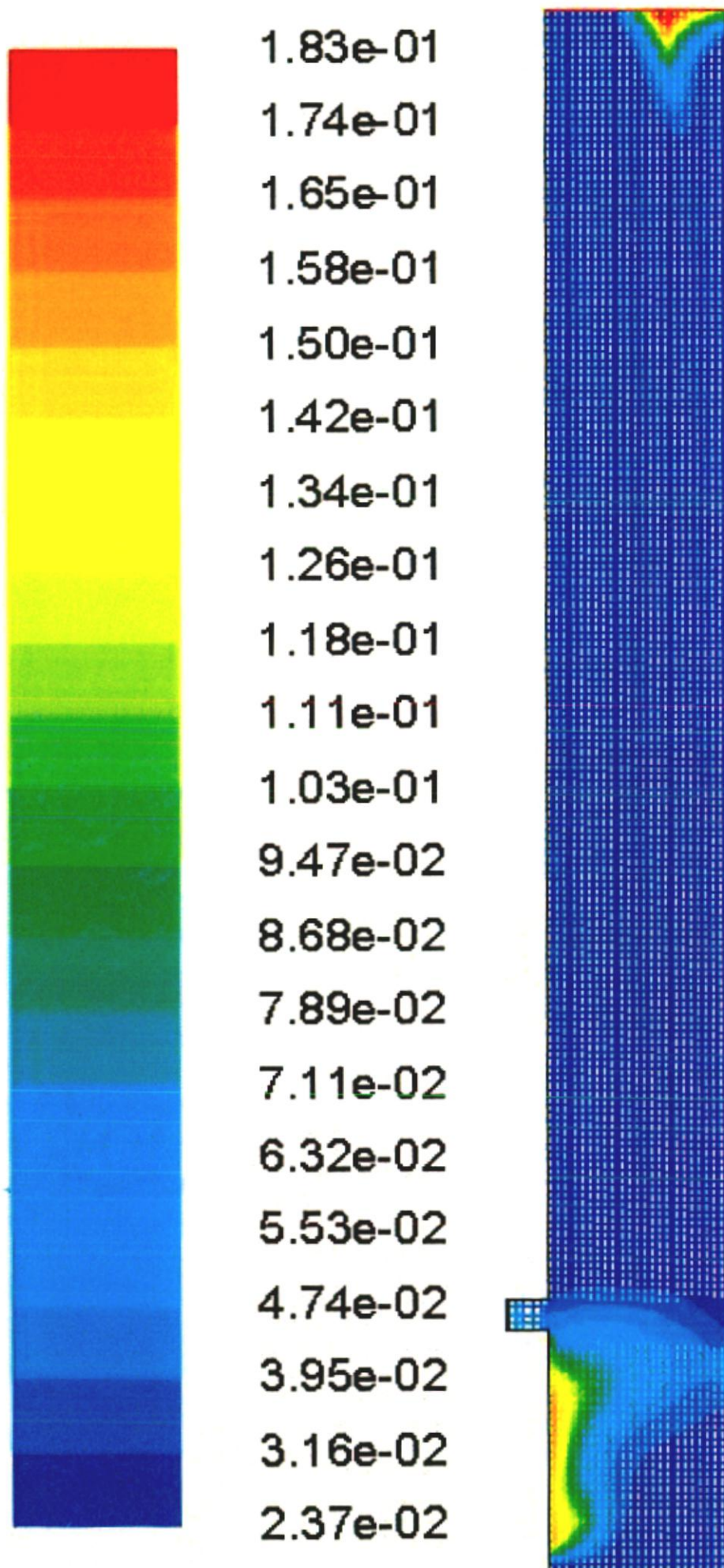


Fig. 5.4 (a) Contours of mole fraction of CO (BASIC MODEL)

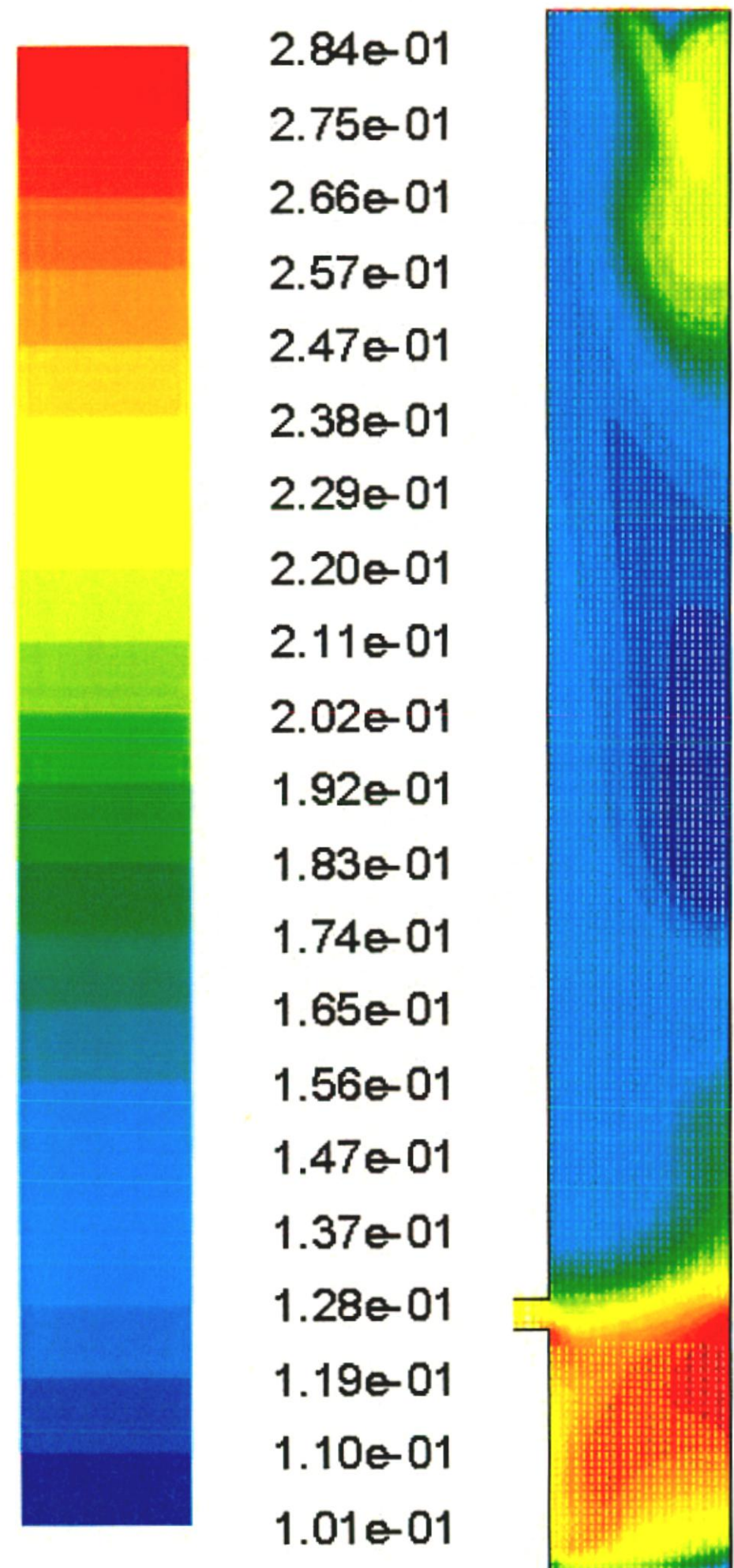


Fig. 5.4 (b) Contours of mole fraction of CO₂ (BASIC MODEL) 100

In this work, the contours of temperature and mole fraction of species have been studied. The contours of CO, CO₂, N₂, H₂O and H₂ are plotted in Fig. 5.4 (a-d) respectively. From these contours, it is evident that both CO & CO₂ are formed at the coal entrance & bed region by the combustion reactions of coal with oxygen and steam as well as through reverse water gas shift and boudouard reaction. However, CO quickly gets consumed to a large extent by the faster water gas shift reaction and CO oxidation when it moves along the height of the gasifier.

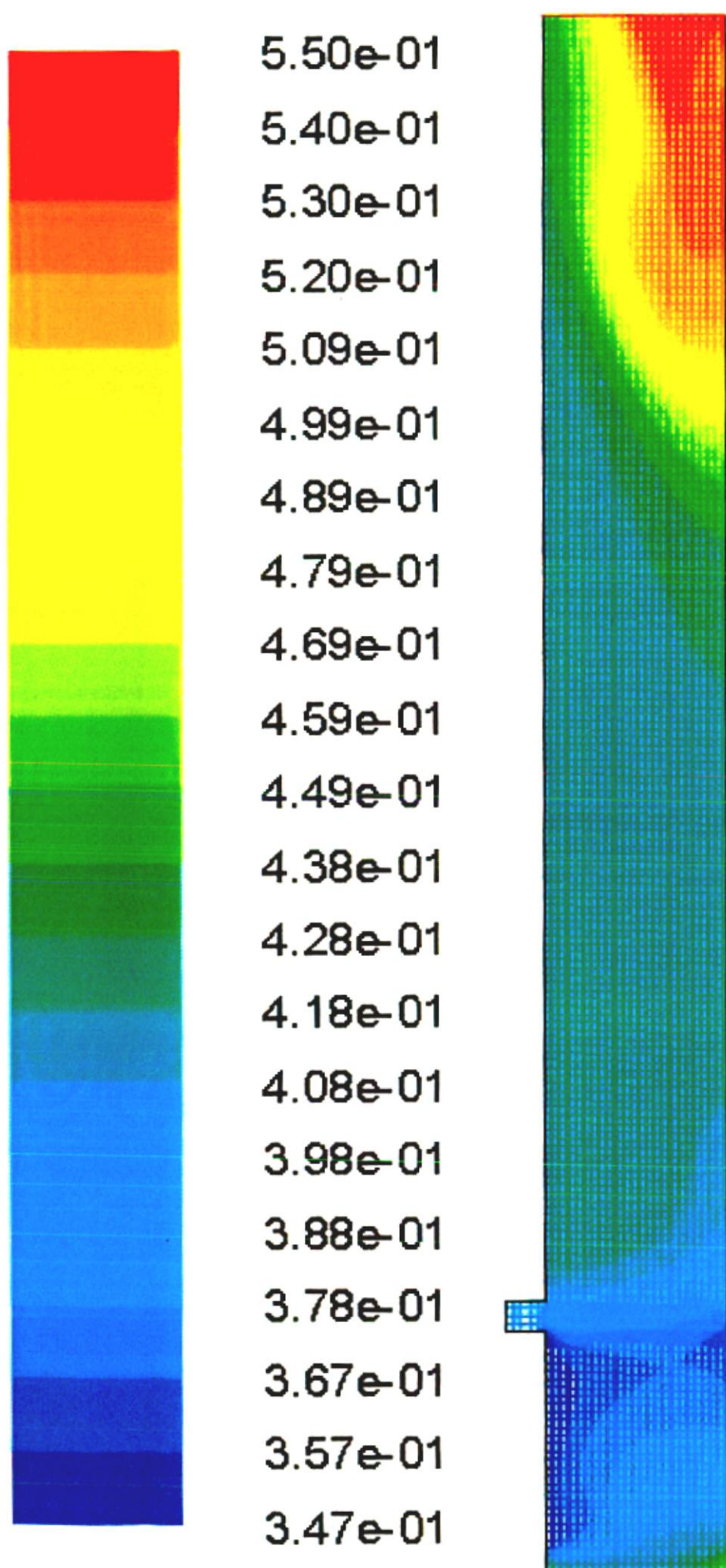


Fig. 5.4 (c) Contours of mole fraction of N₂ (BASIC MODEL)

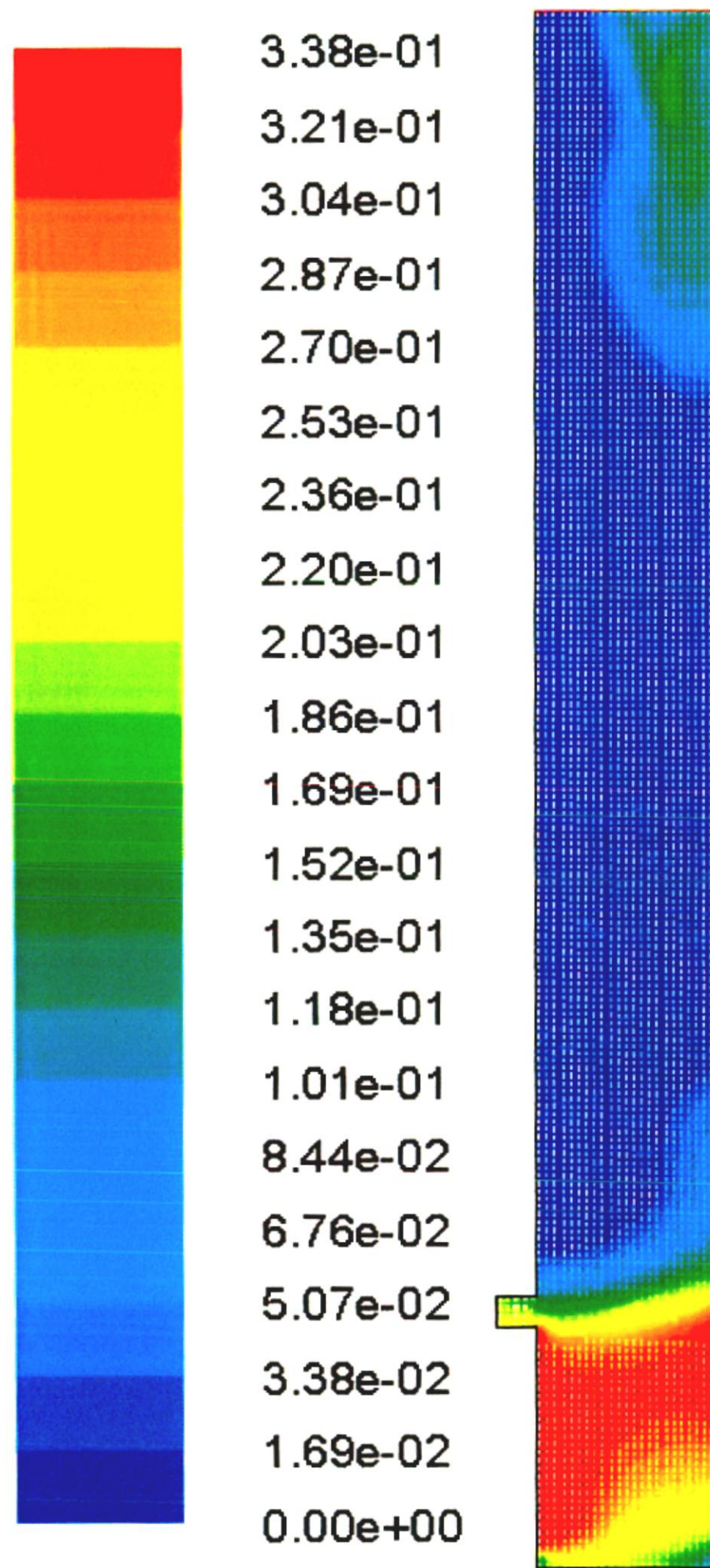


Fig. 5.4 (d) Contours of mole fraction of H₂ (BASIC MODEL)

Similarly, the concentration of H_2 is highest in the bed region owing to combustion in presence of steam and water gas shift reaction, but it decreases quickly due to hydrogen combustion to form water. Again, H_2 forms at top right corner of the gasifier by the water gas shift reaction as shown in Fig. 5.3. The variation in the N_2 contours is due to the formation and consumption of CO , CO_2 and H_2 by these reactions as N_2 itself is an inert gas. The nitrogen in the air ensures greater volume of syngas per ton of coal and helps in maintaining desired temperature profile inside the gasifier.

5.1.6 Bed Fluidization: - The fluidized bed height of the bubbling fluidized bed gasifier was studied at air velocities 0.25 m/ s, 0.5 m/ s, 0.8 m/ s, 1.0 m/ s, 1.3 m/ s and 1.5 m/ s without reaction (cold model) to determine the effect of air velocity on the fluidization process.

In most of the cases, it was observed that the behavior stabilizes between 6- 7 seconds. The contours for the same are shown in Fig. 5.5 (a- d) for air velocity of 0.25 m/ s, 0.5 m/ s, 0.8 m/ s and 1.0 m/ s.

From these contours, it is evident that the bed height increases with air velocity. Also, the turbulence in flow and back mixing increases with air velocity. This results in higher heat and mass transfer between primary phase and secondary phase.

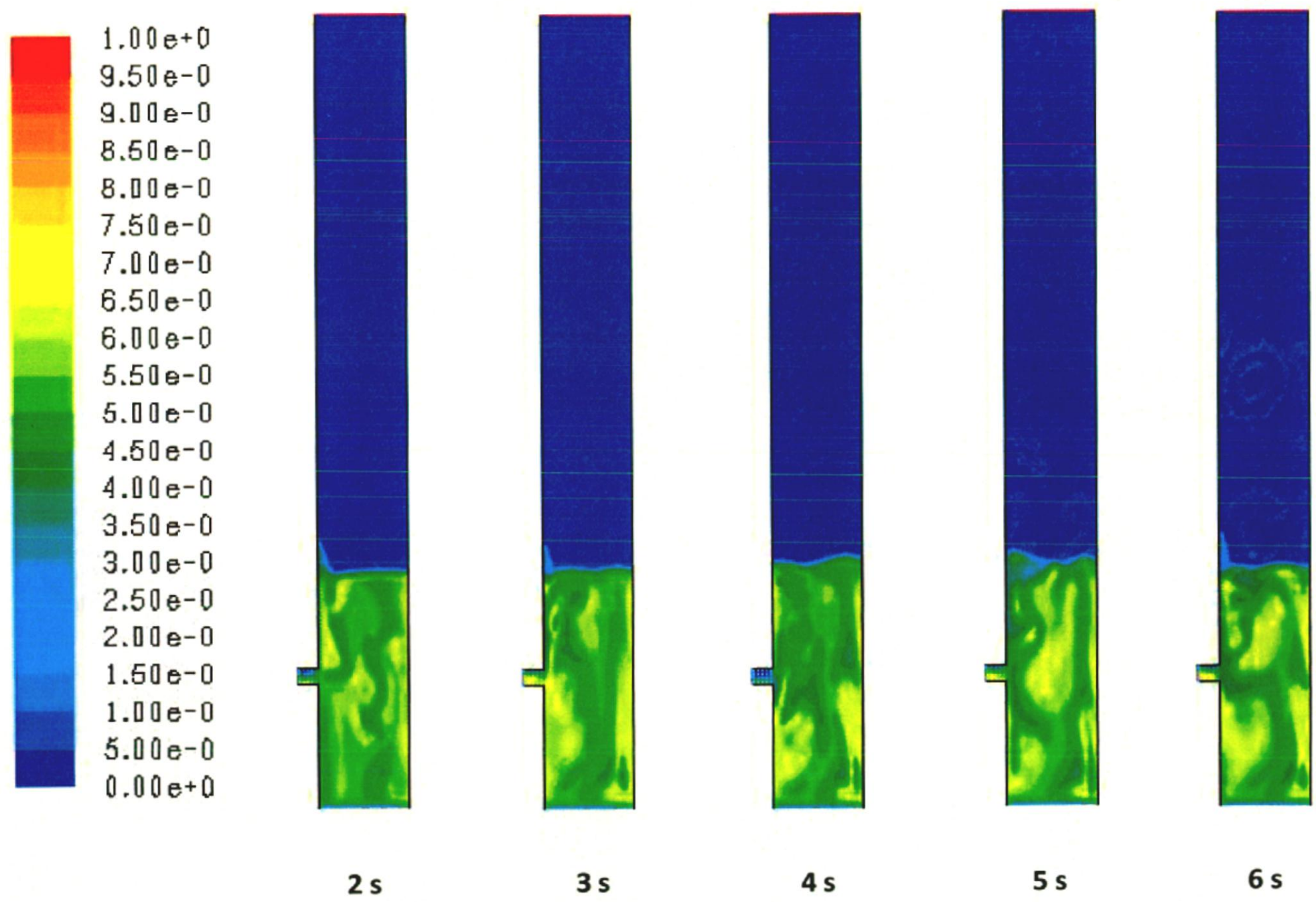


Fig. 5.5 (a) Bed Fluidization at air velocity = 0.25 m/ s

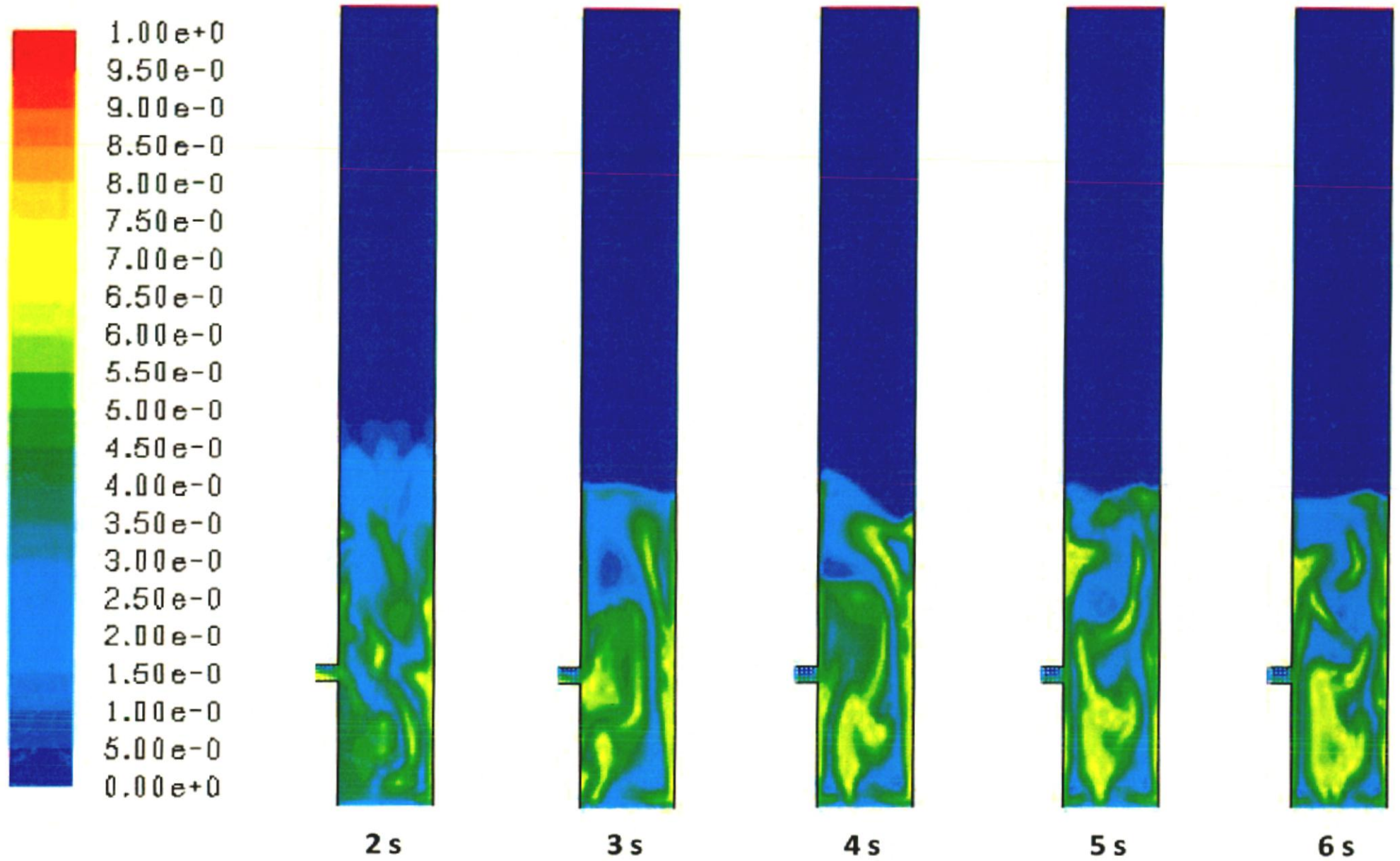


Fig. 5.4 (b) Bed Fluidization at air velocity = 0.5 m/ s

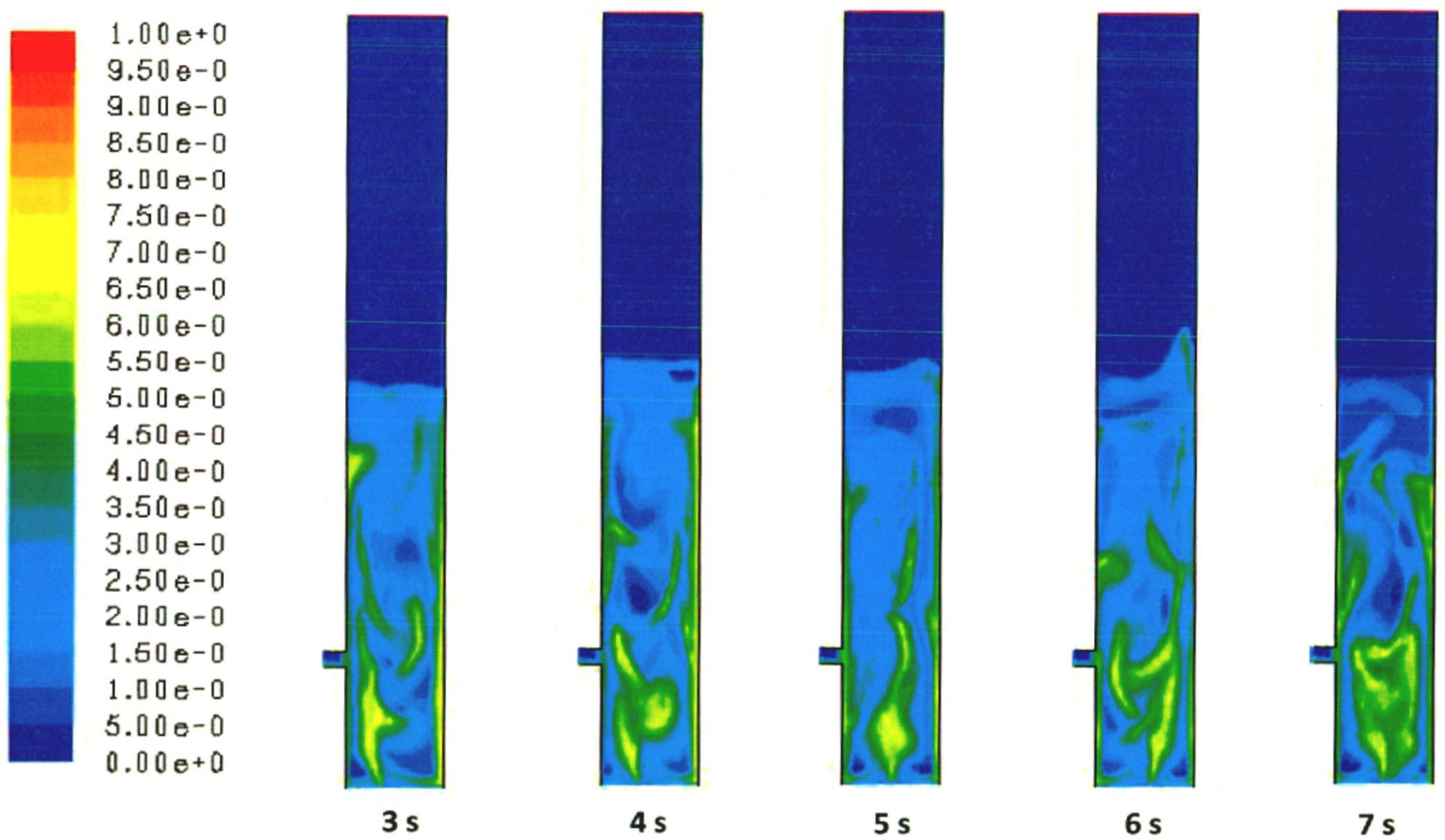


Fig. 5.5 (c) Bed Fluidization at air velocity = 0.8 m/ s

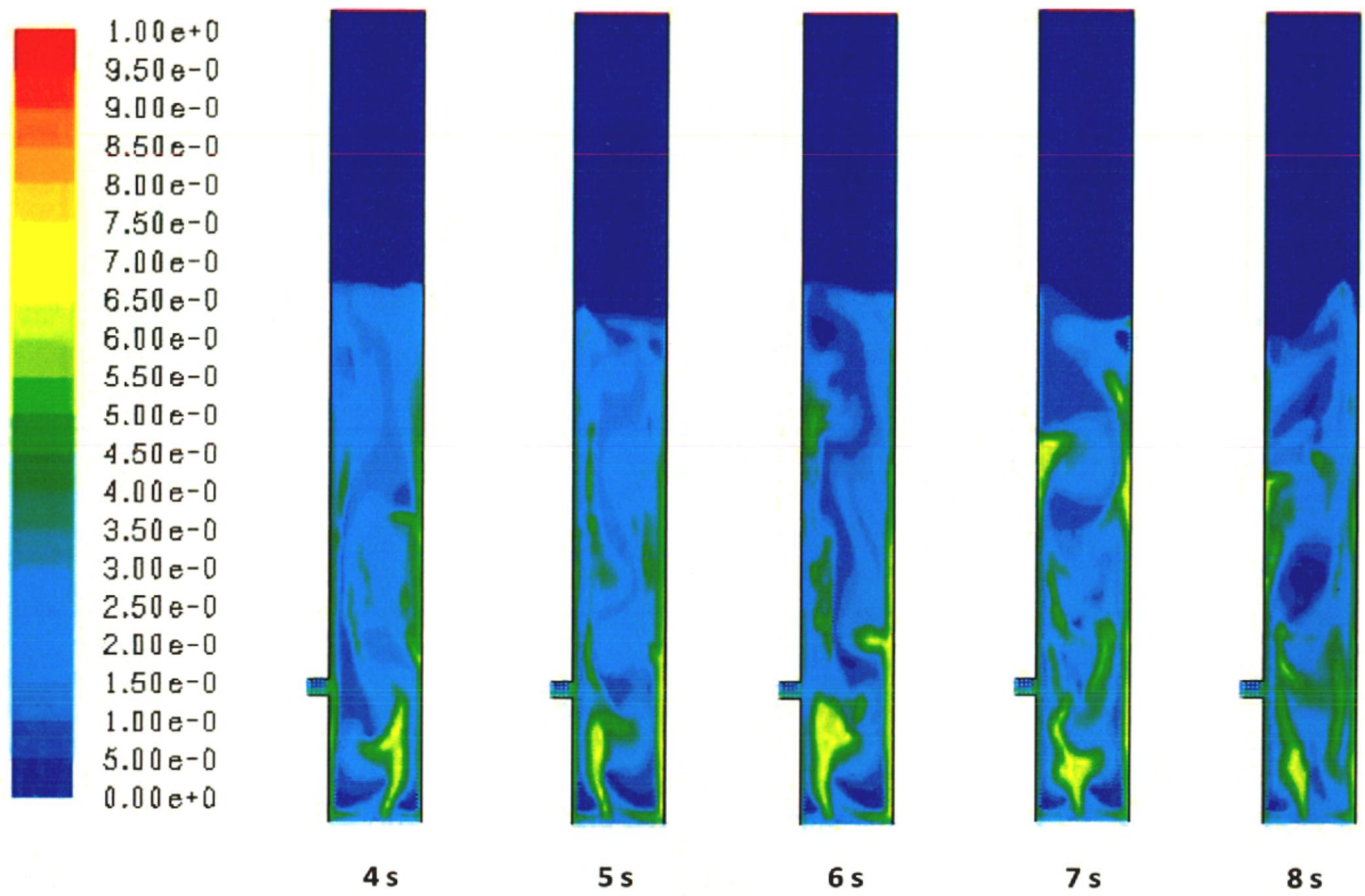


Fig. 5.5 (d) Bed Fluidization at air velocity = 1 m/ s

5.2 CIMFR Gasifier Model

Most of the work available in the literature is based on gasification of low ash coals having ash content in the range of 1- 10 %. However, most of the Indian coal have very high ash content (30- 40 %) for which neither simulation results nor geometry is available in literature. Therefore, to develop a robust model for gasification of Indian coal, CIMFR was contacted to obtain data on detailed geometry of bubbling fluidized bed gasifier pilot plant, composition of Indian coal & composition of syngas obtained from gasification of Indian coal.

5.2.1 Calibration & Validation: -

The composition of syngas & temperature obtained from the FLUENT gasifier model is shown in Table 5.2 along with the experimental results obtained from the CIMFR bubbling fluidized bed pilot plant.

Table 5.2: - Model Validation: predicted values vs. experimental

	Predicted Values	Experimental Values	Error (%)
Syngas Composition	(Mole Fraction, %)	(Mole Fraction, %)	
CO	18.1	18.24	0.84
CO ₂	13.78	14.54	-5.51
H ₂	20.94	19.02	9.16
N ₂	47.17	47.03	0.30
O ₂	0	0	0
H ₂ O	4.33E-05	0	0
Temperature (K)	1228.25	1160.82	5.81

The bar graphs as shown in Fig. 5.6 (a) shows the comparison between experimental and predicted syngas composition whereas Fig. 5.6 (b) compares the predicted and experimental gasifier temperature. From Fig. 5.6 (a) it is evident that the syngas composition & temperature predicted by the model are in good agreement with the experimental results. The maximum error is 9.16 % in case of H₂ mole fraction while for components like CO & N₂, the error is less than 1 %.

The value of temperature predicted by the model is slightly higher than the experimental value as evident from Fig. 5.6 (b). This is due to adiabatic wall condition used in the CIMFR model contrary to actual gasifier, where heat losses are present. The higher value of the H₂ mole fraction is probably due to higher rate of water gas shift reaction at higher temperature and lower rate of hydrogen combustion due to deficiency of oxygen in the gasifier (Table 5.3). A negative error (- 5.51 %) in CO₂ mole fraction is supposed to be due to lower rate of CO combustion and higher rate of boudouard reaction at higher temperature (Table 5.3).

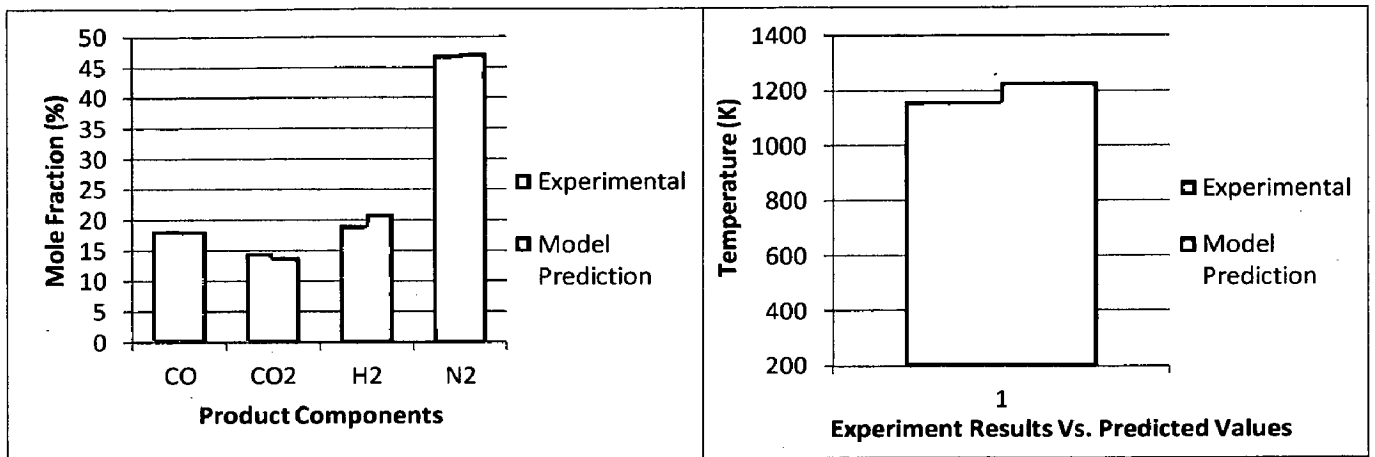


Fig. 5.6: - Comparison of Predicted Values & Experimental results, (a) syngas composition; (b) gasifier temperature

5.2.2 Temperature profile: - The contour of temperature profile of the gasifier is shown in Fig. 5.7. From the figure, it is evident that the temperature of the gasifier rises very quickly at the entrance of the gasifier and afterwards decreases slowly as we move towards the top of the gasifier. This is possibly because at the entrance of the gasifier, coal is virgin and plenty of oxygen is available. So, exothermic combustion reactions results in rapid rise in the temperature in the bed region.

However, as we move upwards, the concentration of O₂ decreases and endothermic reactions like reverse water gas shift reaction and boudouard reaction causes the temperature to decline slowly (Fig. 5.8). The above observation is also supported by the axial temperature distribution of the gasifier as shown in Fig. 5.10.

A schematic representation of various reactions occurring inside the gasifier is presented in Fig. 5.8 along the height of the gasifier. From this figure, it is evident that the combustion reactions such as char, H₂ and CO combustion occur almost completely in the lower portion of the gasifier upto a height of 0.5 m. Since, these reactions are highly exothermic, temperature of coal particles shoots in the gasifier in the height between 0 and 0.5 m as evident from Fig. 5.9.

However, after a height of 0.5 m, mainly Boudouard and reverse water gas shift reaction takes place which are endothermic in nature. Therefore, temperature of the gasifier was observed to decrease gradually afterwards along the height of the reactor. In Fig. 5.9, one can also observe a sharp decrease in temperature between height of 3.5 m and 4 m. This is probably because in this portion of the gasifier, velocity is very less (Fig. 5.14 (a)). Therefore, the residence time is high resulting in higher conversion of CO₂ to CO by endothermic reverse water gas shift reaction (Fig. 5.12 (a) & (b)). This results in sharp decrease in temperature of the gasifier in this region.

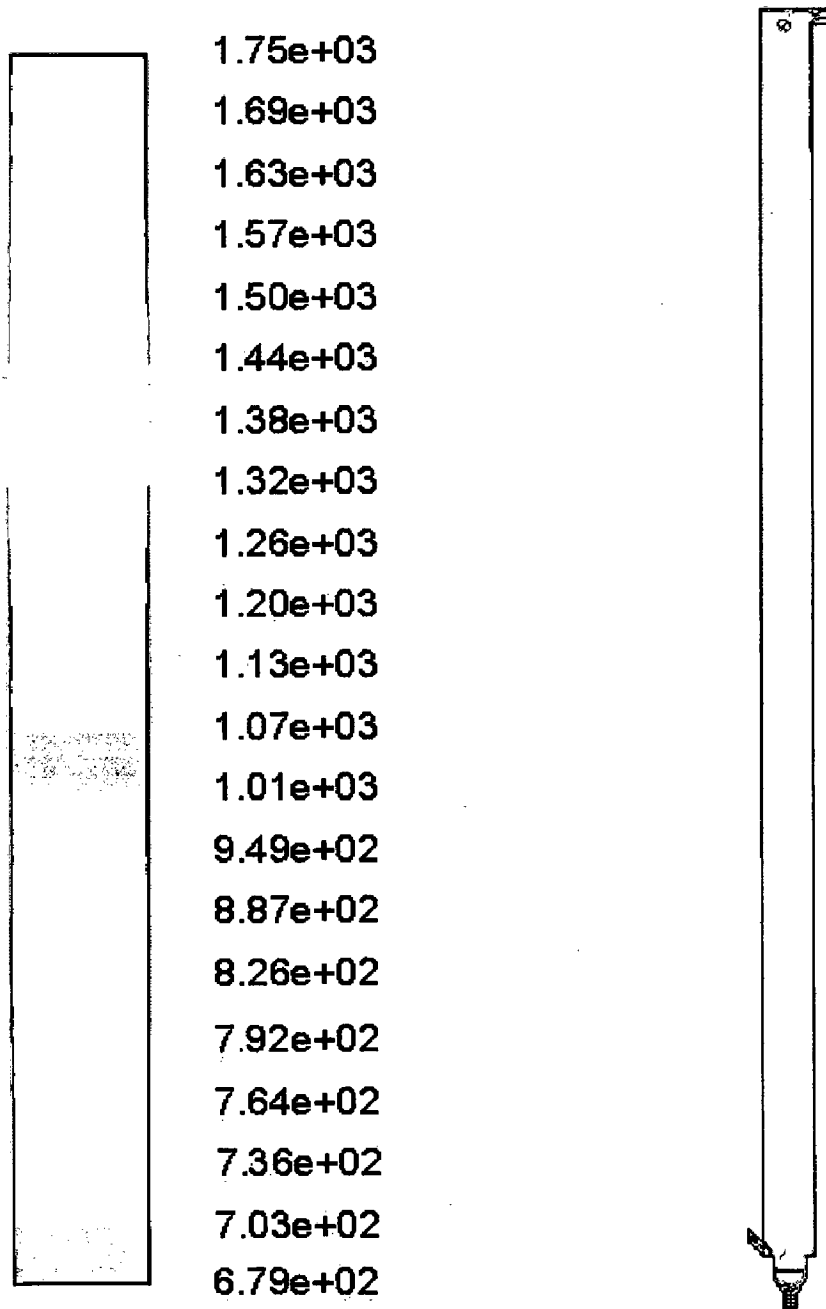


Fig. 5.7: -Contour of Temperature distribution inside the gasifier

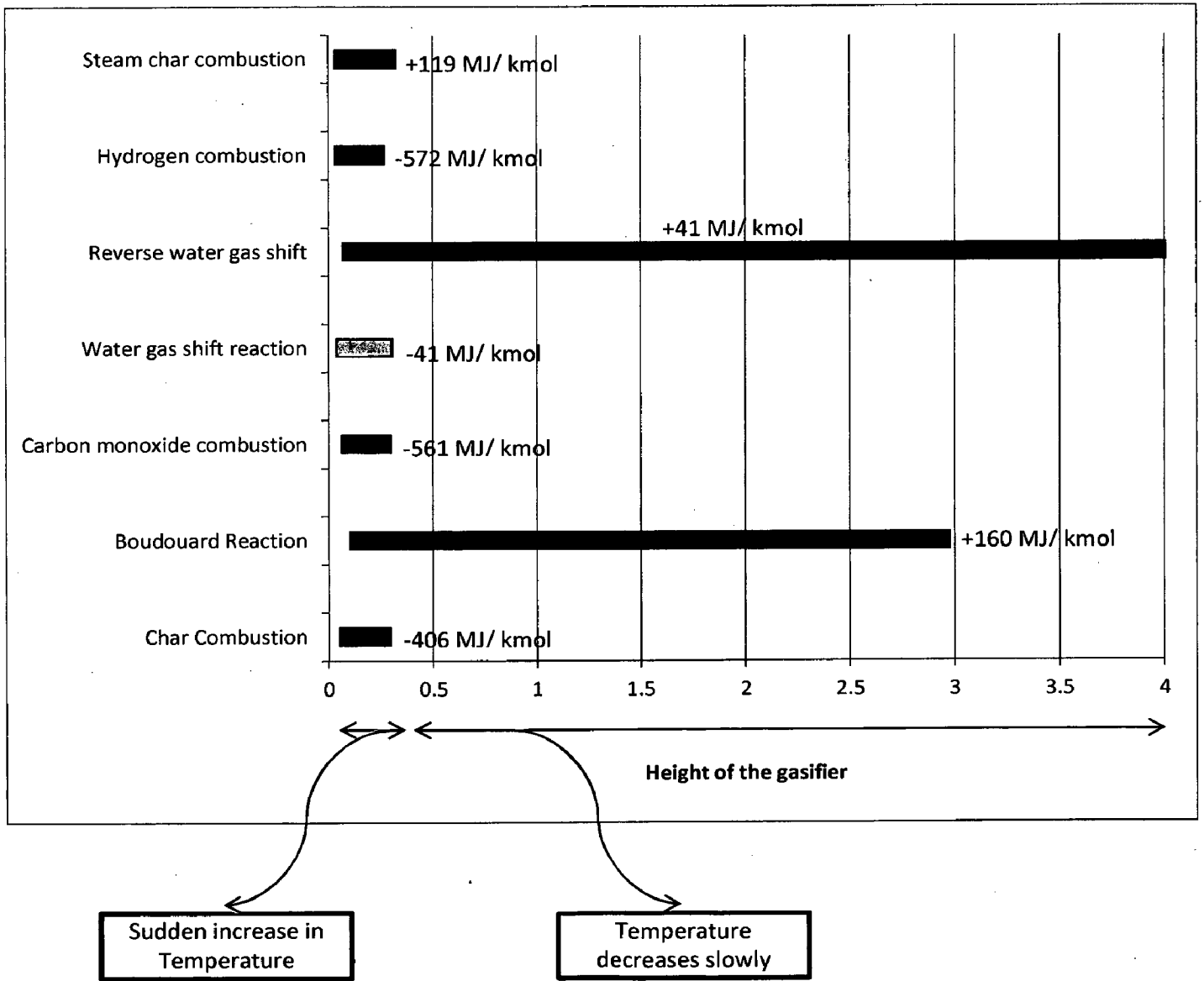


Fig. 5.8: - Reaction pattern along the height of the gasifier

— x-coordinate-7

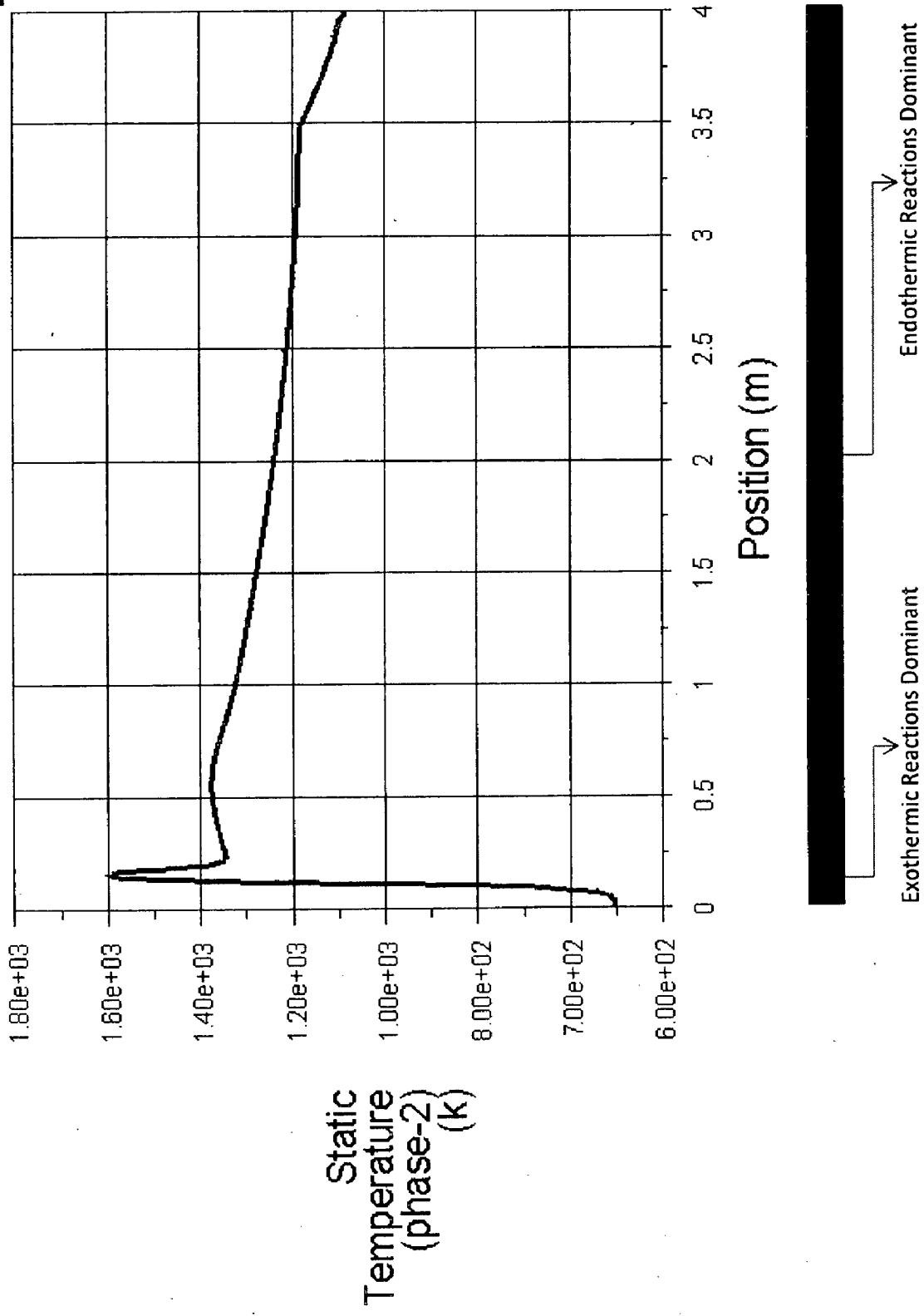


Fig. 5.9: -Axial temperature distribution inside the gasifier

5.2.3 Reaction rate profile: - Fig. 5.10 (a- f) illustrates the axial profile of reaction rates for heterogenous (char oxygen combustion reaction, char CO₂ combustion reaction) and homogeneous (Carbon monoxide combustion reaction, water gas shift reaction, reverse water gas shift reaction, boudourd reaction and hydrogen combustion reaction) gasification reactions.

From these profiles, it is apparent that the combustion reactions like char, carbon monoxide and hydrogen combustion occur very promptly and in a small portion of the gasifier near the coal inlet region and bed zone. The reaction rates for these reactions rises very quickly and reach their peak at a height of 0.2 to 0.3 m along the gasifier.

However, gasification reactions like reverse water gas shift reaction and boudouard reaction occur slowly over a larger portion of the gasifier length. They play a major role in the upper portion of the gasifier, resulting in an increase in the concentration of CO and decrease in the concentration of CO₂ and H₂ as we move towards the top of the gasifier.

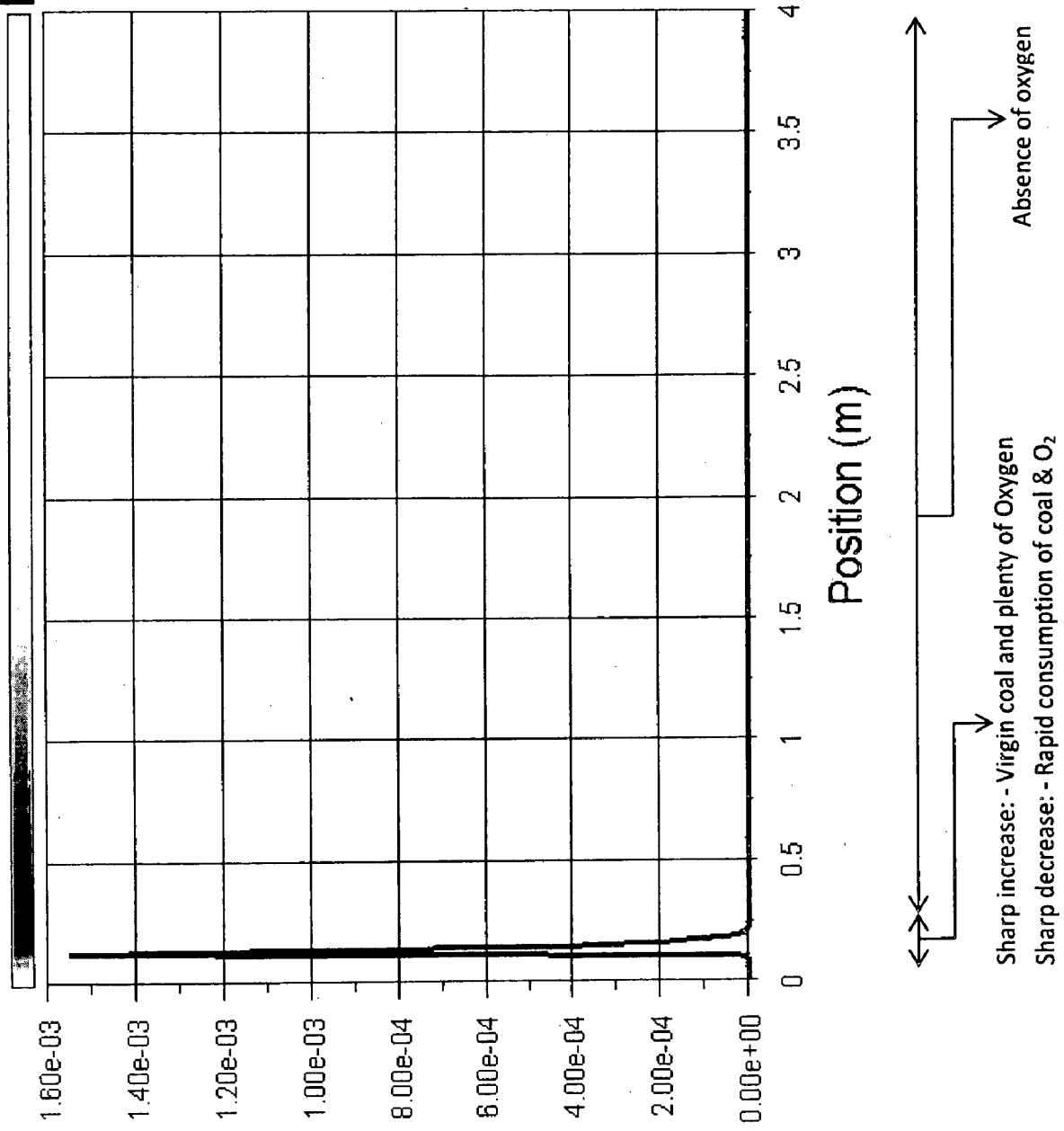
Fig. 5.3 Average rate of reactions

Heterogeneous Reactions	
Reaction	Reaction Rate (kgmol/ m³-s)
C + O ₂ → 0.4 CO + 0.6 CO ₂	9.081e-06
C + H ₂ O → CO + H ₂	1.0759e-10
C + CO ₂ → 2 CO	5.1755e-05
Homogeneous Reactions	
CO + O ₂ → CO ₂	1.7732e-05
CO + H ₂ O → CO ₂ + H ₂	1.689e-04
CO ₂ + H ₂ → CO + H ₂ O	1.711e-06
2 H ₂ + O ₂ → 2 H ₂ O	5.019e-05

The average rate of these reactions over the volume of the gasifier is given in Table 5.3. From the table, it is evident that the reaction rate for water gas shift reaction is higher than hydrogen combustion reaction. Also, Boudouard reaction dominates over carbon monoxide combustion reaction primarily due to higher operating temperature of the gasifier model under assumed adiabatic condition. This is responsible for higher prediction in mole fraction of H₂ and lower prediction in mol fraction of CO₂ from the experimental results.

— x-coordinate-7

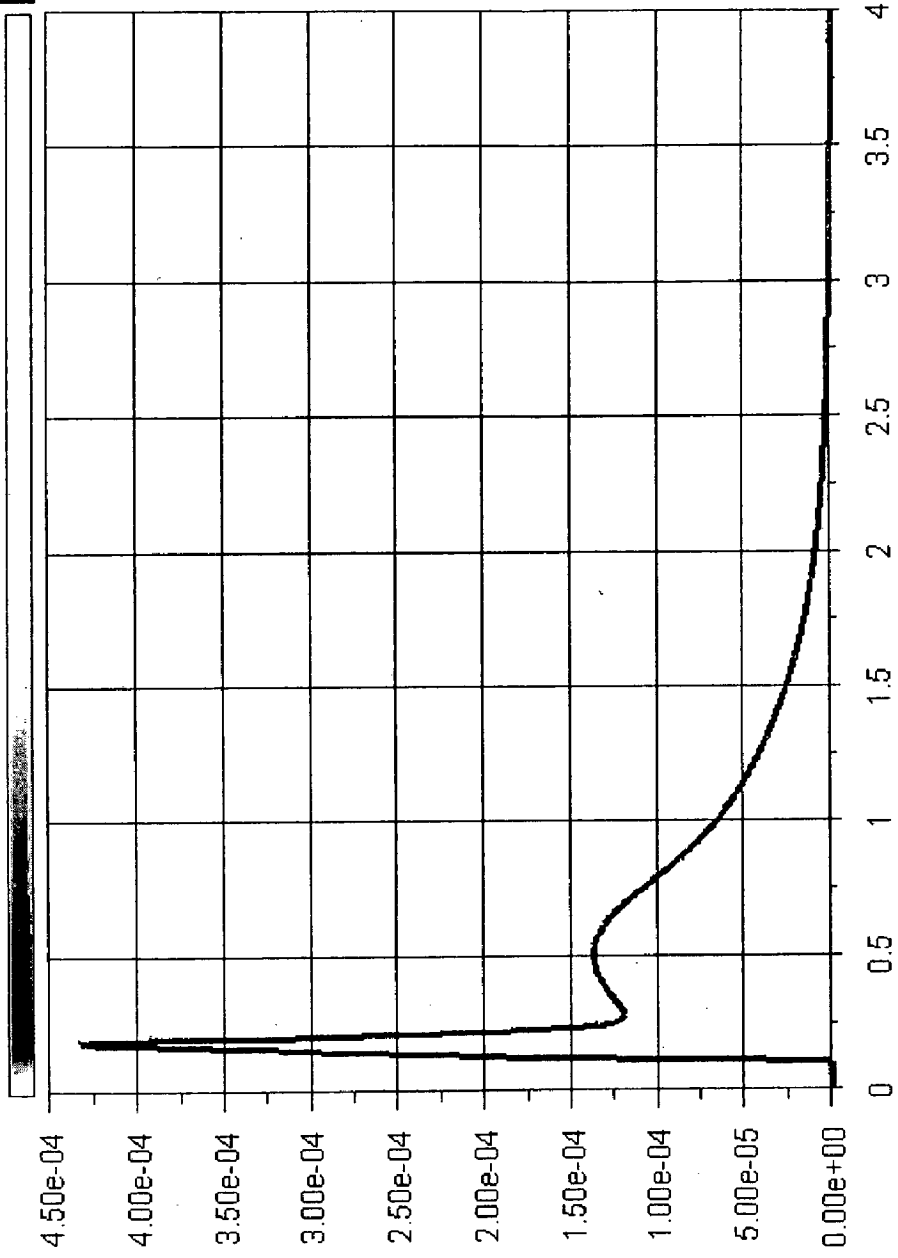
Concentration of coal along the axis of gasifier ↓



Heterogeneous Reaction Rate 1
(mixture)
(kgmol/m³-s)

Fig. 5.10 (a): Axial profile of char oxygen combustion reaction

Concentration of coal along the axis of gasifier



Heterogeneous Reaction Rate 3 (mixture) (kgmol/m³-s)

Position (m)

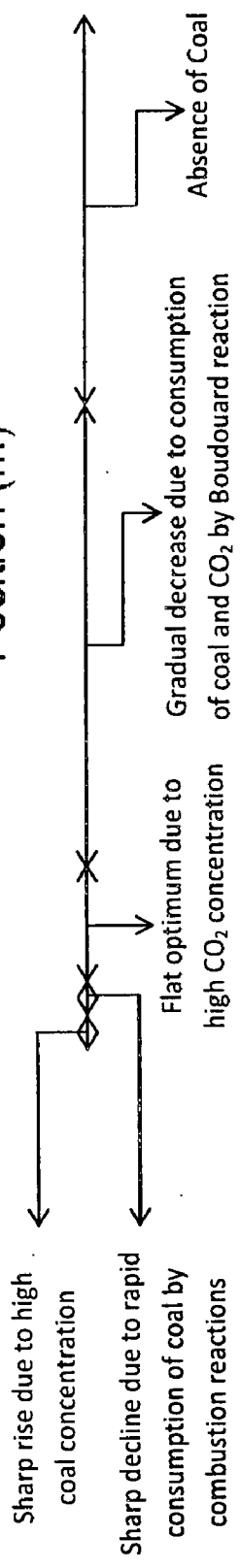


Fig. 5.10 (b): Axial profile of char CO₂ combustion reaction

Fig. 5.10 (a) shows the reaction rate profile for char combustion reaction along the height of the gasifier. From the figure, it is evident that the char combustion reaction occur over a very small portion of the gasifier. The reaction rate increases sharply in the lower portion of the gasifier and reaches its peak of $0.0015 \text{ kmol/ m}^3 \cdot \text{s}$ near the coal inlet section. Afterwards, the reaction rate decreases very sharply. The peak near the coal inlet section is due to high concentration of coal and availability of large amount of oxygen. The char combustion reaction is so fast that most of the coal gets consumed in a very small interval of time and hence the reaction rate decreases very sharply afterwards.

Fig. 5.10 (b) shows the reaction rate profile for boudouard reaction along the height of the gasifier. From the figure, it can be observed that the reaction rate rises very sharply and reaches its peak of $0.000425 \text{ kmol/ m}^3 \cdot \text{s}$ near the coal inlet section of the gasifier. Afterwards, it decreases sharply to a lower value of $0.000125 \text{ kmol/ m}^3 \cdot \text{s}$. The reaction rate again increases slowly and reaches a flat maxima at a height of 0.5 m. Afterwards, it decreases slowly and reaches to zero at a height of 2.5 m. This can be explained as follows: -

The first peak is due to high concentration of coal near the coal inlet section. However, the concentration of coal decreases very quickly due to rapid combustion reaction resulting in sharp decrease in reaction rate of boudouard reaction. The second peak is due to high concentration of CO_2 which has its flat optimum at a height of 0.5 m as evident from Fig. 5.12 (a).

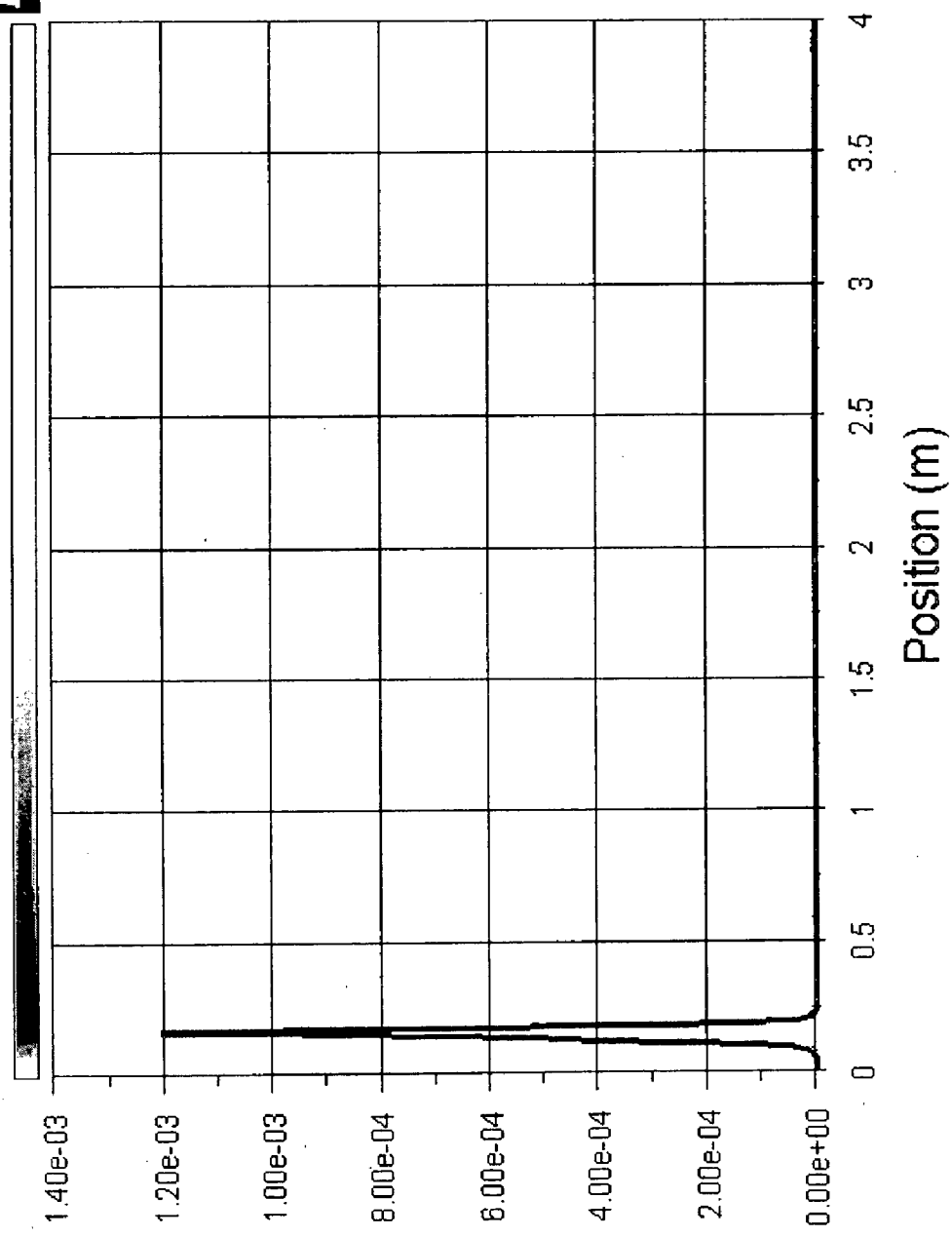
Fig. 5.10 (c) presents the reaction rate profile for CO combustion reaction along the height of the gasifier. CO is formed very quickly near the coal inlet section by char combustion and steam char combustion reaction as evident from Fig. 5.12 (b). However, due to availability of plenty of oxygen in this region, CO combustion reaction starts quickly to convert CO to CO_2 . The reaction rate increases very sharply and reaches its maximum of $0.0045 \text{ kmol/ m}^3 \cdot \text{s}$ at a height of around 0.125 m. Afterwards, it decreases sharply due to sharp decrease in concentration of O_2 due to combustion reactions.

Fig. 5.10 (d & e) shows the reaction rate profile for water gas shift reaction and reverse water gas shift reaction along the height of the gasifier. From Fig. 5.10 (d), it is evident that the reaction rate for water gas shift reaction rises sharply and reaches its peak near the coal inlet section. This is due to the fact that in this region CO is formed by char oxygen and char steam combustion reaction as clear from Fig. 5.12 (b). Also, steam is available in the lower section of the gasifier. The presence of these two reactants initiates the water gas shift reaction and causes it to proceed rapidly. However, steam gets consumed very quickly (Fig. 5.12 (e)) due to char steam combustion and water gas shift reaction causing the reaction rate to decrease sharply.

The reverse water gas shift reaction is a slow reaction. With formation of CO_2 and H_2 in the lower section of the gasifier, its rate increases and reaches a maximum of $0.000180 \text{ kmol/ m}^3 \cdot \text{s}$. Afterwards, it proceed at almost constant rate with slight gradual decrease due to consumption of CO_2 and H_2 by the same reaction along the height of the gasifier.

Concentration of coal along the axis of gasifier

x-coordinate



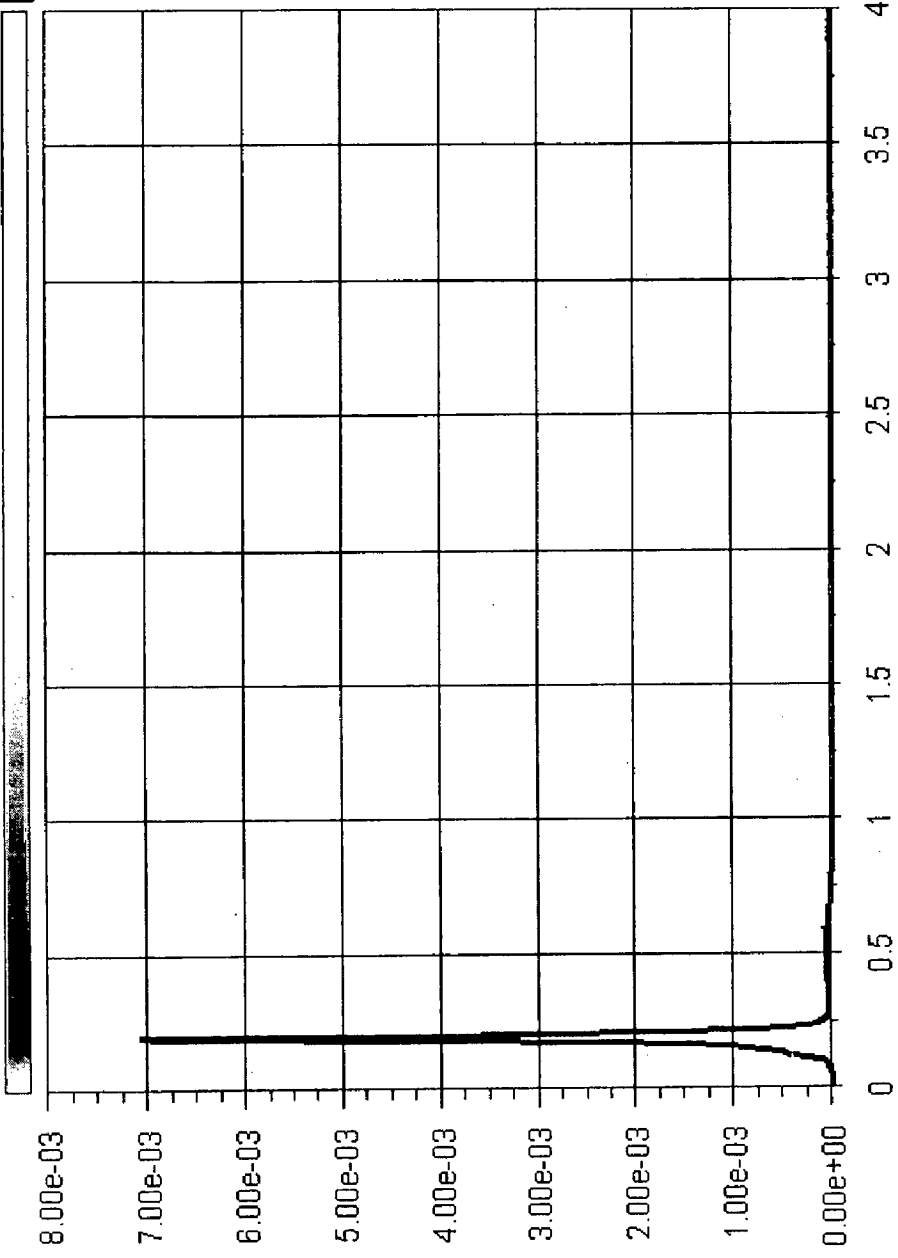
Sharp increase: - Plenty of CO & Oxygen
 Sharp decrease: - Rapid consumption of O₂
 Absence of oxygen

Fig. 5.10 (c): Axial profile of carbon monoxide combustion reaction

x-coordinate-7



Concentration of coal along the axis of gasifier



Rate of Reaction-2 (phase-1) (kgmol/m³-s)

Position (m)

Sharp increase: - Plenty of CO₂ & H₂O
Sharp decrease: - Rapid consumption of H₂O
Absence of H₂O

Fig. 5.10 (d): Axial profile of water gas shift reaction

x-coordinate-7

Concentration of coal along the axis of gasifier

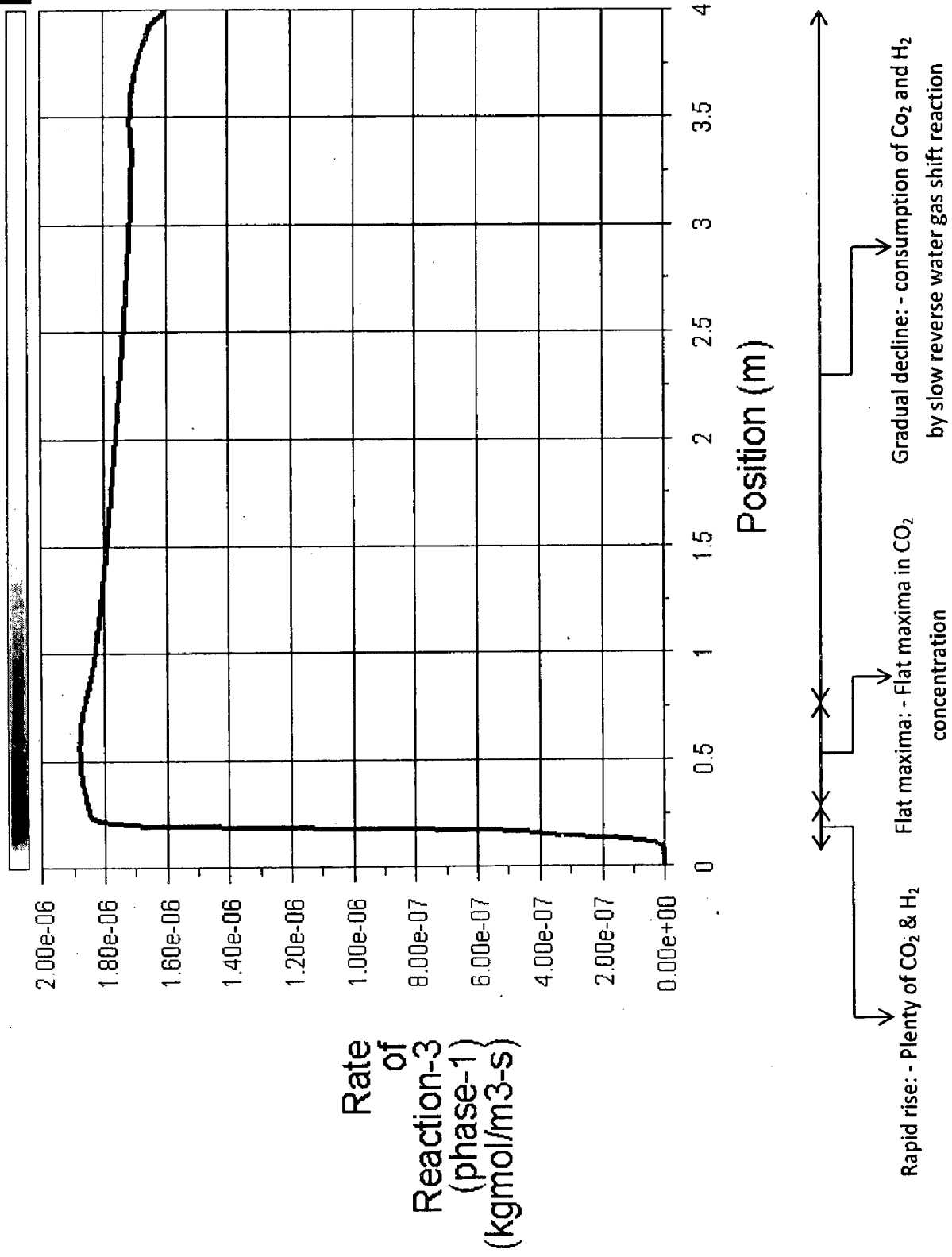


Fig. 5.10 (e): Axial profile of reverse water gas shift reaction

— x-coordinate-7

Concentration of coal along the axis of gasifier ↓

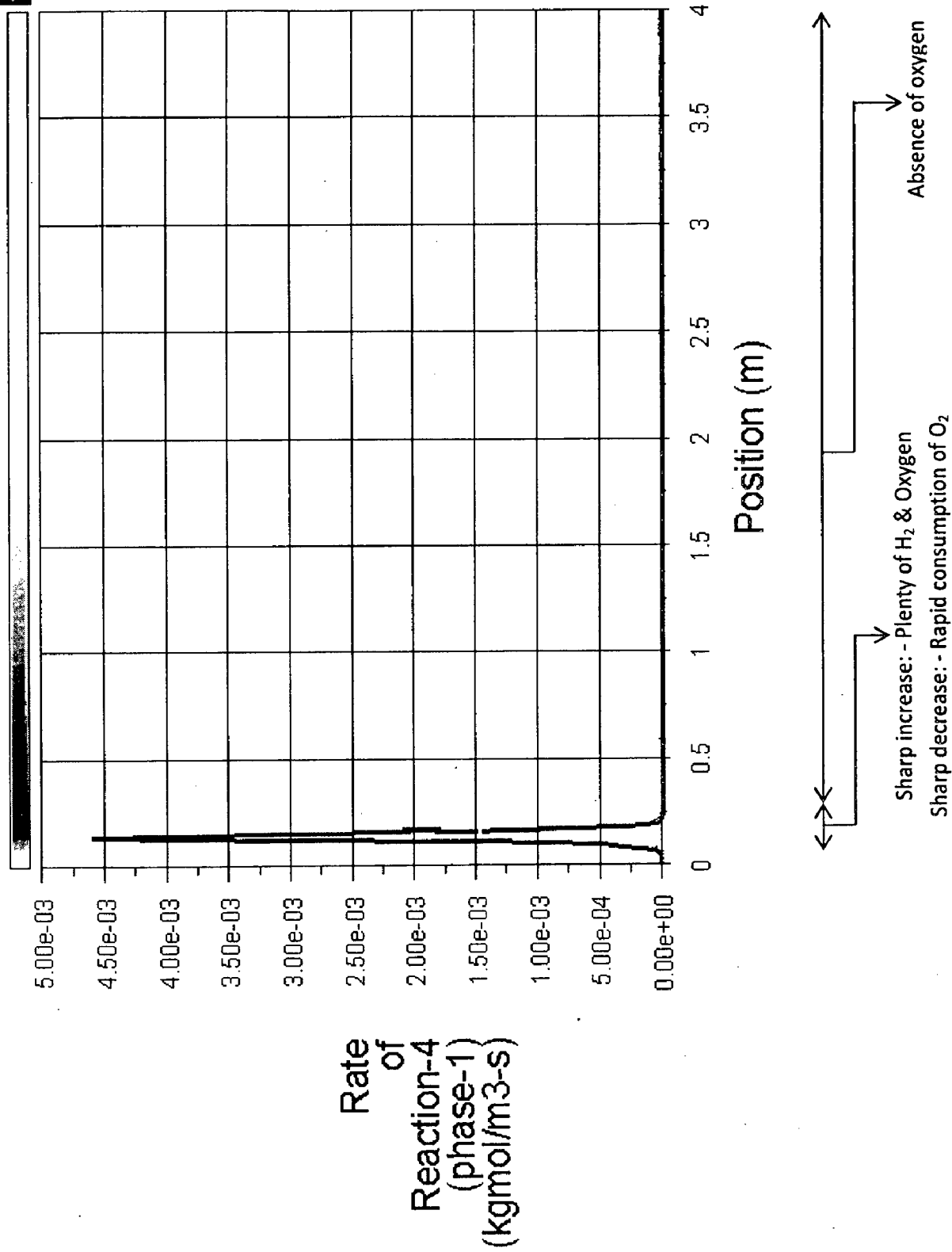


Fig. 5.10 (f): Axial profile of Hydrogen combustion reaction

5.2.4 Contours of species mole fraction: - The contours of the mole fraction of different components (CO, CO₂, N₂ and H₂) in the syngas are shown in Fig. 5.11 (a- d) . From the contours, it is evident that the concentration of CO₂ and H₂ is high in the bed zone but decreases slowly as we move towards the top of the gasifier. However, the trend is opposite for CO, whose concentration is minimum in the bed zone but increases towards the top of the gasifier. This is possibly due to char combustion, CO combustion and forward water gas shift reaction which are dominant in the bed zone due to availability of plenty O₂ and H₂O (Fig. 5.10 (a), (b),(d)).

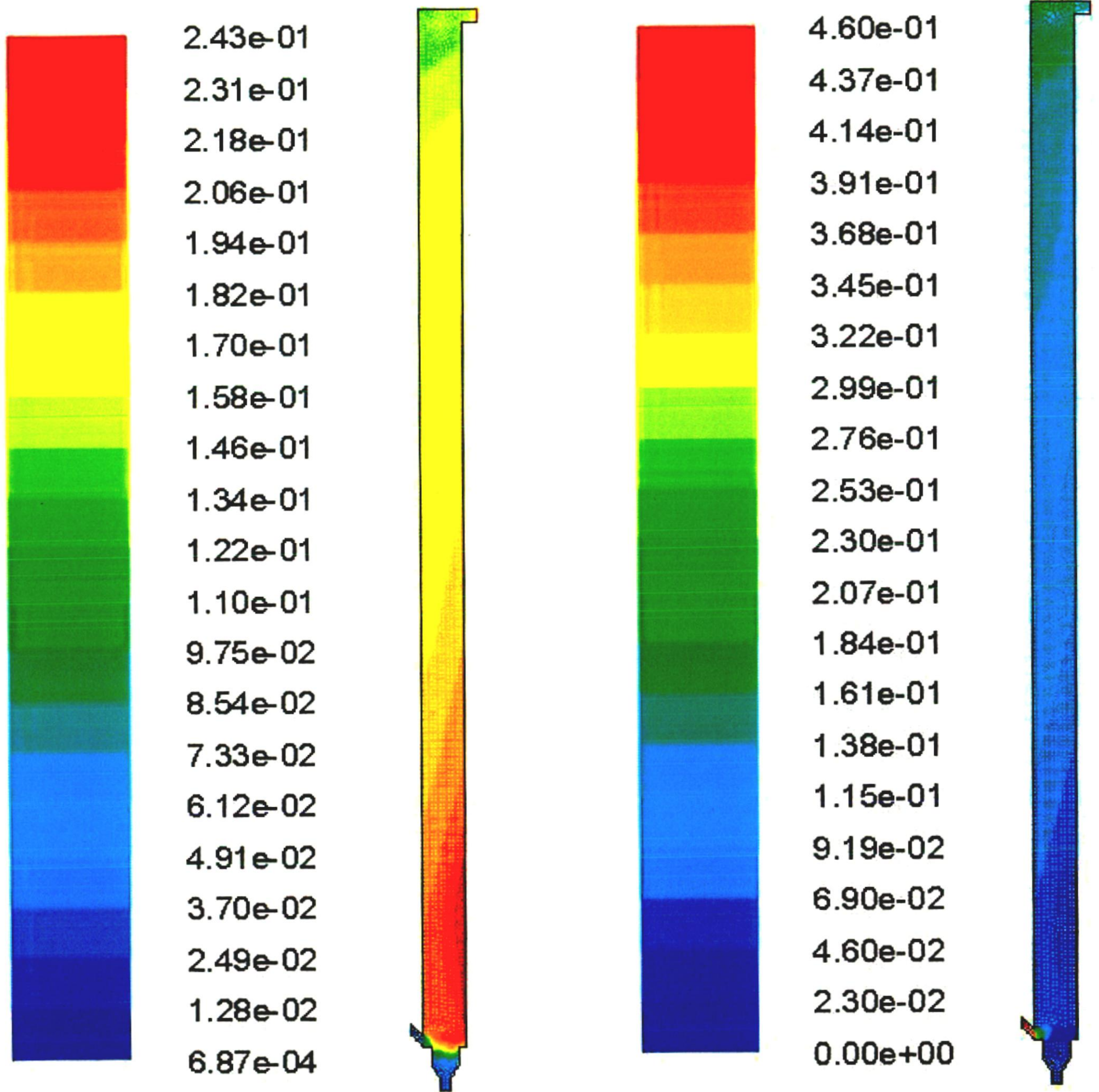


Fig. 5.11 (a): - Contour of Mole fraction of CO₂

Fig. 5.11 (b): - Contour of Mole fraction of CO

However, as we move away from the bed zone, boudouard reation and reverse water gas shift reation becomes dominant resulting the increase in concentration of CO and decrease in concentration of CO₂ & H₂ (Fig. 5.10 (b), (e)).

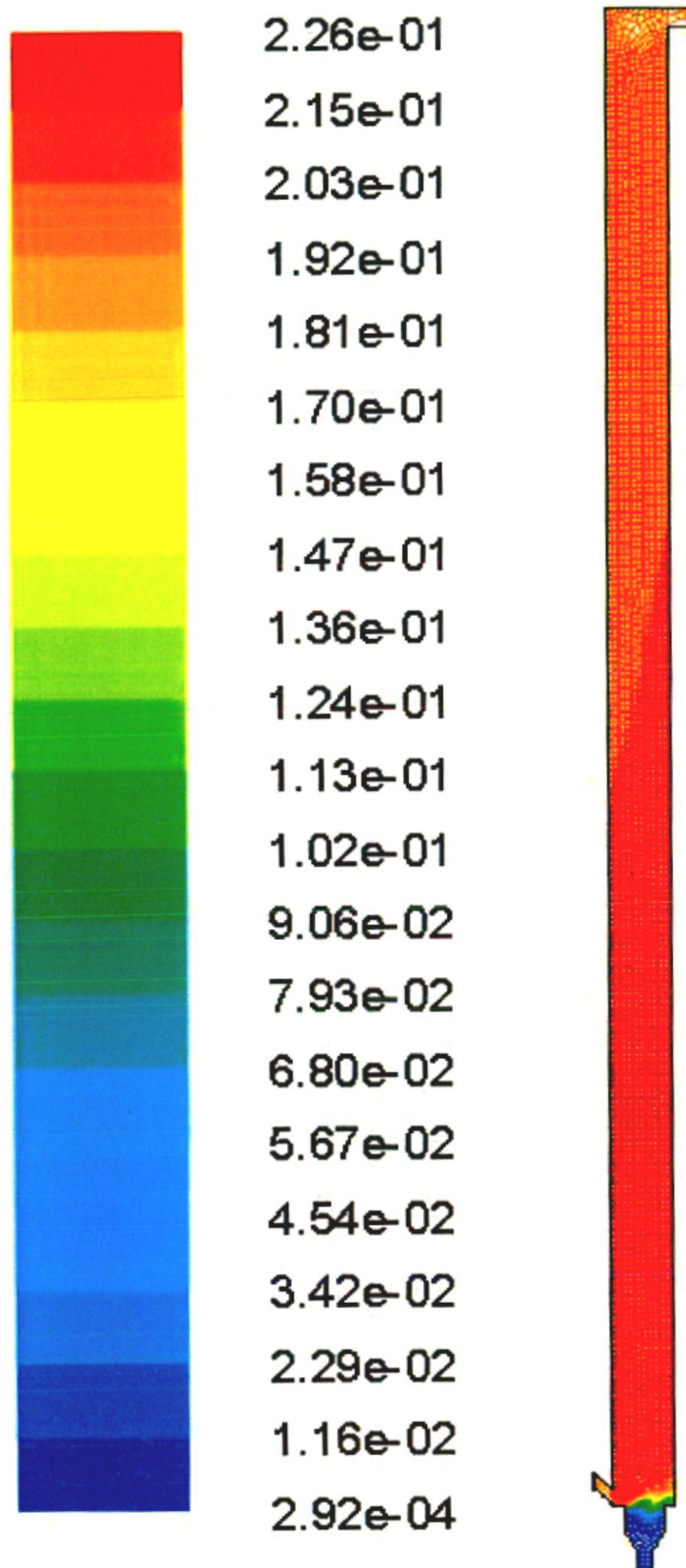


Fig. 5.11 (c): - Contours of Mole fraction of H₂

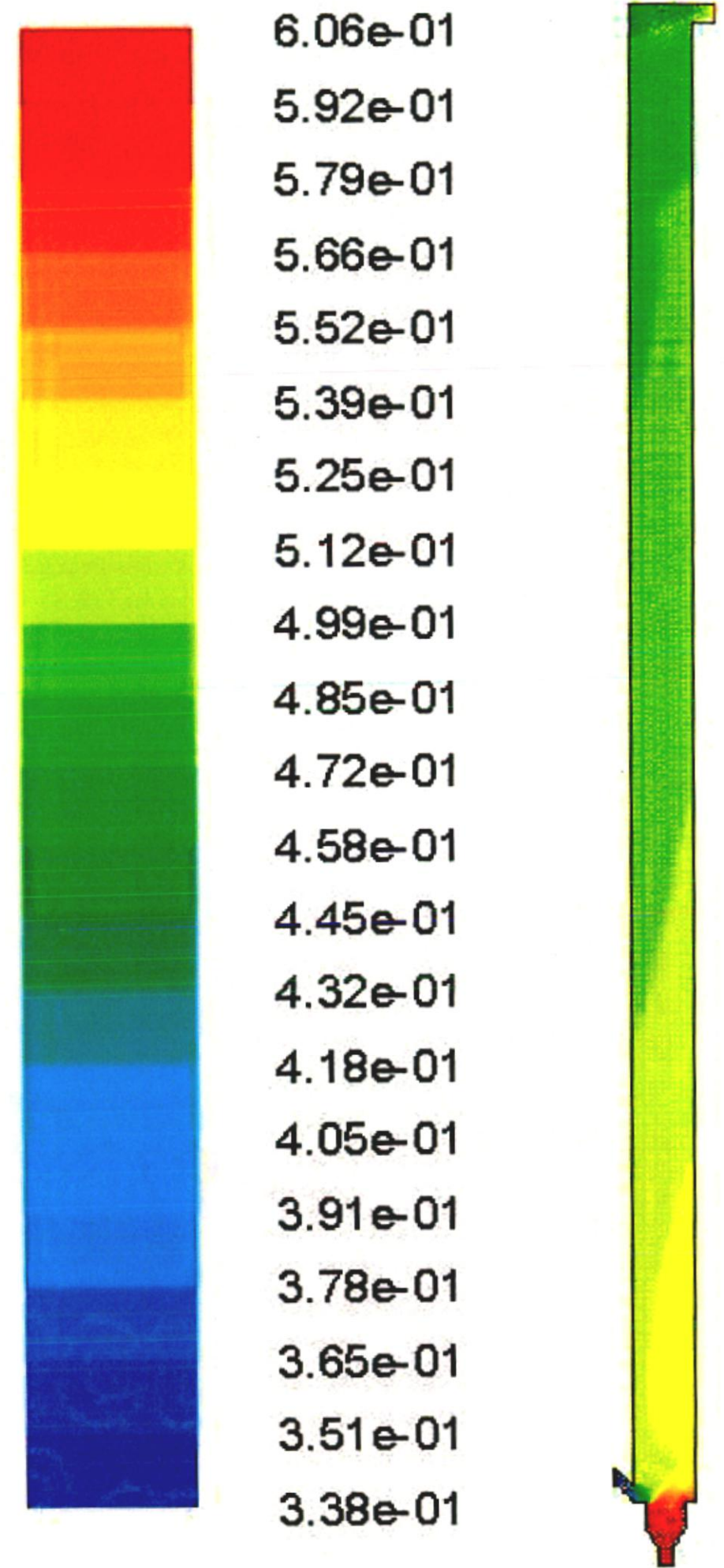


Fig. 5.11 (d): - Contours of Mole fraction of N₂

Also, from fig. 5.11 (c), it is apparent that the concentration of N_2 is highest in the bed zone and decreases as we move towards the top of the gasifier. This is primarily because air (78 % N_2 and 21 % O_2) is used as gasifying medium in this process and is fed through an air distributor at the bottom conical section of the gasifier. Therefore, the concentration of N_2 is high in the lower portion of the gasifier. The decrease in concentration afterwards is due to formation of other gaseous components such as CO_2 , CO and H_2 via gasification reactions. N_2 is itself an inert gas and doesn't undergo any reactions in the operating temperature range of the gasifier.

A similar trend is observed from the axial plot of mole fraction of these components with reactor height as shown in Fig. 5.12 (a- e). From these plots, it is evident that in the upper part of the reactor, boudouard reaction and reverse water gas shift reaction plays a major role resulting in increase in concentration of CO and decrease in the concentration of CO_2 and H_2 as we move upwards in the gasifier as evident from reaction rate plot of Fig. 5.10 (a- f)

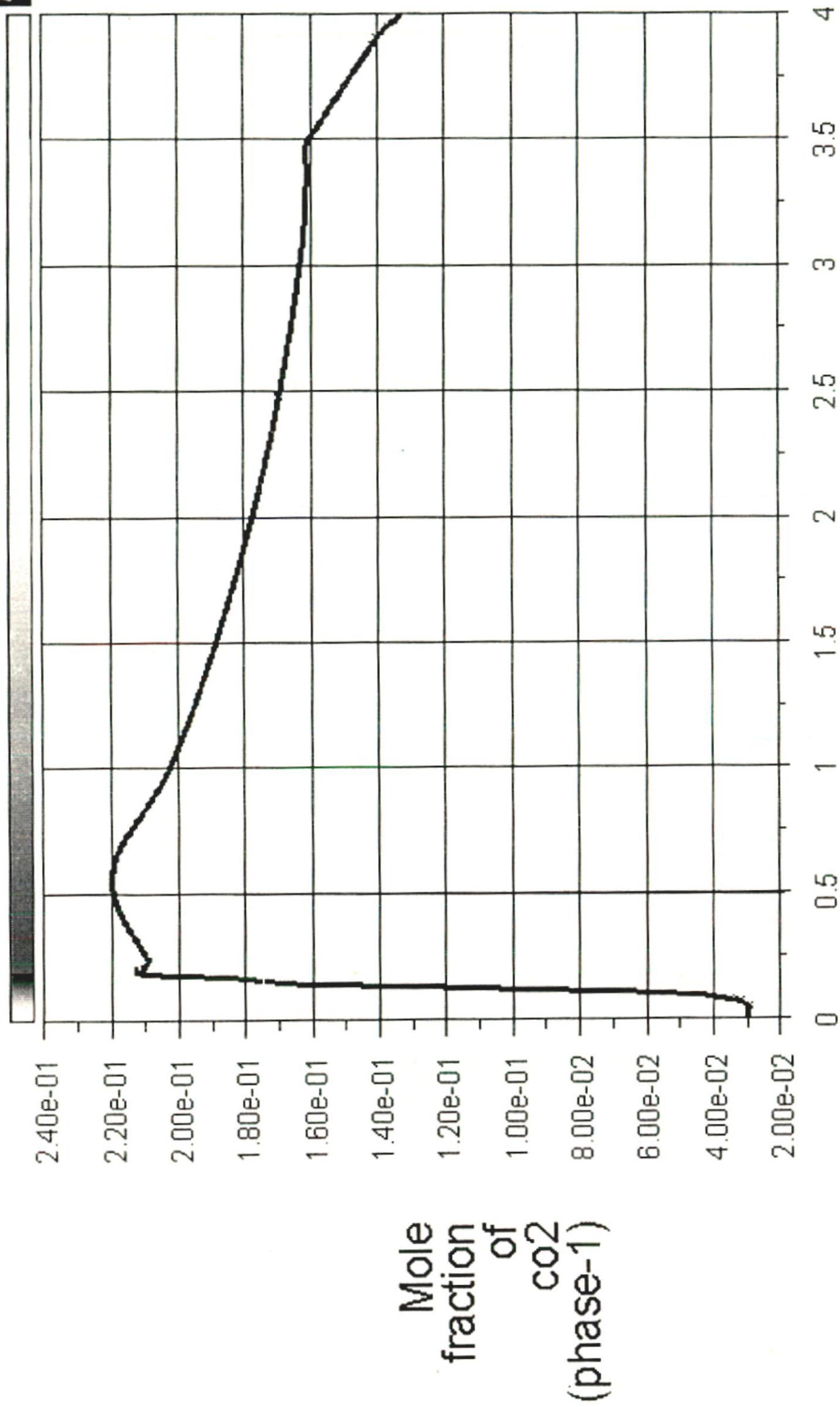
Also, It can be noted that the mole fraction of steam is maximum in the bottom portion of the gasifier. This is due to the steam already present in the gasifying medium and hydrogen combustion reaction which occur almost completely in the lower portion of the gasifier (Fig. 5.10 (f)). However, it is consumed completely in lower portion itself due to dominant water gas shift reaction (Fig. 5.10 (d)).

Fig. 5.12 (b) represents the mole fraction of CO along the height of the gasifier. From the figure, it is evident that the concentration rises sharply and reaches a peak of 0.06 at a height of 0.25 m. However, it drops very quickly to 0.04. Afterwards, it increases continuously. The initial peak is due to formation of CO by char combustion and steam char combustion reaction. However, it decreases sharply due to CO combustion reaction. Afterwards, it increases continuously due to boudouard reaction and reverse water gas shift reaction which occur over a large portion of the gasifier.

Fig. 5.12 (c) shows the mole fraction of N_2 along the height of the gasifier. The concentration is maximum in the lower section of the gasifier and decreases gradually as we move towards the top of the gasifier. This is due to fact that air (containing 78 % N_2) is fed from the bottom of the gasifier. The decrease afterwards is due to formation of other gaseous species as N_2 itself is inert.

Fig. 5.12 (d) shows the mole fraction of H_2 along the height of the gasifier. From the figure, it is evident that the mole fraction of H_2 rises very quickly and reaches its peak of 0.225 at a height of 0.2 m. Afterwards, it decreases slowly along the height of the gasifier. This can be explained as follows.

The sharp increase in the concentration initially is due to steam char combustion reaction and water gas shift reaction which are very rapid in the lower section of the gasifier. The slow decrease afterwards is due to reverse water gas shift reaction which occur slowly throughout the height of the gasifier.



Position (m)

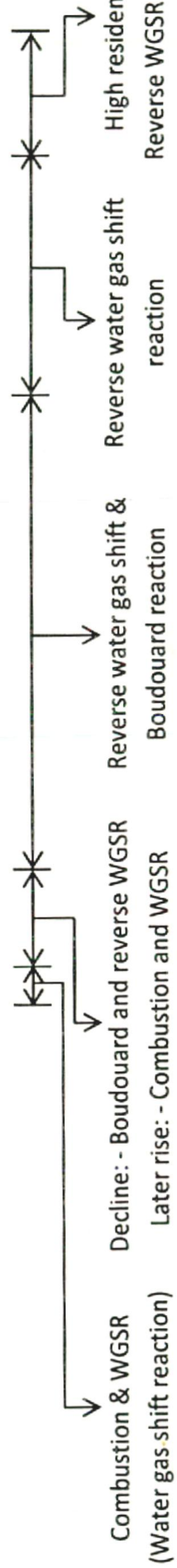


Fig. 5.12 (a): Axial profile of mole fraction of CO₂



Position (m)

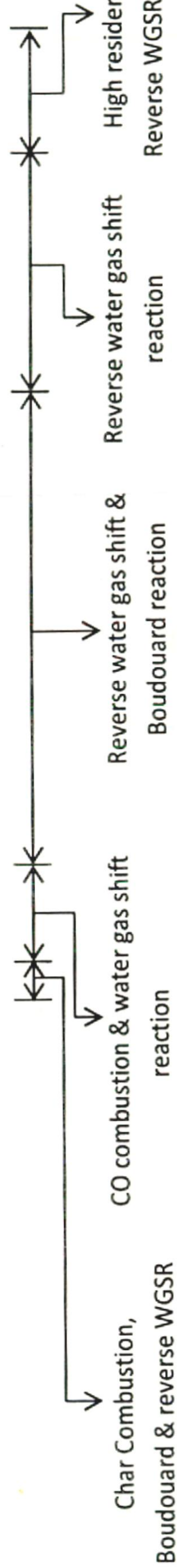
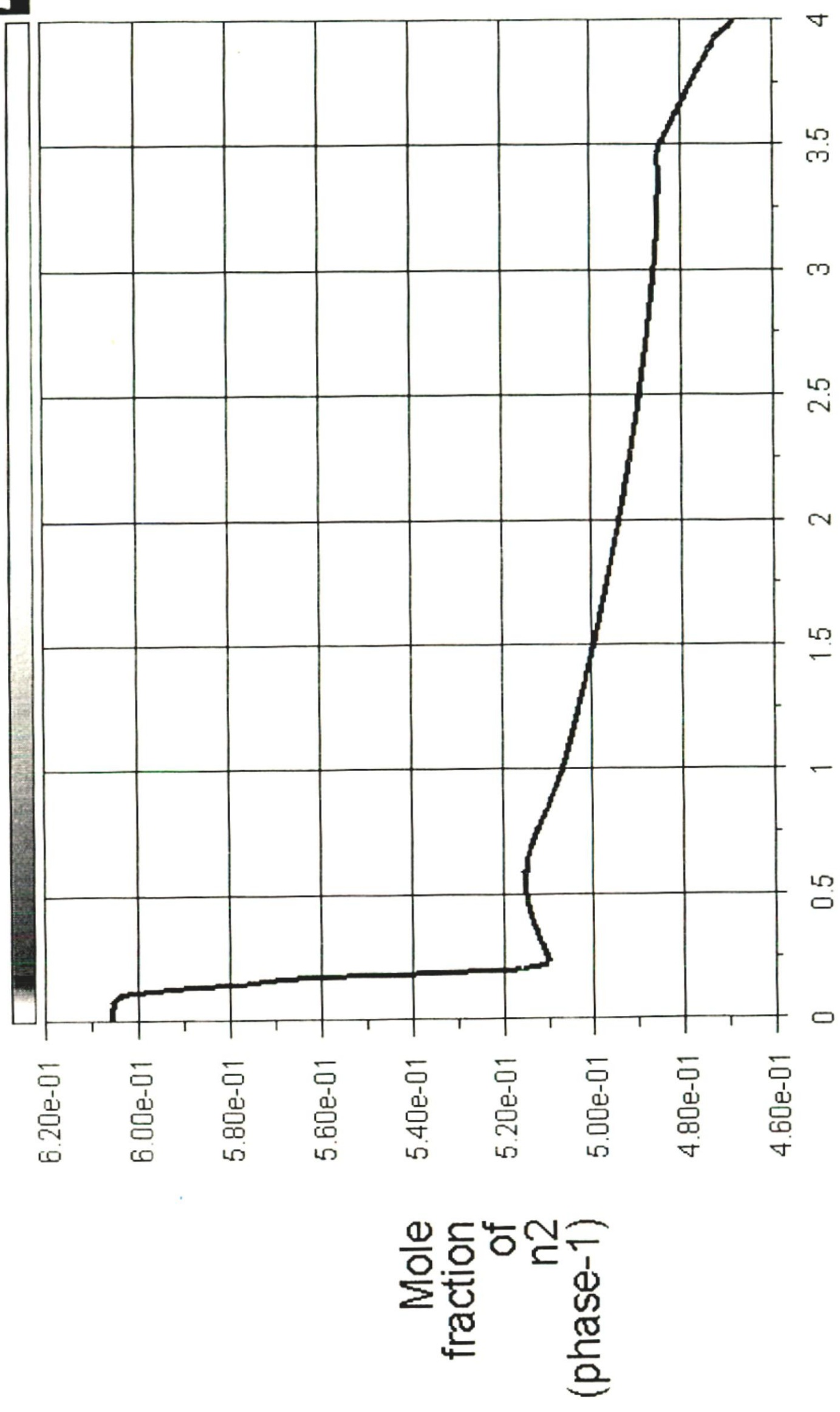


Fig. 5.12 (b): Axial profile of mole fraction of CO



Position (m)

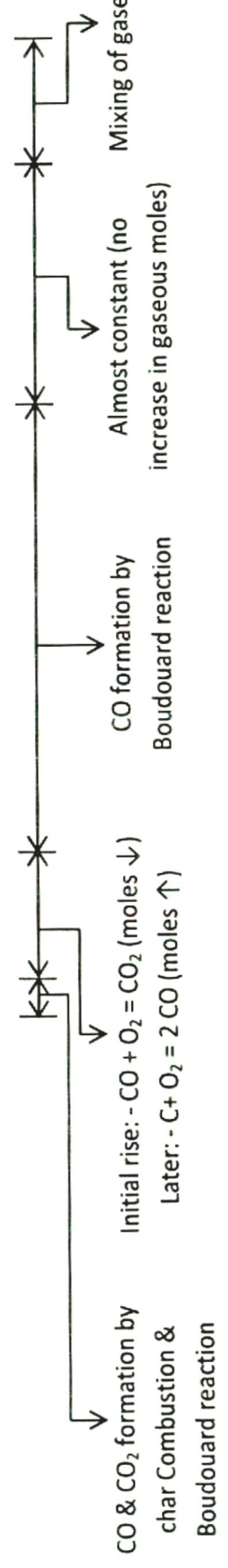


Fig. 5.12 (c): Axial profile of mole fraction of N₂

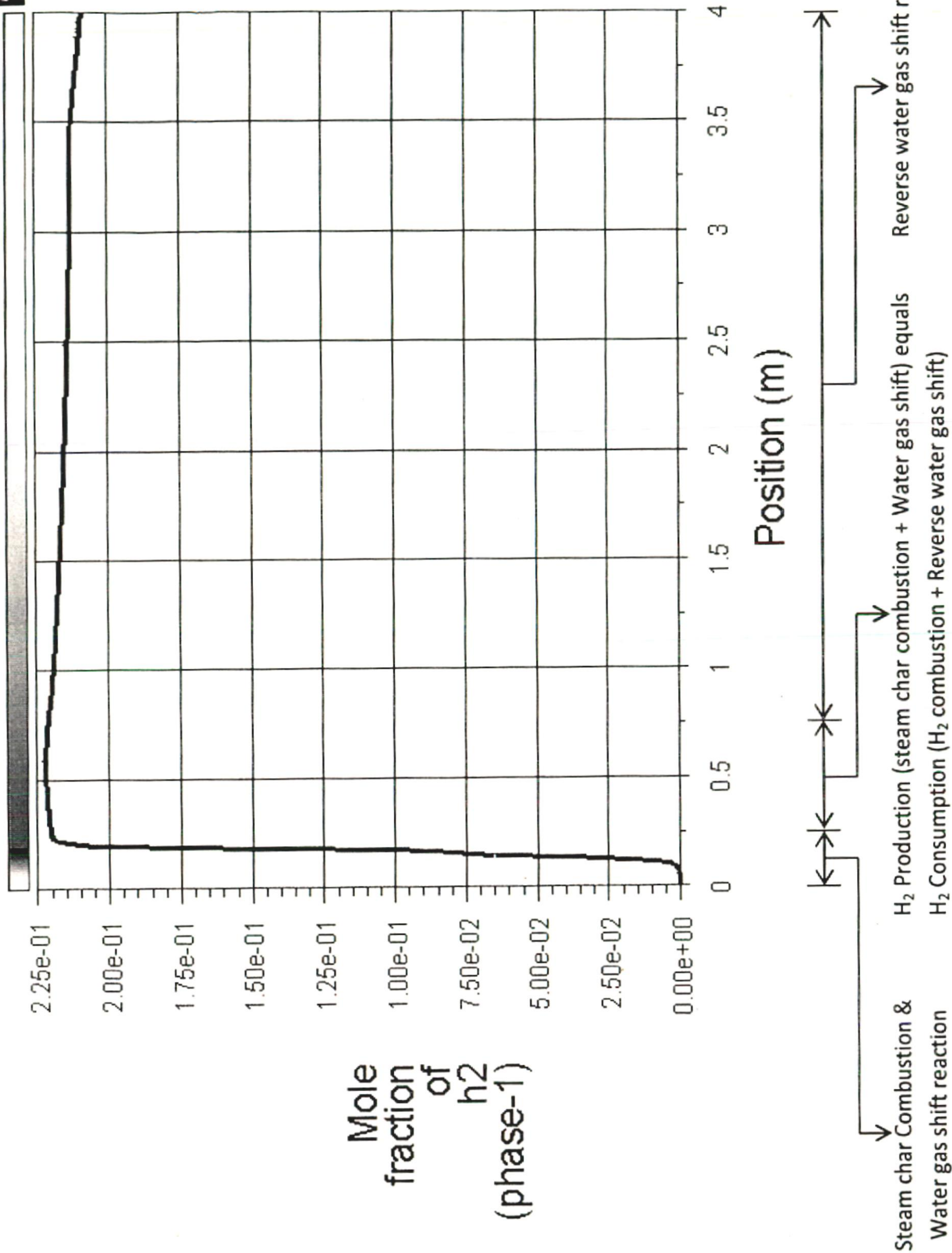


Fig. 5.12 (d): Axial profile of mole fraction of H_2

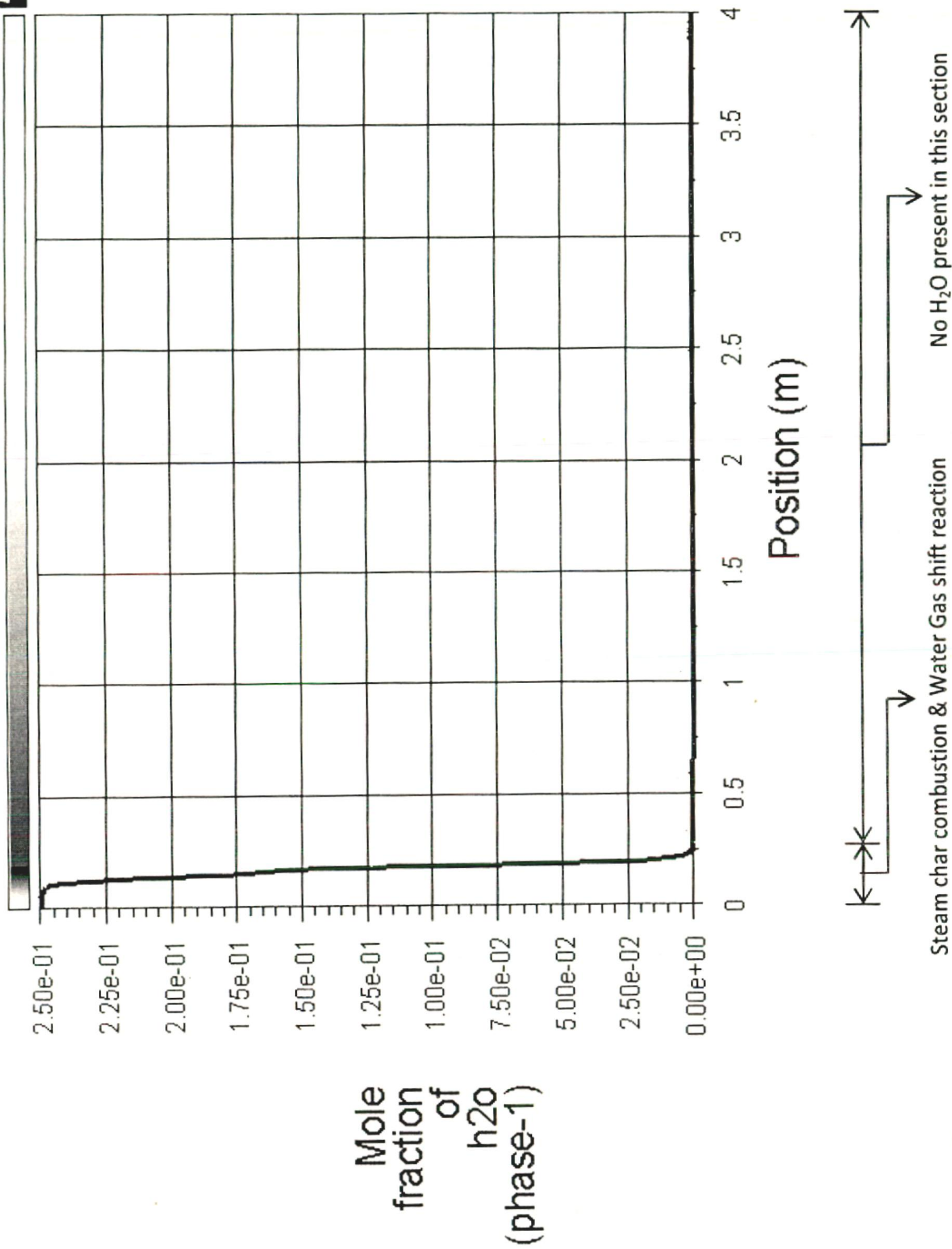


Fig. 5.12 (e): Axial profile of mole fraction of H₂O

5.2.5 Volume Fraction profile: - The volume fraction profile inside the gasifier as a function of time is given in Fig. 5.13. The sharp decrease in the volume fraction of phase 2 near the coal inlet region is due to consumption of char through combustion reaction. Also, devolatilization reaction is very fast and occur in the coal inlet region resulting in formation of tar. Afterwards, the phase 2 volume fraction remains almost constant as ash and tar cannot participate in reaction. The height of the gasifier is such that ash present in the coal cannot pass through the gasifier outlet and instead settles down by gravity as the gas –solid mixture moves upward and leaves the gasifier through the ash outlet at the bottom of the gasifier. Therefore, the volume fraction of phase 2 is zero at the topmost portion of the gasifier.

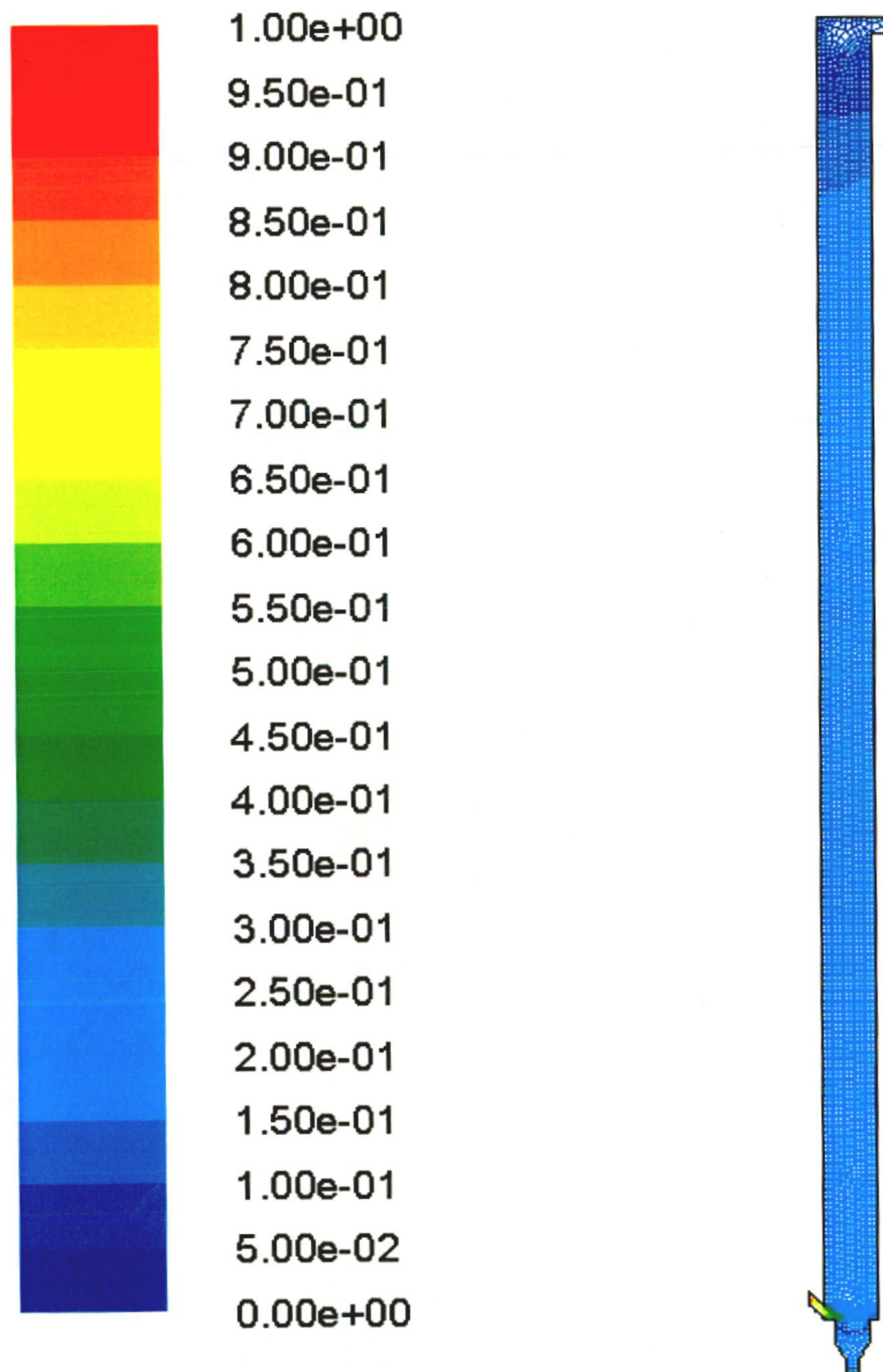


Fig. 5.13: - Contour of Volume fraction of phase 2

5.2.6 Velocity Profile: - The contour of velocity of phase 2 is shown in Fig. 5.14 (a). From the figure, it is evident that the magnitude of velocity decreases as we move upwards. However, once phase 2 reaches the top portion of the gasifier, its velocity suddenly starts increasing. The initial decrease with height is due to effect of gravity acting in the downwards direction. The latter increase is possibly due to pressure gradient (inside pressure > atmospheric pressure) at the pressure outlet. The plot of axial velocity profile of phase 1 & phase 2 inside the gasifier is shown in Fig. 5.14 (c) & (d) respectively.

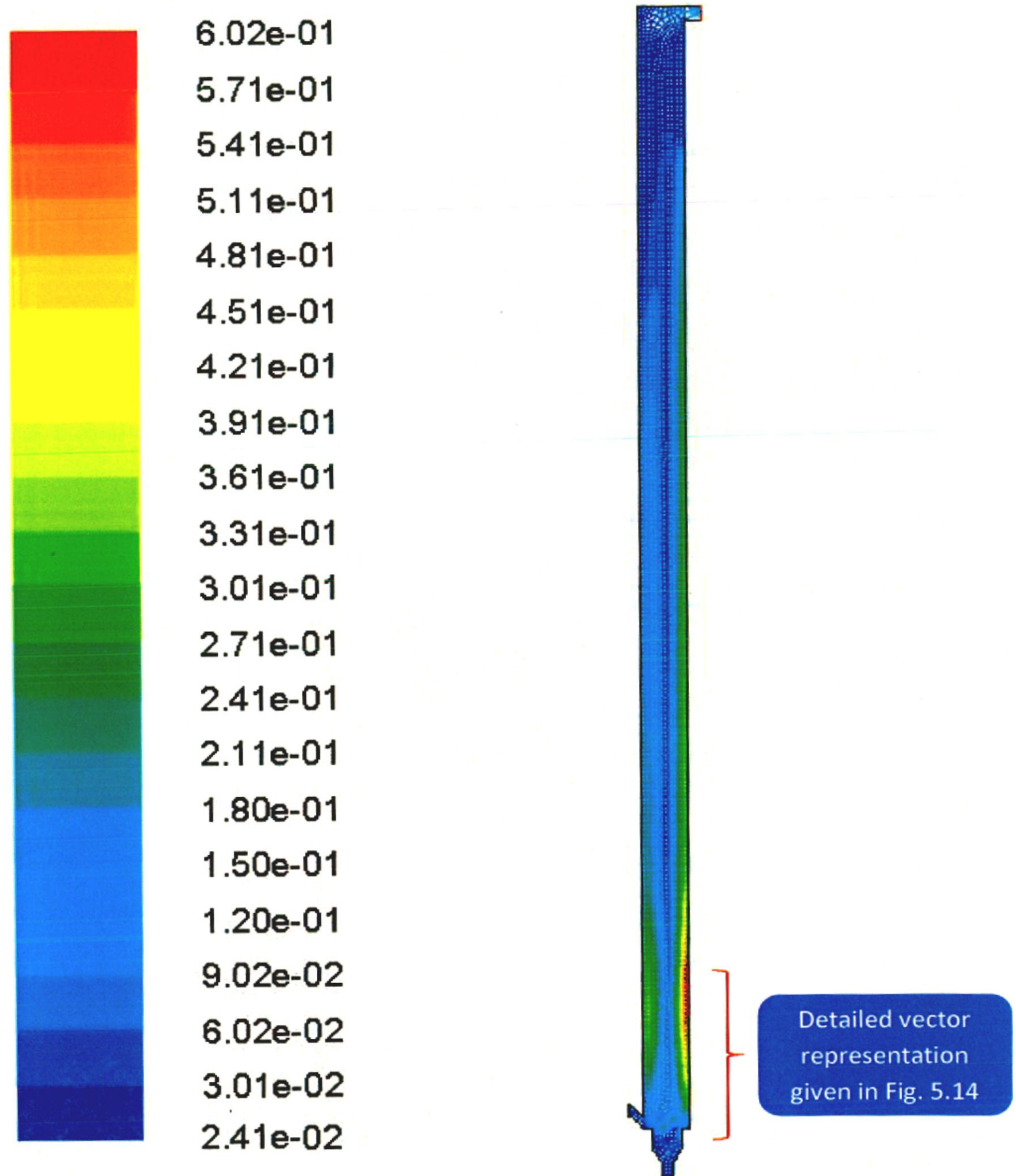


Fig. 5.14 (a): - Contour of velocity profile of phase 2

Fig. 5.14 (b) shows velocity vectors in a section of the gasifier near the coal inlet region. From the figure, it is evident that there is high back mixing due to reverse flow which is responsible for better heat and mass transfer inside bubbling fluidized bed gasifier. Also, from the figure, it is evident that the location and orientation of the coal inlet has a major role play in the hydrodynamics of the gasifier resulting in vortex formation in the central portion of the gasifier. This is responsible for the lower velocity in the axial (y- axis) region of the gasifier as in Fig. 5.14 (c) & 5.14 (d).

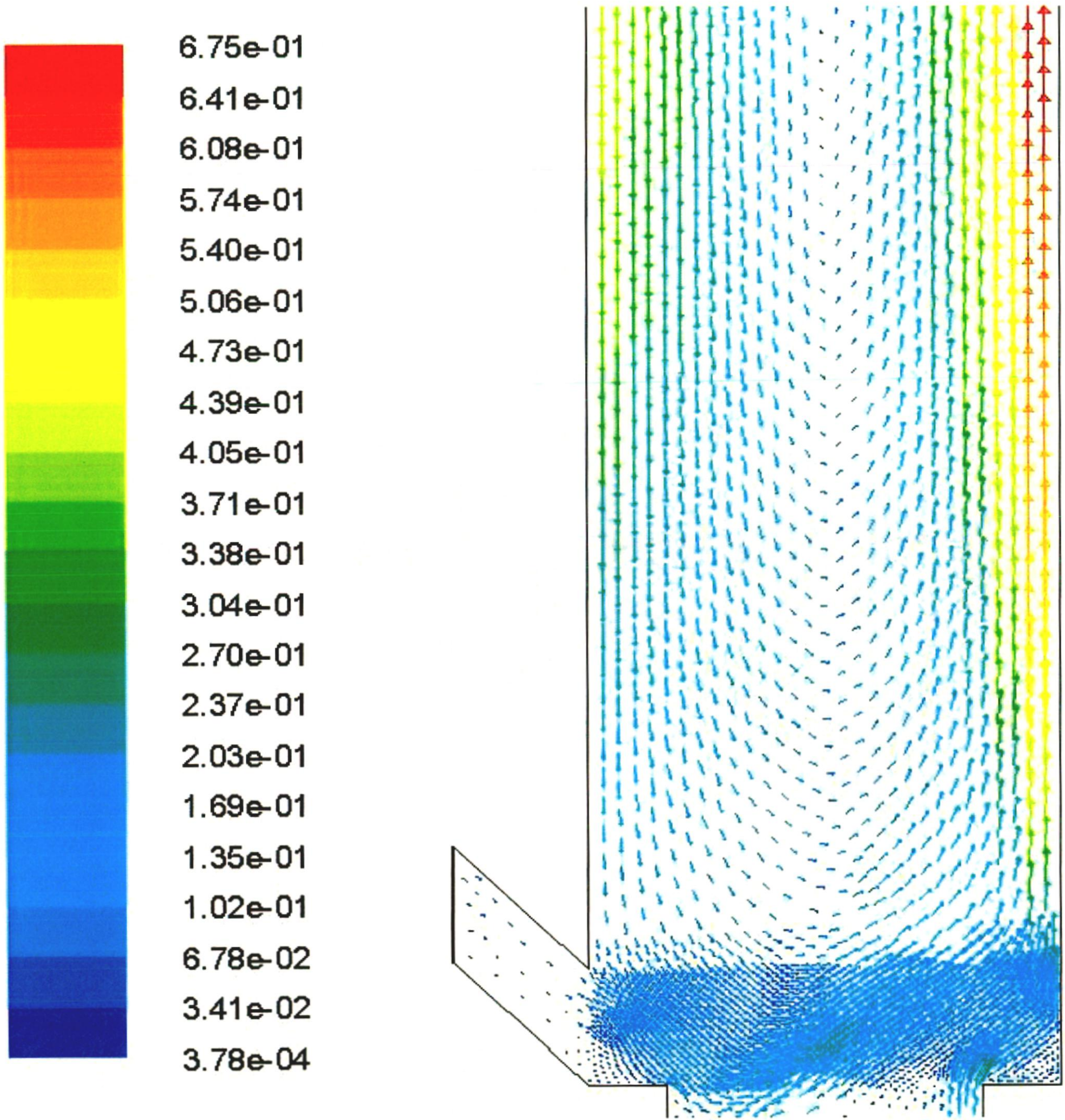
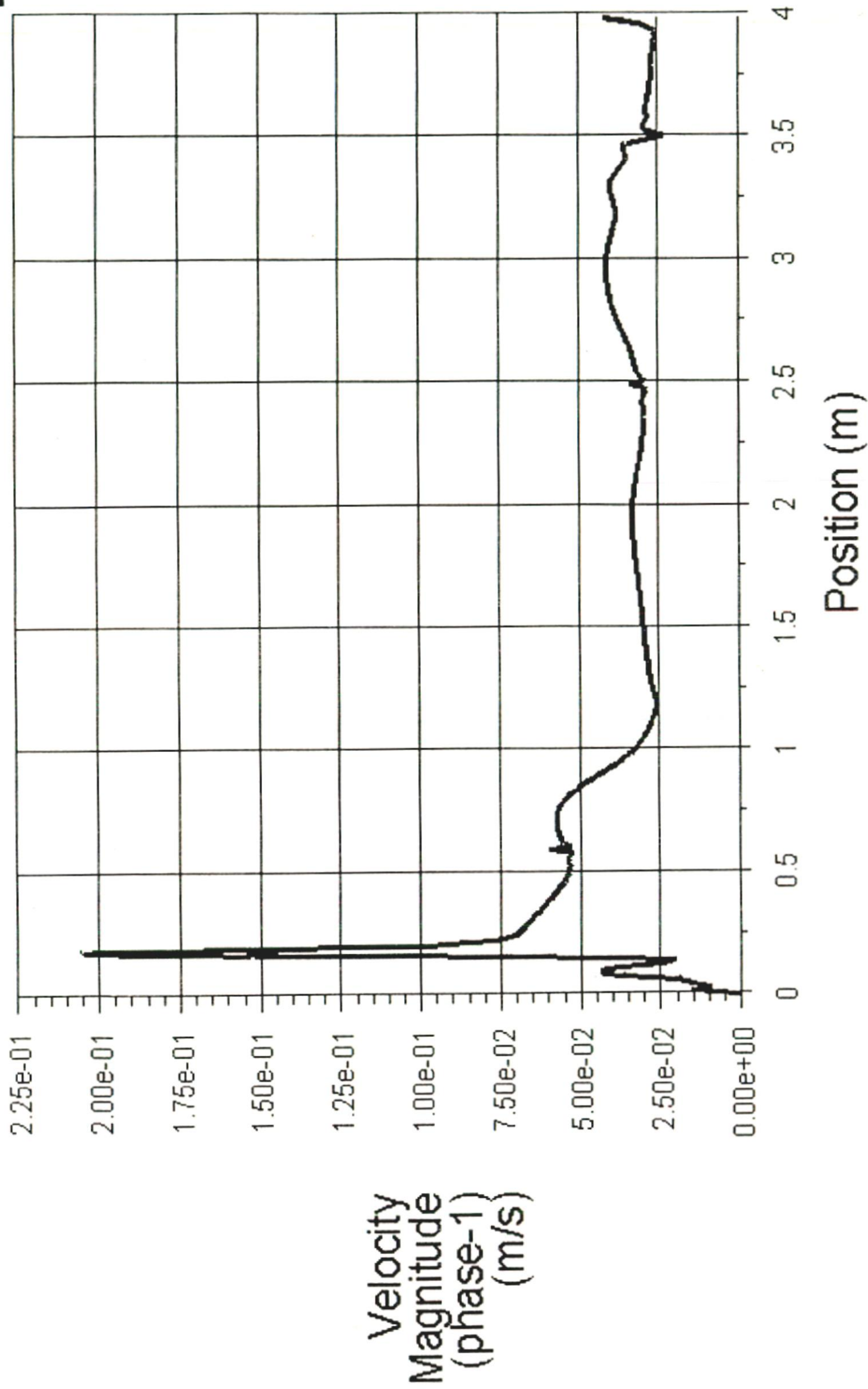


Fig. 5.14 (b): - Velocity vectors in a section of gasifier near coal inlet)

— x-coordinate-7

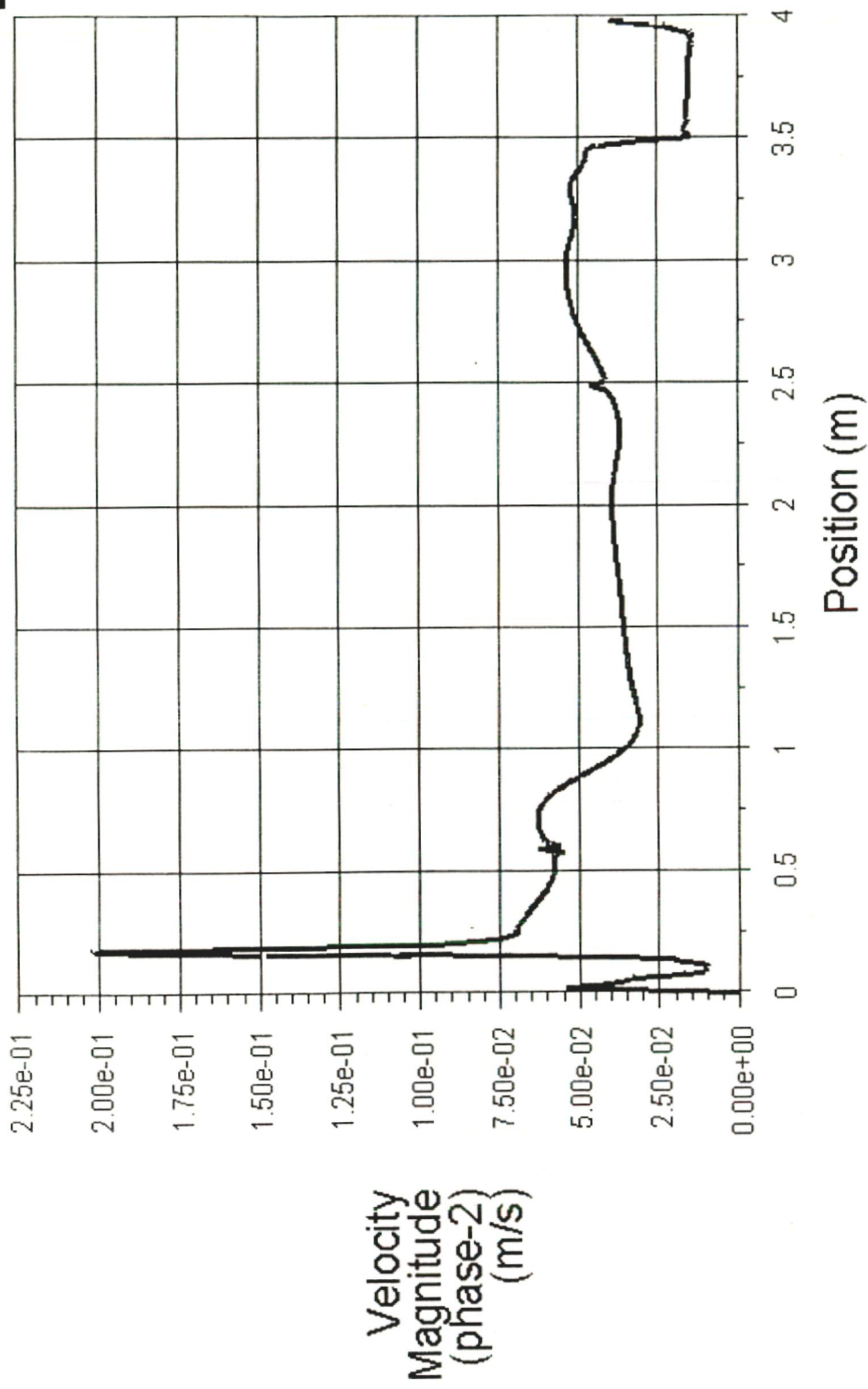


Velocity Magnitude (phase-1) (Time=1.8800e+02)

ANSYS FLUENT 12.0 (2d, dp, pbns, eulerian, spe, rke, transient)

Apr 19, 2012

Fig. 5.14 (c): - Axial velocity distribution of phase 1



Velocity Magnitude (phase-2) (Time=1.8800e+02)

Apr 19, 2012

ANSYS FLUENT 12.0 (2d, dp, pbns, eulerian, spe, rke, transient)

Fig. 5.14 (d): - Axial velocity distribution of phase 2

5.2.7 Tar Concentration profile: - Coal tar is a black or brown liquid of extremely high viscosity. It is a complex and variable mixtures of phenols, polycyclic aromatic hydrocarbons (PAHs), and heterocyclic compounds, about 200 substances in all [4]. It is formed as a by- product in coal gasification during devolatilization of coal. Now, the devolatilization reaction occurs very rapidly as coal enters the gasifier. Therefore, most of the tar is formed in the lower section of the gasifier close to the coal inlet. Afterwards, the mass fraction of tar remains almost constant as evident from Fig. 5.15

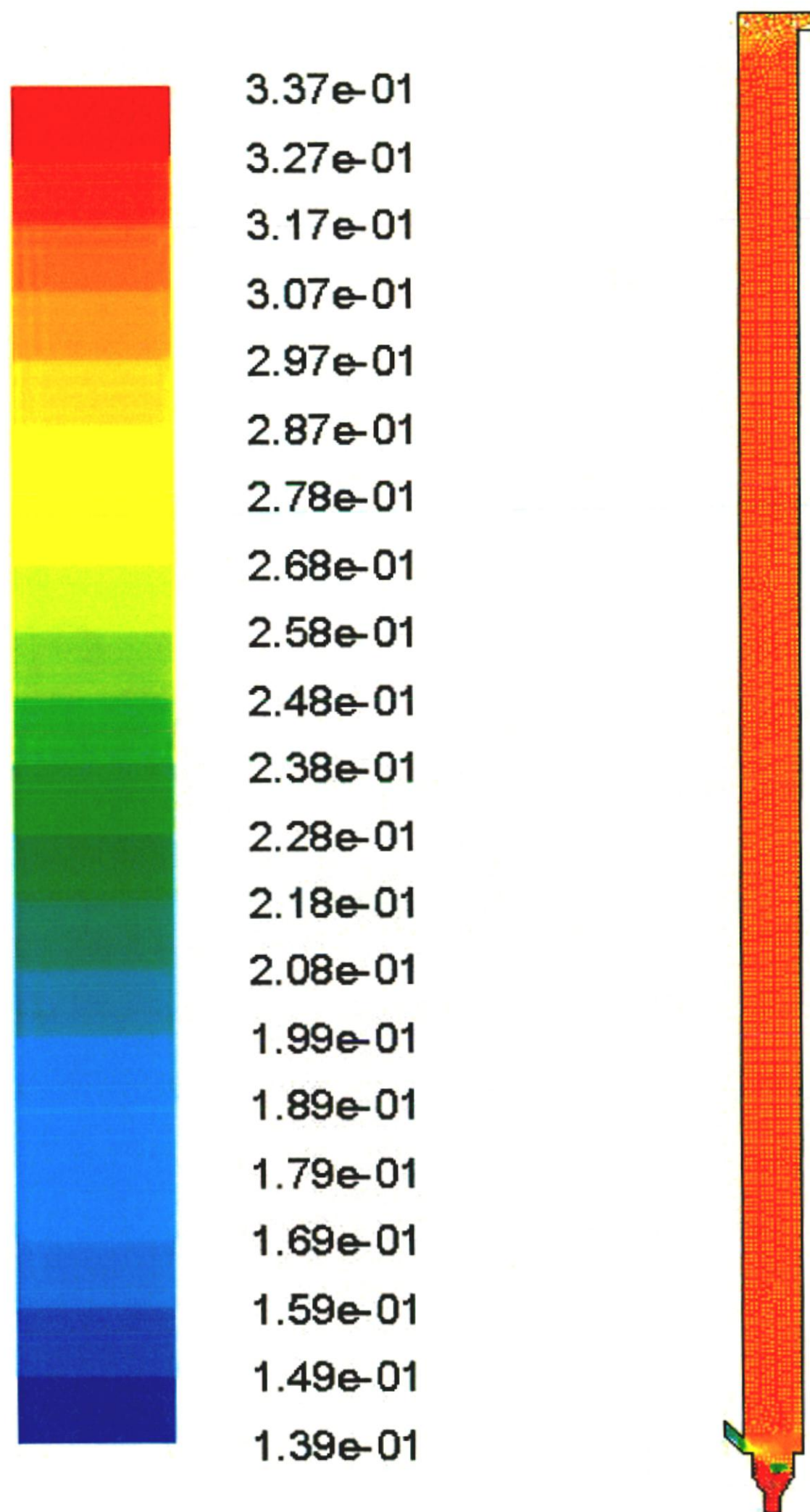


Fig. 5.15 Contours of mass fraction of tar

5.2.8 Calculation of calorific value of Syngas: - The syngas produced from our CIMFR model contains CO, CO₂, N₂, H₂ and a very small amount of H₂O. From these components, only CO and H₂ actually contribute towards the calorific value of exit syngas.

N₂ being an inert gas cannot participate in combustion process. Also, CO₂ is not combustible as the carbon in CO₂ is already in its highest oxidation state. Therefore, N₂ and CO₂ don't contribute towards the calorific value of exit syngas.

Now,

Standard enthalpy of combustion of H₂ = 241.8 MJ/ kmol [105]

Standard enthalpy of combustion of CO = 283 MJ/ kmol [105]

Now,

Mole fraction of H₂ in exit syngas = 0.2094

Mole fraction of CO in exit syngas = 0.181

Hence,

$$\begin{aligned}\text{Calorific value of exit syngas} &= (0.2094 * 241.8) + (0.181 * 283) \\ &= 101.856 \text{ MJ/ kmol}\end{aligned}$$

Also, at standard condition of temperature and pressure, 1 mole of a gas occupies 22.4 liters. Therefore, 1 kmol of gas will occupy a volume of 1 m³.

Therefore,

$$\begin{aligned}\text{Calorific value of exit syngas} &= (101.856 \text{ MJ/ kmol}) / (22.4 \text{ m}^3 / \text{kmol}) \\ &= 4.547 \text{ MJ/ m}^3\end{aligned}$$

This is in range of 3.5 – 10 MJ/ m³ for gasification of coal with air as the oxidizing agent [51].

Fig. 5.16 (a) & 5.16 (b) shows the variation of caloric value of exit syngas as a function of time & temperature at an operating pressure of 3 bars. From the Figure it is evident that the calorific value of exit syngas varies between 85 MJ/ kmol to 105 MJ/ kmol. This observation illustrates the fact that the fluidization process is an unsteady phenomenon. Although the variables like species molar fractions and reactor temperature appear to have converged, they represent only an instantaneous state. The average calorific value of syngas is therefore equal to 94.9 MJ/ kmol or 4.237 MJ/ m³ at STP, considering the behavior of syngas to be similar to ideal gas.

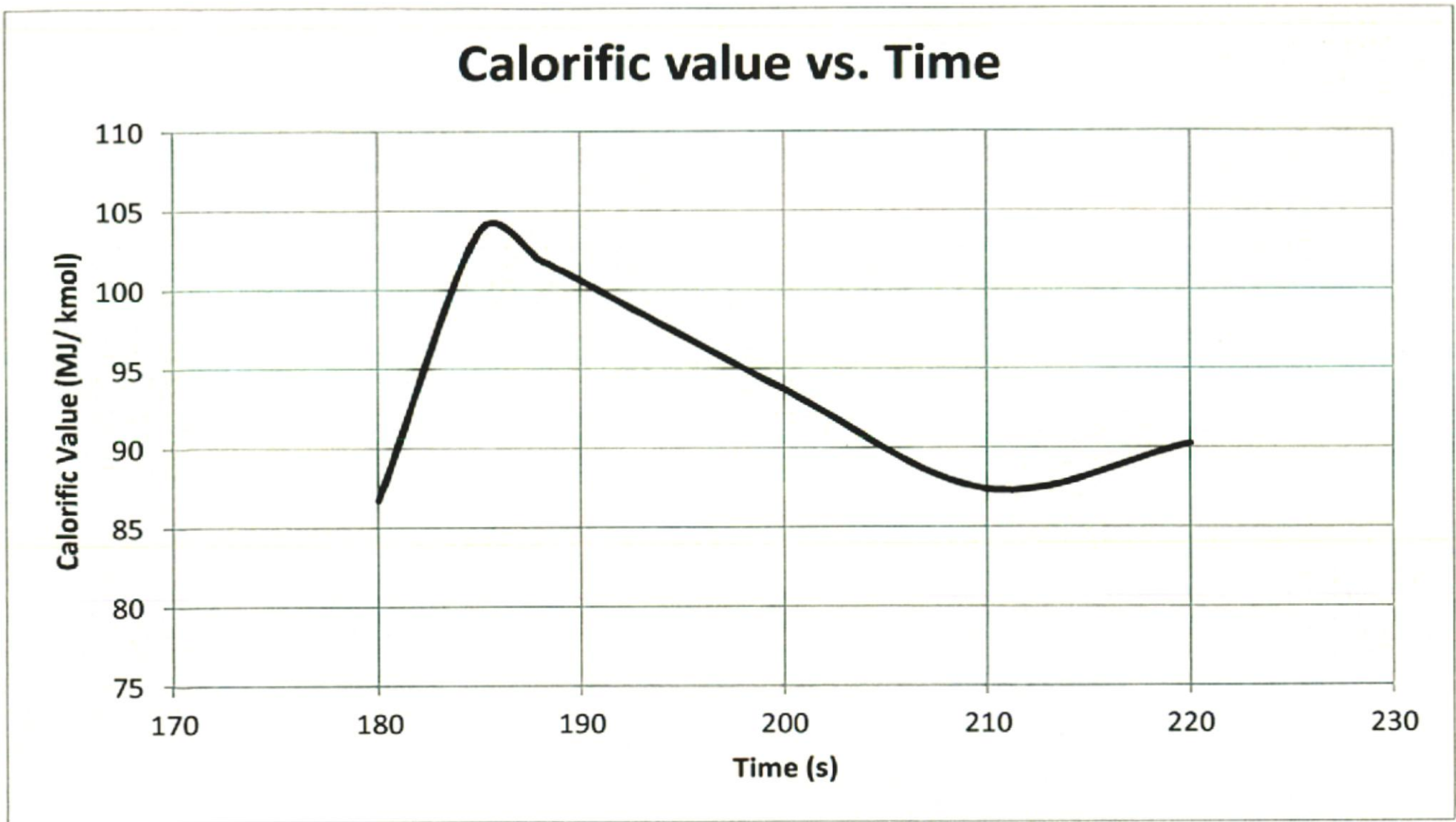


Fig. 5.16 (a) Calorific value of exit syngas as a function of time

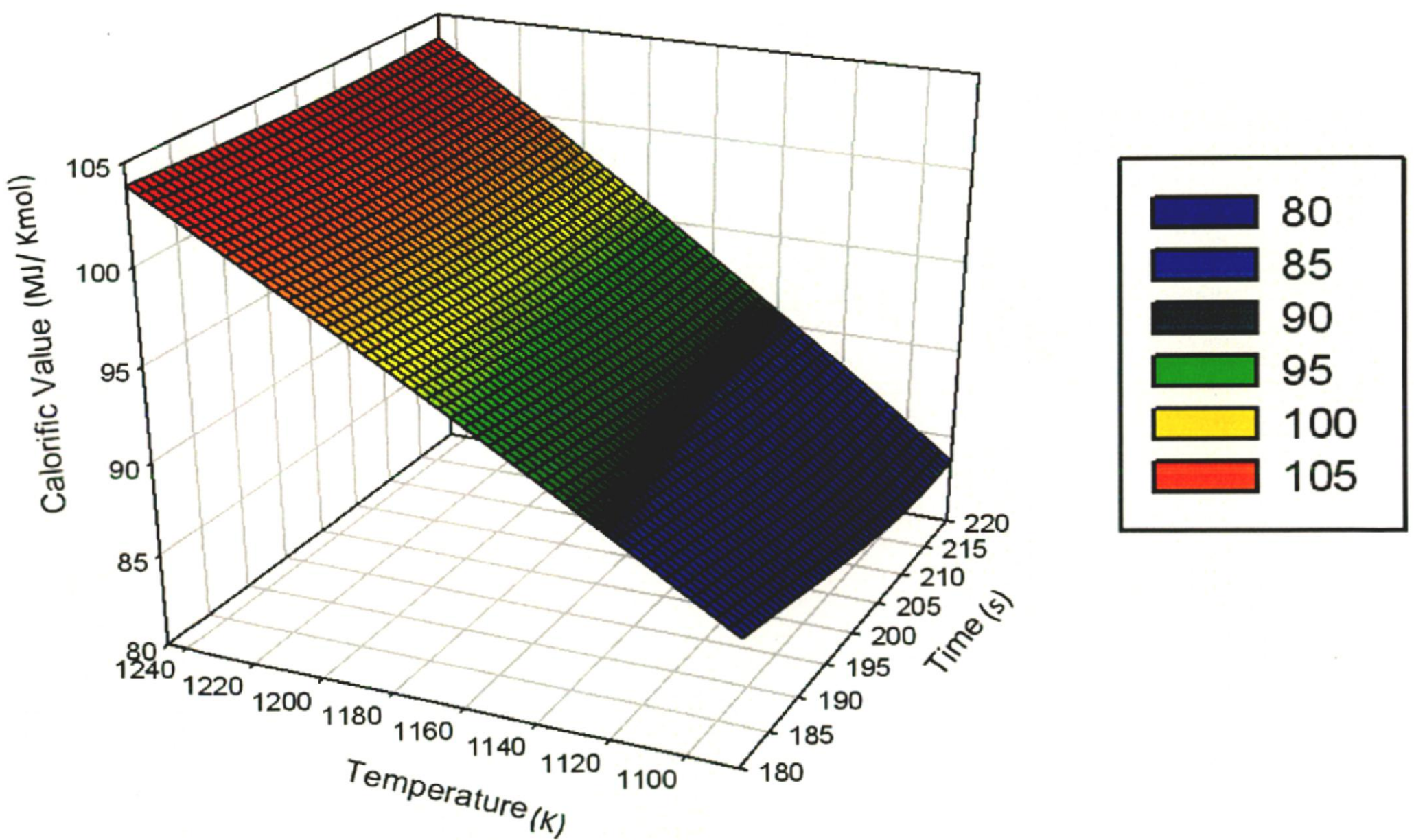


Fig. 5.16 (b) Calorific value of exit syngas as a function of time & temperature 133

5.3 PARAMETRIC STUDY

The CIMFR model after validation was used for parametric study in order to determine the effect of different parameters on the performance of CIMFR bubbling fluidized bed gasifier pilot plant. In this work, the effect of 3 parameters namely superficial air velocity, temperature and pressure were studied. The observations and results obtained from these studies is presented in the following three sections: -

- a) Fluidization at different air velocity
- b) Effect of Temperature on syngas composition
- c) Effect of pressure on syngas composition

5.3.1 Fluidization at different air velocity: - The fluidization bed height of CIMFR bubbling fluidized bed gasifier was studied under cold conditions (without reaction) at air velocities of 0.05 m/ s, 0.1 m/ s, 0.15 m/ s, 0.3 m/ s and 0.5 m/ s to determine the effect of air velocity on fluidization process of the pilot plant gasifier. In most of the cases, it was observed that the behavior stabilizes between 8- 9 seconds.

The contours of the same is presented in Fig. 5.17 (a- e). From the figure, it is evident that the bubbling fluidized bed height increases with air velocity. The bubble formation starts above a certain critical velocity, which in this case is equal to 0.05 m/ s. Also, the turbulence in flow and back mixing increases with air velocity resulting in higher heat and mass transfer between primary phase and secondary phases.

However, above a certain superficial air velocity, pneumatic flow starts resulting in carryover of solid particles from the gasifier by air. In such a situation, a cyclone is required to capture and recycle the un-burnt carbon particles leaving the gasifier. The resulting configuration is known as circulating fluidized bed. Therefore, in order to maintain a bubbling fluidized bed, the air velocity must be maintained between these extremes.

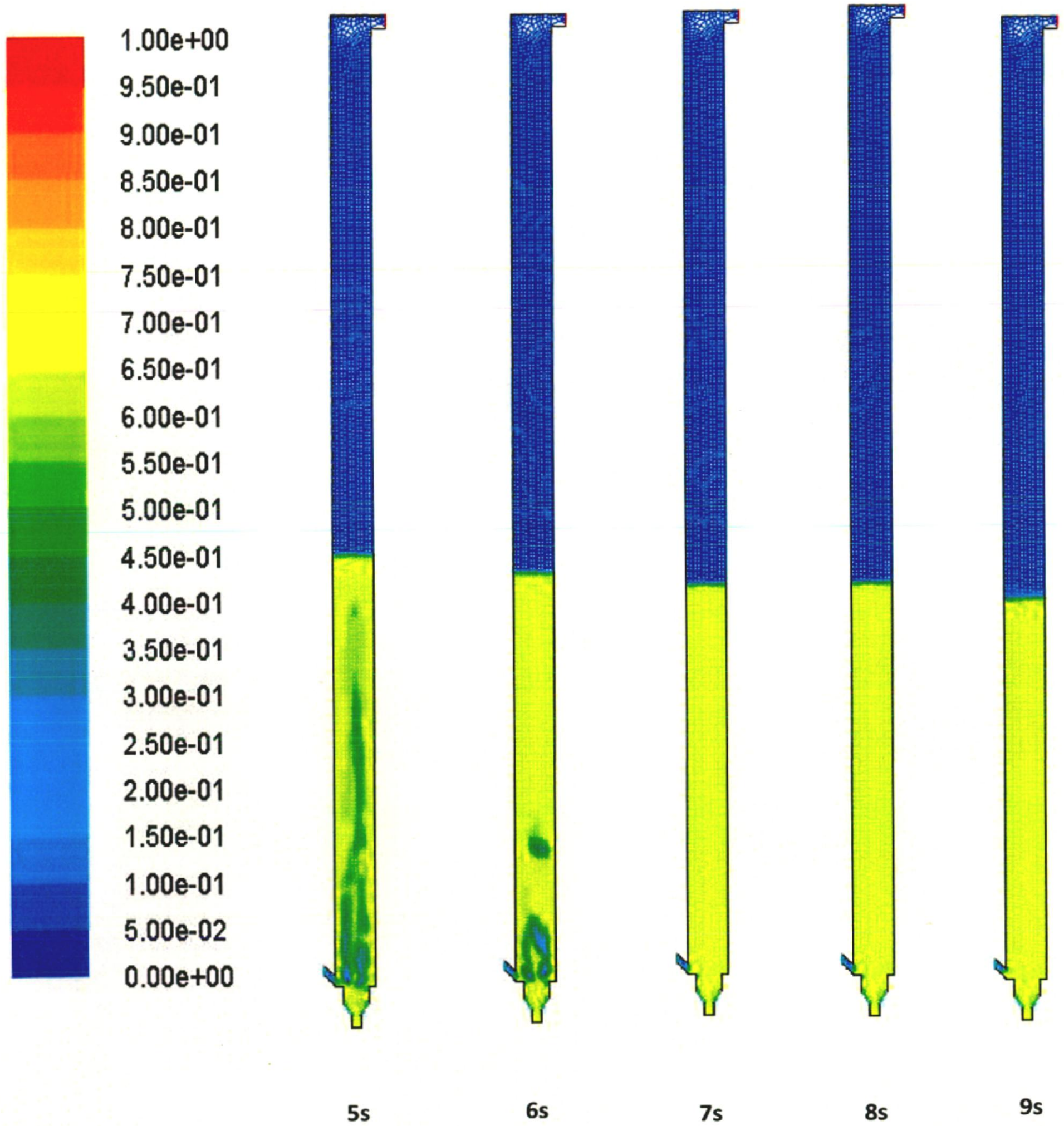


Fig. 5.17 (a): - Fluidization (without reaction) bed height at air velocity = 0.05 m/ s

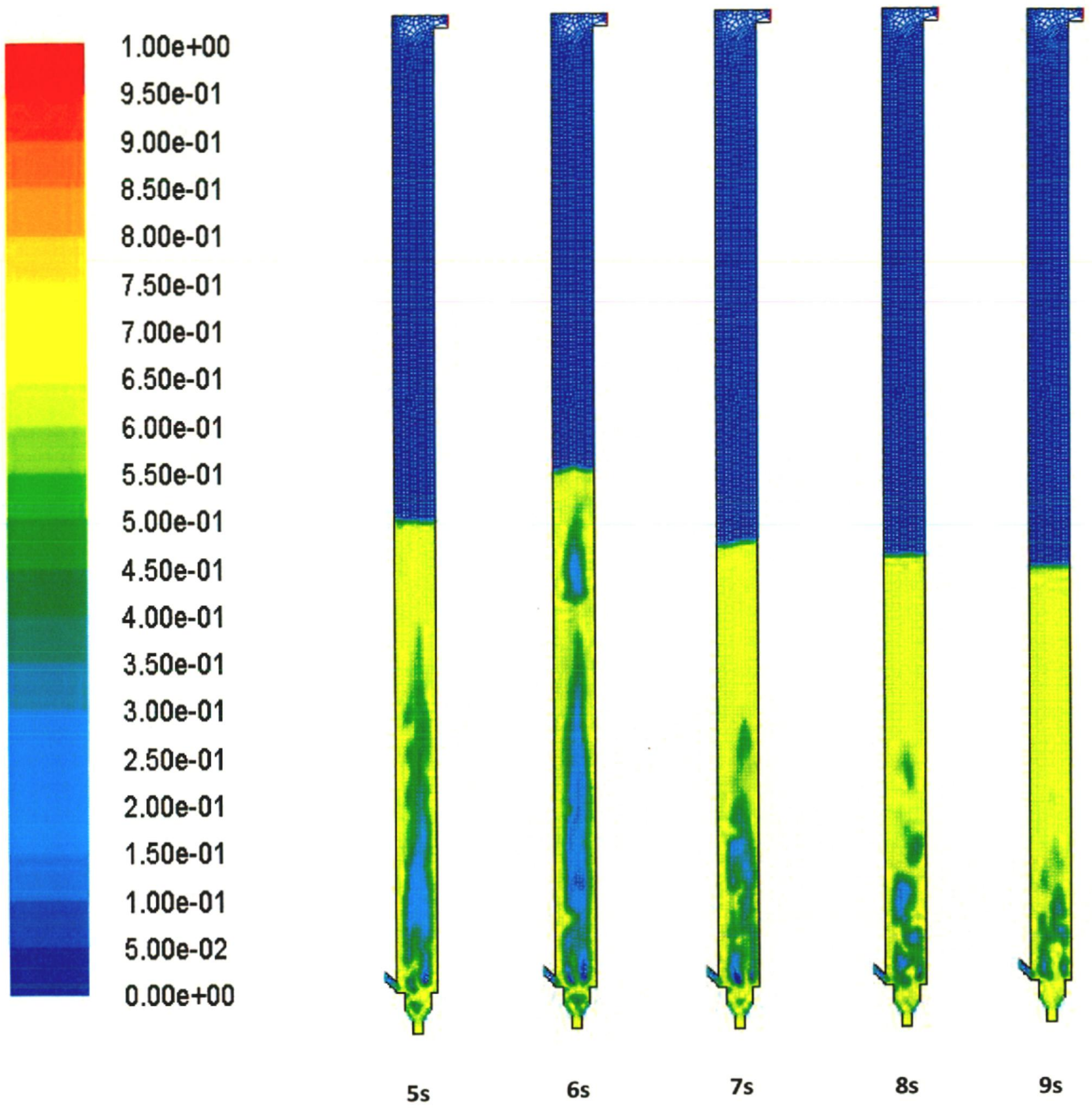


Fig. 5.17 (b): - Fluidization (without reaction) bed height at air velocity = 0.1 m/ s

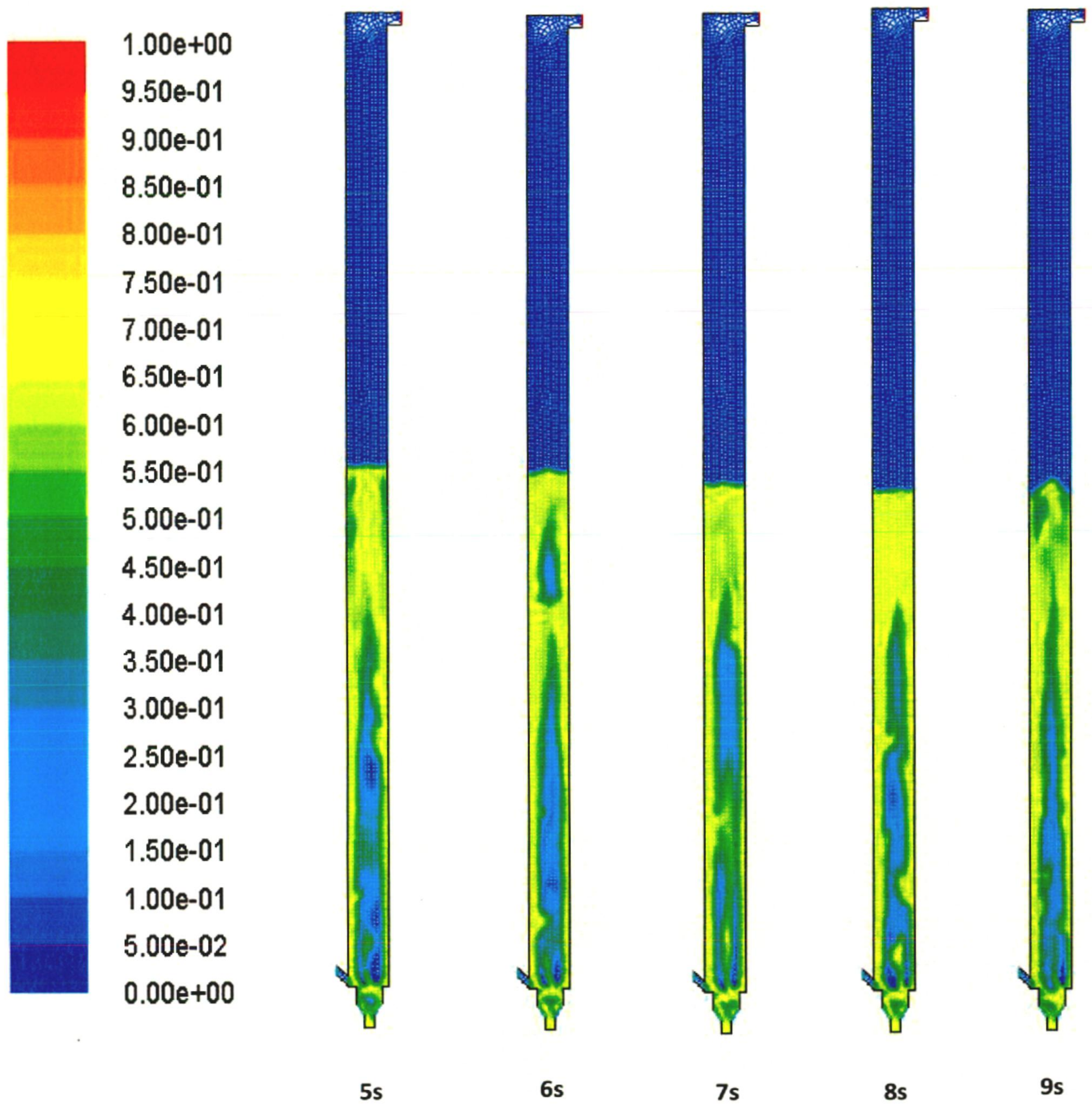


Fig. 5.17 (c): - Fluidization (without reaction) bed height at air velocity = 0.15 m/ s

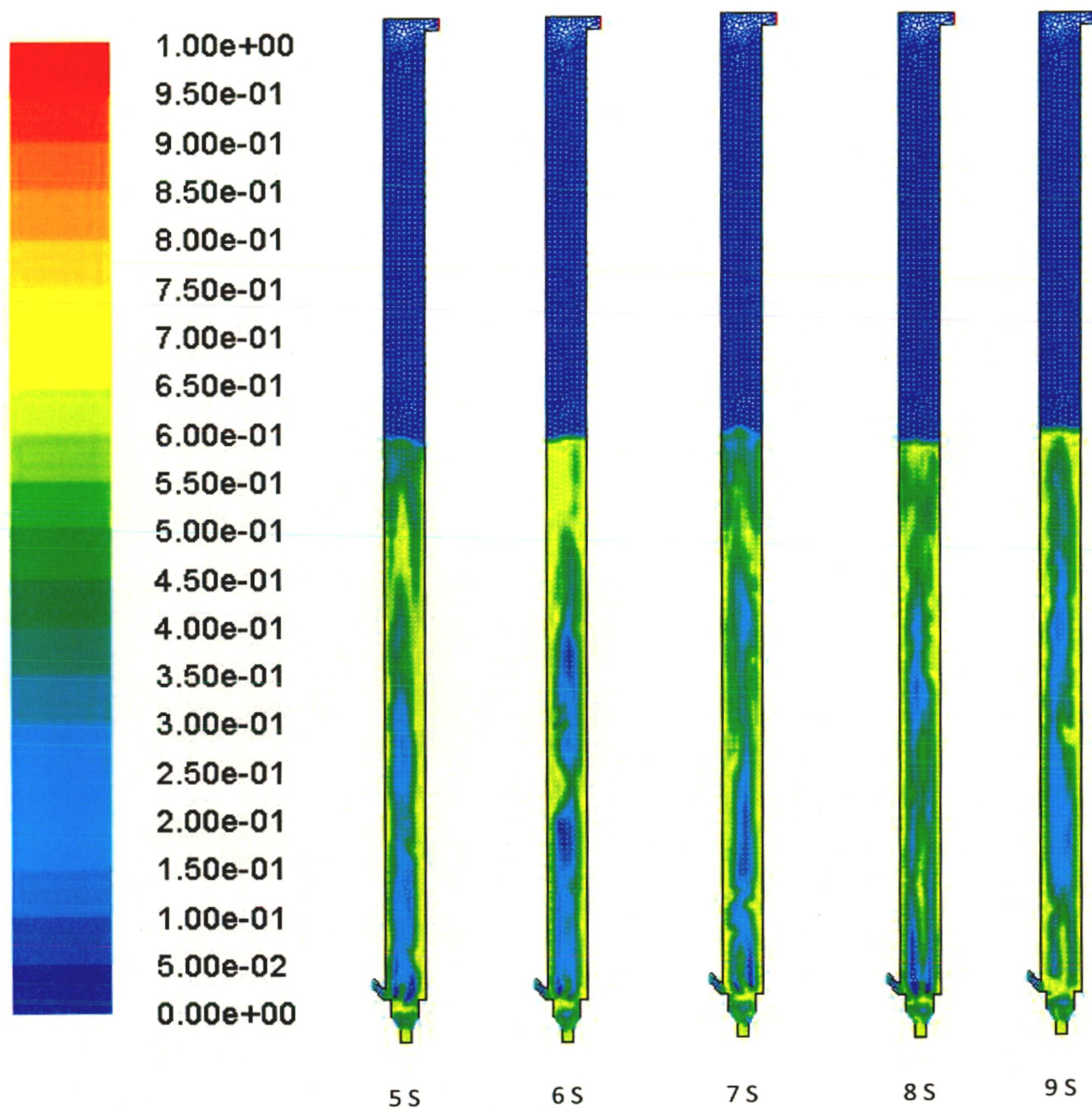


Fig. 5.17 (d): - Fluidization (without reaction) bed height at air velocity = 0.3 m/ s

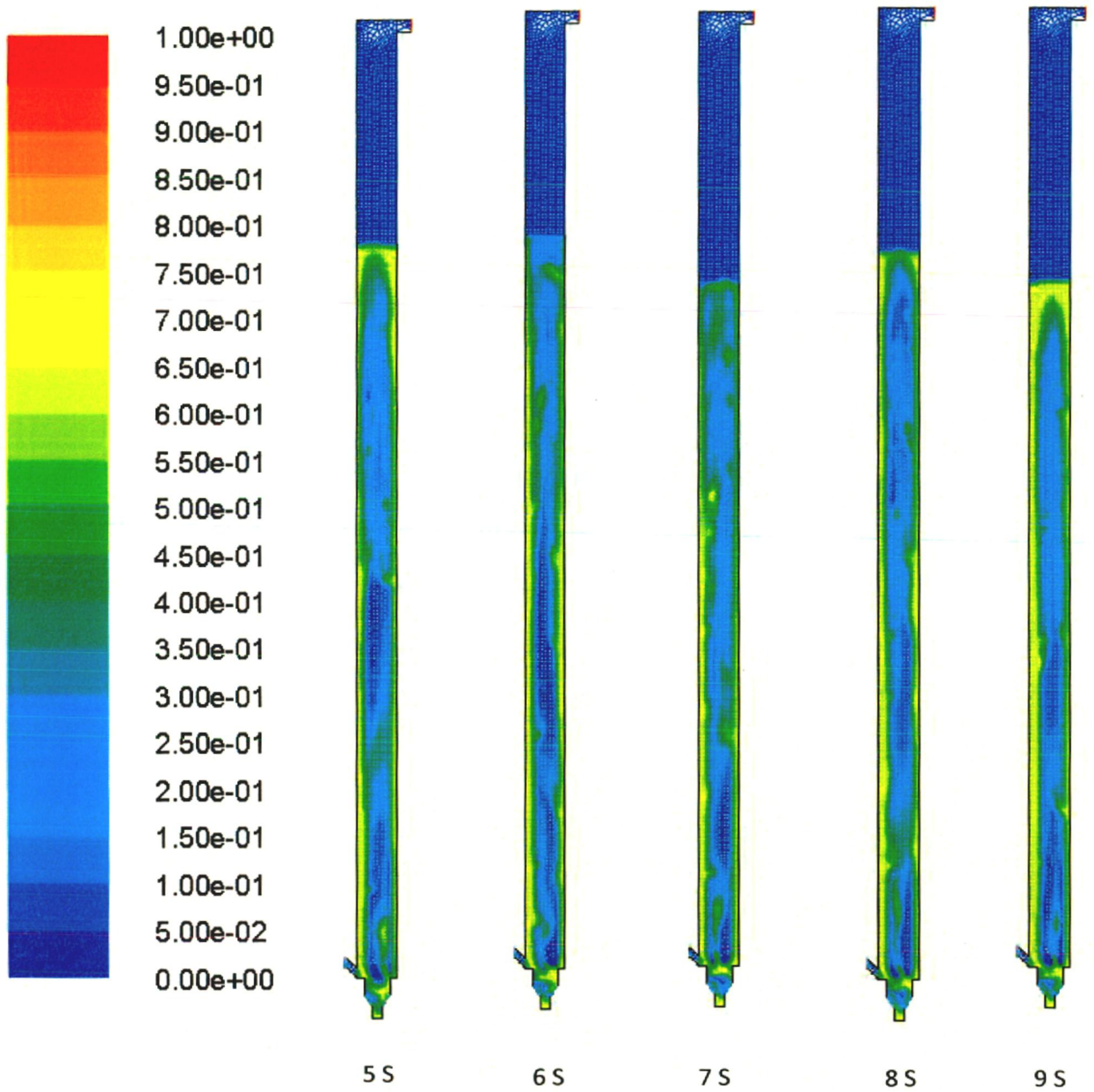


Fig. 5.17 (e): - Fluidization (without reaction) bed height at air velocity = 0.5 m/ s

5.3.2 Effect of Temperature on Syngas composition: - The effect of temperature on syngas composition is shown in Fig. 5.18 (a- d).

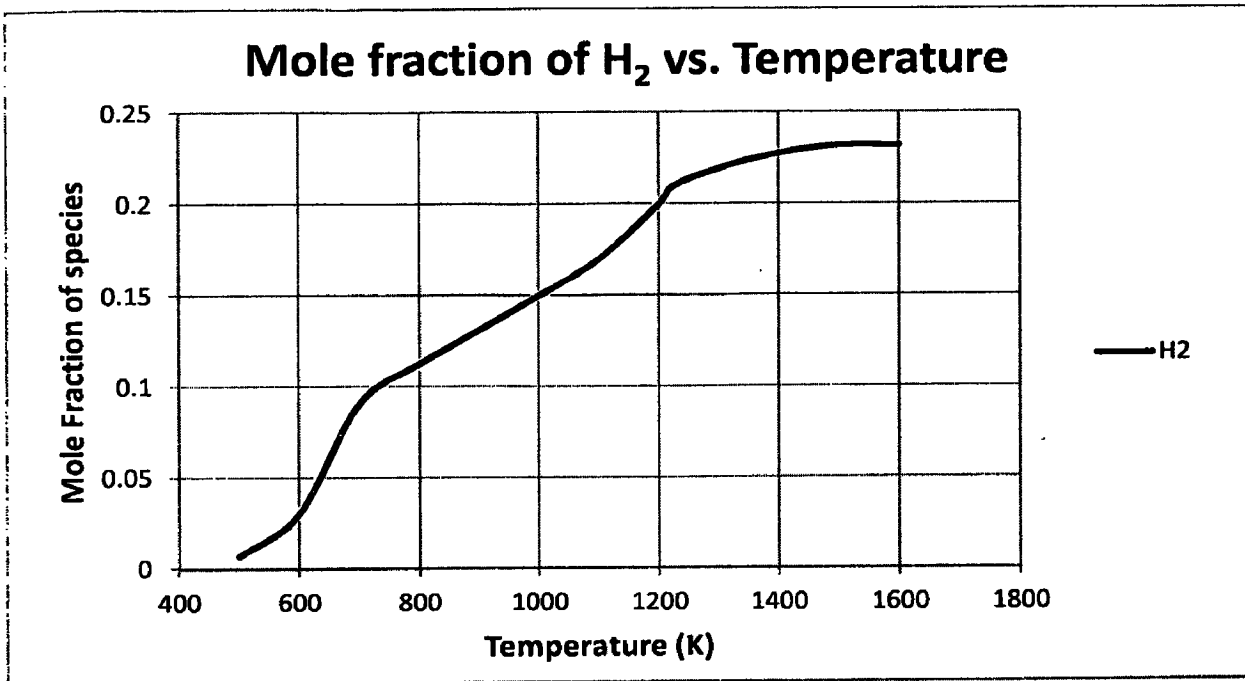


Fig. 5.18 (a): Effect of Temperature on mole fraction of H₂

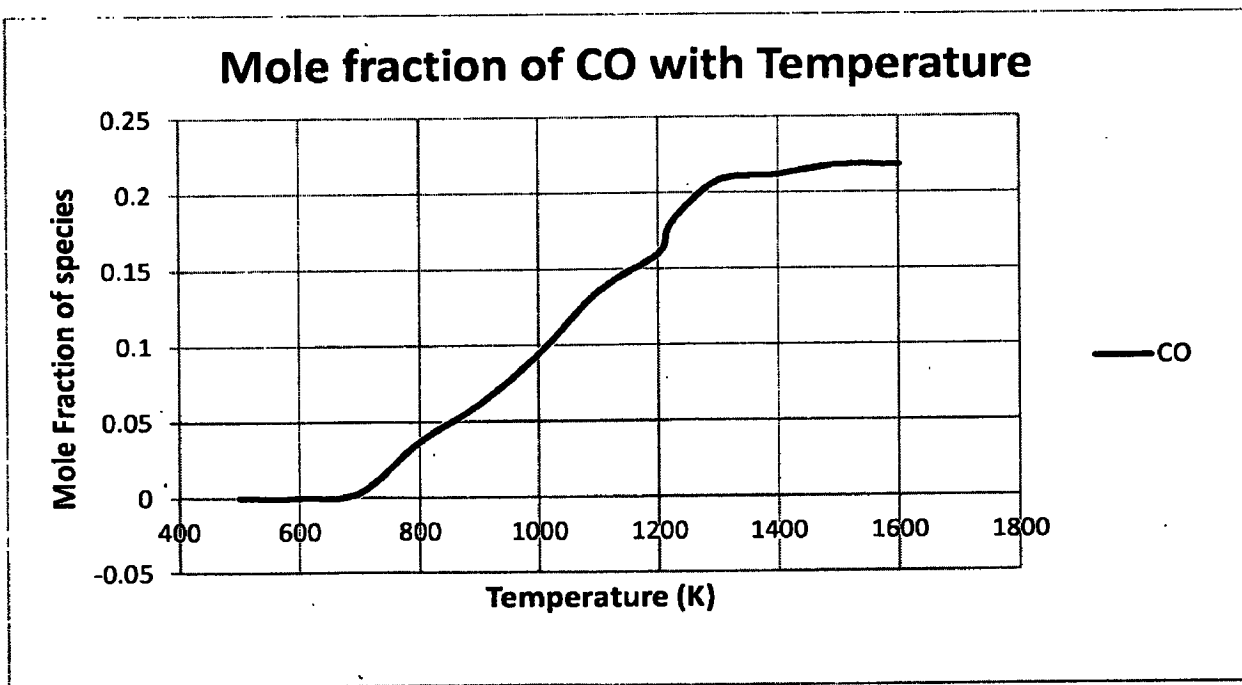


Fig. 5.18 (b): Effect of Temperature on mole fraction of CO

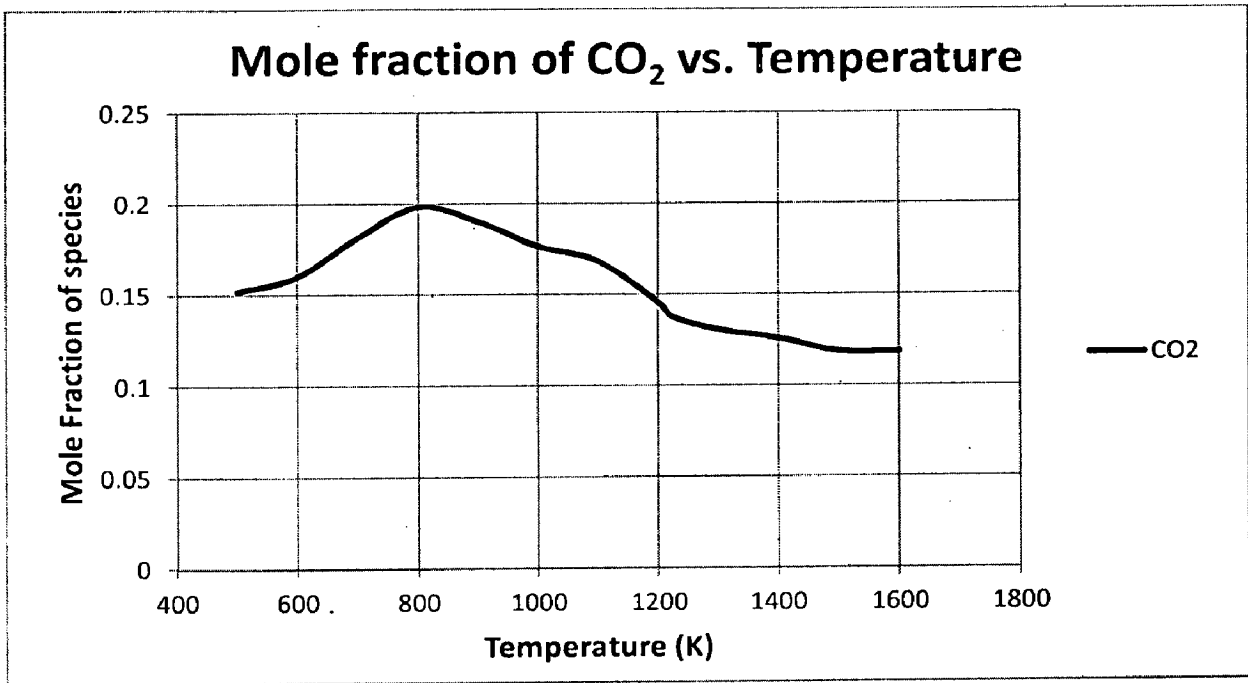


Fig. 5.18 (c): Effect of Temperature on mole fraction of CO₂

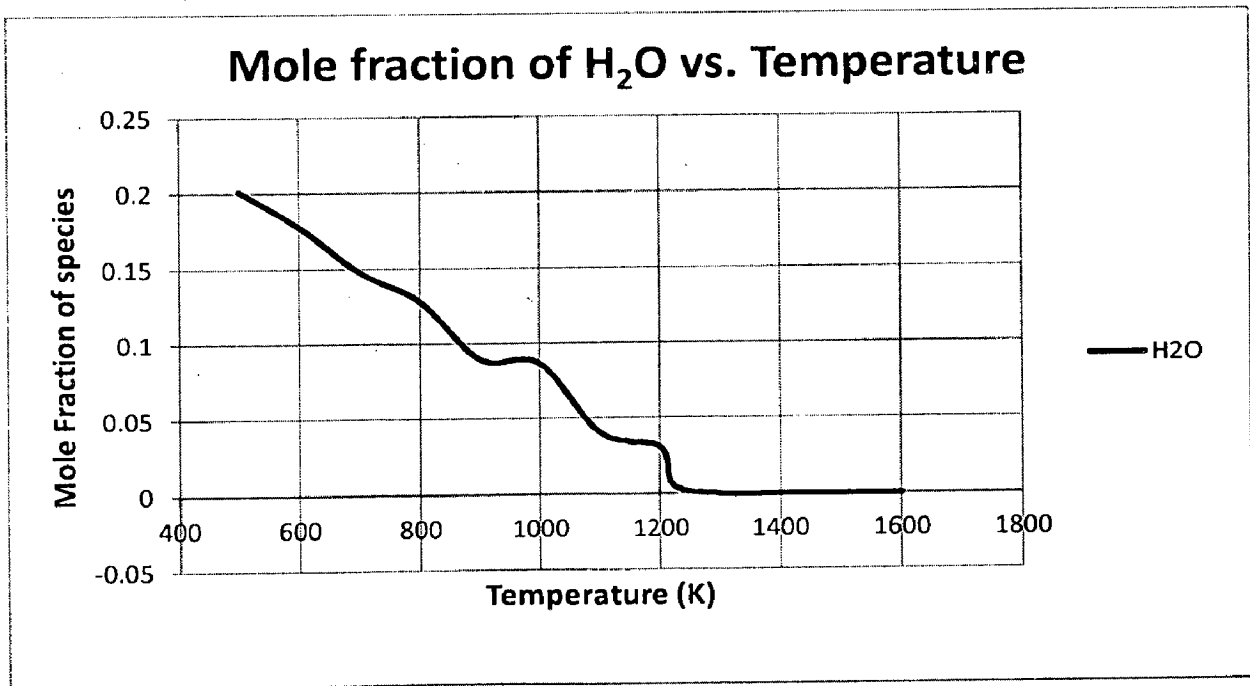


Fig. 5.18 (d): Effect of Temperature on mole fraction of H₂O

Fig. 5.18 (a- d) shows the effect of temperature on the mole fraction of H₂, CO, CO₂ & H₂O respectively. From these figures, it is evident that the concentration of CO & H₂ increases with temperature. The concentration of CO₂ initially increases but decreases with further increase in temperature. The increase in concentration of CO is due to endothermic reactions like boudouard reaction, reverse water gas shift reaction and char steam combustion which are more favored at higher temperatures. Similarly, H₂ content increases with temperature due to char steam combustion. The initial increase in mole fraction of CO₂ is due to increase in rate of reaction (kinetics) with temperature however the later decreases with further increase in temperature is due to the fact that most of the combustion reactions like char combustion, CO combustion are exothermic in nature and therefore are not favored at high temperatures.

5.3.3 Effect of pressure on Syngas composition: - The determine the effect of pressure on syngas composition, case study simulations was done for operating pressure between 1 and 10 atm. The result obtained is shown in Fig. 5.19.

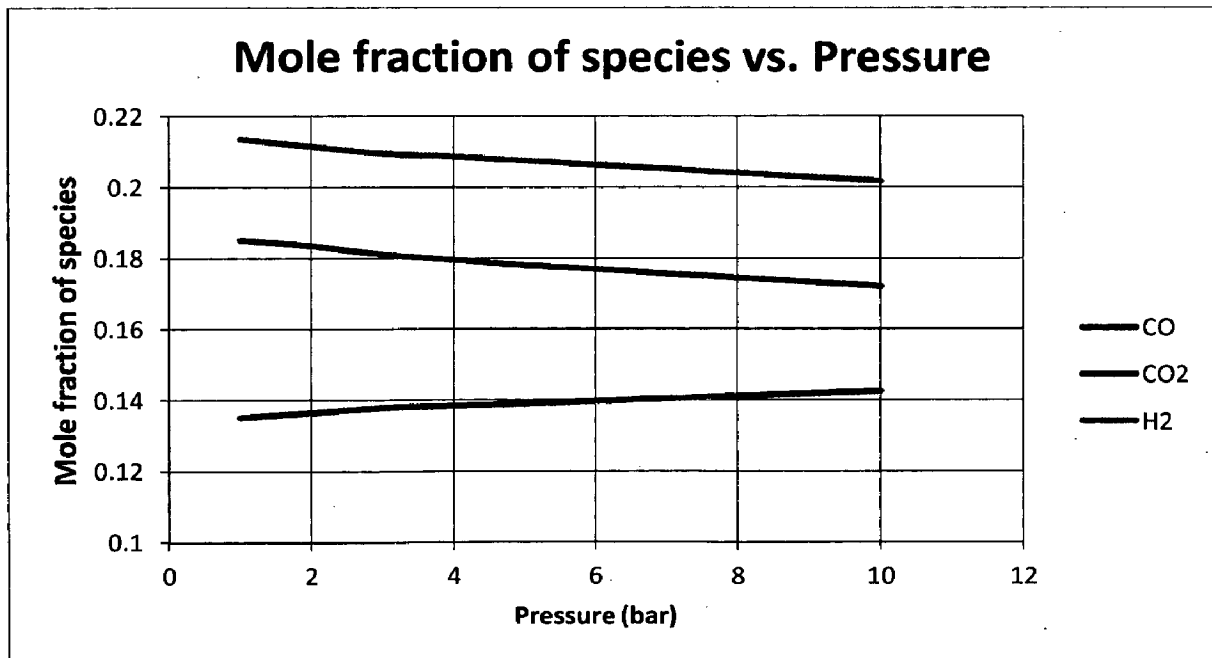


Fig. 5.19: Effect of pressure on syngas composition

From Fig. 5.19, it is evident that the mole fraction of CO & hydrogen decreases with pressure while that of CO₂ increases with pressure. However, the change in all the three cases is very small. This is primarily due to reversible boudouard reaction in which one mole of CO₂ gives 2

mole of CO. Therefore, according to Le-Chatelier's principle, an increase in pressure will shift this reaction in backward direction, resulting in higher concentration of CO₂ and lower concentration of CO. A higher concentration of CO₂ will in turn shift water gas shift reaction in backward direction resulting in decrease in concentration of H₂.

5.4 Some insight on design modification of CIMFR BFBG pilot plant

From the above discussion, it can be observed that the height of the freeboard zone plays a major role in determining the composition of syngas coming out of the gasifier. It provides residence time for the slower reverse water gas shift reaction to take place. In this reaction, CO₂ and H₂ react to form CO and steam. Therefore, if the height of the freeboard zone is increased, the resulting syngas will have higher concentration of CO and lower concentration of CO₂ and H₂. On the other hand, a decrease in the height of freeboard zone will result in syngas having higher concentration of CO₂ & H₂ and lower concentration of CO.

Now, the required composition of syngas depends on its end use. Therefore, the height of the freeboard zone can be varied in accordance with the syngas composition desired for meeting the specific end use requirement. Table 5.4 gives the optimal syngas composition required for producing synthetic fuels, methanol and hydrogen along with the composition of syngas obtained from CIMFR gasifier. [46].

Fig. 5.4 Desired syngas composition for different end uses

Parameters	Synthetic Fuel	Methanol	Hydrogen	CIMFR
H ₂ / CO	0.6	2.0	High	1.0427
CO ₂ (%)	Low	Low	Not important	14.58
N ₂ (%)	Low	Low	Low	47.03
H ₂ O (%)	Low	Low	High	0

The concentration of N₂ in the syngas can be reduced by using pressure swing adsorption to capture N₂ from syngas. As an alternative, Oxygen can be used as gasifying medium instead of air to produce a N₂ free syngas. However, it will require a cryogenic/ pressure swing adsorption unit for separation of Oxygen from air. Also, in case of Oxyfuel gasification, modification in design and recycle of syngas is mandatory to prevent temperature shoot inside the gasifier. However, the syngas obtained from the Oxyfuel gasification will have higher concentration of CO₂ making its removal easier using carbon capture technologies. The final decision will however depend on the economics of the two processes.

CHAPTER- 6

CONCLUSION & RECOMMENDATION

In this work, a modeling approach to illustrate the gasification of Indian coal in bubbling fluidized bed gasifier has been developed within the framework of ANSYS 12. Two models namely BASIC model & CIMFR model has been developed. The preliminary investigation reveals that: -

6.1 BASIC MODEL

- 1) The temperature and syngas composition obtained from the basic model are in good agreement (maximum error $< \pm 9\%$) with the literature data obtained from Liang et al. 2006.
- 2) A multi fluid Eulerian- Eulerian model integrating the kinetic theory of solid particles, along with Arrhenius/ diffusion kinetics (inserted using User Defined Function) for heterogeneous reaction and Arrhenius/ Eddy dissipation kinetics for homogeneous reaction is capable of predicting the behavior of bubbling fluidized bed gasifier.
- 3) This model can be used to study the hydrodynamics, temperature, reactions and species mass fraction profiles inside the gasifier. Hydrodynamic study suggests that there is high back mixing in the bubbling fluidized bed gasifier primarily due to reverse flow and vortex formation. This is responsible for effective heat and mass transfer between gas and solid phases.
- 4) The fluidized bed height under cold condition (without reaction) increases with superficial gas velocity. The behavior stabilizes between 6- 7 seconds.
- 5) Limestone is added with coal in the fluidized bed to capture Sulfur. This limestone may decomposes at a higher temperature of around 1000°C , resulting in higher concentration of CO_2 in syngas.
- 6) The temperature, velocity and mole fraction profiles depends on the specific geometry of the gasifier like height & diameter of the gasifier, location & orientation of coal inlet, air inlet and pressure outlet section. Therefore, they require separate discussion for each type of gasifier under consideration.

6.2 CIMFR MODEL

- 1.) The temperature and syngas composition obtained from the CIMFR model are in good agreement (maximum error $< \pm 10\%$) with the experimental results obtained from CIMFR, Dhanbad bubbling fluidized bed gasifier pilot plant.
- 2.) This model can be used to study the hydrodynamics, temperature, reactions and species mass fraction profiles inside the gasifier. Hydrodynamic study suggests that there is high back mixing in the bubbling fluidized bed gasifier primarily due to reverse flow and vortex formation. This is responsible for effective heat and mass transfer between gas and solid phases.
- 3.) The fluidized bed height under cold condition (without reaction) increases with superficial gas velocity and the behavior stabilizes between 8- 9 seconds. The bubble formation starts at a critical velocity of 0.05 m/ s.
- 4.) Combustion reactions like char combustion, carbon monoxide combustion and water gas shift reaction are very fast in nature and occur almost completely near the coal inlet of the gasifier. However, reverse water gas shift reaction and boudouard reactions are slow in nature and therefore require sufficient residence time to complete. The final product composition depends on the extent of these two reactions.
- 5.) The calorific value of the syngas obtained from CIMFR gasifier lies in the range of 3.84- 4.6 MJ/ m³ which is in the range of 3.5 – 10 MJ/ m³ (Gopal Gautam, 2010) for air gasification of coal.
- 6.) Temperature & CO₂ concentration decreases while CO & H₂ concentration increases along the length of gasifier due to endothermic reverse water gas shift and boudouard reactions prevalent in the freeboard zone of the gasifier.
- 7.) The model can also be used to study the effect of input parameters like temperature & pressure on the performance of the gasifier. The concentration of combustible gases like CO & H₂ increases with temperature while that of H₂O and CO₂ decreases with temperature.
- 8.) The effect of pressure is not very significant on the performance of the gasifier. There is small decrease in concentration of CO & H₂ and increase in concentration of CO₂ with pressure.
- 9.) The height of the freeboard zone plays a major role in determining the composition of syngas coming out of the CIMFR BFBG gasifier. It provides residence time for the

slower reverse water gas shift reaction which converts CO_2 and H_2 to CO and steam. Therefore, the height of the freeboard zone can be varied in accordance with the syngas composition desired for meeting the specific end use requirement.

6.3 RECOMMENDATIONS

For scale up of the pilot plant bubbling fluidized bed gasifier facility available at CIMFR, Dhanbad, further study is required in the below mentioned domains: -

- 1) In this work, a 2D symmetric section has been used for the simulation of CIMFR bubbling fluidized bed gasifier pilot plant, based on assumption of similar results from 2D and 3D simulations, used in literature. This assumption needs to be verified before accepting this model.
- 2) The performance of the gasifier needs to be evaluated for different Indian coals having different ash content from various coal fields by performing case study simulations on the CIMFR model.
- 3) The CIMFR model should be used to predict design improvement required to maximize the concentration of CO & H_2 and minimize the concentration of CO_2 in the exit syngas from the bubbling fluidized bed pilot plant.
- 4) Disperse phase model (DPM) study of the gasifier facility is required
 - a) To determine the effect of air distributor holes on the hydrodynamics of the gasifier &
 - b) To study the trajectory and distribution of coal particles inside the gasifier.

CHAPTER- 7

REFERENCES

- 1.) A Molina, B. S Haynes, C. R. Shaddix, Effect of reactant penetration on inhibition of coal char gasification, *Revista Energetica* 36, Diciembre de 2006.
- 2.) A. Parida, S. Khuntia, J.S. Murty, Combustion of coals with high ash fusion temperatures in a cyclone furnace, *Fuel*, Volume 69, Issue 11, November 1990, Pages 1345–1349.
- 3.) A. Valero, S. Uson, Oxy-co-gasification of coal and biomass in an integrated gasification combined cycle (IGCC) power plant, *Energy* 31 (2006) 1643 –1655.
- 4.) About IGCC power plants, “The Energy Blog”, September 27th 2005, http://thefraserdomain.typepad.com/energy/2005/09/about_igcc_powe.html
- 5.) Ananth P. Chikkatur, A resource and technology assessment of coal utilization in India, coal initiative reports, Kennedy School of Government, Harvard University, Cambridge, MA October 2008
- 6.) Ananth P. Chikkatur* and Ambuj D. Sagar, Positioning the Indian Coal-Power Sector for Carbon Mitigation: Key Policy Options, coal initiative reports, John F. Kennedy School of Government, Harvard University, Cambridge, MA, January 2009.
- 7.) Ansys Fluent 12.0 UDF Manual, April 2009
- 8.) Ansys Fluent 12.0 Theory guide, April 2009
- 9.) APSLEY, D., CFD, Turbulence modeling in CFD, 2004
- 10.) Arastoopour H. Numerical simulation and experimental analysis of gas–solid flow systems: 1999 Fluor-Daniel Plenary lecture. *Powder Technol* 2001; 119:59–67.
- 11.) Association for the study of peak oil & gas- USA (<http://www.aspousa.org/index.php/peak-oil-reference/peak-oil-data>)
- 12.) Avinash Chandra, Some investigations on fly-ash resistivity generated in Indian power plants, Centre for energy studies, IIT Delhi
- 13.) Bi HT, Ellis N, Abba IA, Grace JR. A state-of-the-art review of gas– solid turbulent fluidization. *Chem Eng Sci* 2000; 55:4789–825.
- 14.) Brooks, C.T., Stroud, H.J.F. and Tart, K.R. (1984). British Gas/Lurgi slagging gasifier. In: R.A. Meyers (ed.), *Handbook of Synfuels Technology*. New York: McGraw-Hill, pp. 3–63 to 3–86.
- 15.) C. Y. Wen, Y. H. Yu, Mechanics of fluidization, *Chemical Engineering Progress Symposium Series*, 62:100-111, 1966.

- 16.) Chapman S, Cowling TG. The mathematical theory of non-uniform gases. Cambridge University Press; 1970.
- 17.) Chejne, F. and J. Hernandez (2002): "Modeling and simulation of coal gasification process in fluidized bed," Fuel, 81, 1687–1702.
- 18.) Chen, G., H.Spliethoff, J.Andries, and M. Glazer (2004): "Biomass gasification in a circulating fluidized bed-part i: Preliminary experiments and modeling development," Energy Sources, 26, 485–498.
- 19.) Chen CX, Horio M, Kojima T. Numerical simulation of entrained flow coal gasifiers. Part I: modeling of coal gasification in an entrained flow gasifier. Chem Eng Sci 2000; 55:3861–74.
- 20.) Chiesa M, Mathiesen V, Melheim JA, Halvorsen B. Numerical simulation of particulate flow by the Eulerian–Lagrangian and the Eulerian–Eulerian approach with application to a fluidized bed. Comput Chem Eng 2005; 29:291–304.
- 21.) Chikkatur, A., Sagar, A., Abhyankar, N. and Sreekumar, N., 2007. "Tariff-based incentives for improving coal-power-plant efficiencies in India." Energy Policy: Accepted.
- 22.) Chris Higman and Maarten van der Burgt, Gasification, Elsevier, 2003.
- 23.) Christopher Highman, Marteen van der Burgt, Gasification, Gulf professional publishing, second edition, 2008.
- 24.) Coal Chemistry, FRONTLINE, Volume 25 Issue 22: Oct. 25-Nov. 07, 2008.
- 25.) Coal Utilization, (<http://scienceandtech.cmpdi.co.in/PDF%20Files/Coal%20Utilisation.Pdf>)
- 26.) Cornejo Pablo & Farias Oscar, Mathematical modeling of coal gasification in a fluidized bed reactor using Eulerian granular description, International journal of chemical reactor engineering, volume 9, article A2, 2011
- 27.) DAVIDSON L. An introduction to turbulence models, Chalmers university of technology, Getebörg, Sweden, 2003
- 28.) D. Gidaspow, Multiphase Flow and Fluidization: Continuum and Kinetic Theory Descriptions, Academic Press, New York, 1994.
- 29.) D.S.Santos, solid fuels combustion and gasification, Marcel Dekker, Inc., New York, Basel, 2004.
- 30.) De Souza-Santos ML. Comprehensive modeling and simulation of fluidized bed boilers and gasifiers. Fuel 1989; 68:1507–21.
- 31.) Di-Blasi, C. (2004): "Modeling wood gasification in a countercurrent fixed bed reactor," AIChE Journal, 50, 2306–2319.
- 32.) Ding, J. and D. Gidaspow (1990): "A bubbling fluidization model using kinetic theory of granular flow," AIChE Journal, 36, 523–538.

- 33.) Dr. Samy Sadaka, Gasification, Adjunct Assistant Professor, Department of Agricultural and Biosystems Engineering, Iowa State University
- 34.) Drew, D.A., Lahey Jr., R.T., 1990. Some supplemental analysis concerning the virtual mass and lift force on a sphere in a rotating and straining flow. *Int. J. Multiphase Flow* 16 (6), 1127–1130.
- 35.) E. Furimsky, Gasification of sand coke: review, *Fuel Process. Technol.* 56 (2006) 262–290.
- 36.) E. Furimsky, Gasification in petroleum refinery of 21st century, *Oil Gas Sci. Technol.* 54 (1999) 597– 618.
- 37.) E. Ruckenstein, Homogeneous fluidization, *I & EC Fundam.* 3 (1964) 260.
- 38.) E. Ruckenstein, Nonhomogeneous fluidization, *I & EC Fundam.* 5 (1966) 139.
- 39.) Eaton AM, Smoot LD, Hill SC, Eatough CN. Components, formulations, solutions, evaluation and application of comprehensive combustion models. *Progr Energy Combust Sci* 1999; 25:387–436.
- 40.) Enwald H, Almstedt AE. Fluid dynamics of a pressurized fluidized bed: comparison between numerical solutions from two-fluid models and experimental results. *Chem Eng Sci* 1999; 54:329–42.
- 41.) Enwald H, Peirano E, Almstedt AE, Leckner B. Simulation of the fluid dynamics of a bubbling fluidized bed experimental validation of the two-fluid model and evaluation of a parallel multiblock solver. *Chem Eng Sci* 1999; 54:311–28
- 42.) Ergudenler, A. and A.E. Ghaly. 1992. Determination of reaction kinetics of wheat straw using thermogravimetric analysis. *Journal of Applied Biochemistry and Biotechnology*, 34/35: 75- 91.
- 43.) F.V. Tinaut, A. Melgar, J.F. Pérez, A. Horrillo, Effect of biomass particle size and air superficial velocity on the gasification process in a downdraft fixed bed gasifier. An experimental and modelling study, *Fuel Processing Technology*, 89 (2008) 1076-1089.
- 44.) Feng Duan, Lihui Zang, Yaji Huang, Dependence of bituminous coal gasification on pressure in a turbulent circulating fluidized bed. *Asia pacific journal of chemical engineering*, Curtin University. 12 Oct. 2011.
- 45.) Fletcher, D., B. Haynes, F. Christo, and S. Joseph (2000): “A cfd based combustion model of an entrained flow biomass gasifier,” *Applied Mathematical Modeling*, 24, 165–182.
- 46.) Gasifipedia, Introduction to gasification, the energy lab, NETL, Department of energy, USA.
- 47.) Gasifipedia, Gasification in detail/ types of gasifiers/ entrained bed gasifier, the energy lab, NETL, Department of energy, US.
- 48.) Gera D, Gautam M, Tsuji Y, Kawaguchi T, Tanaka T. Computer simulation of bubbles in large-particle fluidized beds. *Powder Technol* 1998; 98:38–47.

- 49.) Gidaspow D, Jung J, Singh RK. Hydrodynamics of fluidization using kinetic theory: an emerging paradigm 2002 Flour-Daniel lecture. *Powder Technol* 2004; 148:123–41.
- 50.) Gidaspow D. *Multiphase flow and fluidization: continuum and kinetic theory description*. Academic Press; 1994.
- 51.) Gopal Gautam, Parametric study of commercial scale biomass downdraft gasifier, thesis, master of science, Auburn University, December, 2010, pages 6-7, 12-24
- 52.) GTI (2007). *The GTI Gasification Process*. Company leaflet. Des Plaines: Gas Technology Institute.
- 53.) Gunn, D.J., 1978, "Transfer of Heat or Mass to Particles in Fixed and Fluidized Beds," *Int. J. Heat Mass Transfer*, 21, 467-476.
- 54.) Gururajan, V., P. Agarwal, and J. Agnew (1992): "Mathematical modeling of fluidized bed coal gasifiers," *Applied Mathematical Modeling*, 70, 212–238.
- 55.) Guangwen Xu, Tukahiro murakami, Toshiyuki suda, Yoshiyaki Matsuzaw, Hidehisa tani, Two stage dual fluidized bed gasification, *Fuel Processing Technology* 99 (2009).
- 56.) H. Lee, S choi, M. Paek, A simple process modeling for a dry feeding entrained bed coal gasifier, *Proceedings of the Institution of Mechanical Engineers, Part A: Journal of Power and Energy* 2011 225: 74
- 57.) H. tominaga, Y. Matsushita, H. Aoki, T. Yamashita, T. Akiyama, T.Miura, The development of entrained flow coal gasification simulator, *Nihon Enerugi Gakkaishi/ Journal of the Japan Institute of Energy* 85 (n1) (jan 2006) 36-41.
- 58.) H. Watanabe, M.Otaka, J.Inumaru, Development OF numerical Simulation technique for coal gasification on entrained flow gasifier (Modeling of coal gasification reaction and prediction of gasifier performance) *Transaction of the Japan Society of Mechanical Engineers, Part B* 70 (n695) (July 2004) 1856-1863.
- 59.) H.A.M. Knoef, *Inventory of Biomass Gasifier Manufacturers and Installations*, Final Report to European Commission, Contract DIS/1734/98-NL, in, Biomass Technology Group B.V., University of Twente, Enschede, Netherland, 2000.
- 60.) Hamel S, Krumm W. Mathematical modeling and simulation of bubbling fluidized bed gasifiers. *Powder Technol* 2001; 120:105–12.
- 61.) Harris, D., D.Roberts, D. Henderson. 2006. Gasification behavior of Australian coals at high temperature and pressure. *Fuel* 85 (2006) 134–142.
- 62.) Hjertager, H., T. Solberg, and G. Hansen (2005): "Reactive gas solids flow in circulating fluidized beds," *Fourth International Conference on CFD in the Oil and Gas, Metallurgical and Process Industries SINTEF / NTNU, Trondheim, Norway*.

- 63.) Hoomans BPB, Kuipers JAM, Briels WJ, Swaaij WPM. Discrete particle simulation of bubble and slug formation in a two-dimensional gas-fluidised bed: a hard-sphere approach. *Chem Eng Sci* 1996; 51:99.
- 64.) Hoomans BPB, Kuipers JAM, van Swaaij WPM. Granular dynamics simulation of segregation phenomena in bubbling gas-fluidized beds. *Powder Technol* 2000; 109:41–8.
- 65.) <http://www.commodities-now.com/commodities-now-reports/power-and-energy/6391-coal-market-eyes-growing-china-india-demand-japan-recovery.html>
- 66.) http://www.ucsusa.org/clean_energy/coalvswind/c01.html
- 67.) http://www.eia.doe.gov/emeu/aer/pdf/pages/sec11_20.pdf
- 68.) <http://www.prnewswire.com/news-releases/refill-energy-inc-acquires-international-green-energy-and-commercial-downdraft-gasifier-84937387.html>
- 69.) Hydrogen production from coal: Fact Sheet, Fuel cell & hydrogen energy association, www.fcahea.org
- 70.) Implementing clean coal technologies in India, Barriers and prospects, Malti Goel, chapter 13, Jawaharlal Nehru University, Centre for Studies in Science Policy, New Delhi, India
- 71.) Inventory of coal resources in India, <http://coal.nic.in/reserve2.htm>
- 72.) J. B. Roucis, J.M. Kline, J.D. Smith, Advance Modeling of Gasifiers: Gasification Process Modeling using Computational Fluid Dynamics (CFD), Gasification Technologies Conference, Washington, DC Oct 6 2004.
- 73.) J. Wiman, A.E. Almstedt, Influence of pressure, fluidization velocity and particle size on the hydrodynamics of a freely bubbling fluidized bed, *Chemical Engineering Science*, 53 (1998) 2167-2176.
- 74.) Jeffrey Phillips, Different types of gasifier and their integration with gas turbines, <http://www.netl.doe.gov/technologies/coalpower/turbines/refshelf/handbook/1.2.1.pdf>
- 75.) Jenkins, K.T., Richman, M.W., 1998. Plane simple shear flow of smooth inelastic circular disks: The anisotropy of the second moment in the dilute and dense limits. *Journal of Fluid Mechanics* 192, 313–328.
- 76.) John Rezaiyan, Nicholas P. Cheremisinoff, *Gasification Technologies, A primer for engineers and scientists*, Taylor & Francis group, 2005.
- 77.) John L. Guillory, *Gasification of biomass for power and chemicals*, Acadiana Alternative Energy Lecture Series, 12th January 2012.

- 78.) KBR awarded contract for Indian coal gasification project, MSN news, August 26, 2011, American fuels coalition (<http://www.americanfuelscoalition.com/2011/08/26/kbr-india/>)
- 79.) Kim, Y., J. Lee, and S. Kim (2000): "Modeling of coal gasification in an internally circulating fluidized bed reactor with draught tube," *Fuel*, 79, 69–77.
- 80.) Knutson, Ryan Zebadiah, CFD and CFPD modeling of hydrogen production from coal via Lewis ultra-superheated steam fluidized bed gasification, The university of North Dakota, 2011, DAI/B 73-06, p. , Mar 2012
- 81.) L.M. Armstrong, S. Gu & K.H. Luo, Parametric study of gasification process in a BFB coal gasifier, *Industrial & Engineering chemistry research*, ACS publication, 2011.
- 82.) Liang Yu, Jing Lu, X. Zhang, S.Zhang, Numerical Simulation of the bubbling fluidized bed coal gasification by kinetic theory of granular flow (KTGF) 2006.
- 83.) Liu, H. and Kojima, T., 2004. "Theoretical study of coal gasification in a 50 ton/day HYCOL entrained flow gasifier. I. Effects of coal properties and implications," *Energy and Fuels*, Vol. 18, n 4 July/August, pp. 908-912.
- 84.) Lu, J., L. Lu, X. Zhang, S. Zhang, and W. Dai (2008): "Hydrogen production from fluidized bed coal gasifier with in situ fization of co2 part i: numerical model," *Chem. Eng. Technol*, 31, 197–207.
- 85.) Lu Hullin, Wang Shuyan, Zhao Yunhua, Liu Yang, Dimitri Gidaspow, Jimin Ding, Prediction of particle motion in a two dimensional bubbling fluidized bed using discrete hard sphere model, *Chemical Engineering Science*, Volume 60, June 2005, Pages 3217- 3231.
- 86.) Lurgi (1970). *Lurgi Handbuch*. Frankfurt: Lurgi Gesellschaften.
- 87.) Lurgi (1997). *Lurgi, der Technologie- orientierte Anlagenbauer, 1897–1997* . Frankfurt: Lurgi Gesellschaften.
- 88.) M. Ramezan, "Coal-based Gasification Technologies: An Overview" NETL Gasification Technologies Training Course, Sept. 2004.
- 89.) M. Shahnam, M.syamlal, D. Cicero, Numerical Modeling of Combustion and Gasification Process using the discrete Particle Method, *International Joint Power Generation Conf, ASME Fuels & Combustion Technologies Div*, Miami Beach, FL, 2000, July 23-26
- 90.) Ma, R. P., R. M. Felder, and J. K. Ferrell (1988): "Modeling a pilot-scale fluidized bed coal gasification, fuel processing technology," *Energy and Fuels*, 19, 265–290.
- 91.) Magnussen, B. and B. Hjertager (1976): "On mathematical models of turbulent combustion with special emphasis on soot formation and combustion." In 16th Symp. (Int'l.) on Combustion. The Combustion Institute.

- 92.) Martin grabner, Sirko Ogriseck, Bernd Meyer, Numerical simulation of coal gasification at circulating fluidized bed conditions, *Fuel processing technology* 88 (2007).
- 93.) Mathur, M., M. Freeman, and W. O'Down (2001a): "Moisture and char reactivity modeling in pulverized coal combustors," *Combustion Science and Technology*, 172, 35–69.
- 94.) MENTER F. R. Two-equation eddy-viscosity turbulence models for engineering applications, 1994
- 95.) Michael D. mann, Ryan Z. Knutson, John Erjaec, Jason P. Jacobsen, Modeling reaction kinetics of steam gasification for a transport gasifier, *Fuel* 83 (2004).
- 96.) Modeling uniform fluidization in 2D fluidized bed, Fluent Inc., November 22, 2006.
- 97.) Modeling heterogeneous reactions with Eulerian- Granular flow, Fluent Inc., October 28, 2010.
- 98.) N. Syred, K. Kuriawan, T.Griffiths, R.Ray, Development of fragmentation models for solid fuel combustion and gasification as subroutines for inclusion in CFD codes, *Fuel* 86 (2007) 2221-2231
- 99.) O'Brien, T. J., M. Syamlal, and C. Guenther (2003): "Computational fluid dynamics simulations of chemically reactive fluidized bed processes," Third International Conference on CFD in the Minerals and Process Industries CSIRO, Melbourne, Australia.
- 100.) P. Basu, Combustion and gasification in fluidized beds, Taylor and Francis Group, LLC, Boca Raton, FL, 2006
- 101.) P. Mondal, G.S Dang, M.O. Garg, A review on syngas production through gasification of Indian coal and cleanup for downstream applications- recent developments, *Fuel processing technology*, 2011.
- 102.) Patil DJ, Annaland MS, Kuipers JAM. Critical comparison of hydrodynamic models for gas–solid fluidized beds – Part I: bubbling gas–solid fluidized beds operated with a jet. *Chem Eng Sci* 2005; 60: 57–72.
- 103.) Patil DJ, Annaland MS, Kuipers JAM. Critical comparison of hydrodynamic models for gas–solid fluidized beds – Part II: freely bubbling gas–solid fluidized beds. *Chem Eng Sci* 2005; 60: 73–84.
- 104.) Pengmei Lu, Xiaoying Kong, Chaungzhi WU, Zenhong Yuan, Longlong MA, Jie Chang, Modeling & simulation of biomass air steam gasification in a fluidized bed gasifier, *Front. Chem. Eng. China* 2008,2(2):209–213
- 105.) Perry's chemical engineer's handbook, 7th edition, Mc. Graw- Hill, 1997.
- 106.) Pohorely, M., M. Vosecky, P. Hejdova, M. Puncochar, S. Skoblja, M. Staf, J. Vosta, B. Koutsky, and K. Svoboda (2006): "Gasification of coal and pet in fluidized bed reactor," *Fuel*, 85, 2458–2468.

- 107.) Positioning the Indian Coal-Power Sector for Carbon Mitigation: Key Policy Options, coal initiative reports, Ananth P. Chikkatur* and Ambuj D. Sagar, John F. Kennedy School of Government, Harvard University, Cambridge, MA, January 2009.
- 108.) R. Warnecke, Gasification of biomass: comparison of fixed bed and fluidized bed gasifier, *Biomass and Bioenergy*, 18 (2000) 489-497.
- 109.) Ram K. Iyengar and R. Haque, Gasification of high-ash Indian coals for power generation, *Fuel Processing Technology*, 27 (1991) 247-262
- 110.) Reimert, R., and Schaub, G. (1989). Gas production. In: Ullmann's Encyclopedia of Industrial Chemistry, 5th edn, vol. A12. Weinheim: VCH Verlagsgesellschaft
- 111.) Renzenbrink, W., Wischniewski, R., Engelhard, J. and Mittelstädt, A. (1998). "High Temperature Winkler coal gasification: a fully developed process for methanol and electricity production". Paper presented at Gasification Technologies Conference, San Francisco.
- 112.) Rong DG, Mikami T, Horio M. Particle and bubble movements around tubes immersed in fluidized beds – a numerical study. *Chem Eng Sci* 1999; 54:5737–54.
- 113.) Ross D P, Yan H M, Zhong Z P, Zhang D K. A non- isothermal model of a bubbling fluidised- bed coal gasifier. *Fuel* 2005; 84: 1469–81.
- 114.) Rudolf, P. (1984). Lurgi coal gasification (moving-bed gasifier). In: R.A. Meyers (ed.), *Handbook of Synfuels Technology*. New York: McGraw-Hill.
- 115.) Sandeep Tandon, Feasibility study report for 100 MW demonstration project, IGCC technology for future power development in India, greenhouse gas pollution prevention project, USAID, New Delhi, and 20th February, 2008.
- 116.) Saffer, M., A. Ocampo, and C. Laguerie (1988): "Gasification of coal in a fluidized bed in the presence of water vapor and oxygen; an experimental study and a first attempt at modeling the reactor," *International Chemical Engineering*, 28, 46–61
- 117.) Schoeters, J., K. Maniatis and A. Buekens. 1989. The fluidized bed gasification of biomass: Experimental studies on bench scale reactor. *Biomass* 19: 129-143.
- 118.) Simbeck, D. R., Korens, D. R., Biasca, F. E., Vejtasa, S., and Dickenson, R. L. *Coal Gasification Guidebook: Status, Applications, and Technologies*. Palo Alto, Calif.: Electric Power Research Institute (EPRI), 1993.
- 119.) Simbeck, D. (2007). "Gasification opportunities in Alberta". Paper presented at Seminar on Gasification Technologies sponsored by Alberta Government and GTC, Edmonton.
- 120.) Smith, P.V., Davis, B.M., Vimalchand, P., Liu, G. and Longarbach, J. (2002). "Operation of the PDSF transport gasifier". Paper presented at Gasification Technologies Conference, San Francisco.

- 121.) Syamlal, M., The Particle-Particle Drag Term in a Multiparticle Model of Fluidization, Topical Report, DOE/MC/21353-2373, NTIS/DE87006500, National Technical Information Service, Springfield, VA, 1987
- 122.) Syamlal, M., Rogers, W. and O'Brien, T. J. (1993), MFIx documentation, Theory Guide. Technical Note DOE/METC-94/1004. Morgantown, West Virginia, USA,
- 123.) T. Yamazaki, H. Kozu, S. Yamagata, N. Murao, S. Ohta, S. Shiya, T. Ohba, Effect of superficial velocity on tar from downdraft gasification of biomass, *Energy & Fuels*, 19 (2005) 1186-1191.
- 124.) Taghipour, F., N. Ellis, and C. Wong (2003): "Cfd modeling of a two-dimensional fluidized bed reactor," CFD 2003: The Eleventh Annual Conference of the CFD Society of Canada., 265–290.
- 125.) "The future of coal: An interdisciplinary MIT study". Massachusetts Institute of Technology. Retrieved 2008-12-23.
- 126.) "The True Cost of Coal". Greenpeace. Retrieved 2008-12-23. (<http://www.greenpeace.org/raw/international/press/reports/cost-of-coal.pdf>)
- 127.) "The history and present underground coal gasification activities", the oil drum (www.oildrum.com/topic/supply_production).
- 128.) Toomey R D, Johnstone H F. Gaseous fluidization of solid particles. *Chem Eng Prog* 1952; 48:220
- 129.) Tsuji Y, Kawaguchi T, Tanaka T. Discrete particle simulation of two dimensional fluidized bed. *Powder Technol* 1993; 77:79–87.
- 130.) US Department of energy/ Gasification technology Research & Development: - <http://www.fossil.energy.gov/programs/powersystems/gasification/>
- 131.) US Department of Energy (DoE) (2006). Practical Experience Gained During the First Twenty Years of Operation of the Great Plains Gasification Plant and Implications for Future Projects, April. Washington, DC: US Department of Energy.
- 132.) Utioh, A.C, N.N. Bakshi and D.G MacDonald. 1989. Pyrolysis of grain screening in a batch reactor. *Canadian Journal of Chemical Engineering*, 67: 439-442.
- 133.) Van der Burgt, M.J. and Naber J.E. (1983). "Development of the Shell Coal Gasification process (SCGP)". Paper presented at Advanced Gasification Symposium, Shanghai.
- 134.) Weil, S.A., S.P. Nandi, D.V. Punwani and J.L. Johnson. 1978. Peat hydrogasification. Presented at 176th National Meeting of ACS, Miami, FL.
- 135.) Weimer, A. W. and D. E. Clough (1981): "Modeling a low pressure steam-oxygen fluidized bed coal gasifying reactor," *Chemical Engineering Science*, 36, 549–567.

- 136.) Wen, C. Y., & Yu, Y. H. (1966). Mechanics of fluidization. Chemical Engineering Progress Symposium Series, 62, 100–111.
- 137.) WILCOX, D.C. Turbulence Modeling for CFD, DCW Industries, California, USA, 1994
- 138.) X.J. Liu, W.R. Zhang, T. J. Park, Modeling coal gasification in an entrained flow gasifier, Combustion Theory and Modeling 5 (2001) 595-608
- 139.) Xiaofang Wang, Baosheng Jin, Wenqi Zhong, three dimensional simulation of fluidized bed coal gasification, Chemical Engineering and Processing 48 (2009) 695–705.
- 140.) Yan HM, Heidenreich C, Zhang DK. Mathematical modeling of a bubbling fluidized-bed coal gasifier and the significance of ‘net flow’. Fuel 1998; 77:1067–79.
- 141.) Yang TY, Wang AR, Zhang SJ, Zhang XP. Numerical simulation for fluid dynamics in a gas–solid bubbling fluidized bed. Comput Appl Chem 2005; 22:206–10.
- 142.) Yang, Y., Y. Goh, R. Zakaria, V. Nasserzadeh, and J. Swithenbank (2002): “Mathematical modeling of msw incineration on a traveling bed,” Waste Management, 22, 369–380.
- 143.) Yitian Fang, Jiejie Huang, Yang Wang, Bijiang Zang, Experiment & mathematical modeling of bench scale circulating fluidized bed gasifier, Fuel processing technology, volume 69, issue 1, January 2001, pages 29- 44.
- 144.) Yong Tack Kim, Dong Kyun Seo, Jungho Hwang, study of the effect of coal type and particle size on char- CO₂ gasification via gas analysis, Energy & Fuels, ACS publication, 2011.
- 145.) Yu, L., J. Lu, X. Zhang, and S. Zhang (2007): “Numerical simulation of the bubbling fluidized bed coal gasification by the kinetic theory of granular flow,” Fuel, 86, 722–734.
- 146.) Zhou, M., L. feng Yan, Q. xiang Guo, and Q. shi Zhu (2006): “Non-premixed combustion model of fluidized bed biomass gasifier for hydrogen-rich gas,” Thermal Science, 19, 131–136.

APPENDIX- A

PILOT PLANT DATA

Table A4.1 to A4.6 presents the pilot plant data of bubbling fluidized bed gasifier facility at Central Institute of Mining and Fuel Research, Dhanbad used in this study: -

Table A.1 Experimental details for gasification experiments in fluidized bed gasifier

Coal feed rate	12 kg/ hr
Air feed rate	320 LPM
Conveying air flow rate	50 LPM
Steam feed rate	2.7 kg/hr
Ash discharge rate	7 kg/hr

Table A.2 Proximate Analysis of Feed Coal Samples (air dried basis)

Coal	Mineral Matter MM (%)	Moisture M (%)	Volatile Matter VM (%)	Fixed Carbon FC (%)
ECL	48.9	7.1	20.4	23.6

Table A.3 Ultimate Analysis of Feed Coal Samples (air dried basis)

Coal	C (%)	H (%)	N (%)	S (%)	O* (%)
ECL	30.82	1.90	0.60	0.24	5.55

*By difference

Table A.4 Calorific Value of Feed Coal Samples

Coal	Calorific Value GCV (Kcal/kg)
ECL	2670

Table A.5 Ash Analysis of Coal Samples

Coal	SiO ₂ %	Al ₂ O ₃ %	Fe ₂ O ₃ %	TiO ₂ %	P ₂ O ₅ %	SO ₃ %	CaO %	MgO %	Na ₂ O %	K ₂ O %
ECL	62.28	27.56	4.79	1.28	0.17	0.54	1.85	0.68	0.17	0.66

Table A.6 Syngas Composition

Expt. No.	Temperature °C	Syngas Composition, %					
		CO	CO ₂	H ₂	N ₂	CH ₄	O ₂
1	829	10.3	18.49	15.25	54.42	1.54	0
2	837	15.2	16.77	18.46	48.21	1.36	0
3	870	16.80	15.5	18.45	47.96	1.29	0
4	884	17.87	16.00	19.25	46.87	0.002	0
5	892	18.28	15.34	19.35	45.71	1.32	0
6	900	18.78	14.54	18.59	46.81	1.28	0
7	920	19.09	15.07	19.88	44.67	1.29	0
8	849	15.19	15.28	17.94	50.16	1.43	0
9	883	18.66	13.83	18.64	47.6	1.27	0
10	893	18.49	13.55	18.33	48.4	1.19	0

APPENDIX- B

UDF FOR HETEROGENOUS REACTIONS

```
#include"udf.h"

static const real Arrhenius = 1.e15;

static const real E_Activation = 1.e6;

#define SMALL_S 1.e-29

DEFINE_HET_RXN_RATE(arrh,c,t,hr,mw,yi,rr,rr_t)
{
Domain **domain_reactant = hr->domain_reactant;

real *stoich_reactant = hr->stoich_reactant;

int *reactant = hr->reactant;

int i;

int sp_id;

int dindex;

Thread *t_reactant;

real ci;

real T = 1200.; /* should obtain from cell */

/* instead of compute rr directly, compute log (rr) and then take exp */

*rr = 0;

for (i=0; i < hr->n_reactants; i++)
```

```

{
sp_id = reactant[i]; /* species ID to access mw and yi */

if (sp_id == -1) sp_id = 0; /* if phase does not have species,

mw, etc. will be stored at index 0 */

dindex = DOMAIN_INDEX(domain_reactant[i]);

/* domain index to access mw & yi */

t_reactant = THREAD_SUB_THREAD(t,dindex);

/* get conc. */

ci = yi[dindex][sp_id]*C_R(c,t_reactant)/mw[dindex][sp_id];

ci = MAX(ci,SMALL_S);

*rr += stoich_reactant[i]*log(ci);

}

*rr += log(Arrhenius + SMALL_S) -E_Activation/(UNIVERSAL_GAS_CONSTANT*T);

/* 1.e-40 < rr < 1.e40 */

*rr = MAX(*rr,-40);

*rr = MIN(*rr,40);

*rr = exp(*rr);

}

```

APPENDIX- C

SAMPLE DATA & RESULTS

Table C.1: - Effect of Temperature on syngas composition

EFFECT OF TEMPERATURE ON THE SYNGAS COMPOSITION				
Temperature (K)	H₂	CO	CO₂	H₂O
500	0.0067	0	0.152	0.2013
600	0.0302	0	0.1601	0.1779
700	0.0905	0.0034	0.1814	0.1478
800	0.1124	0.0369	0.1982	0.1283
900	0.1311	0.0614	0.1901	0.0898
1000	0.1501	0.0945	0.1765	0.0867
1100	0.1698	0.1358	0.1682	0.0405
1200	0.1997	0.1602	0.1457	0.031
1223	0.2094	0.181	0.1378	0.0052
1300	0.2192	0.208	0.1307	0.00024
1400	0.2274	0.2123	0.1259	0.000058
1500	0.2317	0.2183	0.1187	0.000032
1600	0.2318	0.2185	0.1186	0.000029

Table C.2: - Effect of Pressure on syngas composition

EFFECT OF OPERATING PRESSURE ON SYNGAS COMPOSITION			
Pressure	H₂	CO	CO₂
1	0.0067	0.185	0.152
2	0.0302	0.1834	0.1601
3	0.0905	0.181	0.1814
4	0.1124	0.1795	0.1982
5	0.1311	0.178	0.1901
6	0.1501	0.177	0.1765
7	0.1698	0.1752	0.1682
8	0.1997	0.1747	0.1457
9	0.2094	0.173	0.1378
10	0.2192	0.172	0.1307

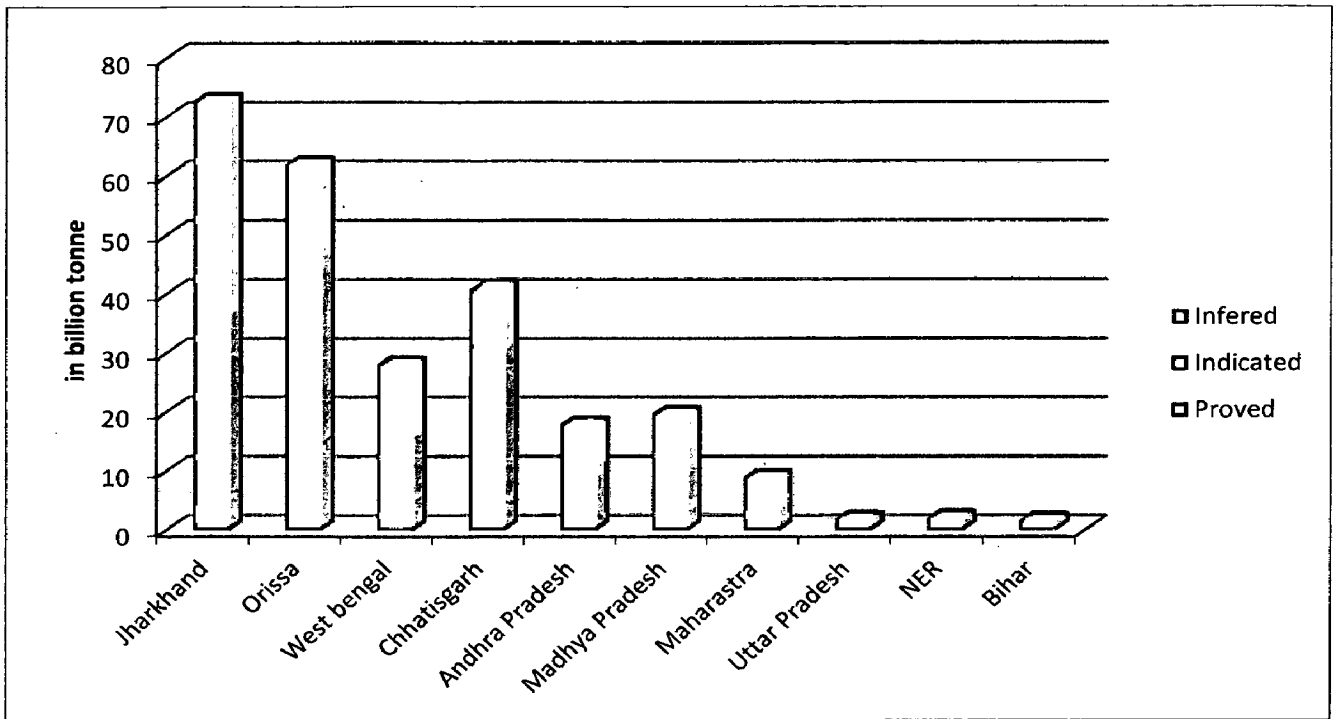


Fig. C.1 State- wise break up of Indian coal reserve

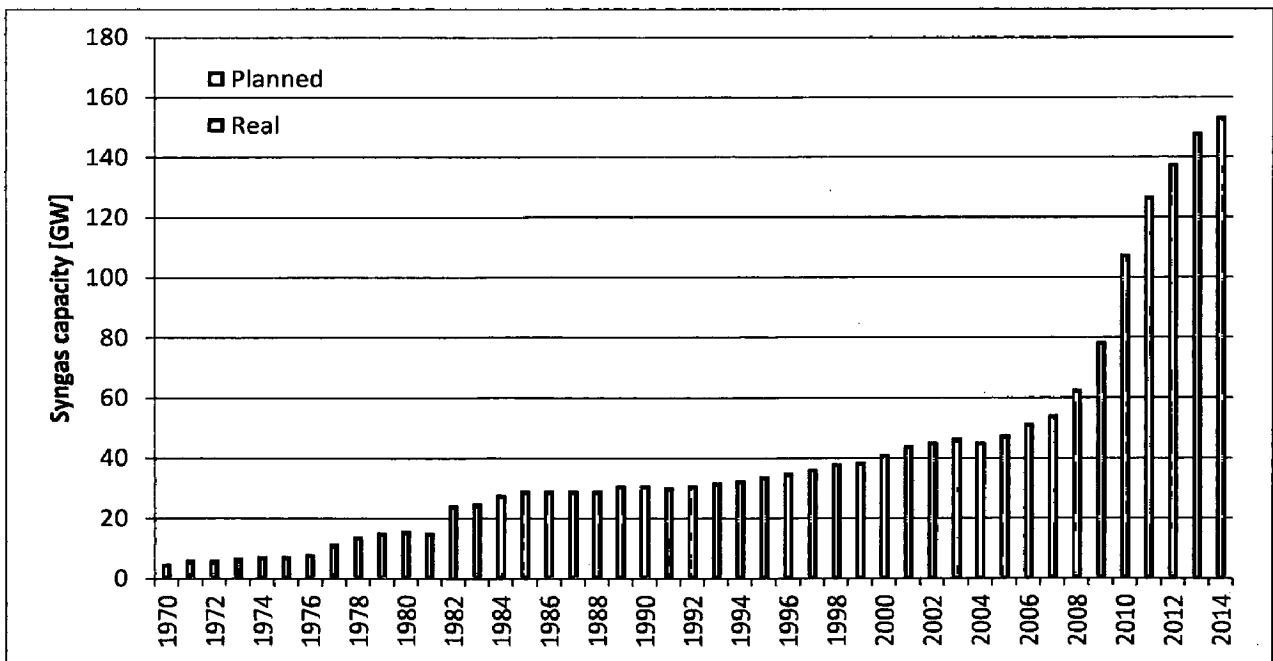


Fig. C.2 Cumulative worldwide gasification facility

Source: Simbeck, 2007